



Huerta Uribe, Alejandro (2019) *Identification and characterisation of small-molecule inhibitors of Shiga toxin expression in Escherichia coli O157:H7*. PhD thesis.

<https://theses.gla.ac.uk/40993/>

Copyright and moral rights for this work are retained by the author

A copy can be downloaded for personal non-commercial research or study, without prior permission or charge

This work cannot be reproduced or quoted extensively from without first obtaining permission in writing from the author

The content must not be changed in any way or sold commercially in any format or medium without the formal permission of the author

When referring to this work, full bibliographic details including the author, title, awarding institution and date of the thesis must be given

Enlighten: Theses

<https://theses.gla.ac.uk/>
research-enlighten@glasgow.ac.uk



University of Glasgow

Identification and characterisation of small-molecule inhibitors of Shiga toxin expression in *Escherichia coli* O157:H7

A thesis submitted to the University of Glasgow for the
degree of Doctor of Philosophy

Alejandro Huerta Uribe BSc, MRes

Submitted September 2018

Institute of Infection, Immunity and Inflammation

College of Medical, Veterinary and Life Sciences

University of Glasgow

Abstract

Shiga toxin (Stx) producing *E. coli* (STEC) infections represent an important public health problem given the severity of the disease and sequelae associated to it. Since the use of antibiotics enhances the virulence of STEC, new therapeutic strategies are urgently required. Thus, the main aim of this project is the study of small molecules that are able to block expression of Shiga toxin in *Escherichia coli* O157:H7.

The genes encoding Stx are located on temperate lysogenic phages integrated into the bacterial chromosome and expression of the toxin is generally coupled to phage induction through the SOS response. We aimed to find new compounds capable of blocking expression of Stx type 2 (Stx2) as this subtype of Stx is more strongly associated with human disease.

High-throughput screening of a small-molecule library identified a lead compound that reduced Stx2 expression in a dose-dependent manner. We show that the optimized compound interferes with the SOS response by directly affecting the activity and oligomerization of RecA, thus limiting phage activation and Stx2 expression. Our work suggests that RecA is highly susceptible to inhibition and that targeting this protein is a viable approach to limiting production of Stx2 by EHEC. This type of approach has the potential to limit production and transfer of other phage induced and transduced determinants.

As a result of the successful identification of a small molecule capable of inhibiting Stx2 expression in *E. coli* O157:H7, an additional high-throughput screening (HTS) of small molecules was performed. Two new compounds with activity against Stx2 production were successfully identified and characterised in biological assays. Finally, we describe the use of a small molecule with previously reported anti-quorum sensing activity. Our findings suggest that the compound furanone C-30 blocks *stx* expression *in vitro*.

Table of Contents

Abstract.....	3
List of Tables	8
List of Figures.....	9
Acknowledgements	12
Author's Declaration.....	13
Abbreviations	14
CHAPTER 1	18
1 Introduction.....	19
1.1 Shiga toxin producing <i>Escherichia coli</i> (STEC).....	19
1.1.1 Virulence factors in <i>E. coli</i> O157:H7	20
1.1.2 Transmission sources	21
1.1.3 Pathogenesis of STEC.....	22
1.2 Shiga toxins	23
1.2.1 Structure of Shiga toxins and cellular receptors.....	23
1.2.2 Shiga toxin types and subtypes	24
1.2.3 Intracellular trafficking of Shiga toxin	25
1.2.4 Shiga toxin mode of action.....	27
1.2.5 Shiga toxin encoding bacteriophages	28
1.2.6 Diversity of Shiga toxin phages	29
1.3 Regulation of Shiga toxin expression.....	31
1.3.1 The SOS response	31
1.3.2 LexA and RecA, the master regulators of the SOS response	32
1.3.3 Filament formation	33
1.3.4 Regulation of RecA and filament formation	34
1.3.5 Induction of the SOS response	35
1.3.6 Expression of Shiga toxin	37
1.4 Shiga toxins and human disease	38
1.4.1 Incidence of STEC infections	38
1.4.2 Detection of STEC.....	39
1.4.3 Haemolytic Uremic Syndrome	42
1.4.4 Antibiotics and STEC infections.....	44
1.5 Anti-virulence approach to treat bacterial infections	45
1.5.1 Concept, advantages and potential limitations	45
1.5.2 Anti-virulence strategies against STEC	47
1.6 The drug discovery process.....	49
1.6.1 Discovery and development	51
1.7 Aims of the project	58
CHAPTER 2	59
2 Materials and methods	60
2.1 Chemicals and molecular reagents.....	60

2.2	Growth media	60
2.3	Cell culture	61
2.3.1	Shiga toxin cytotoxicity assay.....	61
2.4	Storage and handling of bacterial strains	62
2.4.1	Bacterial strains.....	62
2.5	Plasmids	63
2.6	Bacterial growth conditions	63
2.7	Molecular techniques.....	64
2.7.1	Oligonucleotide primers	64
2.7.2	Preparation of genomic DNA	65
2.7.3	Polymerase chain reaction (PCR).....	65
2.7.4	Extraction of plasmid DNA.....	66
2.7.5	Agarose gel electrophoresis	66
2.7.6	Restriction enzyme digests.....	66
2.7.7	DNA gel purification	66
2.7.8	DNA ligation	67
2.7.9	Preparation of electrocompetent <i>E. coli</i>	67
2.7.10	Electroporation transformation.....	67
2.7.11	Heat-shock transformation	68
2.7.12	Gene inactivation using the lambda red recombineering system.....	68
2.7.13	Removal of antibiotic resistance cassettes by FLP recombination	69
2.7.14	Reporter assays.....	70
2.7.15	Phage transduction assays	70
2.8	Biochemical techniques.....	71
2.8.1	RecA Protein overexpression.....	71
2.8.2	SDS-PAGE.....	73
2.8.3	General Western blot procedure	73
2.8.4	RecA ATPase assays.....	73
2.8.5	Sample preparation for metabolomics analysis	74
2.9	Biophysical techniques	75
2.9.1	Microscale thermophoresis	75
2.10	High throughput screening.....	76
2.10.1	Primary screen.....	76
2.10.2	Counter-screen of hit compounds using <i>E. coli rpsM::GFP</i>	77
2.10.3	Dose response calculation	77
2.11	Cytotoxicity of AHU series	77
2.12	Animal experiment.....	78
2.12.1	Mice maintenance.....	78
2.12.2	Infection of mice with <i>C. rodentium</i> λ stx _{2dact}	78
2.12.3	Preparation of peanut butter/hazelnut cocoa pellets and dosing.....	79
2.12.4	Live imaging of infected mice using the IVIS® Spectrum system.....	79
2.12.5	Faecal shedding bacterial counts.....	79

2.12.6	Tissue collection and histology	80
2.13	Organic synthesis	80
2.13.1	General	80
CHAPTER 3	92
3	Identification and characterisation of novel compounds blocking Shiga toxin expression in <i>Escherichia coli</i> O157:H7	93
3.1	Introduction.....	93
3.2	Biological assay used in the screening	94
3.3	Identification of a hit compound with inhibitory activity on <i>stx2</i> expression	95
3.4	The compound AHU3 affects phage lytic development	100
3.5	Effect of AHU3 on <i>Stx2</i> production by EHEC	102
3.6	Finding the target of AHU3	102
3.7	The compound AHU3 does not affect RecA expression	103
3.8	Microscale thermophoresis	104
3.9	The compound AHU3 inhibits the ATPase activity of RecA	106
3.10	AHU3 affects RecA oligomerisation.....	108
3.11	Synthesis of a biotinylated derivative of AHU3 for affinity chromatography	109
3.12	Toxicological profiling of the AHU compounds	116
3.13	Expression and purification of RecA.....	116
3.14	Evaluation of a reported inhibitor of RecA	119
3.15	Discussion.....	123
3.15.1	Electrophilic nature of AHU3 and its implications in the mode of action	123
3.15.2	RecA as a drug target.....	126
3.15.3	Challenges in the development of RecA inhibitors.....	127
3.15.4	RecA-independent prophage induction	129
4	Identification of selective inhibitors of <i>Stx</i> expression by high throughput screening	132
4.1	Introduction.....	132
4.2	Assay development and validation	133
4.2.1	DMSO tolerance	133
4.2.2	Statistical evaluation of the HTS assay	133
4.3	High throughput screening at the Drug Discovery Unit (DDU) University of Dundee ...	137
4.4	Dose response evaluation of putative hit compounds and counter-screen	141
4.5	Characterisation of hit compounds.....	146
4.5.1	The compounds DDD01302463 and DDD01304030 block the phage lytic development 147	
4.5.2	The compounds DDD01302463 and DDD01304030 do not affect bacterial growth and are specific against <i>Stx</i> expression.	150
4.5.3	Evaluation of the compounds DDD01302463 and DDD01304030 in the Shiga toxin cytotoxicity assay.....	151
4.6	Discussion	153
4.6.1	Potential of the compounds DDD01302463 and DDD01304030 as lead compounds	154
4.6.2	Stereochemistry and its implication in drug development	155

4.6.3	Target identification: future work	156
5	Exploring the inhibition of quorum sensing as a potential strategy to prevent Shiga toxin expression in <i>Escherichia coli</i> O157:H7	159
5.1	Introduction.....	159
5.2	Naturally occurring brominated furanones alter AI-2 signalling in <i>E. coli</i>	162
5.3	The compound furanone C-30 reduces <i>stx2</i> ::GFP expression	164
5.4	Furanone C-30 block phage mediated lysis and does not affect bacterial growth in <i>E. coli</i> O157:H7	165
5.5	Furanone C-30 prevents prophage induction and phage lytic development	167
5.6	Western blot analysis of the effect of furanone C-30 on Stx production in <i>C. rodentium</i> λ <i>stx</i> _{2dact}	168
5.7	Evaluation of furanone C-30 in the Shiga toxin cytotoxicity assay	169
5.8	Is the activity of furanone C-30 on Stx expression a result of the inhibition of LuxS? .	171
5.9	Does furanone C-30 inhibit RecA's activity?	172
5.10	<i>In vivo</i> evaluation of furanone C-30 as a potential strategy to prevent Shiga toxin expression.....	173
5.10.1	Animal models for EHEC infections.....	174
5.10.2	Experimental design	175
5.10.3	Preparation of peanut butter/hazelnut spread pellets for the delivery of the drug. 175	
5.10.4	Infection of BALB/c mice with <i>C. rodentium</i> λ <i>stx</i> _{2dact}	176
5.11	Discussion.....	181
5.11.1	<i>In vivo</i> evaluation of furanone C-30 in the <i>Citrobacter rodentium</i> λ <i>stx</i> _{2dact} infection model.	182
6	Final discussion	186
6.1	Targeting the bacterial SOS response to prevent Shiga toxin expression	186
6.2	The use of small molecules to modulate bacterial virulence	187
6.3	Concluding remarks.....	189
	List of References	190
	Annex	230

List of Tables

Table 1 Culture methods for the detection of Stx	40
Table 2 Different types of screening strategies used in drug discovery	53
Table 3 Growth media	60
Table 4 Bacterial strains used in this study	62
Table 5 Plasmids used in this study	63
Table 6 Antibiotics used for the growth of GMO with antibiotic resistance markers	63
Table 7 Primers used in this study.....	64
Table 8 Components of a PCR reaction	65
Table 9 Standard PCR protocol (30 cycles).....	65
Table 10 SOC media recipe (1 L).....	68
Table 11 RecA purification buffers	72
Table 12 Antibodies used in this study.....	73
Table 13 Elutions of samples in HILIC	75
Table 14 Different conditions used for the coupling between AHU1 and biotin	111
Table 15 Toxicological evaluation of the AHU compounds.	116
Table 16 Efficiency of the development of lambdaoid bacteriophages in <i>E. coli</i> and <i>S. aureus</i> after mitomycin C induction and treatment with FePcTs.....	120
Table 17 Average peak intensities of compounds across different groups	122
Table 18 Z' value and its interpretation (modified from Zhan, Chung, and Oldenburg, 1999). .	135
Table 19 Assay validation <i>stx2::GFP</i>	136
Table 20 Assay validation <i>rpsM::GFP</i>	137
Table 21 Conversion table between pXC ₅₀ and μM	143
Table 22 Chemical structures of the hit compounds, potency and activity.....	144
Table 23 Liable functional groups in drug discovery.....	154

List of Figures

Figure 1 STEC transmission cycle.	21
Figure 2. Structure of Shiga toxins.	24
Figure 3 Trafficking of Shiga toxin.	26
Figure 4 Bacteriophages can have lysogenic or lytic cycles.	29
Figure 5 RecA mediates the autocleavage of LexA.	33
Figure 6 RecA filament formation.	34
Figure 7 Triggers of the SOS response.	36
Figure 8 Shiga toxin expression.	37
Figure 9 Incidence of <i>E. coli</i> O157:H7 around the globe.	39
Figure 10 Transfer of Shiga toxin from the circulation to the kidney.	43
Figure 11 Emergence of anti-virulence research.	46
Figure 12 The drug discovery process at a glance.	50
Figure 13 Differences between the phenotype and target-based approaches.	54
Figure 14 Synthesis of compounds with inhibitory activity against Shiga toxin expression.	94
Figure 15 <i>pstx2::GFP</i> reporter assay.	95
Figure 16 Flow chart summarizing the HTS of the ChemBridge library.	96
Figure 17 Effect of AHU1 on <i>stx2::GFP</i> expression.	97
Figure 18 The compound AHU1 does inhibits MMC-induced lysis and does not interfere with bacterial growth rate.	98
Figure 19 Phenotypic half maximum inhibitory concentration for the AHU compounds.	98
Figure 20 Comparison of activity between the analogue compounds AHU1-4.	99
Figure 21 The compound AHU3 affects MMC-induced phage lytic development.	100
Figure 22 AHU3 also affects phage lytic development in <i>S. aureus</i>	101
Figure 23 The compound AHU3 blocks expression in <i>E. coli</i> ZAP1620, a wild-type strain that is lysogenized with both Stx2a- and Stx2c-encoding phages.	102
Figure 24 Effect of AHU3 on RecA expression.	103
Figure 25 Microscale thermophoresis.	105
Figure 26 Exploring the interaction of RecA with the AHU3 and AHU4 compounds using MST. ..	106
Figure 27 AHU3 inhibits RecA-mediated ATP hydrolysis.	107
Figure 28 AHU3 decreases RecA oligomerization.	108
Figure 29 Synthesis of AHU3.	110
Figure 30 Coupling between (+)-biotin and compound <i>vi</i> was attempted using peptide coupling reagents.	110
Figure 31 Synthesis of azidopropylamine.	111
Figure 32 Biotin was converted into its <i>N</i> -hydroxysuccinimide ester (NHS) in order to obtain its <i>N</i> - (3-azidopropyl) derivative <i>xiv</i>	112
Figure 33 Synthesis of 1-(4-(4-(prop-2-yn-1-yl)piperazin-1-yl)phenyl)-1H-pyrrole-2,5-dione	112
Figure 34 Copper-catalysed azide-alkyne cycloaddition.	113
Figure 35 Sonogashira coupling.	113

Figure 36 Sonogashira coupling using tetrakis(triphenylphosphine)palladium(0)	113
Figure 37 The catalytic cycle for the Sonogashira reaction.	114
Figure 38 Copper-catalysed azide-alkyne cycloaddition using AscNa and CuSO ₄	115
Figure 39 The biotinylated derivative of AHU3 was not obtained.	115
Figure 40 Intein-mediated purification of RecA.	117
Figure 41 SDS-PAGE of purification fractions for RecA.	118
Figure 42 Effect of FePcTs on phage production.	120
Figure 43 Effect of FePcTs on Stx2 expression in <i>C. rodentium</i> λ stx _{2dact}	121
Figure 44 Chemical structure of FePcTs.	122
Figure 45 Amino acid sequence of RecA.	125
Figure 46 Proposed molecular mechanism of action of RI-1, an inhibitor of RAD51.	126
Figure 47 Effect of DMSO on bacterial growth.	133
Figure 48 Separation band the suitability of an assay for HTS.	135
Figure 49 Assay performance of the <i>stx2</i> ::GFP reporter strain.	136
Figure 50 Assay performance of the <i>rpsM</i> ::GFP reporter strain.	137
Figure 51 Single point HTS to identify inhibitors of Stx2 expression in <i>E. coli</i> O157:H7.	138
Figure 52 Hit selection from the HTS campaign.	139
Figure 53 Response distribution of the HTS.	140
Figure 54 Secondary screening of the hit compounds using the <i>rpsM</i> ::GFP.	142
Figure 55 Dose-response curves from the hit compounds identified in the primary screen.	145
Figure 56 Re-evaluation of the hit compounds in the <i>stx2</i> ::GFP reporter assay.	146
Figure 57 Effect of the compounds DDU01302463 and DDU01304030 on MMC-induced phage production.	148
Figure 58 Effect of the compounds DDU01302463 and DDU01304030 on MMC-induced cell lysis.	149
Figure 59 Potency of the hit compounds DDD01302463 and DDD01304030	149
Figure 60 Evaluation of effect of compounds DDD01302463 and DDD01304030 in bacterial growth and <i>rpsM</i> ::GFP expression.	150
Figure 61 Effect of DDD01302463 and DDD01304030 on viability of Vero cells treated with lysates of <i>C. rodentium</i> λ stx _{2dact}	151
Figure 62 Effect of DDD01302463 on Stx production in <i>C. rodentium</i> λ stx _{2dact}	152
Figure 63 Chemical structures of the compounds DDD01302463 and DDD01304030.	155
Figure 64 Target identification methods.	157
Figure 65 Adrenergic sensing in EHEC.	160
Figure 66 The LsrR/phospho-AI-2 circuit in <i>E. coli</i>	161
Figure 67 Chemical structures of the brominated furanones isolated from <i>D. pulchra</i>	162
Figure 68 Proposed mechanisms for LuxS by the brominated furanone C-30.	164
Figure 69 The compound furanone C-30 reduces <i>stx2</i> ::GFP expression.	165
Figure 70 Furanone C-30 blocks phage mediated lysis in <i>E. coli</i> O157:H7.	166
Figure 71 Evaluation of effect of furanone C-30 in bacterial growth and <i>rpsM</i> ::GFP expression.	166
Figure 72 Effect of the furanone C-30 on MMC-induced phage production.	168

Figure 73 Furanone C-30 prevents phage-induced lysis in <i>C. rodentium</i> λ stx _{2dact} and decreases Stx _{2dact} production.....	169
Figure 74 Effect of furanone C-30 on viability of Vero cells treated with <i>C. rodentium</i> λ stx _{2dact} lysates.	170
Figure 75 Effect of furanone C-30 on prophage induction in <i>E. coli</i> JP10819 and its Δ LuxS mutant.	172
Figure 76 Furanone C-30 does not inhibit RecA's ATPase activity.....	173
Figure 77 Colonisation of <i>C. rodentium</i> λ stx _{2dact} in BALB/c mice.	177
Figure 78 Colonisation of BALB/c mice with <i>C. rodentium</i> λ stx _{2dact}	178
Figure 79 Weight monitoring of mice.	179
Figure 80 Micrographs of H&E-stained kidney sections from mock infected or <i>C. rodentium</i> λ stx _{2dact} infected mice at day 10 after infection.	180

Acknowledgements

Firstly, I would like to thank Professor Andrew Roe for his continuous and endless support throughout the project. I really appreciate all the guidance, advice and constant motivation even when things were not going well. I will always be grateful for that. Thanks also to Dr Rodolfo Marquez who played a key role at the beginning of the project. Thank you for introducing me to the fascinating world of medicinal chemistry.

I would like to thank Professor Olwyn Byron and Professor Darren Monckton for their valuable support and mentoring at the beginning and throughout the PhD. The programme would not have been the same without you. Many thanks for everything. Thanks also to Dr Gillian Douce for all her support during the project. I really appreciate all the effort you did to help us get the work done.

Thanks to all the members of the Roe lab: Liyana, Glen, James C., James M., Jennifer, Natasha, Nicky, Rebecca, Riccardo, Tom and Zoe. You made the long hours spent in the lab more enjoyable. I will miss you all very much.

Particular thanks to all my friends, both in Glasgow and Mexico. Thanks for always being there, for your support and for all the fun we had! Glasgow would not be the same without you: Alfred, Angel, Andrew, Amin, Dominika, Izaskun, Laura Medina, Laura Mincarelli, Liyana, Luccin, Luis, Maribel, Meri, Miquel, Nerea, Nuria, Riccardo, Rodrigo and Virginia. Let's keep the adventures going!

A big thank you to my parents and brother, who have always given me unconditional support. Thanks for your constant motivation and for giving the courage to make this big jump across the Atlantic. Los quiero mucho papá, mamá y Adrian. Gracias!

Special thanks to Chris, for his patience, constant motivation and support. You have really made a difference. Thank you!

Author's Declaration

I declare that, except where explicit reference is made to the contribution of others, this dissertation is the result of my own work and has not been submitted for any other degree at the University of Glasgow or at any other institution.

Alejandro Huerta Uribe

September 2018

Abbreviations

°C	degrees Celsius
Δ	deletion
A ₆₅₀	Absorbance at 650 nm
A/E	attaching/effacing
AIEC	adherent-invasive <i>E. coli</i>
ANOVA	analysis of variance
APEC	avian pathogenic <i>E. coli</i>
ATP	adenosine triphosphate
ADP	adenosine diphosphate
AUC	analytical ultracentrifugation
AR	acid-resistance
AV	antivirulence
cAMP	cyclic adenosine monophosphate
CTD	carboxy-terminal domain
amp	ampicillin
BLAST	basic local alignment search tool
bp	base pair
CFU	colony forming unit
chl	chloramphenicol
Cys	cysteine
Da	dalton
kDa	kilodalton
DMEM	Dulbecco's Modified Eagle's Medium
DNA	deoxyribonucleic acid
gDNA	genomic DNA
dsDNA	double-stranded DNA
ssDNA	single-stranded DNA
EAEC	enteroaggregative <i>Escherichia coli</i>
EDTA	ethylenediaminetetraacetic acid
EHEC	enterohaemorrhagic <i>Escherichia coli</i>
ELISA	enzyme-linked immunosorbent assay
EPEC	enteropathogenic <i>Escherichia coli</i>

ERAD	endoplasmic reticulum associated pathway
aEPEC	atypical EPEC
EPEC	enterotoxigenic <i>Escherichia coli</i>
ery	erythromycin
FCS	foetal calf serum
Gb3	globotriaosylceramide
GFP	green fluorescent protein
g	gram
mg	milligram
µg	microgram
ng	nanogram
H&E	hematoxylin and eosin
HEPES	4-(2-hydroxyethyl)-1-piperazineethanesulfonic acid
HUS	haemolytic uraemic syndrome
HR	homologous recombination
HTS	high throughput screening
h	hours
ICA	indole-3-carboxaldehyde
IC ₅₀	half maximal inhibitory concentration
IL	interleukin
IPTG	isopropyl β-D-1-thiogalactopyranoside
IVIS	<i>in vivo</i> imaging system
kan	kanamycin
kb	kilobase
L	litre
ml	millilitre
µl	microlitre
LB	Luria-Bertani
LEE	locus for enterocyte effacement
Ler	LEE-encoded regulator
LexA	locus for X-ray sensitivity A
LPS	lipopolysaccharide
M	molar
mM	millimolar
µM	micromolar

nM	nanomolar
MBC	minimum bactericidal concentration
MEM	Minimum Essential Medium
MIC	minimum inhibitory concentration
MMC	mitomycin C
MRSA	multidrug resistant <i>Staphylococcus aureus</i>
MST	microscale thermophoresis
MW	molecular weight
cm	centimeter
mm	millimeter
µm	micrometer
NER	nucleotide excision repair
NMR	nuclear magnetic resonance
NO	nitric oxide
OD	optical density
OMVs	outer membrane vesicles
PBS	phosphate buffered saline
PBST	PBS containing 0.1% Tween
PCR	polymerase chain reaction
PFA	paraformaldehyde
p/s	photons per second
RecA	recombinase A
RFP	red fluorescent protein
RNA	ribonucleic acid
ROS	reactive oxygen species
mRNA	messenger RNA
rRNA	ribosomal RNA
tRNA	transfer RNA
rpm	revolutions per minute
SAR	structure-activity relationship
ssDNA	single stranded DNA
SDS-PAGE	sodium dodecyl sulfate polyacrylamide gel electrophoresis
SMAC	sorbitol MacConkey
SOC	super optimal broth

SOS	save our souls
Str	streptomycin
Stx	Shiga toxin
T3SS	Type 3 Secretion System
TAE	Tris-acetate-EDTA
TBAI	Tetrabutylammonium iodide
TCA	trichloroacetic acid
TLS	translesion synthesis
Tir	translocated intimin receptor
TGN	<i>trans</i> -Golgi network
TNF	tumour necrosis factor
TSB	tryptic soy broth
tet	tetracycline
UK	United Kingdom
UPEC	uropathogenic <i>Escherichia coli</i>
UPR	unfolded protein response
USA	United States of America
UV	ultraviolet
VFA	volatile fatty acid
v/v	volume per volume
w/v	weight per volume
x g	centrifugal force

CHAPTER 1

Introduction

1 Introduction

Escherichia coli is a Gram-negative, facultative anaerobe that is a member of the Enterobacteriaceae family. *E. coli* strains are often classified based on the type of surface antigens present in the cells: the O-antigen found in the outer membrane, the H-antigen present in flagella and the capsular K-antigen (J. L. Smith and Fratamico 2017). Most *E. coli* serotypes are harmless symbionts naturally found in the gastrointestinal tract of warm-blooded animals. However, some strains have acquired virulence genes that make them the causal agents of enteric, urinary tract and extraintestinal infections. Thus, *E. coli* strains can be also classified into pathotypes or groups that have similar forms of disease. These include Enterotoxigenic *E. coli* (ETEC), enteroinvasive *E. coli* (EIEC), enteroaggregative *E. coli* (EAEC), enteropathogenic *E. coli* (EPEC), diffusively adherent *E. coli* (DAEC), Shiga toxin producing *E. coli* (STEC), adherent invasive *E. coli* (AIEC), uropathogenic *E. coli* (UPEC), sepsis-associated *E. coli* (SEPEC), neonatal meningitis *E. coli* (NMEC) and avian pathogenic *E. coli* (APEC). The present work focuses on Shiga toxin producing *E. coli* (STEC).

1.1 Shiga toxin producing *Escherichia coli* (STEC)

The first report of STEC as a human pathogen was in 1983. It was associated with a group of people who fell ill after ingestion of undercooked hamburgers at a fast-food restaurant in the USA (Riley et al. 1983). The symptoms included severe abdominal pain, bloody diarrhoea with little or no fever, manifestations today known as haemorrhagic colitis. Later that year, the presence of a toxin-producing *E. coli* strain in stools of patients with haemolytic uremic syndrome (HUS) revealed the link between the two illnesses (Nataro and Kaper 1998).

STEC is also commonly referred to as Vero-toxin producing *E. coli* (VTEC) as it was discovered that certain diarrheagenic *E. coli* strains produced a cytotoxin that was able to kill Vero cells (Konowalchuk, Speirs, and Stavric 1977). STEC infections are characterised for causing abdominal cramps, bloody diarrhoea followed by the life-threatening haemolytic uremic syndrome (HUS). Over 380

different STEC serotypes have been identified, but only few cause severe disease in humans. *E. coli* O157:H7 has been found to be the most common serotype associated with HUS, but other serotypes have also been linked with severe disease, including O26, O111, O103, O121, O45 and O145, also known as the 'big six'.

1.1.1 Virulence factors in *E. coli* O157:H7

Virulence factors are bacterial components that promote disease by either causing damage to the host or evading the immune system (Casadevall and Pirofski 1999).

The main virulence factor responsible for STEC pathogenesis is Shiga toxin (Stx), a phage-encoded toxin that blocks protein synthesis in the host cells, leading to cell death. A detailed description about Stx and its mechanism of action is provided in Section 1.2. Additional genetic elements contribute to STEC virulence, include the locus of enterocyte effacement (LEE), a pathogenicity island responsible for attaching and effacing activity. The LEE encodes the type three secretion system (T3SS) and effector proteins that make host cells more susceptible to infection. Two key proteins produced from this T3SS are intimin and its receptor Tir (transmembrane intimin receptor). Intimin is the critical adhesin that plays a key role in the adherence to the host cells and formation of attaching and effacing lesions (A/E).

E. coli O157:H7 also contains an F-like plasmid of approximately 92-104 kb known as pO157. The plasmid encodes several virulence factors, including an haemolysin, a catalase-peroxidase, a type II secretion system, a serine protease, a metalloprotease, amongst others (Youn, Yoon, and Hovde 2010). Nevertheless, the importance of the plasmid for the overall virulence has not been fully proved.

STEC strains also carry systems that confer resistance to extreme acidic conditions, a feature that enhances its virulence. Four acid-resistance (AR) mechanisms have been identified in *E. coli*: the oxidative system (AR-1), the glutamate decarboxylase system (AR-2), the arginine decarboxylase system (AR-3) and the lysine decarboxylase system (AR-4) (J. W. Foster 2004). In STEC, the AR-2 system provides better protection to low pH environments than the AR-3

system, but both systems seem to be equally effective in protecting STEC strains against weak acids found in the intestine (Lin et al. 1996).

1.1.2 Transmission sources

Infection occurs when people consume food or water contaminated with STEC (Kintz et al. 2017). Person-to-person transmission is a rare but is a possible route of transmission and normally occurs in nurseries and geriatric care facilities.

Ruminants are the main reservoir for STEC, cattle being the most important source of infection. Consequently, any products that come in contact with cattle or faecal material pose a major risk factor for STEC infection (Persad and Lejeune 2014). Interestingly, STEC does not cause disease in infected cattle, probably as a result of differences in the Stx receptor availability, the influence of the microbiota and the site of colonisation, the terminal rectum. This leads to term ‘super-shedders’, a subset of animals that are colonised at the terminal rectum and release a high number of infectious units. An *E. coli* O157 super-shedder is defined as an animal that excretes $>10^4$ CFU per gram of faeces (Chase-Topping et al. 2008). Super shedders pose an important risk factor for the spreading of STEC in the environment.

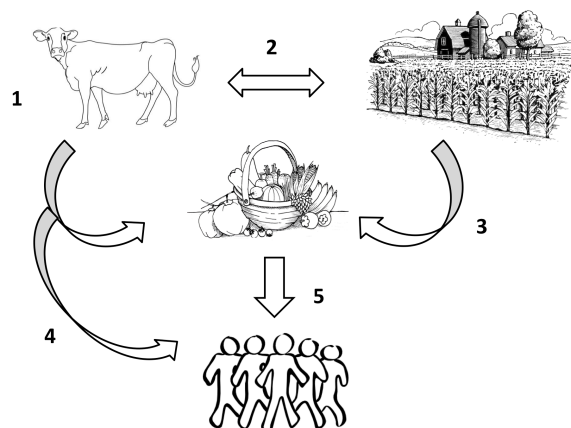


Figure 1 STEC transmission cycle.

1) Ingestion of STEC by cattle, 2) Faecal excretion of STEC leads to contamination of environment, including farms and water reservoirs, 3) Contamination of environment and water leads to contaminated food, including fruits and vegetables, meat, dairy products and water, 4) Transmission animal to person can occur in cases where people are exposed to farms or slaughter houses, 5) People get infected by STEC by consuming contaminated food or by person to person transmission

1.1.3 Pathogenesis of STEC

As previously mentioned, infection occurs when people consume food or water contaminated with STEC. The incubation period varies from 3-10 days. The infectious dose is multifactorial as it depends on the STEC strain, the host susceptibility, age group, etc. However, the acid-resistance of STEC decreases the infectious dose which is thought to be as low as 50 colony forming units (Tilden et al. 1996).

Once STEC has passed through the stomach and reached the intestine, colonisation starts, initiated by binding of intimin to the cell-surface protein nucleolin on the epithelium cells, bringing bacterial cells closer to the intestinal epithelium (Sinclair and O'Brien 2002). Once this first contact has occurred, Tir is secreted into the host cells via the T3SS, also encoded by the LEE. The T3SS forms a needle-like complex that injects Tir and other bacterial effector proteins into the host cells. Tir mediates attachment of intimin to the host cell membrane, hijacking the host cell cytoskeleton and causing the characteristic attaching and effacing lesions (A/E). The additional effector proteins secreted into the host cell contribute to make the cell more susceptible to infection. These include EspA, B and D, which are involved in the delivery of other effectors into the cell; EspG, F, H and Map (mitochondrial associated protein) which are thought to interfere with essential signalling pathways within the cell. Other non-LEE effectors also contribute to STEC pathogenesis, although their function is still unclear.

Shiga toxin (Stx) production also starts when bacteria reach the intestine, normally a few hours after infection. Stxs are responsible for causing the severe complications associated to STEC infections and the mechanisms behind this will be reviewed with detail in the following sections.

1.2 Shiga toxins

Shiga toxins (Stxs) belong to the family of AB toxins. This group of toxins are formed by two components or subunits, the active subunit A and the binding subunit B. Members of this family include ricin toxin found in the castor oil plant *Ricinus communis*, cholera toxin produced by *V. cholerae*, the heat labile enterotoxin from ETEC, pertussis toxin from *Bordetella pertussis* and anthrax toxin from *Bacillus anthracis* (Odumosu et al. 2010). The potent and sometimes mortal bioactivities of these toxins make them a subject of intense research.

Stxs were originally discovered in *Shigella dysenteriae* type 1 by the renowned bacteriologist Kiyoshi Shiga during a dysentery outbreak in 1897 (Trofa et al. 1999). They were later referred to as Verocytotoxins given their toxic effects on Vero cells. For this reason STEC can also be referred to as Verotoxin producing *E. coli* (VTEC). Further studies showed that the toxins were structurally and functionally related.

1.2.1 Structure of Shiga toxins and cellular receptors

Shiga toxins are formed by two non-covalently associated units, the enzymatically active subunit A (StxA) and the homopentameric subunit B (StxB). StxA exhibits a specific RNA *N*-glycosidase activity that cleaves an adenine base on the 28S ribosomal RNA of eukaryotic ribosomes, inhibiting protein synthesis (Johannes and Römer 2010). Two peptide fragments form StxA: A1 (28 kDa) responsible for the toxic effect and A2 (4 kDa) responsible for the association between StxA and StxB.

StxB is responsible for binding the holotoxin to the neutral glycosphingolipid globotriaosylceramide (Gb3) receptor on the cell surface (Figure 2). The B subunits are highly specific to the trisaccharide moiety (Gal α 1-4GalB1-4Glc ceramide) of the Gb3 receptor (Ling et al. 1998). Structural studies on the B subunit of Stx1 revealed that there are three trisaccharide-binding sites per B monomer, giving a total of 15 Gb3-binding sites per StxB unit. This explains the

high affinity of Stx for the host cells (binding constant of 10^9 M^{-1}) (G. Fuchs et al. 1986). Although the same number of binding sites have been found in Stx2, there is an important difference in the binding affinities between Stx1 and Stx2. Stx1 has a 10-fold higher affinity for the Gb3 receptor than Stx2 (Head, Karmali, and Lingwood 1991), even though Stx2 is more potent than Stx1 with an LD₅₀ 400-fold lower than Stx1 (V L Tesh et al. 1993).

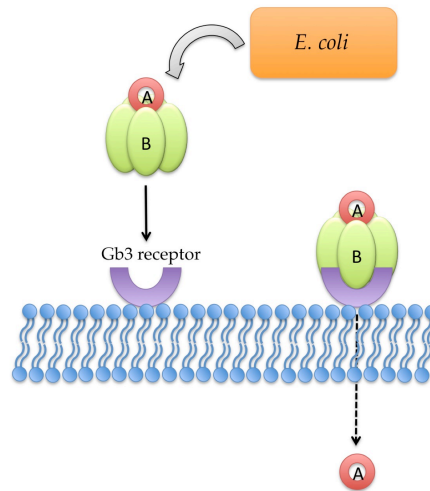


Figure 2. Structure of Shiga toxins.

Shiga toxins are formed by two non-covalently associated units, the enzymatically active subunit A (StxA) and the homopentameric subunit B (StxB).

The Gb3 receptor is mainly expressed in endothelial, epithelial, mesangial and glomerular cells of the kidney, microvascular endothelial cells in brain and intestine, and in some subsets of B lymphocytes (Lingwood 1999; Chan and Ng 2016). This explains the localised damage in both urinary and nervous systems in infected humans.

1.2.2 Shiga toxin types and subtypes

As previously mentioned, there are two types of Shiga toxins: type 1 (Stx1) and type 2 (Stx2). They are structurally similar but differ in their amino acid sequences. The A subunits of Stx1 and Stx2 share 55% similarity, while the B subunits are 62% similar. Additionally, both Stx1 and Stx2 are divided in subtypes: Stx1, Stx1c and Stx1d, Stx2c, Stx2d, Stx2e, Stx2f and Stx2g (Scheutz et al. 2012)

There is a clear relationship between toxin subtype and toxicity. Strains that produce Stx2a, Stx2c or Stx2d usually lead to development of haemorrhagic colitis (HC) and HUS (Melton-Celsa 2014). On the other hand, Stx2b and Stx2e do not seem to cause severe symptoms in affected patients (Fuller et al. 2011). Several factors cause this difference in toxicities amongst Stx subtypes. In general, Stx2 subtypes have been shown to bind tighter to the ribosome than Stx1, explaining the higher toxicity seen in this group. Stx2d is 10-fold more potent than Stx2c, even though they differ by only two amino acids in the A subunit (Bunger et al. 2015). In the case of Stx2e, structural differences in the B subunit makes it more prone to bind to the globotetraosylceramide receptor (Gb4) instead of Gb3 (Tyrrell et al. 1992).

1.2.3 Intracellular trafficking of Shiga toxin

Once Stx has bound to the Gb3 receptor, the complex toxin/receptor is internalised to the host cell by endocytosis (Figure 3). Stx utilises both clathrin-dependent and clathrin-independent endocytosis to enter the cell (Sandvig et al. 1989; Lauvrak, Torgersen, and Sandvig 2004; Römer et al. 2007). After entry, the Stx/Gb3 complex localises to early and recycling endosomes, to be later transferred to the *trans*-Golgi network (TGN) (Johannes et al. 2008; Bonifacino and Rojas 2006).

Stx undergoes retrograde sorting in the early/recycling endosomes in order to bypass recycling and degradation pathways and reach the Golgi apparatus. This process is mediated by clathrin (a nanodomain organising protein essential for the generation of membrane curvatures) and retromer (a heteropentameric complex that mediates retrograde transport of cargo molecules from endosomes to the TGN) (Saint-Pol et al. 2004; Bujny et al. 2007; Johannes and Römer 2010). The mechanism by which clathrin and retromer sort the Stx-containing endosomes remains unclear. However, studies suggest that clathrin mediates the formation of retrograde tubules on the endosome, followed by retromer-dependent scission (Popoff et al. 2007; Johannes et al. 2008). This endosome-sorting process is essential for Stx pathogenesis as it has been proved that cell

lines with defective endosome-sorting pathways are immune to Stx intoxication (Falguières et al. 2001).

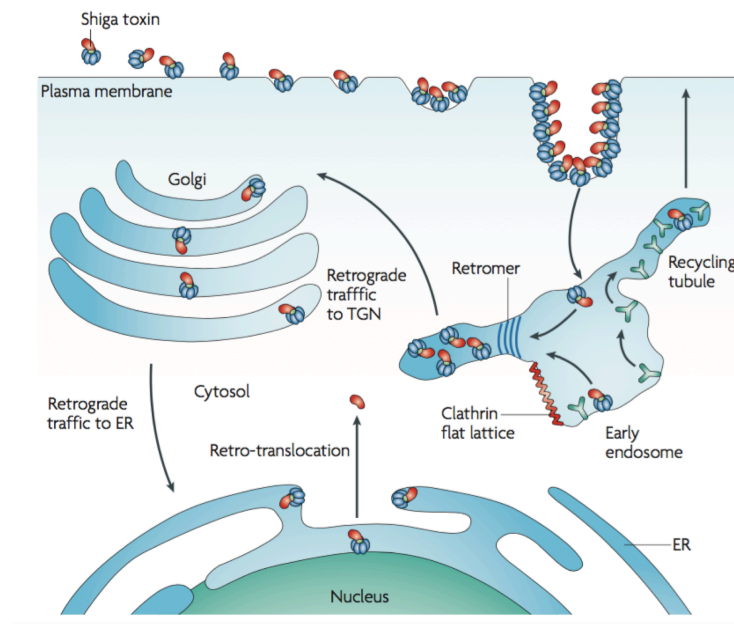


Figure 3 Trafficking of Shiga toxin.

Stxs are internalised by clathrin-dependent and independent pathways. The toxin then undergoes retrograde sorting in early endosomes to bypass recycling and degradation pathways. Stx are then transferred to the trans-Golgi network (TGN) and endoplasmic reticulum. Finally, the cytotoxic subunit A is translocated to the cytosol. (Taken from Johannes and Römer, 2010)

During the retrograde transport, the endoprotease furin divides the StxA fragments A1 and A2 by cleaving a bond between the residues Arg251-Met252 (Garred, van Deurs, and Sandvig 1995). At this point, the A1 fragment remains linked to the A2-StxB complex by a disulfide bond between Cys242 (A1) and Cys261 (A2). Reduction of this disulfide bond in the endoplasmic reticulum (ER) lumen releases the enzymatic A1 fragment (Johannes and Römer 2010).

In order to exert its bioactivity, the A1 fragment has to be translocated to the cytosol via the endoplasmic reticulum associated degradation pathway (ERAD), a pathway in the ER responsible for targeting misfolded proteins for ubiquitylation and degradation by the proteasome (Mukhopadhyay and Linstedt 2013; M. Yu and Haslam 2005; Johannes and Römer 2010). Interestingly, the A1 fragment is able to escape ubiquitin-mediated degradation given its lack of lysine residues and its ability to refold rapidly (Hazes and Read 1997).

Once in the cytosol, the A1 fragment exerts its *N*-glycosidase activity by depurinating a conserved adenine residue in the α -sarcin/ricin loop (SRL) of the

28S ribosomal RNA, blocking the binding of the elongation factor EF-2, which in turn leads to inhibition of translation (Chan and Ng 2016). Although a very small percentage of the A1 fragment reaches the cytosol (approximately 4%), severe cell damage is caused (Tam and Lingwood 2007).

1.2.4 Shiga toxin mode of action

Stx-mediated intoxication is the result of different effects at the cellular level. As previously mentioned, Stxs act on the 28S rRNA of the ribosome, triggering the ribotoxic stress response (W. E. Smith et al. 2003). This regulatory network leads to the activation of mitogen-activated protein kinase (MAPK) signalling pathways that are responsible for controlling cell proliferation and apoptosis. More specifically, it has been shown that Stx activates the p38 MAPK pathway, the c-Jun N-terminal (JNK) pathway and the extracellular signal-regulated kinase (ERK) pathway (Ikeda et al. 2000; Chan and Ng 2016). For a more detailed review on the topic see Vernon L. Tesh 2012.

The ribotoxic stress response has also been associated with cytokine production, promoting local inflammatory responses. The type of cytokines and their levels of expression depend on the type of cell that is being affected. For instance, in proximal tubular cells and glomerular epithelial cells, Stx induce production of IL-1 β , IL-6 and IL-8, whereas an elevation of IL-8 occurs in the intestinal epithelial cells (Cherla et al. 2006; G. H. Foster and Tesh 2002). In addition to this, it has been shown that the tumour necrosis factor alpha (TNF- α) upregulates expression of the Gb3 receptor in endothelial cells, exacerbating the vascular damage in the affected tissues (Eisenhauer et al. 2001).

Stxs have also been associated with the activation of the ER stress response and the unfolded protein response (UPR), a mechanism that ensures proteins are properly folded before leaving the ER (for a detailed description see Schröder 2008). When unfolded proteins are detected, an attenuation of protein translation occurs, together with the activation of genes encoding chaperones and proteins of the ERAD pathway. Stxs activate the UPR by three possible routes. Firstly, the fragment A1 itself contributes to the activation of the UPR

since it has to be misfolded before its translocation to the cytosol. Secondly, the actual host protein synthesis inhibition caused by Stx might lead to accumulation of unfolded host proteins and finally, alteration of intracellular Ca^{2+} . The mechanisms by which the ER stress response induces apoptosis are beyond the scope of this work. For a more detailed description please see Lee et al. 2008.

In addition to the cytotoxicity produced in eukaryotic cells, it has also been shown that Stx promotes intestinal colonisation of STEC. Robinson and co-workers demonstrated that epithelial cells exposed to Stx2 had increased surface expression of nucleolin, the protein to which intimin binds to promote attachment of bacteria to the cell surface (Robinson et al. 2006). Their findings also showed that EHEC O157:H7 strain 86-24 adhere better to epithelial cells *in vitro* compared to its *stx2* isogenic mutant, and that WT EHEC 86-24 colonised mice at a higher rate compared to the *stx2* isogenic mutant.

1.2.5 Shiga toxin encoding bacteriophages

Shiga toxins are encoded by lambdoid bacteriophages that are integrated into the bacterial chromosome. Bacteriophages are viruses that infect bacteria and are the most abundant life form in the planet with an estimated population of approximately 10^{31} (Hendrix, Hatfull, and Smith 2003). Bacteriophages can be classified as lytic or temperate, depending on the life cycle they undergo (Figure 4). Lytic phages are strict bacterial parasites that hijack the cell machineries to produce new phage particles that are released through bacterial lysis. These type of phages follow what is known as the *lytic cycle*. On the other hand, temperate phages integrate their genome into the bacterial chromosome, becoming prophages. Prophages remain in a dormant state, also referred to as the *lysogenic cycle*, in which they are replicated together with the bacterial chromosome and passed along to daughter cells. Under certain conditions, temperate phages shift to the lytic cycle, the Stx-phages being a clear example of this.

Bacteriophages play a key role in the transfer of virulence genes amongst bacteria, making an important contribution to bacterial pathogenesis. Several

toxins are encoded by phages including diphtheria toxin, cholera toxin, botulinum toxin and shiga toxin. Phages also disseminate other virulence traits involved in invasion, immune evasion, superantigens, and adhesion factors, amongst others (Penadés et al. 2015).

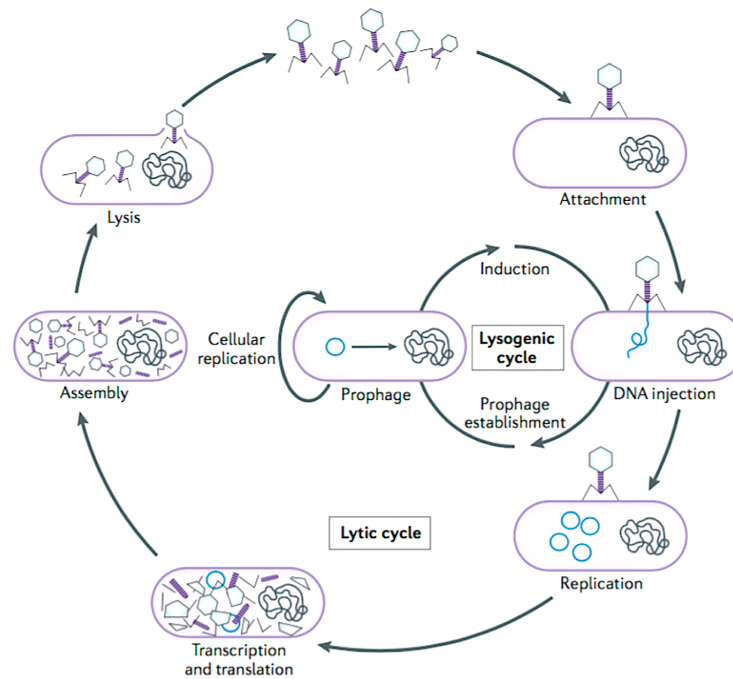


Figure 4 Bacteriophages can have lysogenic or lytic cycles.

Phages infect a host bacterium when they interact with receptors on the cell membrane and inject their genome. The replication strategy will depend on the type of phage, if it is virulent or temperate. Virulent phages, like the phage T4, can only replicate through the lytic cycle. Temperate phages like the phage λ , can enter either the lytic or lysogenic cycle. During lysogeny, the phage genome is termed 'prophage' and it replicates together with the host DNA. Under certain stress conditions, prophages can enter into the lytic cycle and produce new virions that are released via cell lysis. (Adapted from Salmond and Fineran 2015)

1.2.6 Diversity of Shiga toxin phages

Stx-phages show a high degree of heterogeneity in genome composition and morphology. They belong to the family of lambdoid bacteriophages, having all a double stranded DNA genome and roughly similar morphology (icosahedral head and tail). The genetic organisation of Stx-phages is very similar to the archetype phage lambda (λ) but with a genome approximately 50% larger than phage λ .

Some studies suggest that the extra DNA may assist the survival of the bacterial lysogen in the animal host or help promote colonisation (Barondess and Beckwftth 1990; Dziva et al. 2004; van Diemen et al. 2005).

Lambdoid bacteriophages have their genome organised in interchangeable genetic clusters that facilitates recombination and exchange of genes between phages. This results in a high degree of mosaicism amongst Stx-phages. The Stx genes in STEC can be either found in cryptic prophages (phage-like sequences that cannot produce infective phage particles) or inducible prophages (Herold, Karch, and Schmidt 2004). Since multiple cryptic or inducible prophages can reside within the genome of a single host cell (Allison et al. 2003; Perna et al. 2001), recombination events between phage sequences in a single cell can result in the generation of new prophages *in situ*. This phenomenon is enhanced if a recombination system like the λ -Red recombinase is being carried by the phage.

The integration site of the Stx-phages in the bacterial chromosome shows also a high degree of heterogeneity. In *E. coli* O157:H7 the most two common sites are *wrbA* and *yehV*, though the sites *sbcB*, *argW* and *yecE* have also been reported (Krüger and Lucchesi 2015; Shaikh and Tarr 2003; Besser et al. 2007). On the other hand, the prevailing sites in non-O157 strains are *argW*, *potC*, *prfC*, *serU*, *ssrA*, *wrbA*, *yciD*, *yecD*, *yecE*, *yjbM*, *ynfH* and Z2577 (Krüger and Lucchesi 2015; Shringi et al. 2012; Mellor et al. 2012; De Greve et al. 2002).

Stx-phages are able to infect other *E. coli* strains, both pathogenic and non-pathogenic, including strains that are already lysogenized with other Stx-phages. This promotes the spread of Stx genes between *E. coli* and other Enterobacteriaceae. The outbreak that took place in Germany in 2011 is a clear example of this. The enteroaggregative *E. coli* (EAEC) strain O104:H4 acquired a Stx-phage by horizontal transfer, resulting in a hypervirulent strain that caused 2987 cases of acute gastroenteritis, 855 cases of HUS and 53 deaths (Hauswaldt et al. 2013). This outbreak represented a challenge to the German health system and highlighted the serious need for therapeutic strategies to manage STEC infections.

1.3 Regulation of Shiga toxin expression

In spite of the mosaicism in Stx-phages, Stx genes are always located at the late region of the phage genome, downstream of the anti-terminator Q and upstream of the lysis cassette (Pacheco and Sperandio 2012). In lambdoid bacteriophages, the *ci* repressor acts as a genetic switch from the lysogenic state to lytic development. The *ci* protein has a dual functionality by promoting and repressing transcription of the phage genes in the lysogenic cycle. Two *ci* units dimerise and cooperatively bind to the operator regions O_R and O_L to repress transcription of the lytic promoters P_L and P_R , and to stimulate transcription of the P_{RM} promoter to express the *ci* gene in order to maintain the lysogenic replication (Stayrook et al. 2008). Stx expression is initiated upon cleavage of the *ci* repressor, process known as prophage induction. This induction happens under specific environmental conditions, possibly as a survival mechanism so that the phage can move on to better hosts. The bacterial SOS response is the most well known mechanism of prophage induction and will be discussed in the following section (Little and Mount 1982).

1.3.1 The SOS response

The SOS response is a DNA repair system found in most bacterial species (Baharoglu and Mazel 2014). This regulatory network induces the expression of a set of genes that leads to the arrest of cell division, induction of DNA repair, prophages and mutagenesis. There are three DNA repair pathways induced by the SOS response: homologous recombination (HR), nucleotide excision repair (NER) and translesion synthesis (TLS) (Baharoglu and Mazel 2014). The ultimate trigger of all three pathways is the formation of single stranded DNA (ssDNA), either by replication errors or external factors.

1.3.2 LexA and RecA, the master regulators of the SOS response

The protein LexA acts as a repressor of the SOS response by downregulating its own expression and the genes that form the SOS regulon during normal bacterial growth. LexA is a 22 kDa protein formed by two domains that are linked by a flexible hinge region. LexA dimerises by the carboxy-terminal domain (CTD) and interacts with DNA through a helix-turn-helix motif in its amino-terminal domain (NTD) (Schnarr et al. 1988; Knegtel et al. 1995). The consensus DNA sequence for LexA is the 16-bp-long palindromic motif CTGT-N₈-ACAG, also known as the LexA box or SOS box (Butala, Žgur-Bertok, and Busby 2009). The self-cleavage activity of LexA resides within the CTD, where the residues Ser119 and Lys156 mediate the cleavage of the bond between Ala84 and Gly85 (Slilaty and Little 1987; Y. Luo et al. 2001). The CTD in LexA shares a substantial homology with the *cl* repressors found in temperate bacteriophages and this homology is related to the ability to interact with RecA-ssDNA-ATP filaments (Stayrook et al. 2008).

On the other hand, RecA acts as an inducer of the SOS response by promoting the autocleavage of LexA, which results into its dissociation from the SOS promoters. RecA is a 37 kDa multifunctional protein highly conserved in virtually all bacteria. Structural and functional homologues of RecA have been found in archae and eukaryotic cells (Cox 2007). RecA is involved in several cellular processes, including homologous recombination, coprotease activity on LexA, the λ repressor and UmuD, and activation of DNA polymerase V during SOS mutagenesis (Meghna Patel et al. 2010). Structurally, RecA is formed by a 30-residue N-terminal domain involved in monomer-monomer interactions, a 240-residue ATPase core, an 82-residue C-terminal domain and a central domain that shares homology with helicases and DNA transport proteins (Prentiss, Prévost, and Danilowicz 2015). In normal conditions, there are around 9,000 RecA monomers per cell; upon induction of the SOS response, this number rises to over 70,000 (Sommer et al. 1998). In order to cleave LexA, RecA forms a nucleofilament on the damaged DNA region and the resulting ssDNA-RecA filament catalyses the autocleavage of LexA, triggering the SOS response (Figure 5).

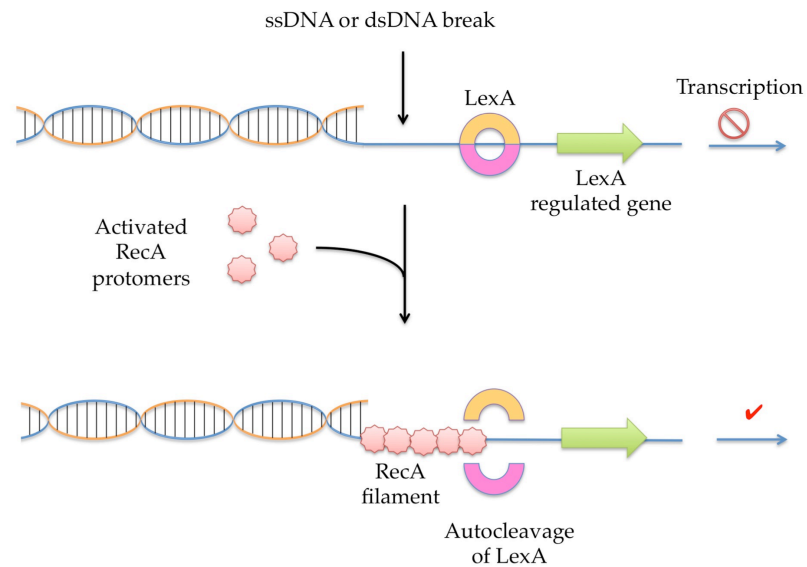


Figure 5 RecA mediates the autocleavage of LexA.

When DNA damage occurs, RecA is activated, forming filaments that mediate autocleavage of LexA (the key SOS response repressor), resulting in expression of the SOS regulon. RecA filaments also mediate autocleavage of prophage repressors, allowing production of phage particles and toxins

1.3.3 Filament formation

The mechanism by which ssDNA induces the SOS response has been well characterised. Briefly, the recombination proteins RecCBD and RecFOR promote the formation of RecA-ssDNA filaments. RecBCD recognises double strand DNA breaks (DSB) or double-strand ends (DSE), whereas RecFOR recognises gaps and nicks in DNA. Filament formation occurs in two steps: *nucleation* and *extension* (Figure 6). Nucleation happens more rapidly on ssDNA than on dsDNA. Only five RecA monomers are sufficient for nucleation but the presence of single-strand DNA binding protein (SSB) significantly slows down this process (Joo et al. 2006). The proteins RecO and RecR help to overcome this inhibitory effect by SSB. Once nucleation has started, the filament extension proceeds from the 5'-to-3' direction where each RecA monomer covers three nucleotides. ATP binding to RecA is essential for filament extension but no ATP hydrolysis. In fact, ATP hydrolysis has the opposite effect, it promotes disassembly of the filament (Arenson, Tsodikov, and Cox 1999; Bork, Cox, and Inman 2001). It has been

reported that the RecA-DNA filament grows at 120-1200 subunits/min whereas dissociation occurs at 70 monomers/min in ssDNA or 120 monomers/min in dsDNA.

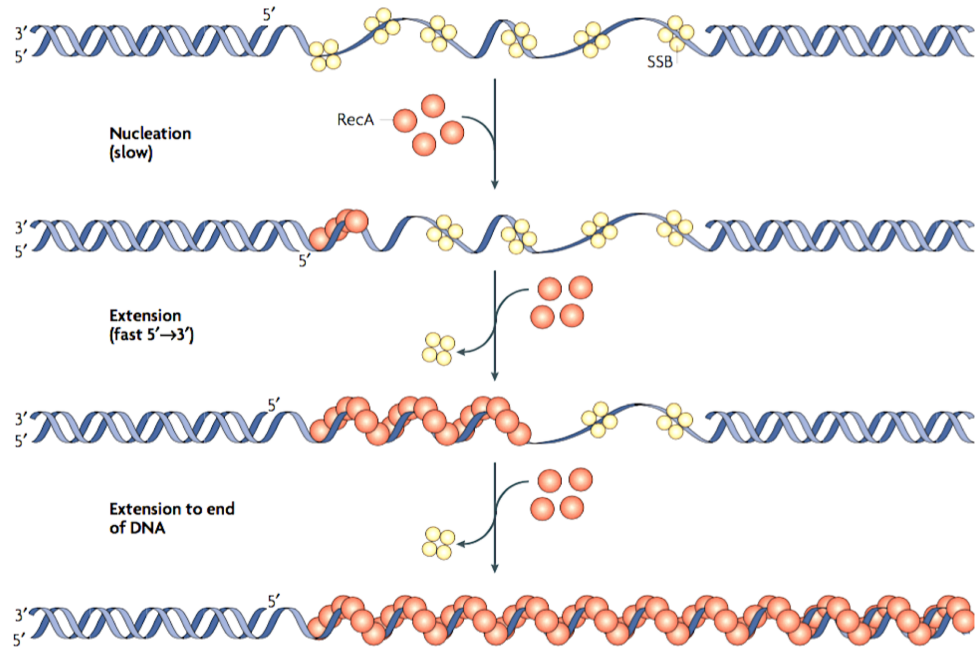


Figure 6 RecA filament formation.

Nucleation occurs slowly due to the single-stranded DNA binding protein (SSB). Then, the filament extends rapidly in the 5' to 3' direction and extends to the end to the DNA. ATP binding to RecA is essential for filament extension. Modified from Cox 2007.

1.3.4 Regulation of RecA and filament formation

Given the complex nature of RecA, the existence of regulatory mechanisms is not surprising. Firstly, there is evidence showing that RecA regulates itself through its C-terminal domain. Different studies on this domain show that the activity of RecA is enhanced when the domain is absent (Benedict and Kowalczykowski 1988; Tateishi et al. 1992). Secondly, a number of accessory proteins intervene in the regulation of RecA, including the RecBCD and RecFOR systems, RecX, DinI, PsiB and RdgC.

As previously mentioned, the RecBCD and RecFOR proteins are required to start and mediate filament formation. The RecBCD proteins create a single-strand

extension on the 3'-ending, allowing the binding of RecA to DNA. On the other hand, the RecFOR proteins mediate the binding of RecA to SSB-coated DNA.

The RecX protein is another important regulator. It acts as an inhibitor of both RecA recombinase and coprotease activities (Stohl et al. 2003). When a RecA monomer dissociates during filament extension, the gap is rapidly filled by another RecA monomer to continue the extension process. RecX exerts its inhibitory activity at this point by capping the assembly ends of the filaments, blocking filament formation (Drees et al. 2004).

The DinI protein is expressed early in the SOS response and has been shown to play a key role in the stabilisation of nucleofilaments after they are formed (Lusetti et al. 2004). The PsiB protein is encoded by conjugative plasmids and is believed to inhibit the SOS response during conjugation. The RdgC protein or recombination-dependent growth protein is a DNA binding protein that competes with RecA for binding sites on the DNA, preventing the cleavage of LexA.

After de-repression of the SOS box, the genes *recA* and *ssb* are induced to protect and stabilize the fork. The genes *uvrA*, *uvrB*, *ydjQ*, *uvrD*, *recN* and *ruvAB* are induced to repair the lesions caused through NER and HR, and the DNA polymerases *polB*, *dinB* and *umuDC* assist in translesion DNA synthesis (TLS). Cell division is also inhibited during the SOS response by induction of the *sulA* gene, which prevents septation by interacting with the *ftsZ* gene product. After the damage has been resolved, the levels of non-activated RecA and uncleaved LexA start rising again.

1.3.5 Induction of the SOS response

As previously mentioned, ssDNA is the main inducer of the SOS response. It can be originated as a result of spontaneous DNA breakage during replication, commonly after fork stalling, or by external factors. Thus, any DNA damaging agent or condition will initiate the SOS response (Baharoglu and Mazel 2014). For instance, UV and gamma radiation activate DNA repair by HR and TLS (Bolsunovsky et al. 2016; Krishna et al. 2007). Reactive oxygen species (ROS) are

also important inducers. For instance, superoxide radicals can lead to the release of iron from iron-containing proteins. High concentration of free ferrous ions leads to the production of hydroxyl radicals through the Fenton reaction, which ultimately cause DNA damage (Henle and Linn 1997; Jena 2012) (Figure 7).

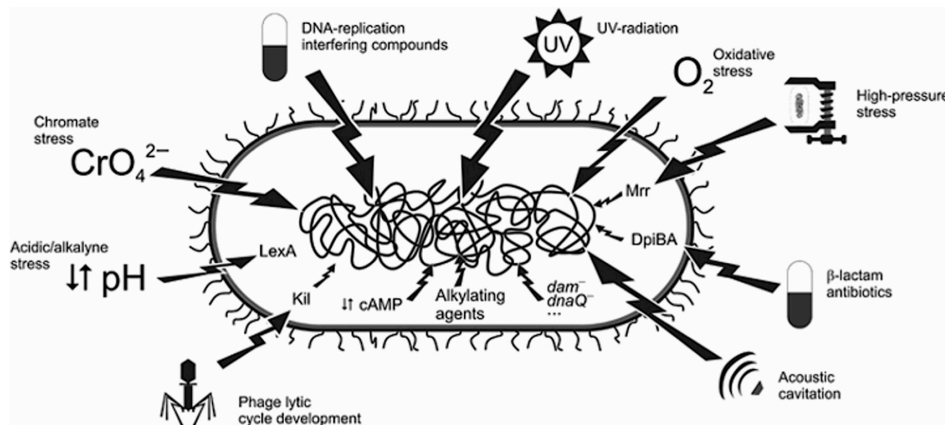


Figure 7 Triggers of the SOS response.

All the different mechanisms responsible for the activation of the SOS response involve DNA damage, either directly or indirectly. Taken from (Erill, Campoy, and Barbé 2007)

Certain antibiotics at both lethal and sublethal concentrations can also induce the SOS response by multiple mechanisms. For example, β -lactam antibiotics have been shown to induce the SOS response by triggering the DpiAB two-component signal transduction system (C. Miller et al. 2004). DNA-damaging agents like mitomycin C or quinolones are powerful SOS inducers (Kimmitt, Harwood, and Barer 2000; Costa de Oliveira, Laval, and Boiteux 1987).

High pressure has been shown to promote DSB formation and trigger the SOS response through the *Mrr* nuclease in *E. coli* (Aertsen and Michiels 2005). The interesting fact of this phenomenon is that, thanks to the SOS induced mutagenesis; the *mrr* gene is inactivated to give origin to bacterial cells resistant to high-pressure conditions. Changes in the intracellular pH have also been associated with the initiation of the SOS response. It has been shown that in acidic media, LexA undergoes a series of conformational changes that lead to a gradual de-repression of the SOS response (Sousa et al. 2006).

1.3.6 Expression of Shiga toxin

The Stx-phages remain dormant when the repressor cl is bound to the right and left operator sites, O_R and O_L respectively, inhibiting the activity of the phage promoters P_R and P_L (Serra-Moreno, Jofre, and Muniesa 2008; Tyler, Mills, and Friedman 2004). When the SOS response is triggered, the protein RecA is activated. This protein cleaves the cl repressor, leading to expression of the anti-terminator Q . Subsequently, the protein Q binds to the promoter $P_{R'}$ and activates transcription of the Stx genes. The fact that Stx is expressed during the lytic cycle eliminates the need for an Stx-secretion system, although an additional secretion mechanism for Stx2 has been reported (Shimizu, Ohta, and Noda 2009).

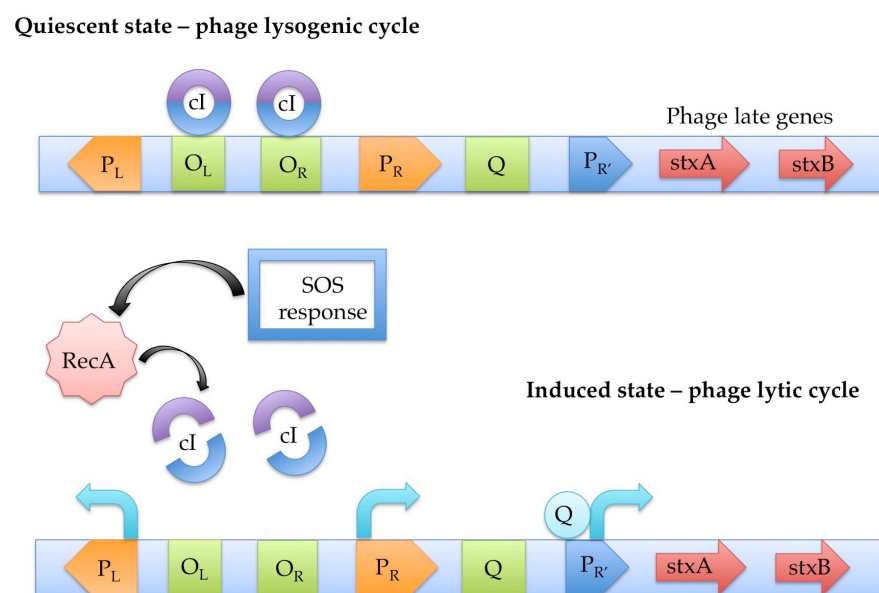


Figure 8 Shiga toxin expression.

Lambdoid phages remain inactive when the repressor cl is bound to the right and left operator sites, O_R and O_L respectively, inhibiting the activity of the phage promoters P_R and P_L . When the SOS response is triggered, the protein RecA cleaves the cl repressor, leading to expression of the anti-terminator Q . Subsequently, the protein Q binds to the promoter $P_{R'}$ leading to transcription of Stx and late phage genes. (Modified from Pacheco and Sperandio, 2012)

There are differences in the mechanisms of gene expression between *stx1* and *stx2*. While expression of *stx2* is promoted by DNA damaging agents (mitomycin C or ciprofloxacin), *stx1* expression is triggered under low-iron conditions. Studies have identified a functional promoter for the *stx1* gene that is regulated by the environmental iron concentration (Calderwood and Mekalanos 1987; Calderwood et al. 1987) .

1.4 Shiga toxins and human disease

1.4.1 Incidence of STEC infections

Given the differences in the surveillance systems in each country, it is difficult to have an accurate number of infections produced by STEC around the world each year. A recent systematic review made by Majowicz and collaborators estimates that STEC causes around 2,800,000 acute illnesses, 3890 cases of HUS, 270 cases of end-stage renal disease (ESRD) and 230 deaths annually, worldwide (Majowicz et al. 2014). Despite the reduced number of cases compared to other microorganisms like *Salmonella* or *Campylobacter*, STEC has a bigger economic impact given the large number of hospitalisations and the costly treatment.

Most outbreaks produced by STEC are caused by the serotype O157:H7. Only in the USA, 350 *E. coli* O157 outbreaks were reported from 1982 to 2002 causing 1493 hospitalisations, 354 cases of HUS and 40 deaths (Rangel et al. 2005). In a more global context, Canada, the United States, Japan and Scotland have reported the highest annual reported incidences of *E. coli* O157:H7 infections during the last 20 years, Scotland being the country with the highest per capita incidence (3-5.73 cases per 100,000 individuals) (Chase-Topping et al. 2008) (Figure 9).

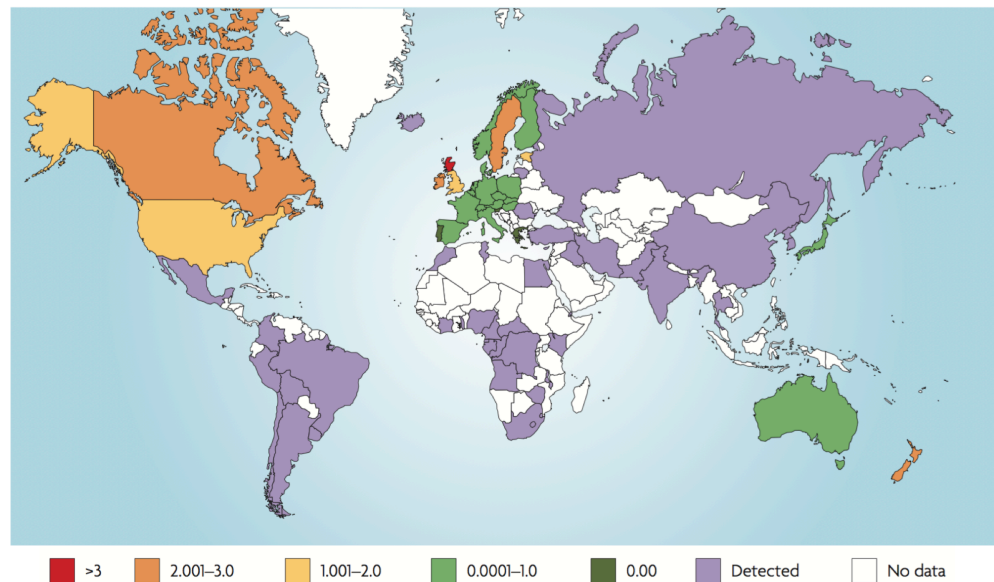


Figure 9 Incidence of *E. coli* O157:H7 around the globe.

Map of the worldwide relative rate of *E. coli* O157:H7 infections per 100,000 individuals in 2005. Purple shading represents detection of *E. coli* O157:H7 in a country where no incidence rate is available. White represents countries where no data are available, although infections may have occurred. Taken from Chase-Topping et al. 2008

In the particular case of Scotland, the high incidence rate has been attributed to the Stx phage type and super-shedding. The phage 21/28 accounted for 50% of the cattle isolates and 72% of isolates obtained from human infections (Chase-Topping et al. 2008). The association between this particular phage type and super-shedding is thought to be due an altered regulation of the type III secretion system that allows for a better colonisation.

1.4.2 Detection of STEC

Given the severity of STEC infections, it is of great importance to have effective detection methods for an appropriate and quick management of the patients. Currently, the methods available include chromogenic agars, enzyme immunoassays (EIA) and molecular techniques. Excellent reviews in the area can be found elsewhere (Parsons et al. 2016), but a brief description follows.

1.4.2.1 Culture methods

Isolation of STEC by culture methods is advisable to identify and characterise the strain. However, sometimes it is difficult to isolate STEC given the low number of bacterial cells present in the sample or interference with other bacteria species. Nevertheless, it is still a valuable method used for the diagnosis of STEC infections. One of the characteristics of *E. coli* O157:H7 is its inability to ferment sorbitol. This peculiarity allowed the use of sorbitol-MacConkey (SMAC) agar to identify the pathogen (Pai et al. 1984). SMAC plates were inoculated with the faecal specimen and examined after 18-24 h, looking for the presence of colourless colonies. However, it was later revealed that SMAC was not able to detect non-O157 STEC strains as well as sorbitol-fermenting O157 isolates lysogenized with Stx phages (Ammon, Petersen, and Karch 1999). More sensitive and specific alternatives to SMAC have been developed and their details are explained in Table 1 (Parsons et al. 2016).

Table 1 Culture methods for the detection of Stx

Name of media	Description	Sensitivity/Specificity	References
CHROMagar™ O157	Detects O157 STEC strains through chromogenic substrates	96.3%/100%	(Church et al. 2007)
CHROMagar™ STEC	Detects O157 STEC and non-O157 strains through chromogenic substrates	84.6-85.7%/87-95.8%	(Wylie et al. 2013)
CHROMagar™ O104 STEC	Detects O104:H4 STEC strains through chromogenic substrates	71.4%/99.1%	(Gouali et al. 2013)
Rainbow® Agar O157	Detects O157 and some non-O157 STEC strains through β-glucuronidase and β-galactosidase activities.	Not determined	(Zelyas et al. 2016)

1.4.2.2 Vero cell cytotoxicity assays

Vero cells - African green monkey kidney cells - have a high number of Gb3 and Gb4 receptors on their cell surface, making them extremely sensitive to the effects of Stx. Historically, this assay played an important role in the diagnosis of STEC infections but lacks of practicality nowadays. Basically, the cells are incubated with a filter-sterilised sample e.g. faecal culture or extract, and examined for cytophatic effects after 48-72 h. Although verocytotoxicity is still considered a gold standard to confirm Stx production, especially in cases where isolation of the organism is difficult, it requires access to tissue culture facilities, trained personnel and long waiting times to give a diagnosis.

1.4.2.3 Enzyme immunoassays

Probably one of the most widely used approaches for the diagnosis of STEC is the immunodetection of Stx. This is achieved through the use of antibody-based Stx detection assays. Since these assays are available as ready to use kits, they are commonly used in routine laboratories. The first ELISA developed for Stx detection was developed in 1987 by Kongmuang and collaborators (Kongmuang, Honda, and Miwatani 1987). The development of more specific and sensitive polyclonal and monoclonal antibodies has led to the commercialisation of ELISA-based assays for the detection of Stx, including the Premier EHEC, Ridascreen Verotoxin, ProSpecT STEC Microplate assay and VTEC Screen Seiken RPLA. These assays normally require enrichment of the sample to be able to detect the toxin but are distinguished for their sensitivity, specificity and robustness.

1.4.2.4 Molecular techniques for the detection of STEC

STEC-specific PCR is the most sensitive assay, for both O157 and non-O157 strains. DNA extracts from single colonies, faeces or food extracts can be used as templates for PCR. The complexity of the samples matrix may sometimes contain inhibitors of *Taq* polymerase and decrease the sensitivity. This problem can be avoided if template DNA is extracted from broth cultures.

Recently, Martinez-Castillo and Muniesa highlighted the importance of free Stx-converting bacteriophages in the environment and how they can influence the

detection of STEC in samples, especially with molecular techniques like PCR (Martínez-Castillo and Muniesa 2014).

1.4.2.5 Serological diagnosis of STEC

When patients in the late course of the disease seek medical attention, it becomes more difficult to detect STEC by both molecular and immunogenic methods because of the low numbers of STEC found in faeces. In these cases, the humoral immune response triggered by STEC can be exploited as a diagnostic tool. Bitzan and collaborators showed a high incidence of serum antibodies to *E. coli* O157 lipopolysaccharide (LPS) in patients with HUS and highlighted the potential of using serological methods for STEC diagnosis (Bitzan et al. 1991). Another study also reported the utility of using antibodies for the detection of LPS O157 when faecal bacteria or Stx cannot be detected (Chart et al. 1991). To date, there are not commercially available serological detection assays for STEC detection but is something that could be exploited in the future.

1.4.3 Haemolytic Uremic Syndrome

Haemolytic uremic syndrome (HUS) is a disease characterised by haemolytic anaemia, low platelet count and renal impairment (Noris and Remuzzi 2005). It is estimated that 15% of STEC infections progress to HUS, children and the elderly being the most susceptible population groups (Tarr, Gordon, and Chandler 2005). The majority of cases of HUS are consequences of STEC infections and around 5-10% of cases is classified as atypical HUS.

Symptoms of HUS develop around 7 days after the first symptoms, when the diarrhoea is improving. These include acute paleness accompanied by renal failure signs, including oedema, nausea, vomit, oliguria and high blood pressure. Neurological, cardiac and respiratory complications may also appear and are normally associated with a worse outcome (Karpman et al. 2017).

Since STEC does not cause bacteraemia, Stx has to gain access to the circulation to reach its target organs. There are different possible mechanisms responsible

for Stx translocation into the circulation. Malyukova and collaborators showed that Stx could be taken up by Gb3-free intestinal cells through macropynocytosis and transcytosis (Malyukova et al. 2008). Another study carried out by Hurley and co-workers suggests that the interaction between STEC and intestinal epithelia results in neutrophil recruitment to the intestinal lumen and this transmigration enhances Stx movement across intestinal epithelial cells (Hurley, Thorpe, and Acheson 2001). A more recent study in the highly virulent *E. coli* O104:H4 strain made by Kunsmann and colleagues shows that Stx could be delivered to the host cells via outer membrane vesicles (OMVs) (Kunsmann et al. 2015).

When Stx gains access to the circulation, it binds to different blood cells, including neutrophils, platelets, monocytes and erythrocytes (Karpman et al. 2017). Stxs are then released from the blood cells in the form of microvesicles in order evade the host immune system and successfully deliver the toxin to target tissues (Figure 10) (Ståhl et al. 2015).

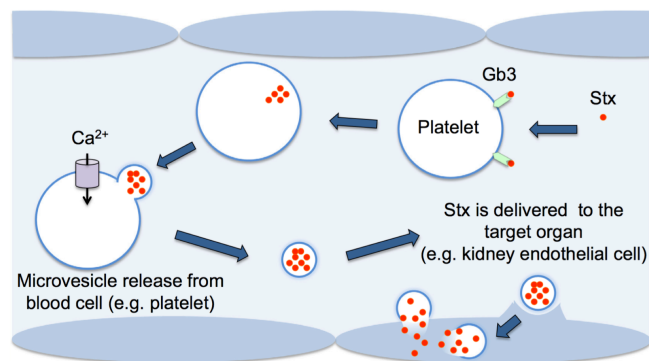


Figure 10 Transfer of Shiga toxin from the circulation to the kidney.

Once Stxs have reached the bloodstream, they bind to the Gb3 receptor on platelets. The toxin is internalised to be later released in microvesicles. These microvesicles circulate and reach the target organ where they are taken up by endothelial cells. Finally, Stx is released from the vesicles inside the cells. Taken from Karpman et al, 2017

Haemolysis and thrombocytopenia are classic indicators of HUS. Stx-induced haemolysis is caused by mechanical breakdown in microthrombi occluded capillaries, oxidative damage and complement activation (Ruggenti, Noris,

and Remuzzi 2001; Túri et al. 1994; Yazdanbakhsh 2005). Thrombocytopenia is the result of platelet activation by Stx, O157 LPS and cytokines.

Currently, treatment of STEC-induced HUS is merely supportive. Administration of isotonic fluids before the onset of HUS seems to have a nephroprotective effect, reducing the need for dialysis. Since STEC-induced HUS causes complement activation via the alternative pathway, inhibition of this pathway using antibodies has been attempted. Eculizumab, a monoclonal anti-C5 antibody has been used as part of the treatment. However, no clear beneficial effect was observed.

The use of antibiotics to treat STEC infections remains controversial and will be discussed with more details in the next section.

1.4.4 Antibiotics and STEC infections

The use of antibiotics to treat STEC infection remains a controversial topic as some studies show that administration of antibiotics enhances the risk of developing HUS whereas other studies claim that antibiotics are neither effective nor harmful. Panos and collaborators did a systematic review about the use of antibiotics for the treatment of STEC infections and its influence in the development of HUS (Panos, Betsi, and Falagas 2006). Their work identified a large amount of contradiction in the literature that makes it difficult to claim if the use of antibiotics is safe or beneficial. Nevertheless, the available data suggests that the class of antibiotic and stage at which they are administered have an impact on the outcome of the treatment. For example, it has been found that the use of doxycycline, phosphomycin, azithromycin and gentamycin decreases Stx production *in vitro* in *E. coli* O157:H7, whereas the use of trimethoprim-sulfamethoxazole, ciprofloxacin and ampicillin showed the opposite effect (McGannon, Fuller, and Weiss 2010). Bielaszewska and collaborators carried out a similar study looking at the effect of different antibiotics on Stx2 expression in *E. coli* O104:H4. Their results showed that ciprofloxacin significantly increases Stx2 expression *in vitro*, fosfomycin,

gentamicin and kanamycin have no significant effect, and chloramphenicol, meropenem, azithromycin, rifamixin and tigecycline decrease expression of the toxin (Bielaszewska et al. 2012). However, further *in vivo* studies are required to prove the potential usefulness of these antibiotics in the clinical setting.

Rifampicin is another antibiotic that has been shown to prevent induction of Stx prophages. Rahal and co-workers found that administration of a MIC of rifampicin prior to bacterial eradication with a minimum bactericidal concentration (MBC) of gentamicin reduces Stx production in *E. coli* O157:H7 by inhibiting transcription of the *stx* genes, both *in vitro* and *in vivo* (Matar and Rahal 2003; Rahal et al. 2011). A subsequent study revealed that the same combination of antibiotics did not activate the SOS response in the pathotype *E. coli* O104:H4, giving as a result a decreased production of Stx2 (Fadlallah et al. 2015). The main drawback of this combinatorial therapy is the rapid development of resistance to rifampicin by *E. coli*, limiting its usefulness.

1.5 Anti-virulence approach to treat bacterial infections

1.5.1 Concept, advantages and potential limitations

During the last few years there has been a growing interest in developing drugs that target bacterial virulence instead of bacterial growth or viability. The large number of putative virulent targets offers an extraordinary source of potential new therapies. This is reflected in the increasing number of publications in this area over the last decade (Figure 11).

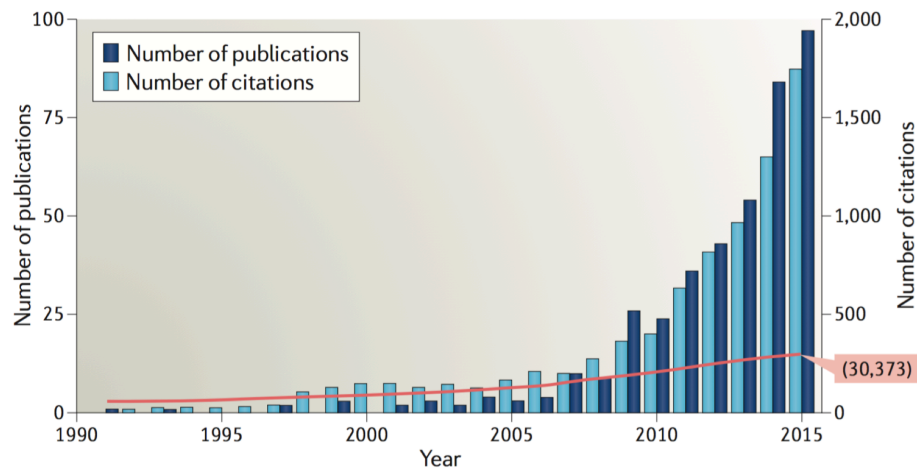


Figure 11 Emergence of anti-virulence research.

During the last decade there has been a steady progress in the anti-virulence field. Taken from Dickey, Cheung, and Otto 2017

Anti-virulence (AV) drugs offer new potential advantages in comparison to traditional antibiotics. For instance, blocking a particular virulence factor is expected to have little or no effect on the survival and propagation of the targeted bacteria, imposing less selective pressure for the development of resistance mechanisms like conventional antibiotics do. In addition, as most virulence factors are restricted to a single or closely related species, horizontal transfer of resistance traits is expected to be unlikely.

From a clinical perspective, AV drugs could be used synergistically with conventional antibiotics in circumstances where their use is contraindicated or when the pathogen is already resistant. Additionally, as antivirulence therapies tend to target processes that are species-specific, they are expected to have little or no effect on the host microbiome.

This approach has, however, some disadvantages or challenges that still need to be addressed. For instance, development of AV drugs is expected to be a more expensive and longer process as large clinical trials might be required to prove clinical efficacy compared to antibiotics alone, especially in cases where there is still an effective treatment. In addition, the narrow spectrum of AV drugs might lead to the use of combination therapies involving the use of different AV drugs or a combination of antibiotic and AV drugs to increase bacterial coverage.

Furthermore, since AV drugs rely on the host immune system to clear the disarmed bacteria from the host, immunocompromised patients might still require the use of traditional antimicrobial agents (Clatworthy, Pierson, and Hung 2007).

AV drugs are highly desirable for pathogens that are already resistant to the current antibiotic arsenal, like the ESKAPE pathogens (*Enterococcus faecium*, *Staphylococcus aureus*, *Klebsiella pneumoniae*, *Actinobacter*, *Pseudomonas aeruginosa* and *Enterobacter*) (Pendleton, Gorman, and Gilmore 2013; Boucher et al. 2009). Toxin-producing bacteria like *C. difficile*, *C. botulinum*, *B. anthracis*, *V. cholerae* and STEC could also be tackled with the AV approach given the current lack of effective treatment strategies.

1.5.2 Anti-virulence strategies against STEC

Efforts to find inhibitors that block the binding of Stx to Gb3 have been attempted, but no success has been achieved yet (Kitov et al. 2000; Trachtman et al. 2003; Watanabe et al. 2004). In the past few years, there has been a growing interest in trying to find strategies to block Shiga toxin activity and its production by STEC strains, with the aim of preventing the complications associated to it. A brief description of the different approaches made to date follows.

A recent study made by Li and collaborators describes the discovery of small peptides with Stx2 neutralising activity both *in vitro* and *in vivo* (T. Li et al. 2016). The peptides TF-1 and WA-8 were found to interact with the StxB subunit, interfering at the receptor-binding step. When administered to mice and rats, TF-1 was able to protect the animals from lethal doses of Stx2 administered intraperitoneally and intravenously respectively, making it a promising anti-Stx agent. Dong and collaborators explored the anti-Stx2 activity of baicalin, a natural occurring flavonoid isolated from *Scutellaria baicalensis* Georgi (J. Luo et al. 2016). Their studies show that baicalin binds to Stx2 and promotes formation of toxin oligomers that lack of cytotoxicity. When used in a HUS mouse model, baicalin provided ~70% protection against Stx2 relative to the non-

treated group; baicalin also ameliorated renal and hematologic damage. Although baicalin was not toxic in mice even when high doses were employed, safety in humans still needs to be evaluated.

As previously mentioned, Stx gets into the hosts cells using the retrograde trafficking pathway (Spooner et al. 2006). Stechmann and collaborators discovered two small molecules, Retro-1 and -2 that selectively block the transport of ricin and Stx (Stechmann et al. 2010). Further studies done by Secher and co-workers demonstrated the protective effects of Retro-2 against Stx (Secher et al. 2015). Administration of 100 mg/kg of Retro-2 to STEC infected mice significantly reduced clinical symptoms and increased survival rates, in comparison to the non-treated group. Another independent study made by Somshuvra and Linstedt showed that manganese (Mn^{2+}) blocks the endosome-to-Golgi transport of Stx, protecting eukaryotic cells from the Stx toxic effects (Mukhopadhyay and Linstedt 2012). *In vivo* evaluation of Mn^{2+} in mice exposed to Stx1 revealed that mice treated with Mn^{2+} did not show any clinical manifestations associated with Stx and survived the entire study, compared to the non-treated group. The low cost and lack of toxicity in humans makes Mn^{2+} a potential anti-virulence adjuvant for STEC infections.

Some other elements have shown to be active against Stx. A recent study made by Surendran-Nair and collaborators showed that selenium (Se) down-regulates the expression of *stx1* and *stx2* in STEC without affecting bacterial growth (Surendran-nair et al. 2016). In addition, Se was also able to reduce expression of the Gb3 receptor in human lymphoma cells, enhancing the anti-Stx activity. However, efficacy *in vivo* as well as the potential toxic effects associated with Se still need to be assessed. In the same area, Crane and collaborators discovered that zinc (Zn^{2+}) downregulates Stx production in STEC without affecting bacterial viability (Crane, Byrd, and Boedeker 2011). Further studies demonstrated that Zn^{2+} blocks the bacterial SOS response by suppressing RecA expression induced by DNA damaging agents such as ciprofloxacin, hydrogen peroxide or mitomycin C (Crane et al. 2014).

Using biochemical methods and NMR-based comparative metabolomics, Bommarius and co-workers discovered indole-based molecules produced by *E.*

coli that are able to regulate the physiology and virulence of other pathogenic *E. coli* strains (Bommarius et al. 2013). Amongst the indole derivatives identified, indole-3-carboxaldehyde (ICA) was able to reduce motility, biofilm formation and Stx production in EHEC. ICA was able to reduce by 10-fold the cytotoxic effects of Stx2 produced by EHEC on mammalian cells. Although indole has been widely studied as signalling molecule between bacteria and could be exploited for the development of antivirulence compounds, the mechanism of action still remains obscure (J. H. Lee, Wood, and Lee 2015; Melander, Minvielle, and Melander 2014; J. Kim and Park 2015).

Lee and collaborators studied the effect of coumarin and several derivatives on the regulation of bacterial virulence in EHEC (J. H. Lee et al. 2014). One compound, esculetin, repressed the expression of the *stx2* gene without affecting bacterial growth and attenuated the virulence *in vivo* when tested in *Caenorhabditis elegans*. More studies are required to elucidate the mechanism of action.

Nowicki and co-workers discovered that certain naturally occurring isothiocyanates (ITCs) block Stx expression in EHEC due to the induction of the bacterial stringent response, a regulatory pathway triggered under nutrient deprivation conditions (Nowicki et al. 2014; Boutte and Crosson 2013; Nowicki et al. 2016). Their findings suggest that ITCs block phage DNA replication by upregulation of (p)ppGpp, a key alarmone involved in the stringent response. ITCs prevented the induction of Stx prophages by agents like hydrogen peroxide or mitomycin C, making them a viable alternative to be used as anti-virulence adjuvants that can be used together with conventional antibiotics.

1.6 The drug discovery process

The driving force to start a drug discovery project is an unmet need for treatment of a disease or clinical condition (Lombardino and Lowe III 2004). This brings together people from different disciplines in order to come up with ideas, hypotheses and a work plan to achieve specific objectives. The drug discovery

process can be divided in three main stages: *discovery and development*, *pre-clinical stage* and *clinical stage* (Figure 12).

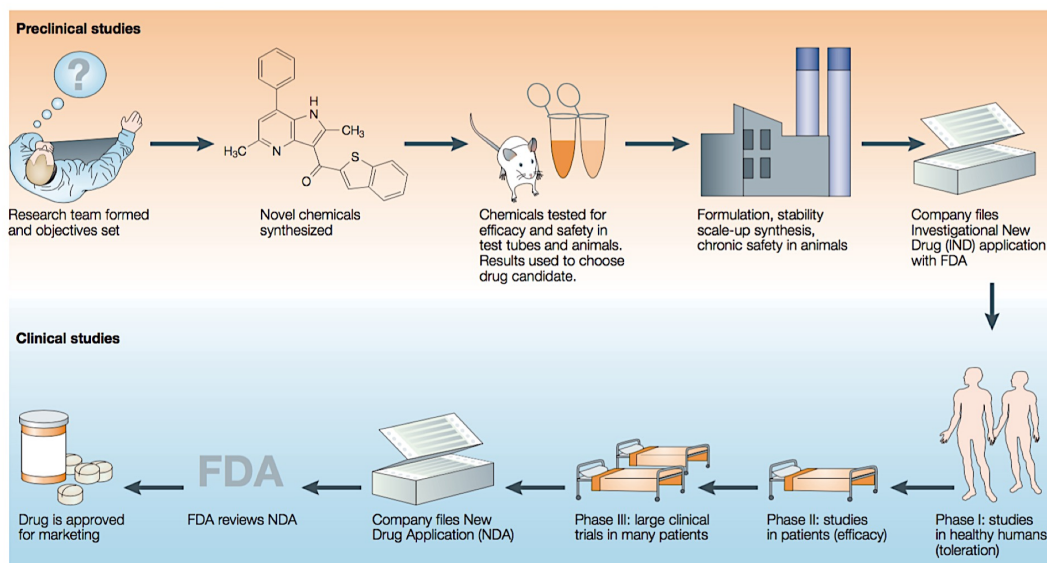


Figure 12 The drug discovery process at a glance.

A drug discovery project starts when a medical problem is identified. Experts from different fields get together to come up with a hypothesis, ideas on how to tackle the problem and specific objectives. Then, testing of chemical libraries in an appropriate biological test begins in order to identify bioactive molecules. Structure-activity relationship (SAR) studies on the hit compounds are usually performed to improve the bioactivity or physicochemical properties. The bioactivity of the new analogues is further validated both *in vitro* and *in vivo*, together with their toxicity profile. Once a drug candidate has been identified, processes like scale-up of the synthesis, chronic safety in animals and formulation start. Next, with consent of the Food and Drug Administration (FDA) in the US or a comparable institution elsewhere, the clinical phase takes. Testing in humans starts with toleration studies in healthy individuals (Phase I), followed by efficacy and dose assessment in individuals who suffer from the disease (Phase II) and finally a larger study in several thousands of patients to confirm efficacy and safety (Phase III). This provides the required data to get an approval from the FDA and release the drug into the market. Modified from Lombradino 2004.

1.6.1 Discovery and development

1.6.1.1 Target identification and validation

This stage usually starts with the identification and validation of a ‘druggable’ target i.e. a biological entity involved in the development of the disease whose activity can be modulated to prevent or revert the disease. Different sources of information including scientific publications, gene expression and proteomics data, transgenic phenotyping, etc. can be used to have a more in-depth understanding of the problem. One of the approaches used in target identification involves comparing the genomes of healthy individuals with those of people with the disease. Differences in the genomes can help to formulate hypotheses on which proteins are involved in the development of the disease. A similar approach involves changing one gene at a time (knock-out) in cells or simpler organisms and see if the phenotype has similarities with the disease state. This provides clues about the relationship between the mutated gene and the disease. In microbial drug discovery, genes or pathways that are essential for bacterial growth or virulence are good starting points.

Once a target has been identified, the next step is the validation using *in vitro* and *in vivo* tools. The process of validation basically demonstrates that the target is essential for the development of the disease. Cell-based or animal models of the disease are frequently employed, but best results are achieved when a combination of approaches is used.

A common deviation from the classic target identification and validation approach occurs when there is already a compound with demonstrated activity, or when known drugs show unexpected pharmacological effects, but with an undefined mechanism of action. In these cases, the project focuses on the identification of the target(s) and mode of action. Failure to identify the target does not necessarily disqualify a compound as a drug candidate, but might interfere with the potential improvement of the pharmacological properties.

It is also worth mentioning that important discoveries have been made by accident throughout history, phenomena known as *serendipity*. Many of the

commercially available drugs today were discovered in this way, including penicillin, imipramine or sildenafil, which reminds us that luck truly plays a role in drug discovery (Ban 2006)

1.6.1.2 Hit discovery

Following target identification and validation, the hit discovery process starts. A 'hit' can be defined as 'a compound which has the desired activity in a compound screen and whose activity is confirmed upon retesting' (J. P. Hughes et al. 2011). High-throughput screening (HTS) is one of the most popular approaches used to discover bioactive compounds and can be defined as the automated testing of large numbers of small molecules in order to identify inhibitors (antagonists) or activators (agonists) of a particular biological target or process (Broach and Thorner 1996). There are different screening strategies available. The selection is usually based on the available knowledge of the target or biological process (Table 2).

Table 2 Different types of screening strategies used in drug discovery

Screening strategy	Description
High throughput	Automated analysis of large numbers of compounds in a relevant biological assay, generally in 384-well plate format. No prior knowledge of the chemical scaffold likely to have activity is required.
Focused screen	The screening uses compounds that have been previously identified as bioactive against a specific class of targets (e.g. kinases) and that have a similar chemical scaffold. May limit the discovery of novel bioactive structures.
Fragment screen	Usually, crystals of the protein of interest are soaked with small molecule fragments (<300 Da) and the fragment-protein binding interactions are analysed using biophysical techniques like NMR or X-ray crystallography. This allows for the design of larger molecules with improved affinity for the target.
Physiological screen	This approach uses physiological models of the disease (e.g. a tissue-based model) to screen compounds. It is considered to be low-throughput given the complexity of the assay, but its phenotypic nature provides a broader pool of targets and signalling pathways.
Structure-based drug design	It is normally used as an adjunct to other screening strategies. This approach uses the crystal structure of the target and molecular modelling techniques to design compounds with improved activity and/or selectivity.
Virtual screen	Large virtual libraries of compounds are evaluated using <i>in silico</i> models based on the X-ray structure of the target in order to find bioactive molecules. It can help to identify a particular chemical scaffold that can be used in a focused screen, reducing the number of compounds to be tested.

1.6.1.3 The importance of the biological assay used in HTS

The type of assay used for the screening of compounds has a great impact on the outcome of the project. There are two types of assays used in HTS campaigns: *phenotype-based* and *target-based* assays. The choice of the assay depends on the biology of the problem studied, infrastructure, resources, experience of the scientists involved, etc. (Figure 13).

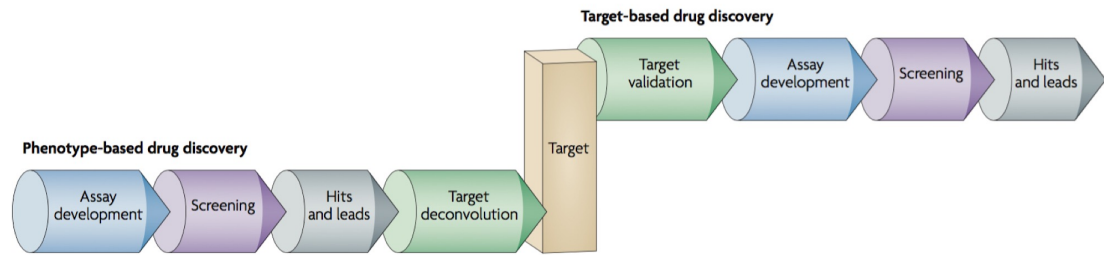


Figure 13 Differences between the phenotype and target-based approaches.

With the phenotype-based approach, the biological assay is developed first in order to start the screening of compounds. Then, studies to understand the mode of action start. On the other hand, the target-based approach starts with a defined target. Based on the properties of the target, an assay is developed, followed by the screening of compounds to identify the hits. Taken from Terstappen et al. 2007

Phenotypic-based assays consist in testing libraries of compounds in a physiologically relevant platform to find molecules that produce a specific phenotype or response. This approach has gained more popularity in recent years as it permits to study multiple targets or pathways that are otherwise overlooked in the target-based approach (Haasen et al. 2017).

Historically, phenotypic assays were the pioneers of the discovery of new drugs when defined substances were tested in complex living systems or isolated organs, looking for changes in the phenotype (Terstappen et al. 2007). Two possible downsides of the phenotypic-based approach are the lower throughput compared to the target-based method and the complex task of target deconvolution.

With the advances in biochemistry and molecular biology, the target-based approach emerged with the hope of making the discovery process more 'rational and efficient'. This approach involves overexpression and purification of the target protein in order to develop an assay able to measure the effect of compounds on the target's activity, followed by testing in a biological model.

Even though the pharmaceutical sector perceived a decline in productivity after the introduction of the target-based approach (Sams-Dodd 2005), it is still widely used in drug discovery programmes. One of the main disadvantages of this

approach is that it underestimates the complexity of the target's activity in physiological conditions. It also increases the risk of finding compounds with poor physicochemical properties that prevent their progression to biological testing (e.g. solubility issues, poor cell permeability, biotransformation, etc.).

1.6.1.4 Hit confirmation

Once the active compounds or 'hits' have been identified, it is important to confirm that the activity observed in the primary assay is correct. This starts by the generation of dose-response curves, preferably with freshly synthesised or repurchased samples of the compounds. This enables to compare the potencies of the compounds and to confirm that the activity is not due to a degradation impurity from the compound stock (Keserű and Makara 2006).

The use of counter-screens to eliminate false positives or compounds with undesirable mechanisms is also a common practice at this stage (Thorne, Auld, and Inglese 2010). For example, a hit compound can be tested against a different member of the target family using the same assay conditions. If the compound shows activity in both assays, it is likely to be non-specific or a false positive. These molecules are known as pan-assay interference compounds (PAINS). PAINS tend to react in a non-specific manner with different biological targets, giving false signals in assays (Baell J. B. and Holloway G. A. 2010). This class of compounds give false redouts in different ways, including autofluorescence or colour, chelation of metals essential for the assay or chemical modification of the protein of interest.

Some of the best-known PAINS include toxoflavin, a redox cycler that activates or inactivates proteins, polyhydroxylated natural products like curcumin, epigallocatechin gallate and resveratrol, phenol sulphonamides, isothiazolonones, amongst others (Priyadarsini K. I. 2013).

Awareness of these molecules and precautionary practices could help to prevent spending time and resources in the optimisation of compounds that are very unlikely to become drugs.

These practices include the identification of the most common structural classes found in PAINS, the use of software tools that can filter PAINS from screening libraries, assess the hits using secondary assays and verify the purity and identity

of the hits to discard that the activity is a result of breakdown product of the compound identified in the screen (Baell J. B. and Walters M. A. 2014).

1.6.1.5 The hit to lead process

The next step after hit identification involves the performance of structure-activity relationship (SAR) studies on the lead compound(s). A lead compound can be defined as 'a chemical structure or series of structures that show activity and selectivity in a pharmacological or biochemical relevant assay' (Lombardino and Lowe III 2004).

The medicinal chemists play an important role at this stage, as systematic chemical modifications need to be performed on the lead compound. The aim of this is to improve or manipulate the pharmacological properties of the compound, such as potency or undesired effects. It also allows for the modification of the pharmacokinetic properties, including the distribution and elimination profiles, biotransformation and chemical stability under physiological conditions.

There are two ways of doing SAR on a lead compound (Guha 2013). The first one involves the crystallisation of the target protein and the compound in order to identify the binding interactions. However, this might not be always possible if the target is a difficult protein to crystallise or if the target is yet to be determined. In these situations, a certain number of compounds with structural variations are synthesised and the effect that such modification have on the biological activity is studied.

1.6.1.6 Preclinical stage

Once a lead compound has been selected as a potential drug candidate, the next step is the toxicity testing. This usually starts with *in vitro* tests using cell culture assays and/or *in vivo* testing, commonly using transgenic mice to assess any possible carcinogenic or teratogenic properties (Strovel et al. 2004). The

assays consist of the administration of large doses to induce a toxic effect for a short period of time. The animals studied are euthanized and their organs examined to see any possible alterations. Long-term toxicological tests are also performed using lower doses of the drug to see if the drug shows any chronic toxicity. The toxicity of a given drug can be measured by its LD₅₀ value i.e. the dose required to kill 50% of the population.

It is also important to study the biotransformation of the compounds in the human body. This includes the study of the drug metabolites formed and see what biological activity they might have. This is an important safety issue, as some metabolites might be toxic or have undesired side effects. Ideally, drug metabolites should be inactive and quickly eliminated from the body (Shu, Johnson, and Yang 2008).

1.6.1.7 Clinical stage

The next stage in the drug discovery process consists in the design of clinical trials to test the drug in humans. In order to reach this stage, more in-depth studies on the pharmacology of the drug are required, to see whether it has off-target activity or simply to gain more insights on the drug's mechanism of action. In addition, formulation studies need to take place in order to develop a dosage form of the drug that is both stable and suitable for the condition to be treated. These studies include the characterisation of the drug's chemical and physical properties in order to choose suitable ingredients for the preparation. It also involves pharmacokinetic studies in order to ensure a successful delivery of the drug.

The formulation studies do not have to be finalised in order to start the clinical studies, as simple preparations can be used at early stages. Long-term stability studies will still need to be carried out. The clinical trials are divided in phase I, II, III and IV. A complete review of each stage is out of the scope of this work but the reader is referred to excellent literature material (J. P. Hughes et al. 2011; Hefti 2008).

1.7 Aims of the project

The general aim of this project was to develop small-molecule inhibitors of Shiga toxin expression in *E. coli* O157:H7.

This interdisciplinary project involved the high- throughput screen of chemical libraries, synthesis and biological evaluation *in vitro* and *in vivo* of new chemical entities able to suppress Shiga toxin expression and affect bacterial virulence. This novel approach is attractive as, unlike traditional bactericidal antibiotics, there is far less selective pressure for the development of resistance.

CHAPTER 2

Materials and Methods

2 Materials and methods

2.1 Chemicals and molecular reagents

Chemicals used in the present work were purchased from Sigma-Aldrich, Fisher Scientific and Invitrogen, unless otherwise stated.

2.2 Growth media

All bacterial growth media was prepared using deionised water, and sterilised in autoclave.

Table 3 Growth media

Media	Components per litre	
LB broth	Tryptone	10 g
	Yeast extract	5 g
	NaCl	10 g
LB agar	Tryptone	10 g
	Yeast extract	5 g
	NaCl	10 g
	Agar	15 g
M9 salts	Na ₂ HPO ₄ 7H ₂ O	64 g
	KH ₂ PO ₄	15 g
	NaCl	2.5 g
	NH ₄ Cl	5 g
M9 media	M9 salts	200 mL
	MgSO ₄ 1 M	2 mL
	Glucose 20% w/v	20 mL
	CaCl ₂ 1 M	100 µL

2.3 Cell culture

2.3.1 Shiga toxin cytotoxicity assay

Vero cells were grown in Minimum Essential Medium Eagle, HEPES modification (Sigma Aldrich) supplemented with 10% heat-inactivated fetal bovine serum (Gibco), 1% penicillin-streptomycin (Gibco) and 1% L-glutamine (Gibco) and incubated at 37 °C in a humidified 5% CO₂ incubator. On the previous day before the experiment, Vero cells were seeded at 1x10⁴ cells/well in 96-well plates and incubated overnight.

In order to evaluate Shiga toxin production, overnight cultures of *C. rodentium* (λ stX_{2dact}) were diluted 1/100 in fresh LB medium supplemented with 100 µg/mL chloramphenicol and grown until an OD₆₀₀ of 0.3. Then, the culture was split in samples containing 2 mL of culture and the compound was added at different concentrations, taking care of maintaining the final DMSO concentration below 1%. Shiga toxin production was triggered by the addition of 1 µg/mL of MMC to the samples containing the compound and to the positive control. Cultures were filter sterilised using 0.2 µm syringe filters and serially diluted, starting at 1:5. The growth media of the Vero cells plates was replaced by 100 µL of diluted lysate, and the cells were incubated for further 48 h at 37 °C in a humidified 5% CO₂ incubator. Cytotoxicity was assessed using the methylthiazolyldiphenyl-tetrazolium bromide (MTT) assay. MTT (Sigma Aldrich) was dissolved in phosphate-buffered saline (PBS) to 1 mg/mL and filter sterilised. The growth media in the Vero cells plates was substituted with 100 µL of the MTT solution and incubated for 4 h. After this time, the liquid was removed from the wells and the precipitate - purple formazan - was dissolved by addition of 100 µL DMSO. Plates were read at 540 nm to quantify cell viability.

2.4 Storage and handling of bacterial strains

Bacterial stocks were prepared by adding 0.5 mL of bacterial culture to 1 mL glycerol (40%) and peptone (2%) and stored at -80°C. To obtain a bacterial working plate, bacteria from the frozen stock were streaked onto fresh LB plates (supplemented with antibiotics if required), grown overnight at the required temperature and stored at 4°C for approximately 2-3 weeks.

2.4.1 Bacterial strains

All bacterial strains used in this work are listed and described in table 4.

Table 4 Bacterial strains used in this study		
Strain	Description and genotype	Source
<i>Escherichia coli</i>		
TUV93-0	Stx-negative derivative of O157:H6 EDL933	Campellone et al, 2002
ZAP0273	Stx-negative derivative of O157:H7 Sakai	Prof. David Gally, University of Edinburgh
JP10819	MG1665 strain lysogenic for ϕ P27, <i>stx2::Tet</i>	Quiles-Puchalt et al, 2014
K-12 MG1665	Non-lysogenic laboratory strain	Blattner et al, 1997
BL21 (DE3)	Protein expression strain	New England Biolabs
<i>Staphylococcus aureus</i>		
JP5011	RN4220 strain lysogenic for ϕ SLT, <i>pvl::tet</i>	Ferrer et al, 2011
RN4220	Non lysogenic laboratory strain	Nair et al, 2011
<i>Citrobacter rodentium</i>		
<i>Citrobacter rodentium lux</i>	<i>lux</i> -positive <i>C. rodentium</i> with <i>stx2</i> prophage λ <i>stx2</i> _{dact}	Mallick et al 2012

2.5 Plasmids

All plasmids used in this work are listed and described in table 5.

Table 5 Plasmids used in this study

Plasmid	Vector type	Antibiotic resistance	Source
<i>pstx2::GFP</i>	Reporter	Chloramphenicol	Prof. D. Gally
<i>prpsM::GFP</i>	Reporter	Chloramphenicol	Roe et al, 2003
pKD46	Helper	Ampicillin	Datsenko et al, 2000
pKD4	Template	Kanamycin	Datsenko et al, 2000
pKD3	Template	Chloramphenicol	Datsenko et al, 2000
pTXB1	Expression	Ampicillin	New England Biolabs
pCP20	Helper	Ampicillin	Datsenko et al, 2000

2.6 Bacterial growth conditions

Unless otherwise specified, overnight cultures consisted on a single colony taken from an agar plate suspended in 5 mL of LB (supplemented with antibiotics if required), and grown overnight in a shaking incubator at 37 °C, 200 rpm. Subcultures were obtained by 1/100 dilution of the overnight culture in fresh LB and grown to the desired OD₆₀₀.

Table 6 Antibiotics used for the growth of GMO with antibiotic resistance markers

Antibiotic	Final concentration (µg/mL)
Ampicillin	100
Chloramphenicol	35
Erythromycin	500
Kanamycin	50
Tetracycline	6

2.7 Molecular techniques

2.7.1 Oligonucleotide primers

Primers used in the present study were designed using MacVector and synthesised by Life Technologies. A 100 µM working stock was used in PCR. All primers are listed in table 7

Table 7 Primers used in this study

Name	Sequence 5' to 3'
Lambda red <i>luxS</i> 5' <i>E. coli</i> Sakai	GAGGTGGCTAAATGCCGTTGTTAGATAGCTTCACAGTCGGTGTAGGCTGG AGCTGCTTC
Lambda red <i>luxS</i> 3' <i>E. coli</i> Sakai	CTGACTAAATGTGCAGTTCCTGCAACTTCTCTTTCGCATATGAATATCCTC CTTAG
Lambda red <i>luxS</i> 5' check	GAGGTGGCTAAATGCCGTTGTTAGA
Lambda red <i>luxS</i> 3' check	CTGACTAAATGTGCAGTTCCTGCAA
Lambda red <i>sdiA</i> 3' <i>E. coli</i> Sakai	AGGGGCGTTGCGGTTTACTATGCAGGATACGGATTTTTGTGTAGGCTGGA GCTGCTTC
Lambda red <i>sdiA</i> 5' <i>E. coli</i> Sakai	GACAGAAAAGAGATCAAATTAAGCCAGTAGCGGCCGCGTCATATGAATAT CCTCCTTAG
Lambda red <i>sdiA</i> 5' check Sakai	ACTCTCAGGGGCGTTGCGGTTTACT
Lambda red <i>sdiA</i> 3' check Sakai	TCTGGCACGCAGGACAGAAAAGAGA
Lambda red <i>luxS</i> 5' <i>E. coli</i> MG1665 φ27	GTGGCTAAATGCCGTTGTTAGATAGCTTCACAGTGTAGGCTGGAGCTGCT TC
Lambda red <i>luxS</i> 3' <i>E. coli</i> MG1665 φ27	TGTGAAGATAGTTTACTGACTAGATGTGCAGTTCCTGCAACATATGAATAT CCTCCTTAG
Lambda red <i>luxS</i> 5' check Sakai	AAATGCCGTTGTTAGATA
Lambda red <i>luxS</i> 3' check Sakai	TACTGACTAGATGTGCAGTT
Lambda red <i>sdiA</i> 5' <i>E. coli</i> MG1665 φ27	GTTGCGGTTTACTATGCAGGATAAGGATTTTTTCAGCTGGGTGTAGGCTG GAGCTGCTTC
Lambda red <i>sdiA</i> 3' <i>E. coli</i> MG1665 φ27	GACAGAAAAGAGATCAAATTAAGCCAGTAGCGGCCGCGTAACATATGAAT ATCCTCCTTAG
Lambda red <i>sdiA</i> 5' check MG1665	CAGGGGCGTTGCGGTTTACT
Lambda red <i>sdiA</i> 3' check MG1665	TGGCACGCAGGACAGAAAAGAGA
Cloning RecA 5'	GGAATTCATATGATGGCTATCGACGAAAACAACAGAAA
Cloning RecA 3'	CCGTGATGCAGGAAGAGCCAAAATCTTCGTTAGTTTCTGC
pTXB1 check 5'	CGACTCACTATAGGGGAATTGTGAGCGGATAACAATT
pTXB1 check 3'	CTCGGGTAGGGCAACTAGTCATCTCCCGT

Stx2dact B subunit 5'	ATGAAGAAGATATTTGTAGCGGCTTTATTTGCTT
Stx2dact B subunit 3'	TTAATTAAACTGCACTTCAGCAAATCCTGAACCT
Stx2dact A subunit 5'	ATGAAGTGTATATTATTTAAATGGGTACTGTGCCT
Stx2dact A subunit 3'	TTATTCTCCGGATGTATTTAAAGAGTGGGC

2.7.2 Preparation of genomic DNA

Genomic DNA was extracted from 1 mL overnight culture of the desired strain using the ChargeSwitch gDNA mini bacteria kit (Invitrogen) following the manufacturer's instructions. The DNA was dissolved in 200 µL of nuclease free water and stored at -20 °C

2.7.3 Polymerase chain reaction (PCR)

All reactions were performed in nuclease free PCR tubes. When the template used was plasmid or genomic DNA, samples were diluted to a 1/100 stock and used in the reaction. For colony PCR, a colony was picked from a fresh working plate using a micropipette tip and resuspended in 50 µL sterile H₂O. The mix was boiled at 95 °C for 10 minutes and 1 µL used as template for the reaction.

Table 8 Components of a PCR reaction

GoTaq Green Master Mix	12.5 µL
10 µM 5' primer	0.5 µL
10 µM 3' primer	0.5 µL
Template DNA	1 µL
Nuclease free H ₂ O	10.5 µL

Table 9 Standard PCR protocol (30 cycles)

Step	Temperature (°C)	Time (s)
Initial denaturation	95	300
Denaturation	95	45
Annealing	55	45
Extension	72	60 per kb
Final extension	72	600
Hold	4	Hold

2.7.4 Extraction of plasmid DNA

An overnight culture (5 mL) of the desired strain was centrifuged at 3750 rpm for 10 minutes. The plasmid was purified using the QIAprep® Spin Miniprep kit protocol (Qiagen). The purified plasmid was eluted in 25-40 µL of nuclease free water (Ambion) and the concentration was determined using a NanoDrop™ (Thermo Fisher) at 200 nm, followed by storage at -20 °C.

2.7.5 Agarose gel electrophoresis

To separate DNA using agarose gel electrophoresis, 1% w/v agarose gels were prepared by heating 1 g of ultrapure agarose in 100 mL of 1X Tris-acetate-EDTA (TAE) buffer and cooled down at room temperature. SYBR™ Safe DNA gel stain (Thermo Fisher) was added at a 1:10,000 dilution before the solution was poured into a gel tray and allowed to set. Samples were loaded using the BlueJuice™ loading buffer (Thermo Fisher), using 1 Kb Reference DNA ladder as standard marker of size. Gels were run at 100 V for 40 minutes and visualised using an Alphamager transilluminator (Alpha Innotech)

2.7.6 Restriction enzyme digests

All restriction enzyme digests were performed according to the manufacturer's procedures (New England Biolabs). Each digestion consisted of 20 µL containing 1µg/µL DNA (1 µL), 1x digestion buffer (1 µL), 10 units/µL restriction enzyme (1 µL) and nuclease-free water (7 µL). Reactions were incubated at 37 °C for 2 h, and the digestion products were resolved by agarose gel electrophoresis.

2.7.7 DNA gel purification

PCR products or linearised DNA from restriction enzyme digestion were resolved by agarose gel electrophoresis. DNA was visualised using an Alphamager transilluminator (Alpha Innotech) and the band of interest was excised from the gel a purified using the QIAquick Gel Extraction Kit (Qiagen) following the manufacturer's instructions. The purified DNA was then eluted with 25-50 µL of

nuclease free water and the concentration determined using a NanoDrop™ (Thermo Fisher) at 200 nm, followed by storage at -20 °C

2.7.8 DNA ligation

Ligation reactions were performed following manufacturer's instructions (New England Biolabs). Briefly, reactions were carried out in a final volume of 10 µL containing 100 ng/µL of linearized plasmid (1 µL), 100 ng/µL of insert DNA (3 µL), T4 ligase (1 µL), 10x T4 DNA ligase buffer (1 µL) and nuclease-free water (4 µL). Reactions were incubated at room temperature overnight or at 16 °C.

2.7.9 Preparation of electrocompetent *E. coli*

An overnight culture of the desired strain is diluted (1/100) in 25 mL of fresh LB. The subculture is grown at 37 °C and 200 rpm until an OD₆₀₀ of 0.6. Culture was centrifuged at 3000 x g for 10 minutes at 4 °C. The supernatant was discarded and the cell pellet resuspended in 20 mL of ice-cold 10% (v/v) glycerol (or cold sterile water) before a further centrifugation for 10 min. The pellet is resuspended again in 1 mL of ice-cold 10% glycerol and centrifuged for 2 minutes, and this step was repeated a further 4 times. Finally, the pellet was resuspended in 100 µL of ice-cold 10% glycerol and used for transformation.

2.7.10 Electroporation transformation

For each transformation, 40 µL of electrocompetent cells were mixed either 2 µL of purified plasmid or 2-5 µL of the ligation reaction and immediately electroporated at 2.5 kV and a capacitance of 25 µF using an Eporator electroporator® (Eppendorf). 1 mL of pre-warmed SOC media was added to the transformation mixture and transferred to a 1.5 mL eppendorf tube. Cells were recovered with incubation at either 30 or 37 °C with shaking for 2 h. The cells were plated onto LB agar plates supplemented with the required antibiotic, and incubated overnight at the appropriate temperature.

Table 10 SOC media recipe (1 L)

Tryptone	20 g
Yeast extract	5 g
NaCl 5 M	2 mL
KCl 1 M	2.5 mL
MgCl ₂ 1 M	10 mL
MgSO ₄ 1 M	10 mL
Glucose 1 M	20 mL
dH ₂ O	Q.S. 1 L

2.7.11 Heat-shock transformation

For each transformation, 50 µL of chemically competent BL21 Star (DE3) were mixed with 4 µL of purified plasmid and incubated on ice for 30 min. The cells were then heat shocked for 45 seconds at 42 °C, followed by a 2 min incubation in ice. Then, 1 mL of pre-warmed SOC media was added and the cells recovered with incubation at 37 °C, 200 rpm for 2 h. Finally, cells were plated onto LB agar plates supplemented with the appropriate antibiotic and incubated overnight.

2.7.12 Gene inactivation using the lambda red recombineering system

Gene ‘knockouts’ were performed using lambda red recombineering. Briefly, the technique involves the amplification of an antibiotic resistance cassette that contains 5’ and 3’ overhangs that flank the gene of interest. The PCR product is transformed into bacterial cells and the gene of interest is replaced with the resistance cassette, which allows for identification of such mutants. The lambda red recombineering system requires three components to work: *gam* (encodes a protein that prevents the digestion of linear DNA introduced into the cells), *exo* (encodes a 5’ to 3’ exonuclease that degrades linear dsDNA) and *beta* (encodes a ssDNA annealing protein that protects the ssDNA created by Exo and promotes its annealing to a complementary ssDNA). These elements are encoded on the arabinose-inducible pKD46 plasmid. In this way, when the resistance cassette PCR product is transformed into the cells that have pKD46, the Gam protein prevents degradation, Exo converts the 5’ ends into 3’ ssDNA overhangs and Beta

uses these overhangs to pair them with their complementary target (Datsenko and Wanner 2000)

Experimentally, the procedure involved the transformation of the Amp^R pKD46 plasmid into the target strain. The plasmid is temperature sensitive so cells had to be grown at 30°C. To design the antibiotic resistance with flanking regions of the knockout gene, the kanamycin or chloramphenicol genes are amplified from the pKD4 or pKD3 plasmids respectively. Primers should have internal overlap with the resistance marker and external overlap with the target gene (50 bp upstream and downstream). The PCR products from 10 reactions were run on 0.5% agarose gel, DNA excised, purified and pooled.

Cells transformed with the pKD46 plasmid were grown in 25 mL of LB media supplemented with ampicillin and 0.1 M arabinose at 30°C. Once the culture reached an OD₆₀₀ of 0.6, the cells were made electrocompetent following the 'preparation of electrocompetent *E. coli*' protocol. Cells were transformed with approximately 3-4 µL of the PCR product, plated onto agar plates supplemented with the corresponding antibiotic, and grown at 42°C. Colonies were re-streaked on LB agar plates + antibiotic and incubated at 42°C for 2-3. This was done to allow curing of the mutant of the pKD46 plasmid. Successful gene knockouts were identified by colony PCR, using primers that only flank the target gene.

2.7.13 Removal of antibiotic resistance cassettes by FLP recombination

In order to remove the antibiotic resistance cassette as a consequence of the lambda red gene inactivation process, competent cells of the mutant of interest were prepared following the 'preparation of electrocompetent *E. coli*' protocol. Cells were transformed with the plasmid pCP20, which has a temperature sensitive origin of replication resistant to chloramphenicol and ampicillin. Cells were recovered at 30°C, 200 rpm, for 3 h and plated onto ampicillin plates.

Few transformants were picked and inoculated into 5 mL of LB (no antibiotic) and incubated at 42°C overnight to induce FLP recombinase expression and

select for the loss of pCP20. After the incubation period, transformants were plated onto two ampicillin plates, one was incubated at 30°C and the other one at 42°C. Colonies that only grew on the 42°C plate were picked and resuspended in 10 µL of LB and 3 µL were plated onto a set of three plates: chloramphenicol, 37°C; Ampicillin 30°C; no selection, 37°C. Colonies that only grew on the no selective plate had lost both the pCP20 plasmid and the Cm^R cassette. This was confirmed through PCR.

2.7.14 Reporter assays

Shiga toxin expression assays were performed using the *pstx2::GFP* reporter fusion plasmid (pNY16). The plasmid was transformed by electroporation into ZAP0273 and transformants cultured overnight in LB medium containing 35 µg/mL chloramphenicol. Overnight cultures were diluted into fresh LB (1/100) and grown to an OD₆₀₀ of 0.3 at 37°C and 200 rpm. Compounds and mitomycin C (MMC, 1 µg/mL) were added at this point, and fluorescence and optical density of cultures measured hourly. GFP fluorescence of 200 µL aliquots was measured in a 96-well blank microtiter plate using a FLUOstar Optima plate reader (BMG, Germany).

2.7.15 Phage transduction assays

Overnight cultures of *E. coli* JP10819 and *S. aureus* JP5011 (Quiles-Puchalt, et al., 2014) were diluted 1/100 in LB (*E. coli*) or TSB (*S. aureus*) media and grown at 37°C, 200 rpm until an OD₆₀₀ of 0.25 was reached. Compounds and 1 µg/ml MMC were added at this point and cultures were incubated at 32°C, 80 rpm shaking for 4 h, followed by room temperature without shaking for 16 h.

On the next day, cultures were filter sterilised using 0.2 µm syringe filters, and serially diluted in phage buffer (100 mM NaCl, 0.5 M tris pH 7.8, 1 mM MgSO₄, 4 mM CaCl₂). In parallel, cultures of the recipient strains MG1655 (*E. coli*) or RN4220 (*S. aureus*) were grown to an OD₆₀₀ of 1.4, after which CaCl₂ was added to a final concentration of 10 mM. 100 µl of phage lysate was added to 1 ml

aliquots of the recipient strain and samples were incubated without shaking at 37 °C for 30 minutes. Then, 3 ml of pre-warmed (45 °C) top agar was added, and samples were poured onto LB or TSB agar plates containing 6 µg/ml tetracycline and 1.7 mM sodium citrate. A negative control lacking addition of phage lysate was also included to confirm the absence of phage contamination. Colonies were subsequently counted to define the number of transduction events per sample.

2.8 Biochemical techniques

2.8.1 RecA Protein overexpression

For expression of RecA, *E. coli* BL21(IDE3) cells were heat-shock transformed with the pTXB1-*recA* expression vector. Cells were cultured in M9CA medium supplemented with 100 µg/ml ampicillin and grown at 37 °C, 200 rpm to an OD₆₀₀ of 0.8. When the desired OD₆₀₀ was reached, IPTG was added to a final concentration of 500 µM and the culture flasks were transferred to a shaker incubator set at 18 °C, 200 rpm and incubated for 16-18h. The next day, cells were harvested by centrifugation and resuspended in sucrose lysis buffer (3.5 mL per gram of cell pellet). Cells were sonicated at 75 W, 40% output for 5 min with pulses of 5 seconds on and 10 seconds off, using a Soniprep 150 sonicator (MSE). The soluble fraction was centrifuged at 13000 rpm for 15 min at 4 °C. Chitin beads (New England Biolabs) were loaded in a 1.5x12 cm column and washed with chitin binding buffer (10 column volumes) prior to the loading of the soluble fraction. Generally, 10 mL of chitin beads can be used for one-liter culture purification, so the bed volume and column size should be adjusted accordingly. Once the column was equilibrated with the chitin-binding buffer, the soluble fraction was loaded onto the column at a flow rate between 0.5-1 mL/min. When the entire soluble fraction was loaded, the column was washed with 10 bed volumes of chitin-binding buffer. Two bed volumes of chitin cleavage buffer were quickly flushed to homogeneously distribute the DTT through the column. The column was then sealed and incubated at 4 °C overnight to allow intein autoproteolysis. The next day, the released RecA was eluted with 3-5 bed volumes of elution buffer in fractions of approximately 1 mL. The protein concentration in each fraction was determined using the Bradford Assay and the most concentrated fractions were pooled and dialyzed overnight against 2 L of

dialysis buffer. On the next day, the protein was concentrated to approximately 1 mg/mL using 25 mL concentrators 30 MWCO (Vivaspin).

In order to regenerate the chitin resin, the column was washed with 3 bed volumes of 0.3 M NaOH (stripping solution) and allowed to soak for 30 min and then washed with 7 bed volumes of stripping solution. The column was then rinsed with 20 bed volumes of distilled water and 5 bed volumes of chitin-binding buffer for storage.

Table 11 RecA purification buffers

Buffer	Components	
Lysis buffer	Sucrose	25% (w/v)
	Tris HCl pH 7.5	80 mM
	Brij-35	0.5% (v/v)
	EDTA	5 mM
Chitin binding buffer	Tris HCl pH 7.5	20 mM
	NaCl	1.5 mM
	EDTA	1 mM
	CHAPS	0.5 % (w/v)
Chitin cleaving buffer	Tris HCl pH 8	20 mM
	Glycerol	10% (v/v)
	EDTA	0.1 mM
	Triton X-100	0.1% (v/v)
	DTT	50 mM
Elution buffer	Tris HCl pH 8	20 mM
	Glycerol	10% (v/v)
	EDTA	0.1 mM
	Triton X-100	0.1 % (v/v)
Dialysis buffer	Tris HCl pH 7.5	20 mM
	Glycerol	10% (v/v)
	DTT	1 mM

2.8.2 SDS-PAGE

Protein samples for analysis by SDS-PAGE were mixed with 4x NuPAGE[®] LDS loading buffer and boiled for 10 min at 70°C prior to the loading onto NuPAGE[®] 4-12% Bis-Tris pre-cast gels (Invitrogen). A total of 10-15 µL of sample were loaded and SeeBlue plus2 pre-stained protein standard (Invitrogen) was used as a molecular weight marker. The gels were run using NuPAGE MES SDS Running buffer for 45-50 min at 150 V. The gels were stained with Coomassie blue for protein visualization or taking for immunoblotting. Coomassie blue stain is formed by dissolving Coomassie blue R-250 (0.1% w/v) in water-methanol-glacial acetic acid (5:4:1).

2.8.3 General Western blot procedure

Proteins for immunoblotting were transferred from SDS-PAGE to PVDF membrane (Millipore) at 30 V for 90 minutes using the Mini Blot module (Thermo Fisher). The membrane was then blocked with 4% skimmed milk (Marvel) suspended in PBST for 1 h at room temperature in an orbital shaker. This was followed by an overnight incubation with the primary antibody dissolved in PBST in an orbital shaker at 4°C. On the next day, the membrane was washed with PBST three times, followed by incubation with the secondary horseradish-peroxidase conjugated antibody for 1 h at room temperature. At the end of this incubation, the membrane was washed with PBST a further three times. Finally, the membrane was developed with SuperSignal West Pico Chemiluminescent ECL substrate (Thermo Scientific) according to the manufacturer's specifications.

Table 12 Antibodies used in this study

Primary antibody	Dilution	Secondary antibody
Mouse anti-StxB (Abcam)	1:1000	Goat anti-mouse
Rabbit anti-GroEL (Enzo)	1:10,000	Goat anti-rabbit
Rabbit anti-RecA (Abcam)	1:6000	Goat anti-rabbit

2.8.4 RecA ATPase assays

RecA ATPase activity was assessed using an Innova Biosciences ATPase assay kit (#601-0120) following the manufacturer's protocol. Briefly, the assays were

performed in 96-well plates; each reaction consisted in 50 μL containing 0.25 μM RecA, 5 μM ssDNA, 25 μL of SB mix (0.5 M Tris pH 7.5, 0.1 M MgCl_2 , 10 mM ATP, H_2O) and nuclease free water q.s. 50 μL . The small molecule inhibitors were added to the wells before addition of ssDNA. Care was taken to keep the DMSO at a final concentration of 1% to avoid interference with the assay. The plate was incubated at 37°C for 30 minutes and reactions were stopped by addition of 12.5 μL of PiColorLock™, followed by addition of 5 μL of stabilizer. Absorbance was measured at a wavelength 590-660 nm.

2.8.5 Sample preparation for metabolomics analysis

Preparation of samples for metabolomics was adapted from Creek et al. 2011. Briefly, bacterial cultures were grown in 10 mL of M9 minimal medium to an OD_{600} of 0.9. 2.5 mL of the bacterial culture were mixed with 2.5 mL of fresh M9 medium, followed by addition of the compound of interest at the desired concentration. The solution was incubated for 1 h at room temperature. 1 mL of the incubated solution was mixed with 100 μL of 10-bromodecade oil and the mixture was centrifuged at 13000 rpm, 4°C for 2 min. 12.5 μL of supernatant were transferred into a sterile micro-centrifuge tube and mixed with 500 μL of a 1:3:1 chloroform:methanol:water extracting solution, generating the supernatant sample. The rest of the supernatant was removed and the cell pellet was resuspended in 200 μL of the extracting solution to create the cell sample. All the samples were performed in triplicate and stored at -80°C until MS analysis. Dr. Karl Burgess and Dr. Stefan Weidt from the University of Glasgow Polyomics Division carried out the metabolomics analysis. Samples were analysed through hydrophilic interaction liquid chromatography (HILIC) on Dionex UltiMate 3000 RSLC system (Thermo Fisher Scientific, Hemel Hempstead, UK) using a ZIC-pHILIC column (Merck Sequant). Samples were eluted with a linear gradient using A) 20 mM ammonium carbonate in water and B) acetonitrile over 26 min at a flow rate of 0.3 mL/min as shown in table 13.

Table 13 Elutions of samples in HILIC

Time/min	%A	%B
0	20	80
15	80	20
15	95	5
17	95	5
17	20	80
24	20	80

The injection volume was 10 μ L and samples were maintained at 4°C prior to injection. The MS analysis was performed using a Thermo Orbitrap Exactive (Thermo Fisher Scientific), operated in polarity switching mode with a resolution of 50'000. Samples of cell-free medium and appropriate compound concentration were used as controls.

2.9 Biophysical techniques

2.9.1 Microscale thermophoresis

RecA protein was covalently labelled with NT-647 Red dye (Nanotemper technologies). The dye carries a reactive NHS-ester group that modifies primary amines present in amino acids like lysine. Excess dye was removed using a gravity flow column. The compound AHU3 was dissolved in a PBS-DMSO (4%) solution and diluted from 200 μ M to 12 pM. RecA was dissolved in PBS at 100 μ M. RecA was incubated with the different concentrations of AHU3 for 5 minutes at room temperature, followed by loading into MST NT.115 glass capillaries and the MST analysis was performed using a Monolith NT (NanoTemper Technologies)

2.10 High throughput screening

2.10.1 Primary screen

A high-throughput screening campaign to find inhibitors of Stx expression was carried out at the Drug Discovery Unit (DDU), University of Dundee. A total of 29,504 were screened using the *stx2*::GFP reporter assay as described below.

Compounds from the Gates and DDU targeting sets, the Epigenetics set and Easyset libraries were dispensed into barcoded clear-bottomed black 384-well plates (Greiner#781091) using an Echo 550 acoustic dispenser (Labcyte) to reach a final concentration of 30 μM (125 nL). Separately, an overnight culture of *E. coli stx2*::GFP was diluted (1:50) into freshly prepared M9 minimal media supplemented with chloramphenicol (35 $\mu\text{g}/\text{mL}$). The culture was grown at 37°C, 200 rpm until an OD_{600} of 0.2-0.25 was reached. The culture was split in two flasks. Flask 1 was treated with MMC (1 $\mu\text{g}/\text{mL}$) and flask 2 was not. Using a Multidrop™ Combi reagent dispenser (Thermo Scientific), 30 μL of the bacterial culture in flask 1 were dispensed into columns 1-23 of all assay plates. Culture from flask 2 was dispensed into column 24 using a VIAFLO II electronic pipette (Integra Biosciences). The plates were sealed with parafilm, placed into a moist box and incubated at 37°C, 150 rpm for 6 h. Care was taken to avoid stacking more than 4 plates high. Using a Pherastar plate reader (BMG Labtech), the plates were read for GFP 485/520 nm set at 10 flashes per well and settling time 0.2 s. The raw data was processed using ActivityBase software version 8.0.2.15 (IDBS)

For all the data analysis, the relative fluorescence units (RFU) measured were normalized to a percentage effect of the positive control using the following formula:

$$\% \text{ Effect} = \frac{\text{Raw data} - \text{Median (MMC+)}}{\text{Median (MMC -)} - \text{Median (MMC-)}}$$

2.10.2 Counter-screen of hit compounds using *E. coli* *rpsM::GFP*

An overnight culture of *E. coli rpsM::GFP* was diluted (1:50) into freshly prepared M9 minimal media supplemented with chloramphenicol (35 µg/mL). The culture was split in two flasks. Flask 1 was treated with ampicillin (100 µg/mL) and flask 2 was not. Using a Multidrop™ Combi reagent dispenser (Thermo Scientific), 30 µL of the bacterial culture in flask 2 were dispensed into columns 1-11 and 13-24 of all assay plates. Culture from flask 1 was dispensed into columns 12 and 24 using a VIAFLO II electronic pipette (Integra Biosciences). The plates were sealed with parafilm, placed into a moist box and incubated at 37°C, 150 rpm for 6 h. Care was taken to avoid stacking more than 4 plates high. Using a Pherastar plate reader (BMG Labtech), the plates were read for GFP 485/520 nm set at 10 flashes per well and settling time 0.2 s. The raw data was processed using ActivityBase software version 8.0.2.15 (IDBS)

2.10.3 Dose response calculation

The dose response evaluation of the compounds was calculated using MathIQ model 203 in ActivityBase XE. The potency of the hit compounds was assessed using the *stx2::GFP* assay, two-fold serial dilutions of the compounds. For all data analysis, the RFU of each well was normalised to as percentage effect (% Effect) of the positive control. ActivityBase XE (IDBS) was used for all data processing. Potency was determined using a 4-parameter logistic fit (minimum, maximum, hill slope and IC₅₀), being defined in reference to the negative logarithm of the molar value at the point of inflection of a sigmoidal dose-response curve (pIC₅₀). All the plates assessed were subject to quality control analysis, ensuring that the SB ratio ≥ 2 , CV % < 10% and Z' ≥ 0.4 .

2.11 Cytotoxicity of AHU series

Cytotoxicity evaluation of the AHU1-3 compounds was carried out at the European Screening Port (Hamburg, Germany). Human embryonic kidney 293 (HEK 293) cells were grown on surface modified T175 cell culture flasks (Greiner

Bio-One) in DMEM (Life Technologies) with 10% FCS, streptomycin (100 µg/mL) and 100 U/mL penicillin G. Cells were incubated at 37°C in the presence of 5% CO₂ and were harvested at 80-90% confluency. The compounds (200 nL of 10 mM DMSO stock) were spotted onto polystyrene 384-well cell culture microtitre plates (Greiner Bio-one) using the Echo 550[®] Liquid Handler (Labcyte). Each assay plate also contained 16 wells for the positive control (cells treated with 3 mM cisplatin) and 16 wells for the negative control (cells treated with 0.1% DMSO). To harvest the cells, 1.5 mL of trypsin/EDTA was added per flask and incubated at 37°C in a 5% CO₂ incubator for 2 min. Detached cells were resuspended in pre warmed media to a density of 0.2x10⁶ cells/mL. A total of 20 µL were added to each well of the 384-well plate, giving a final compound concentration of 100 µM and 0.1% v/v DMSO. The plates were incubated 24 h at 37°C in a 5% CO₂ incubator, followed by addition of 20 µL of Cell Titer-Glo reagent (Promega) to each well and the plate was placed upon a linear shaker for 1 minute at room temperature and further incubated at room temperature without shaking for 10 min. Luminescence was read using the EnVision[®] Multilable Reader (PerkinElmer) with 0.5 sec read time per well. The compounds were tested on three different days in duplicate.

2.12 Animal experiment

2.12.1 Mice maintenance

Female inbred BALB/c mice, aged 6-8 weeks were purchased from Harlan Laboratories, UK. Mice were housed in groups of 4 and 5 in a room with controlled temperature 22°C, with a 12 h light/darkness cycle. Animals had access to BK001E Beekay rat and mouse diet (Special Diet Services) and water at all times.

2.12.2 Infection of mice with *C. rodentium* λ stx_{2dact}

LUX marked *C. rodentium* λ stx_{2dact} was cultured overnight in LB at 37°C and subcultured in pre-warmed DMEM and grown to an OD₆₀₀ of 0.8. Bacteria were harvested by centrifugation and resuspended in sterile PBS to get a 100x

concentrate of the original culture. The infection dose was determined by serial dilution of the inoculum and plating onto LB agar plates and was determined to be 3.1×10^{10} CFU/mL.

2.12.3 Preparation of peanut butter/hazelnut cocoa pellets and dosing

Pellets were prepared mixing equal amounts of peanut butter and hazelnut cocoa spread. Approximately $100 \text{ mg} \pm 2.5 \text{ mg}$ of the mixture were dispensed in 1.5 mL eppendorf tubes. The compound furanone C-30 was added from a 10 mM ethanol stock in order to get doses of $4 \mu\text{g}$ per gram of weight. Placebo pellets contained an equal amount of vehicle only. The pellets were thoroughly mixed by hand with a spatula, spun down in a bench centrifuge, and stored at -20°C until use. Doses were voluntarily administered by oral route twice a day at 9:00 and 18:00 hrs using sterile micropipette tips.

2.12.4 Live imaging of infected mice using the IVIS[®] Spectrum system

The extent and location of colonisation in mice was monitored using the IVIS[®] Spectrum imaging system. Animals were anesthetized by inhalation of 2% isofluorane and bioluminescence produced by the LUX marked *C. rodentium* $\lambda\text{stx}_{2\text{dact}}$ strain was measured as photons per second (p/s) using an exposure time of one minute, with large or medium binning.

2.12.5 Faecal shedding bacterial counts

Bacterial colonization was determined by faecal shedding. Faecal samples were collected from individual mice and resuspended in sterile PBS to get a faecal concentration of 100 mg/mL. The samples were incubated at 4°C for 30 min, then vortexed to disrupt the pellets and release the bacteria. After a very short centrifugation, the supernatant was serially diluted using sterile PBS and 10 μL of each dilution were spotted in triplicate onto LB agar plates containing erythromycin and chloramphenicol. The number of colony forming units was

calculated from the dilution that contained between 5-30 colonies. The following equation was used for the calculation of colony forming units (CFUs)

$$\text{CFU/mL} = \frac{(\text{\#colonies})(\text{dilution factor})}{\text{volume plated (mL)}}$$

2.12.6 Tissue collection and histology

To assess the intestinal and kidney damage caused by *C. rodentium* $\lambda\text{stx}_{2\text{dact}}$ in infected mice, at necropsy, distal colon (≈ 0.5 cm) and one kidney were removed, opened longitudinally and placed in 10% formal saline for histological assessment. Five-micrometer tissue sections were cut and stained with H&E stain at the Veterinary Diagnostics department, University of Glasgow. Slides were scanned at the Academic Unit of Medical Genetics and Clinical Pathology, Queen Elizabeth University Hospital and visualized Leica Biosystems visualization software.

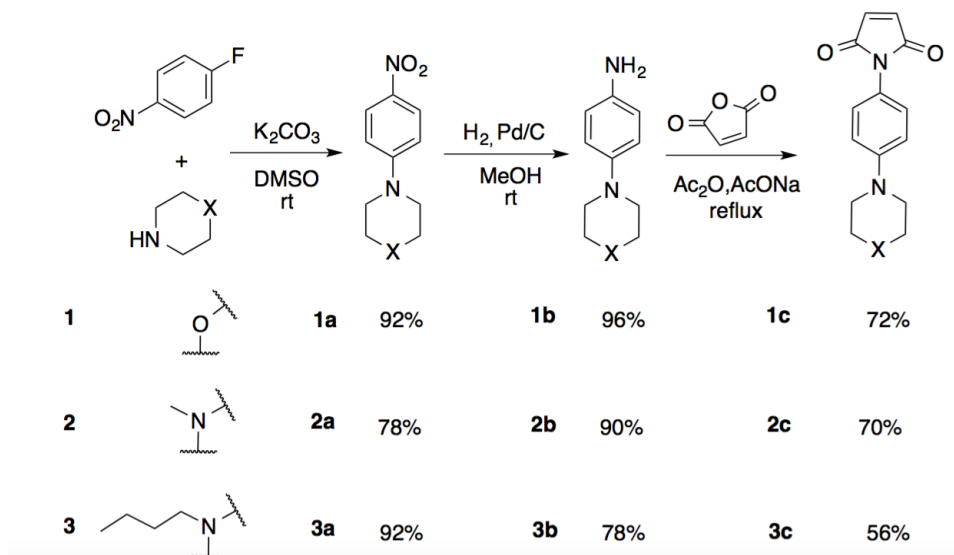
2.13 Organic synthesis

2.13.1 General

All chemicals and solvents were used as received. Tetrahydrofuran, toluene and acetonitrile were purified through a Pure Solv 400-5MD solvent purification system (Innovative Technology, Inc). Solvents were evaporated under reduced pressure at 40°C. All reactions described were performed under argon atmosphere unless otherwise stated and monitored by thin layer chromatography (TLC) with precoated TLC plates (Merck Silica Gel 60 F254). Plates were visualized by UV light (254 nm), iodine vapours or stained with anisaldehyde. Compounds were purified using flash column chromatography using silica gel (Fluro Chem Silica LC 60A) as the stationary phase. ^1H NMR and ^{13}C NMR spectra were recorded at 400 MHz and 100 MHz or at 500 MHz and 125 MHz using either a Bruker DPX Avance400 instrument or a Bruker Avancell500 instrument,

respectively. IR spectra were obtained using a Shimadzu FTIR-8400 spectrometer.

2.13.1.1 Synthesis of AHU compounds



4-(4-nitrophenyl)morpholine (1a). 1-fluoro-4-nitrobenzene (0.50 g, 3.5 mmol) and K_2CO_3 (0.53 g, 3.8 mmol) were stirred in DMSO (0.75 mL) for 0.5 h at room temperature. Then, morpholine (0.30 mL, 3.5 mmol) was added slowly to the reaction mixture and this was left stirring overnight. Subsequently, the contents were poured into ice-water and the precipitate was filtered and dried to afford **1a** (0.6 g, 92%) as a yellow powder.

1-methyl-4-(4-nitrophenyl)piperazine (1b). Following the procedure for compound **1a**, 1-fluoro-4-nitrobenzene (0.50 g, 3.5 mmol), K_2CO_3 (0.53 g, 3.8 mmol), DMSO (0.75 mL) and 1-methylpiperazine (0.40 mL, 3.5 mmol) afforded **1b** (0.72 g, 92%) as a yellow powder. The NMR data obtained is in accordance with the literature.

1H NMR ($CDCl_3$, 400 MHz): 8.14 (2H, d, $J=9.5$ Hz), 6.85 (2H, d, $J=9.5$ Hz), 3.46 (4H, m), 2.58 (4H, m), 2.38 (3H, s).

1-butyl-4-(4-nitrophenyl)piperazine (1c). Following the procedure for compound **1a** 1-fluoro-4-nitrobenzene (0.50 g, 3.5 mmol), K_2CO_3 (0.53 g, 3.8 mmol), DMSO (0.75 mL) and 1-butylpiperazine (0.50 mL, 3.5 mmol) afforded **1c** (0.72 g, 78%) as a yellow powder.

^1H NMR (CDCl_3 , 400 MHz): 8.15 (2H, d, $J=9.5$ Hz), 6.85 (2H, d, $J=9.5$ Hz), 3.47 (4H, m), 2.61 (4H, m), 2.43 (2H, m), 1.54 (2H, m), 1.35 (2H, sextet, 7.2 Hz), 0.97 (3H, t, 7.3 Hz).

4-morpholinoaniline (1b). To a mixture of 4-(4-nitrophenyl)morpholine (0.50 g, 2.4 mmol) in anhydrous methanol (7 mL) under atmosphere of argon was added Pd/C (50 mg, 10%) followed by replacement of the argon with a hydrogen atmosphere. The reaction mixture was stirred at room temperature until completion (2 h). The crude mixture was filtered over celite and the methanol was removed in vacuo to afford **1b** (0.41 g, 96%) as a beige powder.

^1H NMR (CDCl_3 , 400 MHz): 6.83 (2H, d, $J=8.8$ Hz), 6.70 (2H, d, $J=8.8$ Hz), 3.88 (4H, m), 3.05 (4H, m).

4-(4-methylpiperazin-1-yl)aniline (2b). Following the procedure for compound **2a**, 1-methyl-4-(4-nitrophenyl)piperazine (0.70 g, 3.1 mmol), anhydrous methanol (15 mL) and Pd/C (70 mg, 10%) afforded **2b** (0.47 g, 78%) as a brown powder. The NMR data obtained is in accordance with the literature (Galstukhova N. B et al 1972).

^1H NMR (CDCl_3 , 400 MHz): 6.85 (2H, d, $J=8.9$ Hz), 6.69 (2H, d, $J=8.9$ Hz), 3.10 (4H, m), 2.61 (4H, m), 2.38 (3H, s).

4-(4-butylpiperazin-1-yl)aniline (3b). Following the procedure for compound **2a**, 1-butyl-4-(4-nitrophenyl)piperazine (0.70 g, 2.7 mmol), anhydrous methanol (15 mL) and Pd/C (70 mg, 10%) afforded **3b** (0.63 g, 90%) as a brown powder.

^1H NMR (CDCl_3 , 400 MHz): 6.84 (2H, d, $J=8.9$ Hz), 6.67 (2H, d, $J=8.9$ Hz), 3.09 (4H, m), 2.63 (4H, m), 2.41 (2H, m) 1.53 (2H, m) 1.37 (2H, sextet, $J=7.2$ Hz) 0.95 (3H, t, $J=7.3$ Hz).

1-(4-morpholinophenyl)-1H-pyrrole-2,5-dione (1c). A solution of 4-morphoaniline (0.20 g, 1.1 mmol) in DCM (5 mL) was treated by the slow addition of maleic anhydride (0.10 g, 1.1 mmol). The reaction was stirred at room temperature for 1 h. Then, the DCM was removed in vacuo to afford the maleanilic acid, which was dissolved in acetic anhydride (5 mL) and sodium acetate (22 mg, 10%). The mixture was heated for 2 h under reflux. Then the reaction was cooled down, quenched with water and neutralised with a K_2CO_3

saturated solution. The solution was then transferred to a separation funnel and extracted with DCM. The combined organic layers were dried with Na_2SO_4 and concentrated in vacuo. The product was purified through column chromatography (petroleum ether/AcOEt, 5/5) giving 0.20 g (72%) of **1c** as an orange powder.

^1H NMR (CDCl_3 , 400 MHz): 7.13 (2H, d, $J=9.1$ Hz), 6.89 (2H, d, 9.1 Hz), 6.75 (2H, s), 3.79 (4H, m), 3.11 (4H, m).

^{13}C NMR (CDCl_3 , 100 MHz): 169.9, 150.9, 134.1, 127.1, 122.8, 115.7, 66.8, 48.9.

IR ν_{max} (film)/ cm^{-1} 30071, 2358, 1707, 1517. MS (EI) calcd for $\text{C}_{14}\text{H}_{14}\text{N}_2\text{O}_3$ $[\text{M}]^+$ 258.10 m/z, found 258.2 m/z.

1-(4-(4-methylpiperazin-1-yl)phenyl)-1H-pyrrole-2,5-dione (2c). Following the procedure for compound **1c**, 4-(4-methylpiperazin-1-yl)aniline (0.2 g, 1.04 mmol), maleic anhydride (0.1 g, 1.12 mmol), DCM (5 mL), acetic anhydride (5 mL) and sodium acetate (22 mg, 10%) yielded 0.13 g (56.2%) as an orange solid.

^1H NMR (CDCl_3 , 400 MHz): 7.22 (2H, d, $J=9.1$ Hz), 7.01 (2H, d, $J=9.1$ Hz), 6.86 (2H, s), 3.28 (4H, m), 2.61 (4H, m), 2.39 (4H, m).

^{13}C NMR (CDCl_3 , 100 MHz): 169.9, 150.9, 134.1, 127.1, 122.3, 116.6, 55.8, 48.7, 46.1.

IR ν_{max} (film)/ cm^{-1} 3089, 2947, 2804, 2359, 1700, 1517. MS (EI) calcd for $\text{C}_{15}\text{H}_{17}\text{N}_3\text{O}_2$ $[\text{M}]^+$ 271.13 m/z, found 271.2 m/z.

1-(4-(4-butylpiperazin-1-yl)phenyl)-1H-pyrrole-2,5-dione (3c). Following the procedure for compound **1c**, 4-(4-butylpiperazin-1-yl)aniline (0.2 g, 0.85 mmol), maleic anhydride (0.08, 0.85 mmol), DCM (5 mL), acetic anhydride (5 mL) and sodium acetate (22 mg, 10%) yielded 0.19 g (70%) as an orange solid.

^1H NMR (CDCl_3 , 400 MHz): 7.22 (2H, d, $J=9.1$ Hz), 7.01 (2H, d, $J=9.1$ Hz), 6.86 (2H, s), 3.28 (4H, m), 2.61 (4H, m), 2.39 (4H, m).

^{13}C NMR (CDCl_3 , 100 MHz): 169.9, 150.9, 134.1, 127.1, 122.2, 116, 58.4, 53.1, 48.7, 29, 20.7, 14.

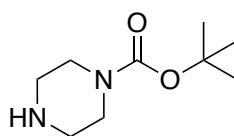
IR ν_{\max} (film)/ cm^{-1} 3086, 2925, 2359, 1700, 1517. MS (EI) $[\text{M}]^+$ calcd for $\text{C}_{18}\text{H}_{23}\text{N}_3\text{O}_2$ 313.18, found 313.3 m/z .

2-(4-morpholinophenyl)isoindoline-1,3-dione. Following the procedure for compound **1c**, 4-morpholinoaniline (0.090 g, 0.5 mmol), maleic anhydride (0.07 g, 0.5 mmol), DCM (3 mL), acetic anhydride (3 mL) and sodium acetate (0.01 g, 10%) yielded 0.14 g (96.5%) as a yellow solid.

^1H NMR (CDCl_3 , 400 MHz): 7.96 (2H, dd, $J = 5.5, 3$ Hz), 7.80 (2H, dd, $J = 5.4, 3$ Hz), 7.34 (2H, m), 7.03 (2H, m), 3.90 (4H, m), 3.24 (4H, m).

^{13}C NMR (CDCl_3 , 100 MHz): 167.6, 150.9, 134.2, 131.9, 127.4, 123.6, 123.2, 115.78, 66.83, 49. IR ν_{\max} (film)/ cm^{-1} 2952, 2864, 2364, 1707, 1517.

***tert*-butyl piperazine-1-carboxylate (ii)**

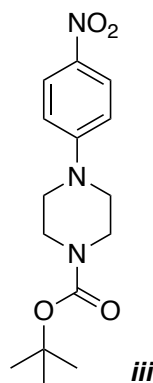


ii

A solution of di-*tert*-butyl-dicarbonate (1.26 g, 5.77 mmol) in *i*-PrOH (7.5 mL) was added dropwise to a stirring solution of piperazine (1 g, 11 mmol) in *i*-PrOH (7.5 mL) and NaOH (0.6 mL of a 2.5 M solution). The reaction mixture was stirred at room temperature for 2 h. The solvent was evaporated in rotavapor. The solid was redissolved in H_2O (7 mL) and the 1,4-diprotected piperazine was filtered off. The pH of the aqueous layer was increased to 10 using saturated NaHCO_3 solution and extracted with CH_2Cl_2 (3x40 mL). The combined organic layers were dried with Na_2SO_4 and concentrated *in vacuo* to give a white solid (0.9 g, 83%). The NMR data is in accordance with the literature (M. T. Wu et al. 1990).

^1H NMR (CDCl_3 , 400 MHz) δ (ppm): 3.24 (4H, m), 2.66 (4H, m), 1.31 (9H, br s).

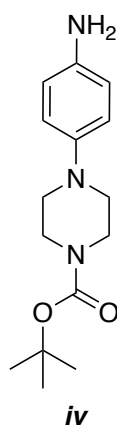
***tert*-butyl-4-(4-nitrophenyl)piperazine-1-carboxylate (iii)**



To a mixture of *tert*-butyl piperazine-1-carboxylate (0.2 g, 1 mmol), K_2CO_3 (0.17 g, 1.2 mmol), in DMSO (1 mL) was added 4-fluoronitrobenzene (0.17 g, 1.2 mmol) dissolved in DMSO (0.5 mL). The reaction mixture was stirred at room temperature overnight. The crude mixture was washed with a $NaHCO_3$ saturated solution (3x20 mL) and brine (3x20 mL) and extracted with CH_2Cl_2 (3x30 mL). The combined organic layers were dried with Na_2SO_4 and concentrated in *vacuo*. The product was obtained as a yellow powder (0.26 g, 81%). The NMR data is in accordance with the literature (Patel and Telvekar 2014).

1H NMR ($CDCl_3$, 400 MHz) δ (ppm): 8.05 (2H, *d*, $J=9.4$ Hz), 6.76 (2H, *d*, $J = 9.4$ Hz), 3.54 (4H, *m*), 3.35 (4H, *m*), 2.53 (9H, *br s*)

***tert*-butyl-4-(4-aminophenyl)piperazine-1-carboxylate (*iv*)**

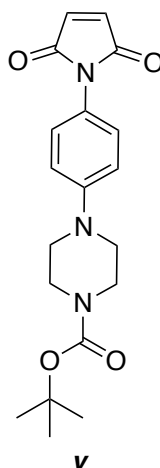


To a mixture of *tert*-butyl-4-(4-nitrophenyl)piperazine-1-carboxylate (0.1 g, 0.3 mmol) in anhydrous methanol (5 mL) under atmosphere of argon was added Pd/C (0.01 g, 10% w/w) followed by replacement of argon with a hydrogen atmosphere. The reaction mixture was stirred at room temperature until completion (3 h). The crude mixture was filtered over celite and the methanol

was concentrated *in vacuo* to afford *iv* (0.084 g, 92%) as a brown powder. The NMR data is in accordance with the literature (VanderWel et al. 2005).

^1H NMR (CDCl_3 , 400 MHz) δ (ppm): 6.81 (2H, d, $J = 8.8$ Hz), 6.65 (2H, d, $J = 8.8$ Hz), 3.55 (4H, m), 2.98 (4H, m), 1.49 (9H, s).

***tert*-butyl 4-(-4-(2,5-dioxo-2,5-dihydro-1H-pyrrol-1-yl)phenyl)piperazine-1-carboxylate (*v*)**

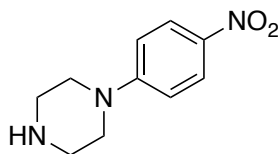


To a solution of *tert*-butyl-4-(4-aminophenyl)piperazine-1-carboxylate (0.2 g, 0.72 mmol) in DCM (5 mL) was dropwise added a solution of maleic anhydride (0.15 g, 1.53 mmol) in DCM (2 mL). The reaction was stirred at room temperature for 1 h. Then, the CH_2Cl_2 was evaporated *in vacuo* to afford the maleanilic acid, which was redissolved in acetic anhydride (5 mL) and sodium acetate (0.04 g, 0.49 mmol). The mixture was heated for 2 h under reflux. Then the reaction was cooled down, quenched with water (7 mL) and neutralised with K_2CO_3 (10 mL) saturated solution. The solution was then extracted with CH_2Cl_2 (3 x 20 mL). The combined organic layers were dried with Na_2SO_4 and concentrated *in vacuo*. The product was purified through column chromatography (petroleum ether/AcOEt, 5/5) giving *v* (0.16 g, 63%) as a red powder.

^1H NMR (CDCl_3 , 400 MHz) δ (ppm): 7.13(2H, d, $J = 9.1$ Hz), 6.91 (2H, d, $J = 9.1$ Hz), 6.76 (2H, s), 3.51 (4H, m), 3.10 (4H, m), 1.42 (9H, s).

^{13}C NMR (CDCl_3 , 125 MHz) δ (ppm): 170.1, 154.7, 148.5, 135.9, 130.7, 121.8, 118.5, 80.4, 50.1, 43.2, 28.3

1-(4-nitrophenyl)piperazine (*xvii*)

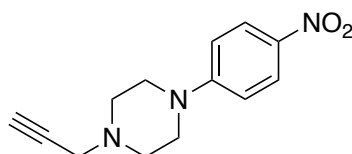


xvii

To a mixture of piperazine (0.4 g, 4.6 mmol), K_2CO_3 (0.73 g, 5.42 mmol), TBAI (0.013 g, 0.035 mmol) in DMSO (1 mL) was added 4-fluoronitrobenzene (0.50 g, 3.5 mmol) dissolved in DMSO (0.5 mL). The reaction mixture was stirred at room temperature overnight. The crude mixture was washed with a $NaHCO_3$ saturated solution and brine and extracted with CH_2Cl_2 . The combined organic layers were dried with Na_2SO_4 and concentrated in vacuo. The product was obtained as a yellow powder (0.77 g, 81%). The NMR data is in accordance with the literature (Hepperle, Eckert, and Gala 1999).

1H NMR ($CDCl_3$, 400 MHz) δ : 8.16 (2H, *d*, $J = 9.5$ Hz), 6.86 (2H, *d*, $J = 9.5$ Hz), 3.41 (4H, *m*), 3.06 (4H, *m*).

1-(4-nitrophenyl)-4-(prop-2-yn-1-yl)piperazine (*xviii*)



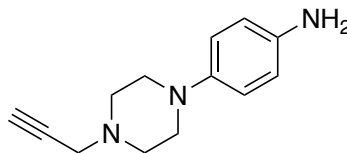
xviii

A solution of 1-(4-nitrophenyl)piperazine (0.20 g, 0.96 mmol) and K_2CO_3 (0.40 g, 2.9 mmol) in MeCN (5 mL) was treated by the slow addition of propargyl bromide (0.10 mL, 1.3 mmol) dissolved in MeCN (1 mL). The mixture was heated overnight at $90^\circ C$. Then the reaction was cooled down, washed with a $NaHCO_3$ saturated solution and AcOEt. The combined organic layers were dried with Na_2SO_4 and concentrated in vacuo. The product was purified through column chromatography (petroleum ether/AcOEt, 5/5) giving *xviii* (0.05 g, 21%) as a yellow powder. The NMR data obtained is in accordance with the literature (Risseuw et al. 2013).

1H NMR ($CDCl_3$, 400 MHz) δ : 6.84 (2H, *d*, $J = 8.6$ Hz), 6.62 (2H, *d*, $J = 8.7$ Hz), 3.35

(2H, *d*, $J=2.4$ Hz), 3.08 (4H, *m*), 2.71 (4H, *m*), 2.28 (1H, *t*, $J=2.4$ Hz)

4-(4-(prop-2-yn-1-yl)piperazin-1-yl)aniline (*xix*)

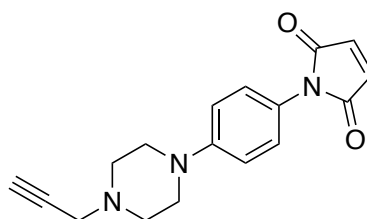


xix

A solution of 1-(4-nitrophenyl)-4-(prop-2-yn-1-yl)piperazine (0.14 g, 0.57 mmol), SnCl_2 (0.64 g, 2.9 mmol) in EtOH (5 mL) was heated overnight at 70°C . The reaction was cooled down and the pH of the crude mixture was increased to 7-8 using a NaHCO_3 saturated solution. The compound was extracted with AcOEt. The combined organic layers were dried with Na_2SO_4 and concentrated *in vacuo*. The product was purified through column chromatography (AcOEt/MeOH:Ammonia 90/10) giving ***xix*** (0.10 g, 87%) as a brown solid. The NMR data obtained is in accordance with the literature (Risseuw et al. 2013).

^1H NMR (CDCl_3 , 400 MHz) δ : 6.84 (2H, *d*, $J = 8.6$ Hz), 6.62 (2H, *d*, $J = 8.7$ Hz), 3.4 (2H, *br s*), 3.35 (2H, *d*, $J = 2.4$ Hz), 3.08 (4H, *m*), 2.71 (4H, *m*), 2.28 (1H, *t*, $J = 2.4$ Hz)

1-(4-(4-(prop-2-yn-1-yl)piperazin-1-yl)phenyl)-1H-pyrrole-2,5-dione (*xx*)



xx

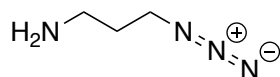
To a solution of 4-(4-(prop-2-yn-1-yl)piperazin-1-yl)aniline (0.1 g, 0.5 mmol) in DCM (5 mL) was dropwise added a solution of maleic anhydride (0.05 g, 0.5 mmol) in CH_2Cl_2 (2 mL). The reaction was stirred at room temperature for 1 h. Then, the CH_2Cl_2 was evaporated *in vacuo* to afford the maleanilic acid, which was redissolved in acetic anhydride (5 mL) and sodium acetate (0.01 g, 0.12 mmoles). The mixture was heated for 2 h under reflux. Then the reaction was

cooled down, quenched with water (5 mL) and neutralised with K_2CO_3 (10 mL) saturated solution. The solution was then transferred to a separation funnel and extracted with CH_2Cl_2 . The combined organic layers were dried with Na_2SO_4 and concentrated *in vacuo*. The product was purified through column chromatography (petroleum ether/AcOEt, 5/5) giving **xx** (0.07 g, 52%) as a red solid.

1H NMR ($CDCl_3$, 400 MHz) δ : 7.48 (2H d $J=10.1$ Hz), 7.21 (2H, d, $J=9.1$ Hz), 7.10 (2H, d, $J=9.1$ Hz), 3.40 (2H, d, $J=2.5$ Hz), 3.30 (4H, m), 2.76 (4H, m), 2.31 (1H, t, $J=2.5$ Hz)

^{13}C NMR ($CDCl_3$, 125 MHz) δ : 169.5, 148.1, 135.1, 131.3, 120.5, 116.4, 75.9, 72.8, 51.1, 50.1, 42.1.

3-azidopropan-1-amine (**xi**)

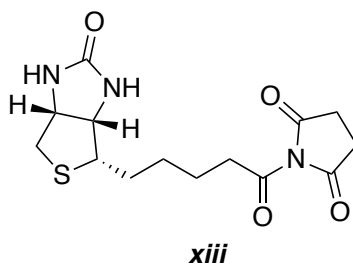


xi

To a solution of 3-chloropropylamine hydrochloride (1.2 g) dissolved in water, sodium azide was added. The reaction mixture was heated to $80^\circ C$ overnight. Adding saturated K_2CO_3 aqueous solution increased the pH of the solution and the compound was extracted with Et_2O (3x50 mL). The combined organic layers were dried with Na_2SO_4 , filtered and concentrated in rotavapor. A light yellow volatile liquid was obtained. The NMR data obtained is in accordance with the literature (Landi et al. 2010).

1H NMR ($CDCl_3$, 400 MHz) δ : 3.35 (2H, t, $J=6.8$ Hz), 2.90 (2H, $J=6.8$ Hz), 1.83 (2H, *quintet*, $J=6.8$ Hz), 1.35 (2H, *br s*).

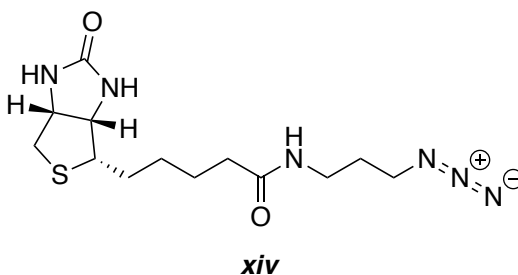
1-(5-((3a*S*,4*S*,6a*R*)-2-oxohexahydro-1*H*-thieno[3,4-*d*]imidazol-4-yl)pentanoyl)pyrrolidine-2,5- dione (*xiii*)



To a solution of (D)-biotin (0.97 g, 4 mmol) in DMF (4 mL) was added *N*-hydroxysuccinimide (0.68 g, 6 mmol) and the reaction was stirred at room temperature overnight. Ice-water was added to the reaction flask and the precipitate was filtered, washed with water (3 x 5 mL) and dried in rotavapor. A white solid (0.78 g, 60%) was obtained. The NMR data obtained is in accordance with the literature (F. Yu et al. 2013).

^1H NMR (CDCl_3 , 400 MHz) δ : 5.22 (1H, *s*), 4.94 (1H, *s*), 4.53 (1H, *m*), 4.33 (1H, *m*), 3.15 (1H, *m*), 2.88-2.96 (1H, *m*), 2.85 (4H, *s*), 2.75 (1H, *d*, $J=12.8$ Hz), 2.57-2.71 (2H, *m*), 1.6-1.91 (4H, *m*), 1.51-1.59 (2H, *m*).

***N*-(3-azidopropyl)-5-((3a*S*,4*S*,6a*R*)-oxohexahydro-1*H*-thieno[3,4-*d*]imidazole-4-yl)pentanamide (*xiv*)**



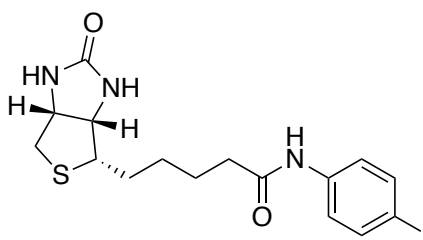
To a solution of **22** (0.1 g, 0.30 mmol) in anhydrous methanol (4 mL) was added 3-azidopropan-1-amine (0.075 g, 0.75 mmol). The reaction was stirred overnight at room temperature. The crude was purified by column chromatography using CH_2Cl_2 :MeOH: NH_4OH (9:1:0.1) giving **xiv** as a white solid (0.047 g, 48%). The NMR data obtained is in accordance with the literature (F. Yu et al. 2013).

^1H NMR (CD_3OD , 400 MHz) δ : 4.65 (1H, *dd*, $J=7.1$ Hz), 4.48 (1H, *dd*, $J=7.5$ Hz),

3.53 (2H, *t*, $J=6.8$ Hz), 3.41 (2H, *t*, $J=6.8$ Hz), 3.37 (2H, *m*), 3.10 (1H, *dd*, $J=5.3, 12.8$ Hz), 2.39 (2H, *t*, $J=7.2$ Hz), 1.98-1.77 (6H, *m*), 1.65-1.59 (2H, *m*).

^{13}C NMR (CD_3OD , 125 MHz) δ : 176.1, 166.2, 63.4, 61.7, 57.1, 50.3, 41.1, 37.8, 36.9, 29.8, 29.6, 26.9.

***N*-(4-iodophenyl)-5-((3*a*S,4*S*,6*a*R)-2-oxohexahydro-1*H*-thieno[3,4-*d*]imidazole-4-yl)pentanamide (*xxiii*)**



xxiii

To a solution of (D)-biotin (0.05g, 0.2 mmoles) in anhydrous CH_2Cl_2 (3 mL) was added EDCl (0.047g, 0.25 mmoles), DMAP (0.037 g, 0.3 mmoles) and the reaction mixture was heated to reflux for 30 min. Then, 4-iodoaniline was added and the reaction mixture was stirred overnight under reflux. The crude was purified by column chromatography using $\text{CH}_2\text{Cl}_2:\text{MeOH}:\text{NH}_4\text{OH}$ (9:1:0.1) giving *xxiii* as a white powder (0.026g, 30%).

^1H NMR (CD_3OD , 400 MHz) δ : 7.45 (2H, *dd*, $J=8.67$ Hz), 6.86 (2H, *dd*, $J=8.67$ Hz), 2.98-2.85 (1H, *m*), 2.79 (2H, *s*), 2.70 (1H, *d*, $J=12.8$ Hz), 2.8-2.4 (2H, *m*), 1.8-1.6 (4H, *m*), 1.57-1.50 (2H, *m*).

^{13}C NMR (CD_3OD , 125 MHz) δ (ppm): 175.2, 160.2, 136.1, 135.6, 124.8, 96.2, 66.4, 62.7, 54.2, 36.9, 32.6, 31.8, 23.8, 23.0

CHAPTER 3

Identification and characterisation of novel
compounds blocking Shiga toxin expression in
Escherichia coli O157:H7

3 Identification and characterisation of novel compounds blocking Shiga toxin expression in *Escherichia coli* O157:H7

3.1 Introduction

Production of Shiga toxin by EHEC is essential for the development of HUS in infected patients. The use of conventional antibiotics results in increased Stx release and thus greater risk of HUS manifestation. New therapeutic strategies that aim to prevent or decrease the production of Stx may be an effective way to prevent EHEC-mediated disease.

Recently, in order to identify potential inhibitors of Shiga toxin expression in *E. coli* O157:H7, a high-throughput screen (HTS) of 17,500 compounds using a *stx2::GFP* reporter assay was performed. A total of 76 hit compounds were identified in the primary screen, which were then narrowed to 6 compounds following dose-response validation assays. This was followed by the generation of a focused set of derivatives based on the best performing compound in order to get structure-activity (SAR) information and improve their activity. This optimisation resulted in the compound AHU3, a 2,5-pyrroledione synthesised in four steps (Figure 14). SAR studies determined that the 2,5-pyrroledione moiety was responsible for activity, whilst the two remaining rings could tolerate manipulations.

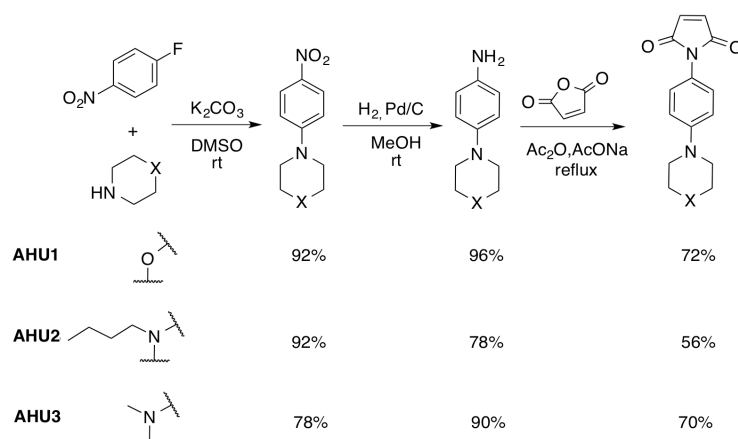


Figure 14 Synthesis of compounds with inhibitory activity against Shiga toxin expression

Once the compound was proven active against Stx expression, the next step was therefore the elucidation of the molecular mechanism responsible for activity. The work presented in this chapter describes the approaches used to find the molecular target of AHU3. Our data suggests that the compound interferes with the SOS response and autocleavage of the λ phage repressor *ci* by directly affecting the activity and oligomerization of RecA, thus limiting prophage induction and *stx2* expression. The findings suggests that RecA is highly susceptible to inhibition and that targeting this protein is a viable approach to limiting production of Stx2 by STEC.

3.2 Biological assay used in the screening

As previously described, Shiga toxin is expressed at very low levels under non-inducing conditions and its expression is up-regulated in the presence of DNA-damaging agents that activate the bacterial SOS response. Under laboratory conditions this is usually achieved by addition of MMC, a potent DNA crosslinker. In order to identify potential small-molecule inhibitors of *stx2*, the *pstx2::GFP* promoter fusion plasmid containing the *stx2* promoter fused to the GFP gene was transformed into Stx-negative *E. coli* Sakai ZAP0273 strain. The compounds were tested in bacterial cultures in mid-logarithmic growth, and the SOS response was

induced by addition of 1 $\mu\text{g}/\text{mL}$, a concentration low enough to allow the growth during the first couple of hours but that eventually leads to bacteriophage induced lysis after 3-4 h. Fluorescence and bacterial growth were monitored at intervals of 1 h, for a 6-8 h after addition of the compounds and MMC (Figure 15).

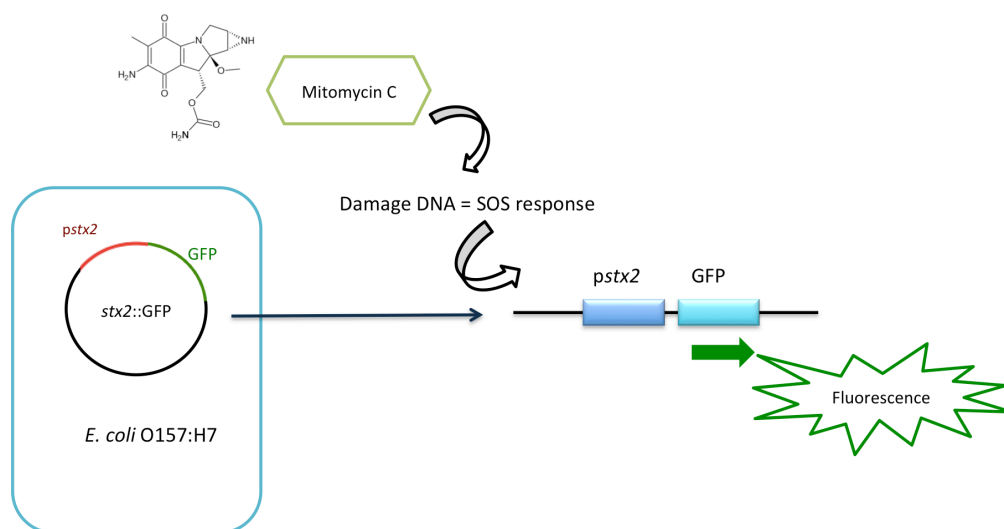


Figure 15 *pstx2::GFP* reporter assay.

The lysogenic Stx-negative Sakai *E. coli* strain transformed with *pstx2::GFP* reporter fusion are treated with a DNA damaging agent (mitomycin C). Induction of the SOS response leads to activation of the *stx2* promoter, which can be measured as means of fluorescence. Any small-molecule with that has an antagonistic effect on the expression of Stx will therefore cause a decrease in fluorescence.

3.3 Identification of a hit compound with inhibitory activity on *stx2* expression

Using the *stx2::GFP* reporter assay previously described, a high throughput screening of small molecules was carried out at the Laboratory for Chemical Biology, Umeå. The ChemBridge library comprised 17,500 chemically diverse compounds that have previously proven valuable for the identification of novel therapeutics. Compounds were initially tested at a concentration of 50 μM for the ability to suppress MMC-induced expression of *stx2::GFP* in ZAP0273. Two additional reporter fusions were used in the screen, *sulA::GFP* and *rpsM::GFP*.

SulA is a LexA regulated protein essential for the arrest of cell division during SOS response, and the *rpsM* promoter activity (30S ribosomal subunit) was chosen as a housekeeping gene control as it is not related to Stx expression. In total 76 hits, comprising 48 compounds that reduced fluorescence in the *stx2*::GFP screen only and 28 compounds that reduced fluorescence in the *stx2*::GFP and *sulA*::GFP screen, were selected (Figure 16).

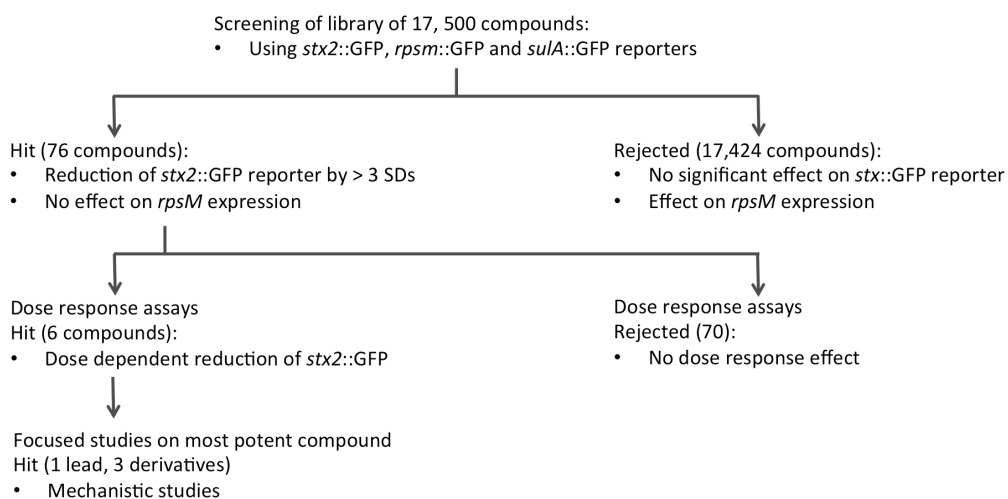


Figure 16 Flow chart summarizing the HTS of the ChemBridge library.

A library of 17,500 compounds was screened using *stx2*::GFP, *rpsM*::GFP and *sulA*::GFP reporter fusions. Seventy-six compounds that showed significant activity on *stx2*::GFP and *sulA*::GFP were identified from this initial screen, and further dose-response assays narrowed this to six hits that reduced *stx2*::GFP expression in a dose-dependent manner. The single most potent compound was taken forward for mechanistic studies.

For the hit validation step, the compounds were studied in dose-response experiments. Concentrations of compounds ranging from 0.2 to 200 μ M were prepared using 2-fold serial dilutions. The dose-response experiments were performed in the *stx2*::GFP and *rpsM*::GFP reporter assay to evaluate inhibitor potency and specificity, respectively. From the initial screen of 76 primary hits, 6 compounds showed a reproducible dose-dependent reduction of MMC-induced *stx2*::GFP expression. The most effective of these was the Hit2Lead compound ID 5324836, a phenyl pyrroledione henceforth called AHU1. The compound showed a reproducible dose-dependent reduction of MMC-induced *stx2*::GFP expression (Figure 17).

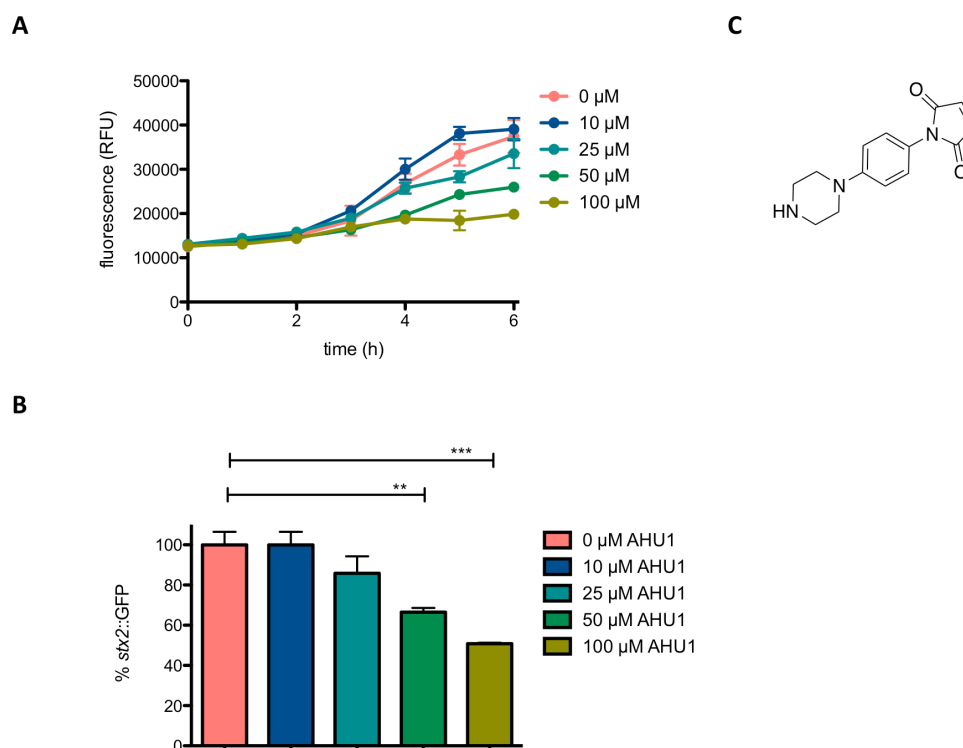


Figure 17 Effect of AHU1 on *stx2*::GFP expression.

ZAP0273 transformed with *pstx2*::GFP was cultured in the presence of 25- 100 μM AHU1, and induced with 1 μg/ml MMC. Expression of *stx2*::GFP was measured by fluorescence. (A) Inhibition of MMC-induced *stx2*::GFP expression by AHU1 over time. (B) AHU1 significantly decreases *stx2*::GFP expression in a dose dependent manner. (C) Chemical structure of AHU1, a phenyl pyrroledione. Experiments were performed in triplicate, and data plotted as the mean with standard deviation from the mean displayed by error bars

Bacterial growth was also monitored during the assay. An interesting observation was that the compound was also able to block the MMC-induced phage mediated lysis, at concentrations 50 and 100 μM (Figure 18). More importantly, the compound did not affect bacterial growth rate in the absence of MMC, a desirable feature in anti-virulence drugs.

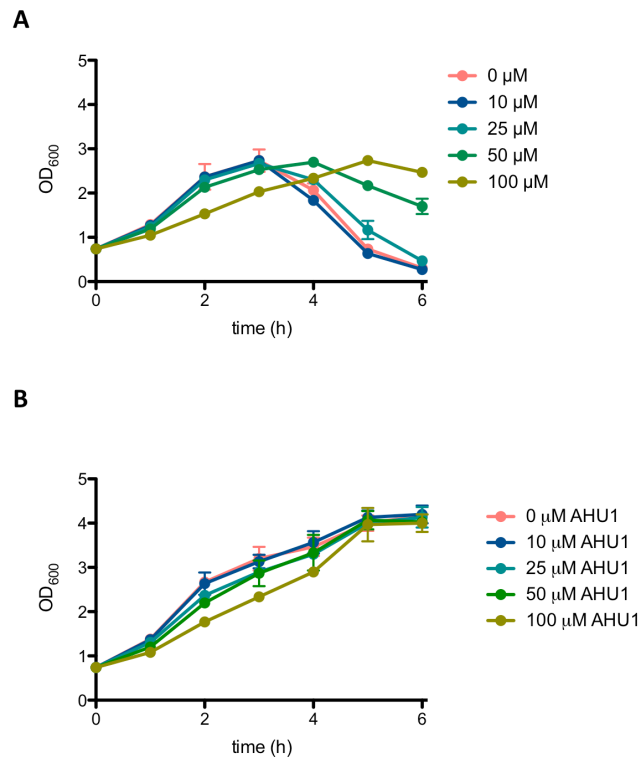


Figure 18 The compound AHU1 does not inhibit MMC-induced lysis and does not interfere with bacterial growth rate.

(A) Inhibition of MMC-induced lysis by AHU1. (B) Effect of AHU1 on bacterial growth in the absence of MMC. Experiments were performed in triplicate, and data plotted as the mean with standard deviation from the mean displayed by error bars.

In order to obtain an IC_{50} for the AHU compounds, a range of different concentrations were tested in the *stx2::GFP* assay. The IC_{50} values obtained were AHU1= 17 μ M, AHU2=30 μ M and AHU3=19 μ M (Figure 19).

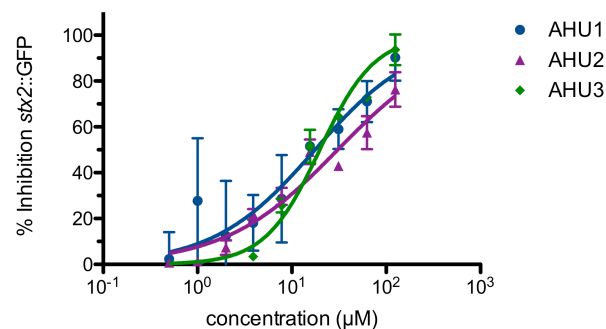


Figure 19 Phenotypic half maximum inhibitory concentration for the AHU compounds.

Different concentrations of the compounds were analysed in the *stx2::GFP* assay. The IC_{50} values obtained were AHU1= 17 μ M, AHU2=30 μ M and AHU3=19 μ M

Three structural analogues of AHU1 were synthesized in order to get structure-activity relationship (SAR) information on AHU1 (Figure 20-C). Evaluation of the three analogues against AHU1 revealed that the maleimide moiety was essential for activity, and a more potent inhibitor was obtained: AHU3. The compound AHU3 produced a greater increase in inhibitions at 25 μM when compared to AHU1 (Figure 20-A). Thus, it was selected for use in all further experiments.

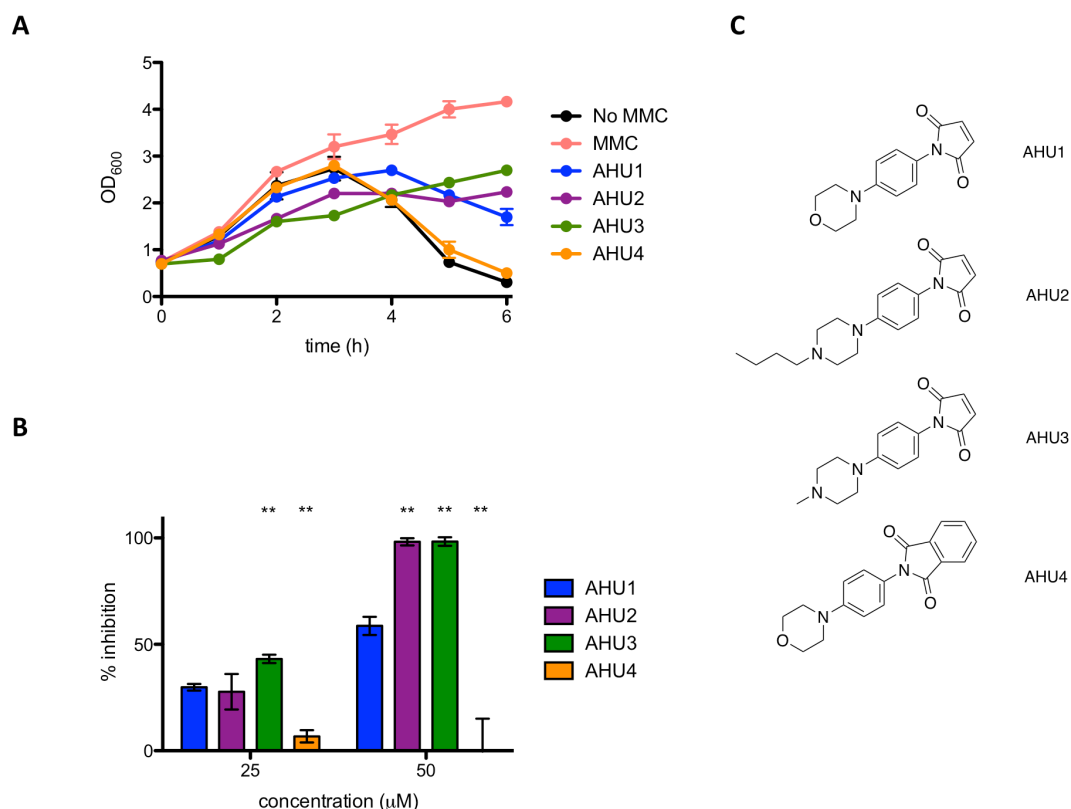


Figure 20 Comparison of activity between the analogues AHU1-4.

(A) Inhibition of MMC-induced bacterial lysis after addition of AHU1-4 and MMC. AHU3 showed to be more potent compared to the other compounds. (B) Inhibition of *stx2*::GFP expression by 25 and 50 μM AHU1-4 at 6 h after addition of AHU1-4 and MMC. (C) Chemical structures of the AHU compounds. Data were calculated from triplicate experiments and displayed as the mean inhibition with error bars showing the standard deviation from the mean. Asterisks indicate a significant difference (** $p < 0.001$) from the original AHU1 concentration inhibition, determined by Student's unpaired *t*-test

3.4 The compound AHU3 affects phage lytic development

When the compound AHU3 was tested on the *stx2::GFP* reporter assay, it was observed that the compound also blocked phage mediated lysis, in comparison to the untreated control. This observation prompted exploration in more detail of the effect of the compound on prophage induction in EHEC. To this end, phage transduction assays were performed using the strain *E. coli* JP10819 that carries only the lysogenic Stx2 prophage ϕ P27, which contains a tetracycline resistance cassette inserted into the *stx2* gene (Quiles-Puchalt et al. 2014). The Stx2 prophage was induced by the addition of mitomycin C (MMC) in the presence and absence of 50 μ M AHU3, and the phages produced were isolated by filtration. The non-lysogenic *E. coli* strain K-12 MG1665 was used as a recipient strain, which was treated with serial dilutions of the cell lysate and grown on agar plates containing tetracycline.

As shown in figure 21, bacterial cultures that were not induced with MMC produced low levels of Stx phage (10^4 PFU/mL), whereas the presence of MMC increased the levels by four logs to 10^8 . The presence of 50 μ M of AHU3 significantly decreased the amount of Stx phage produced with a titre of 10^5 PFU/mL. This demonstrated that the compound inhibits the production of functional Stx phages.

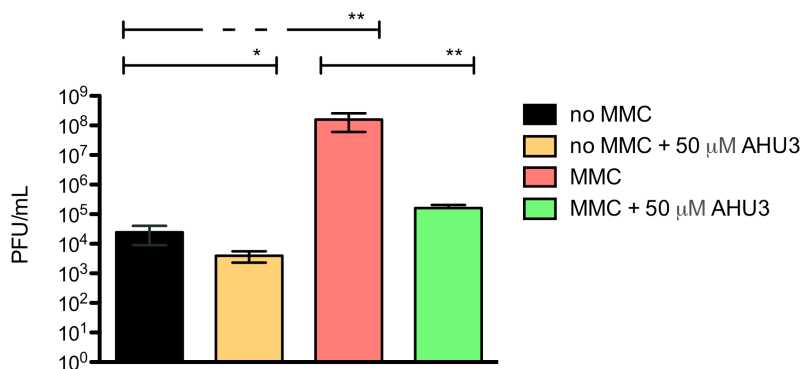


Figure 21 The compound AHU3 affects MMC-induced phage lytic development.

Induction of JP10819 with 2 μ g/ml MMC resulted in significantly increased Stx phage production. Addition of 50 μ M AHU3 produced a significant decrease in phage production by both non-induced and MMC-induced JP10819. The interaction between MMC and AHU3 was determined to be

significant ($p < 0.001$), implying that the reduction in phage production by MMC-induced cells observed is not the result of the inhibitory effect of AHU3 on bacterial growth. The data shown are the average of triplicate individual experiments with standard deviation from the mean displayed as error bars. Statistical significance was determined by GLM analysis

The next step was studying if the compound also had effect on phage-mediated lysis in Gram-positive bacteria. To assess this, the strain of *Staphylococcus aureus* JP5011, which carries the ϕ SLT phage containing a tetracycline resistance cassette inserted into the *plv* gene, was used. Induction of *S. aureus* JP5011 with MMC produced approximately 10^6 PFU/mL. Addition 50 μ M of AHU3 decreased the titre more than a log as shown in Figure 22.

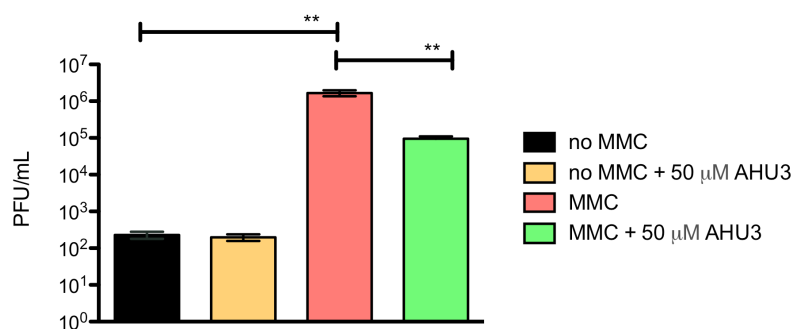


Figure 22 AHU3 also affects phage lytic development in *S. aureus*.

Induction of JP5011 with 2 μ g/ml MMC resulted in significantly increased SLT phage production. Addition of 50 μ M AHU3 produced a significant decrease in phage production by MMC-induced JP5011. Asterisks indicate a significant difference ($*p < 0.05$, $**p < 0.001$) in phage production between the groups indicated by capped lines. The data shown are the average of triplicate individual experiments with standard deviation from the mean displayed as error bars. Statistical significance was determined by GLM analysis

While the inhibitory effect of AHU3 on *S. aureus* is less potent than the observed in *E. coli*, the transduction assay demonstrated that the compound does not exclusively target expression of the Stx2 phage only, but has a broader mechanism of action, likely involving aspects of phage biology.

3.5 Effect of AHU3 on Stx2 production by EHEC

To assess if AHU3 could impact on Stx2 production in EHEC we directly assayed toxin production in ZAP1620, a wild-type strain that is lysogenized with both Stx2a- and Stx2c-encoding phages and was isolated from a human patient. ZAP1620 was cultured to mid-exponential phase and MMC added to induce toxin expression. Culture supernatants were isolated and the levels of toxin assessed using an ELISA-based assay (RIDASCREEN R verotoxin, R-Biopharm). Data were calculated as a percentage of expression compared with the positive control (100%), consisting of inactivated Stx. Analysis of the supernatant of ZAP1620 showed strong MMC-dependent production of Stx2, at 85% ($\pm 7\%$) activity compared with the positive control. Addition of 50 μM AHU3 reduced Stx2 expression to 47% activity ($\pm 3\%$) compared with the positive control, demonstrating that AHU3 markedly inhibits Stx2 production in wild-type isolates (Figure 23).

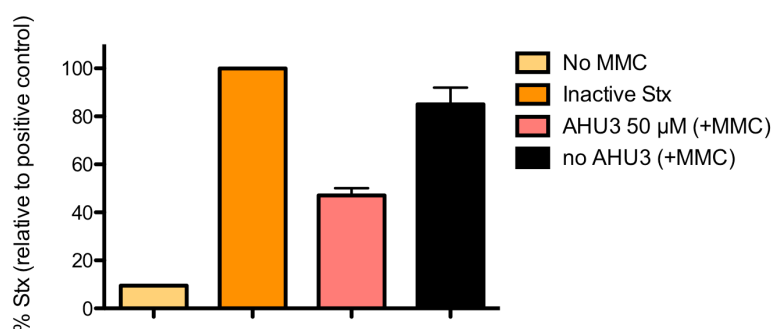


Figure 23 The compound AHU3 blocks expression in *E. coli* ZAP1620, a wild-type strain that is lysogenized with both Stx2a- and Stx2c-encoding phages.

Addition of 50 μM of AHU3 significantly decreased the MMC-induced production of the toxin in comparison to the untreated control.

3.6 Finding the target of AHU3

Transduction assays showed that AHU3 blocks phage production in both Gram-negative and positive organisms, including phages unrelated to Stx. As discussed in section 1.3, the SOS response plays a key role on prophage induction, so it

appeared likely that AHU3 could be acting on an essential component of this pathway. Prophage genes are under the control of repressors that help prevent the phage from entering the lytic cycle and causing bacterial lysis. When the SOS response is initiated, protein filaments of RecA induce the autocleavage of the phage repressors as well as autocleavage of LexA, the key repressor of the SOS genes.

Since AHU3 showed activity in both Gram-negative and positive organisms, the compound would need to target a protein highly conserved across bacteria. We therefore hypothesised that RecA could be a potential target, either by preventing it binding to ssDNA, preventing the formation of activated filaments or interacting with the phage repressor *ci*. Inhibition of the expression or function of other SOS components was considered unlikely, as while this would affect the SOS response, the prophage would be unaffected.

3.7 The compound AHU3 does not affect RecA expression

Studies have shown that production of Stx in *recA* mutant strains of *E. coli* O157:H7 is considerably decreased than that of the wild-type strains, and complementation with a *recA* vector restores the toxin production (S. Fuchs et al. 1999). This is due to the key role that RecA plays in prophage induction (Matsushiro et al. 1999). We therefore decided to assess whether the compound was exerting its inhibitory activity by down-regulation of RecA expression. Expression of RecA was studied in response to AHU3 and MMC, AHU3 and MMC. Immunoblotting for RecA did not show a decrease of expression when AHU3 was added to *E. coli* O157:H7 cultures (Figure 24).

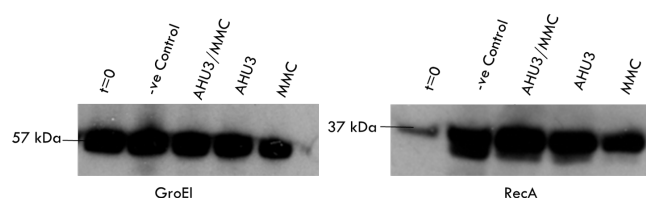


Figure 24 Effect of AHU3 on RecA expression.

Bacterial cultures of *E. coli* O157:H7 were incubated in the presence and absence of AHU3 in order to study its effect on RecA expression. Samples were processed after 3 h incubation with the compound and the cell lysates were processed for a Western Blot analysis of RecA. The compound did not affect RecA expression. GroEL was used as a housekeeping protein control

Since the compound did not have an effect on RecA expression, the next step was to assess if AHU3 was interfering with the activity of RecA, as explained in the following sections.

3.8 Microscale thermophoresis

The use of methods for the study of interactions between proteins and other biomolecules like DNA, RNA or small molecules is of great importance for the understanding of cellular processes and for the development of new drugs. There is a wide range of techniques already available for this purpose but there are still some caveats that limit their use. Microscale thermophoresis is a relatively new biophysical technique used in the study of biomolecular interactions based on the thermophoresis of molecules in solution. Thermophoresis can be defined as the direct movement of molecules through a temperature gradient (Rainard, Pandarakalam, and McElroy 2018). Amongst the advantages that this technique offers are the easy sample preparation, low quantity of sample required and the broad range of dissociation constants that can be measured (pM to mM).

A typical MST experiment consists of one fluorescent binding partner and one non-fluorescent, also known as titrant. Usually, fluorescence is provided by a fusion protein like GFP or by using a fluorescent label covalently attached to the molecule of interest. The concentration of the fluorescent molecule is normally kept low (around 50 pM-100 nM) and the non-fluorescent partner is prepared at different concentrations (titration). It is important to keep the buffer and other elements like DMSO constant throughout samples. During the experiment, an infrared laser induces a microscopic temperature gradient and the directed movement of molecules is detected and quantified (Figure 25). The thermophoresis signal is plotted against the ligand concentration, obtaining a dose-response curve from which the binding constant can be calculated (Jerabek-Willemsen et al. 2014) .

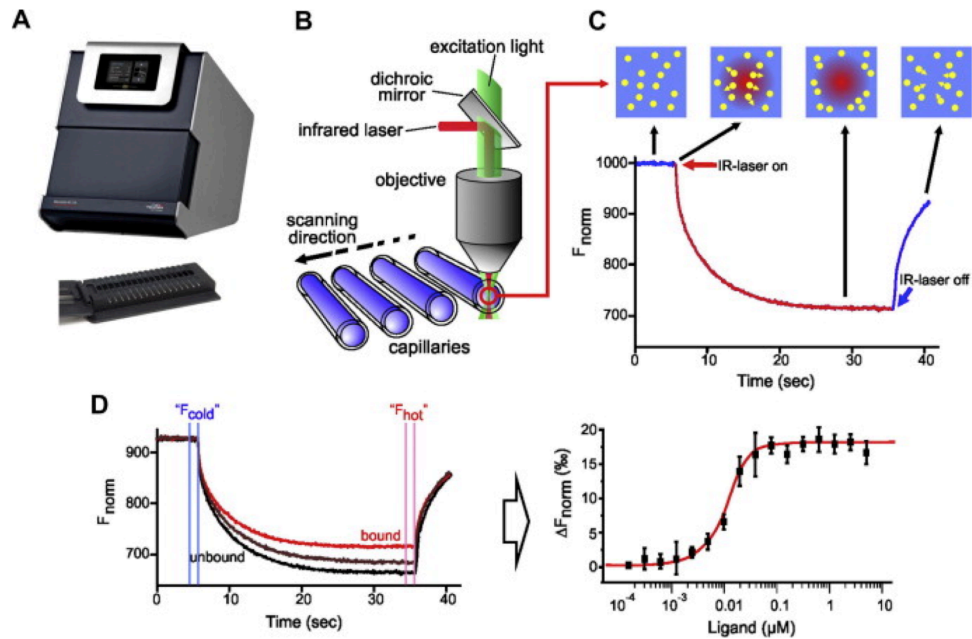


Figure 25 Microscale thermophoresis.

(A) The Monolith NT.115 from NanoTemper Technologies. (B) The samples are loaded in capillaries with a total volume of 4 μL . The fluorescence of the samples is excited and detected through the same objective. The IR laser heats a defined sample volume and the thermophoresis of fluorescent molecules through the temperature gradient is detected. (C) Initially, the molecules in the samples are homogeneously distributed and a basal fluorescence is detected. After activation of the IR laser, a rapid change in fluorophore properties due to the fast temperature change is observed. Then, a movement of the fluorescently labeled molecules out of the heated sample volume is detected. When the IR laser is deactivated, the molecules diffuse back to their initial state. (D) The thermophoretic movement of a fluorescent molecule (black, 'unbound') changes when it binds to a non-fluorescent ligand (red, 'bound'). The change in thermophoresis is expressed as the change in the normalized fluorescence (ΔF_{norm}), which is defined as $F_{\text{hot}}/F_{\text{cold}}$ (F -values are the average fluorescence values between defined areas marked in the figure). The gradual change in thermophoresis is caused by the titration of the non-fluorescent ligand. Such gradual change is plotted as ΔF_{norm} , generating a binding curve that can be fitted to obtain binding constants. (Taken from Jerabek-Willemsen et al. 2014)

In order to investigate the possible interaction between RecA and AHU3, the RecA protein was fluorescently labeled with NT-647 Red dye (NanoTemper technologies). The dye carries a reactive NHS-ester group that modifies primary amines present in amino acids like lysine. Since AHU4 did not show activity on the *stx2::GFP* assay, it was used as a negative control during the experiment.

The concentrations of both AHU3 and AHU4 were varied between 200 μM - 12 nM. As shown in Figure 26, AHU3 showed to be interacting with RecA whereas AHU4 did not show to have affinity towards RecA.

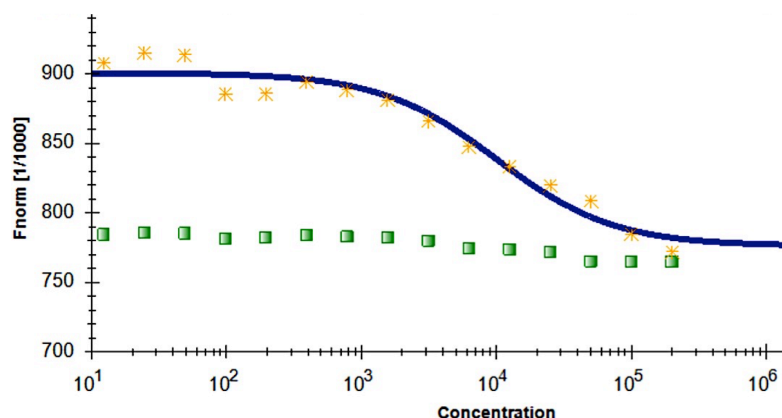


Figure 26 Exploring the interaction of RecA with the AHU3 and AHU4 compounds using MST.

The concentration of the fluorescent labeled RecA was kept constant throughout the experiment, while the concentrations of the non-labeled components (AHU3 in yellow asterisks and AHU4 in green squares) were between 200 μM - 12 nM. Concentrations are plotted in nM. The results indicate that RecA is interacting with AHU3, whereas no interaction is observed in the presence of AHU4.

3.9 The compound AHU3 inhibits the ATPase activity of RecA

As previously mentioned, ssDNA is the main inducer of the SOS response. Most of the different functions of RecA involve the formation of helical homopolymeric filaments of ATP-bound RecA monomers around the ssDNA. This RecA-DNA complex has the ability to hydrolyze ATP. As a consequence, monitoring the ATPase activity of this RecA-DNA complex can be exploited as a diagnostic assay to monitor RecA's activity. This approach has been used to identify small molecule inhibitors of RecA by *in vitro* screening (Peterson et al. 2012; Wigle et al. 2009).

We decided to apply this concept to investigate if the compound AHU3 was interfering with RecA's activity. We attempted to use the phosphomolybdate-blue ATPase assay described by Sexton and collaborators, but we were unable to reproduce the assay (Sexton et al. 2010). We then decided to use the Innova Biosciences ATPase kit. Following the manufacturer's instructions, the optimal concentrations for the reaction were found to be 0.25 μM RecA and 5 μM ssDNA.

The DMSO concentration was kept below 2% to avoid any possible interference with the assay. The ability of AHU3 to inhibit RecA mediated ATP hydrolysis was investigated at concentrations between 0.1 to 100 μM . A dose-response curve was plotted using the data obtained, giving to AHU3 an IC_{50} of 7.72 μM (Figure 27). While the inhibition of the ATPase does not give insights into the mechanism of action of AHU3, it provides evidence that the compound is acting as an inhibitor of RecA and validates the results obtained through MST (Section 3.8). The inactive AHU4 compound was used as a negative control and the reported RecA inhibitor curcumin as a positive control.

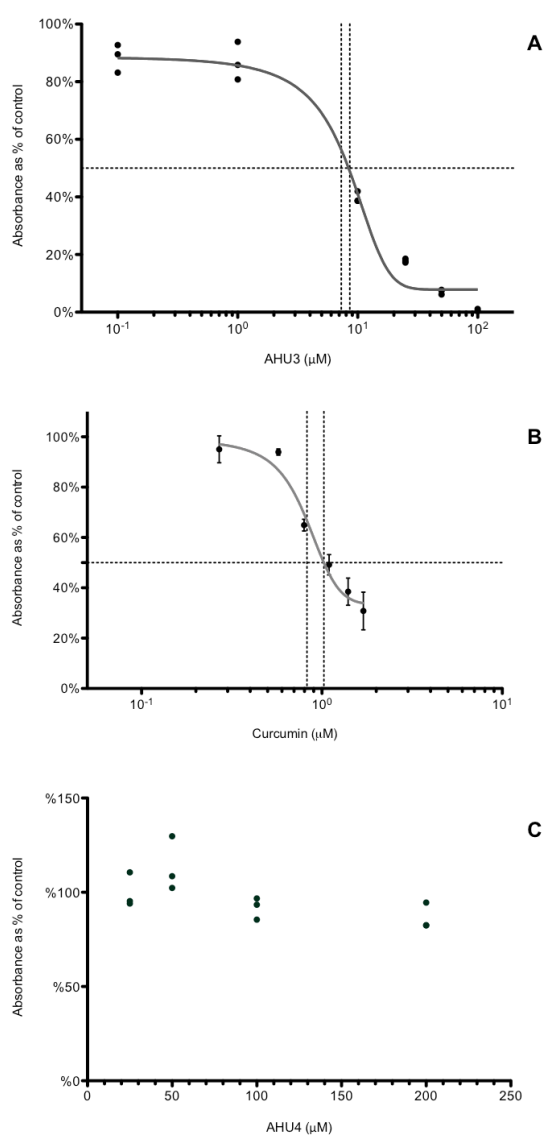


Figure 27 AHU3 inhibits RecA-mediated ATP hydrolysis.

(A) Dose-response inhibition of RecA's ATPase activity by RecA. Data are plotted as a percentage of the average absorbance of the assay well containing 0 μM AHU3. The curved showed an IC_{50} of 7.72 μM for AHU3. (B) Dose-response curve for the known RecA inhibitor curcumin, exhibiting an

IC₅₀ of 6.69 μ M. (C) Dose-response curve for AHU4, showing no inhibition of RecA's ATPase activity.

3.10 AHU3 affects RecA oligomerisation

A crucial process for a successful induction of the SOS response is the formation of the RecA filaments. Thus, we decided to explore if the compound was interfering with the formation of RecA filaments. Analytical ultracentrifugation (AUC) is a biophysical technique that allows the quantitative analysis of macromolecules in solution. Previous studies have used AUC sedimentation equilibrium experiments (SE) to analyze the oligomerization of *E. coli* RecA, revealing monomers in reversible equilibrium with trimers, hexamers and dodecamers. To assess whether AHU3 affects the oligomerization dynamics of the protein, we performed SE for RecA in the presence and absence of AHU3 in collaboration with Prof. Olwyn Byron and Dr Zoe Marjenberg. We also controlled for any influence of DMSO, included as a solvent for AHU3, on protein behavior. The SE data were analyzed with SEDPHAT using the species analysis model with a single species, in order to gain a model-independent measure of the whole-cell weight average molecular mass. The average molecular mass of RecA oligomers in the absence of AHU3 and DMSO was 556 kDa at 10,000 rpm and 404 kDa at 14,000 rpm (Figure 28).

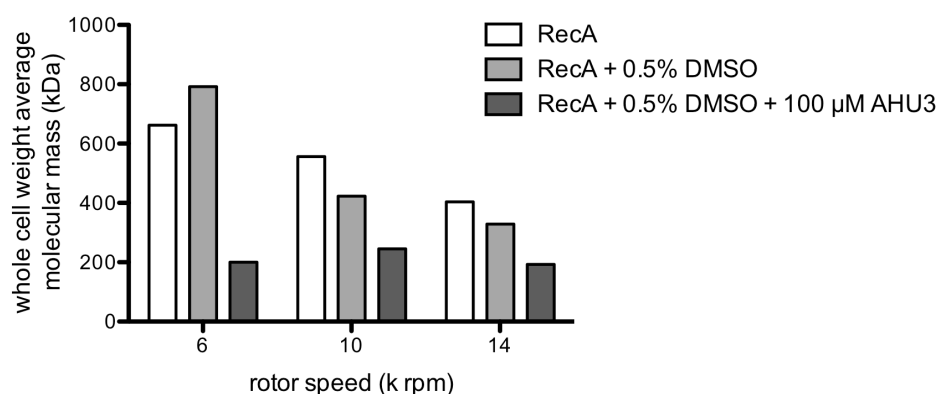


Figure 28 AHU3 decreases RecA oligomerization.

Whole cell weight average molecular mass of RecA at AUC rotor speeds of 6, 10, and 14 k rpm. Ten micrometer RecA was studied alone, in the presence of 0.5% DMSO, and in the presence of 0.5% DMSO and 100 μ M AHU3.

In the presence of AHU3, the average molecular mass of RecA oligomers was greatly reduced at all rotor speeds tested. The greatest changes were observed at 6,000 rpm, with a 70% decrease in the average molecular mass compared with untreated RecA. At 10,000 and 14,000 rpm, the decreases were still marked, at 56 and 52%, respectively. As a control we also compared the average molecular mass of RecA with that of the same protein in the presence of DMSO and found only very minor effects on RecA oligomerization. These data demonstrate that AHU3 is affecting the formation of larger oligomeric RecA species, resulting in an increase in lower molecular mass oligomers.

3.11 Synthesis of a biotinylated derivative of AHU3 for affinity chromatography

Affinity chromatography is one of the most widely used methods for target identification. Typically, this approach starts with structure-activity relationship (SAR) studies on the molecule of interest. This allows for the identification of the functional groups responsible for activity and the nonessential sites that can be used as points of attachment to an affinity tag (e.g. biotin) or solid matrix (e.g. Affi-Gel agarose beads) (Lomenick, Olsen, and Huang 2011). In cases where biotin is used as an affinity tag, a biotinylated version of the compound is synthesized. The compound will have the ability to bind to streptavidin beads, due to the strong non-covalent interaction that biotin has with streptavidin ($K_d = 1 \times 10^{-14}$ M) (Taldone et al. 2013). The beads are incubated with lysates of the strain or cells of interest in order to ‘pull-down’ the target. After a certain period of time, washes to remove non-specific interactions are performed and the protein(s) bound to the beads are eluted using either an excess of the compound or denaturing conditions. Finally, the proteins are analysed by SDS-PAGE and the protein bands are identified by mass spectrometry.

There are several examples of the application of this approach for target identification. A good example is the identification of the target proteins for the salicylidene acylhydrazides, a family of novel anti-virulence compounds that inhibit the type three secretion system in Gram-negative bacteria (Dai Wang et al. 2011). Using this approach, Wang and collaborators identified the bacterial

proteins that are targeted by this class of compounds using a biotinylated derivative of the hit compound ME0052.

Given the potential that this approach offers and the SAR information of AHU3 already available, it was decided to synthesise a biotinylated derivative of AHU3 in an attempt to identify the molecular target. Since AHU3 has a secondary amino group on the piperazine ring that is labile to chemical modifications and it was not required for bioactivity, it was decided to try to couple the secondary amino group with biotin using peptide-coupling chemistry. Firstly, compound **vi** was synthesised following the synthetic route showed in Figure 29.

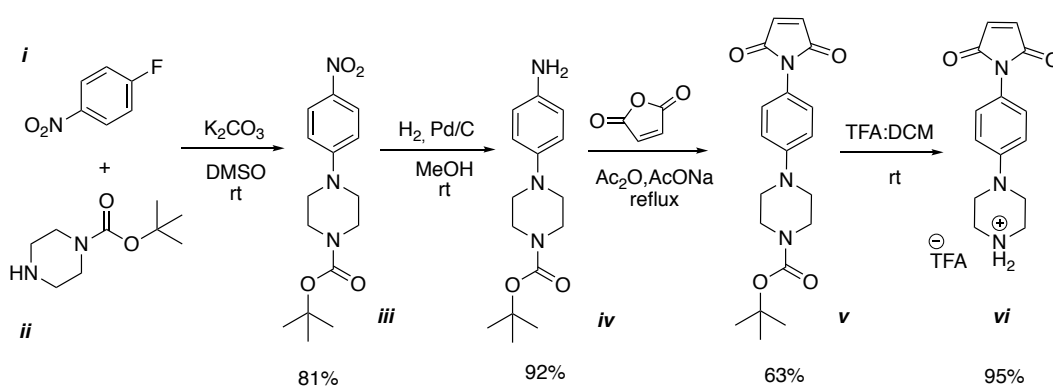


Figure 29 Synthesis of **vi**.

Compound **vi** was subjected to different coupling conditions in order to link it to (+)-biotin **vii**. Unfortunately, the desired product **viii** was not obtained (scheme 2). Different reagents and conditions were attempted (table 14) however the product **viii** was never isolated. Intermediates of **vii** formed with the coupling reagents were isolated in some cases and decomposition of the starting materials was observed when high temperatures were used.

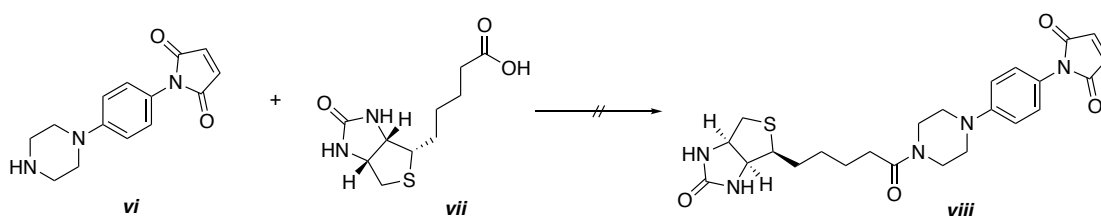


Figure 30 Coupling between (+)-biotin and compound **vi** was attempted using peptide coupling reagents.

Table 14 Different conditions used for the coupling between AHU1 and biotin

Reagents	Temperature	Reaction time	Product(s)
HBTU, DIPEA, CH ₂ Cl ₂	rt	12 h	Active ester of <i>vi</i> + <i>vii</i>
HBTU, DIPEA, CH ₂ Cl ₂ :DMF	40 °C	12 h	Active ester of <i>vi</i> + <i>vii</i>
HBTU, DIPEA, DMF	140 °C	12 h	Decomposition
SOCl ₂ , CH ₂ Cl ₂	rt	12 h	Decomposition
DCC, DMAP, CH ₂ Cl ₂	40 °C	12 h	Starting materials
EDCI, DMAP, DMF	80 °C	12 h	Starting materials
EDCI, DMAP, DMF	Mw, 110 °C	1 h	Decomposition

Given the unsuccessful results trying the amide coupling, the copper-catalysed azide-alkyne cycloaddition was considered as an alternative, a 1,3-dipolar cycloaddition between an azide and a terminal or internal alkyne to produce 1,2,3-triazoles (Berg and Straub 2013). The azide component was obtained by reacting 3-chloropropylamine hydrochloride (*ix*) with sodium azide (*x*) to give the corresponding azidopropylamine (*xi*). Low yields were obtained in this reaction owing to the volatility of the product (Figure 31).

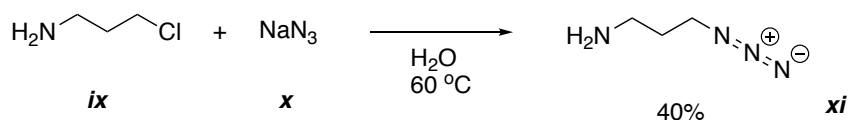


Figure 31 Synthesis of azidopropylamine.

To add the azide functionality to (D)-biotin, it was converted in to the *N*-hydroxysuccinimide ester (NHS) by reacting it with *N*-hydroxysuccinimide using EDCI in DMF. Then, compounds *xi* and *xiii* were reacted in methanol at room temperature to give *xiv* in moderate yields (Figure 32).

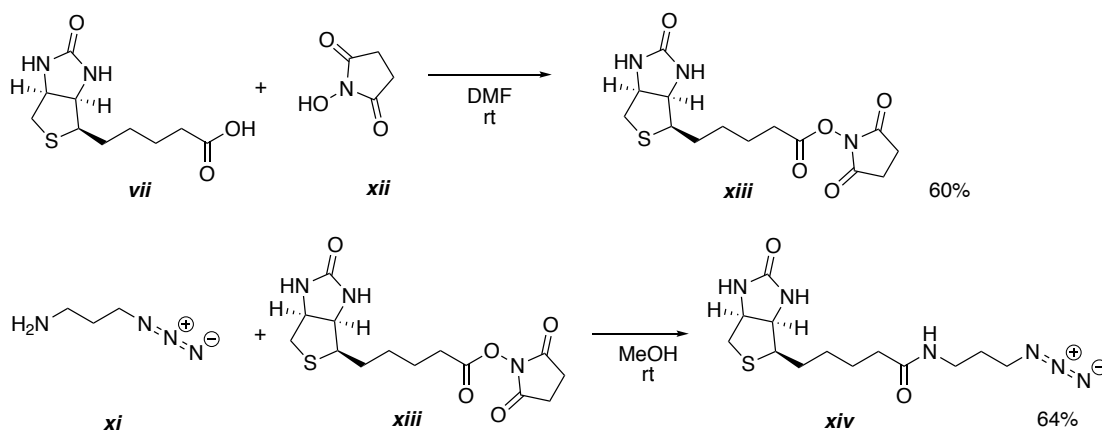


Figure 32 Biotin was converted into its *N*-hydroxysuccinimide ester (NHS) in order to obtain its *N*-(3-azidopropyl) derivative **xiv**.

The coupling partner bearing the alkyne functionality was then synthesised producing **xx**. To do so, piperazine (**xvi**) was arylated by reacting it with 4-fluoronitrobenzene (**xv**) in presence of tetrabutylammonium iodide (TBAI), giving the nitroaryl piperazine compound **xvii**, which was then *N*-alkylated using propargyl bromide under basic conditions, forming the nitro alkyne **xviii**. Reduction of the nitro group using tin(II) chloride gave the aniline **xix**, which was subsequently refluxed with maleic anhydride in acetic anhydride to give the alkyne-functionalised maleimide **xx** (Figure 33).

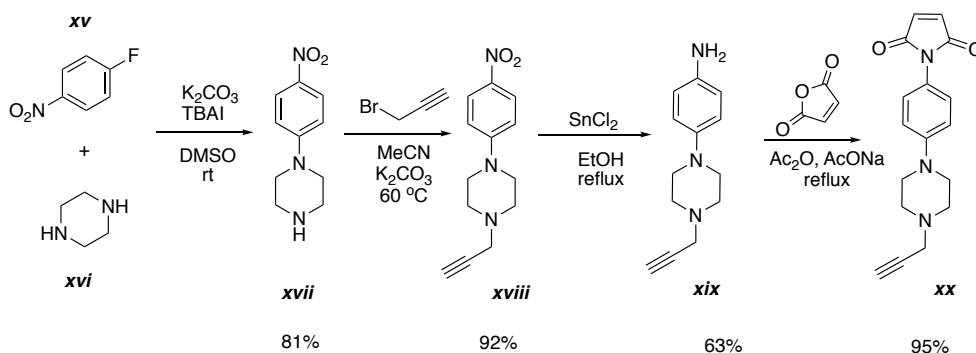


Figure 33 Synthesis of 1-(4-(4-(prop-2-yn-1-yl)piperazin-1-yl)phenyl)-1H-pyrrole-2,5-dione

The click reaction was tried using the conditions reported by Yu and collaborators (F. Yu et al. 2013). They described a base-free click reaction to synthesise a biotinylated derivative of echinocystic acid, using copper sulphate and sodium ascorbate in a mixture of THF:H₂O. Unfortunately, the use of these conditions did not produce the desired product **xxi** (Figure 34). Purification of the reaction mixture only showed decomposition products.

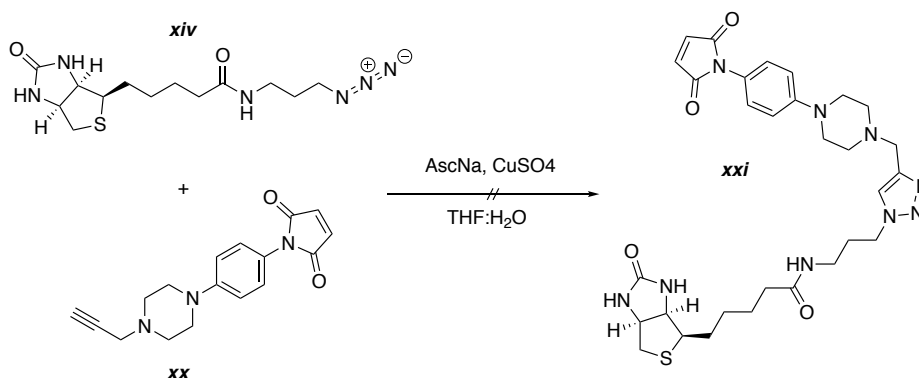


Figure 34 Copper-catalysed azide-alkyne cycloaddition.

Given the difficulties experienced with the click reaction, it was decided to try a different approach. Since the compound **xx** was already synthesised, the possibility of using the Sonogashira coupling was considered. To this aim, (D)-biotin (**vii**) was reacted with 4-iodoaniline (**xxii**) to obtain the aryl halide **xxiii** (Figure 35). The coupling was performed using EDCl, DMAP in CH_2Cl_2 under reflux. The product **xxiii** was obtained although in low yields.

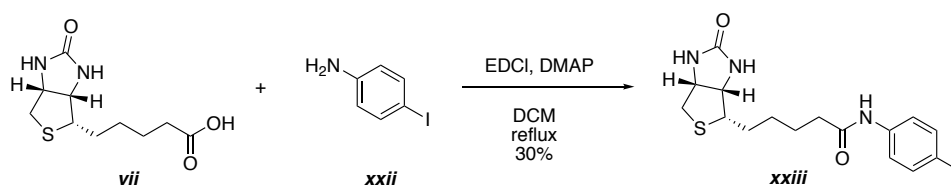


Figure 35 Sonogashira coupling.

Guilagaber and co-workers developed a methodology to perform Sonogashira couplings using mild conditions (Ghilagaber, Hunter, and Marquez 2007). The reaction was carried out using tetrakis(triphenylphosphine)palladium(0) and copper iodide as catalysts. Unfortunately, the desired product (**xxiv**) was not obtained (Figure 36).

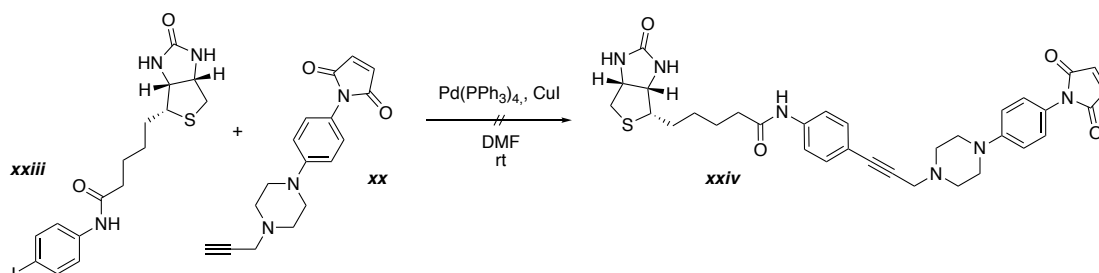


Figure 36 Sonogashira coupling using tetrakis(triphenylphosphine)palladium(0)

After purification through column chromatography, ^1H NMR analysis showed the recovery of the starting material **xxiii** and a by-product of **xx**. The by-product showed the loss of the alkynyl hydrogen but signals of aromatic protons were observed instead, suggesting that either the intermediate complex alkyne-Pd (shown as **(8)** in Figure 37) or the homocoupling product of **xx** were formed. Longer reaction times (up to 72 h) and higher temperatures were tried (up to 80°C), but no product formation was observed.

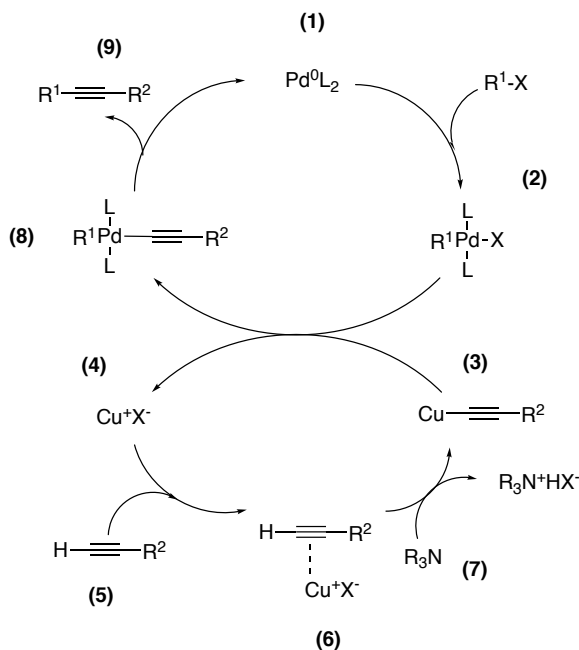


Figure 37 The catalytic cycle for the Sonogashira reaction.

The reaction consists of a fast oxidative addition of $\text{R}^1\text{-X}^1$ (R^1 =aryl, hetaryl, vinyl; $\text{X} = \text{I}, \text{Br}, \text{Cl}, \text{OTf}$) to the catalyst Pd^0L_2 formed by reduction of different palladium(II) complexes. The next step involves a transmetalation with the copper acetylide formed during the copper catalytic cycle to generate a $\text{R}^1\text{Pd}(\text{-C}\equiv\text{CR}^2)\text{L}_2$ species, which gives the coupled alkyne after *cis/trans* isomerisation and reductive elimination with regeneration of the catalyst (Chinchilla and Najera 2007).

Hansen and collaborators reported the synthesis of a biotinylated derivative of phorbazole A via Sonogashira coupling using $\text{PdCl}_2(\text{PPh}_3)_2$, CuI and Et_3N in THF, reporting moderate yields (Hansen, Engler, and Forsyth 2003). The aryl iodide **xxiii** and the alkyne **xx** were subjected to these conditions. The desired product **xxiv** was not obtained and loss of the alkyne in **xx** was again observed in the ^1H NMR spectra. The reaction was also attempted using microwave radiation but yet again no product was isolated.

Given the unsuccessful results using the Sonogashira coupling, it was decided to stop trying it. In the copper-catalysed azide-alkyne cycloaddition, the main issue was the stability of the maleimide moiety. Thus, it was decided to build up the molecule in a way that the click reaction could be done at early stages, before the maleimide group was added. Hence, biotin azide (**xiv**) was reacted with the nitro alkynyl compound **xxv** and the desired product **xxvi** was obtained with moderate yield (Figure 38).

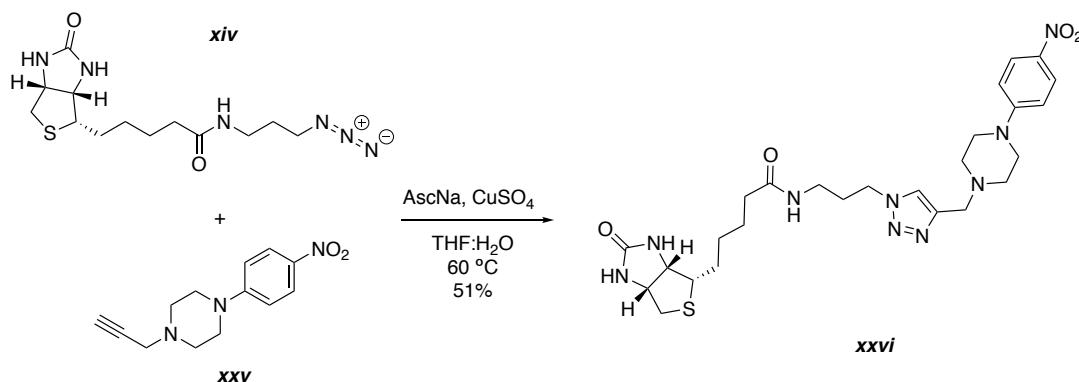


Figure 38 Copper-catalysed azide-alkyne cycloaddition using AscNa and CuSO₄.

Reduction of the nitro compound of **xxvi** yielded the corresponding aniline **xxvii**, which was then refluxed with maleic anhydride in acetic anhydride to obtain the final product **xxviii** (scheme 12). Unfortunately, after purification, the ¹H NMR spectra showed decomposition products of **xxviii**, probably due to the high temperatures employed (130 °C). Lower temperatures were tried, but no difference was observed (Figure 39).

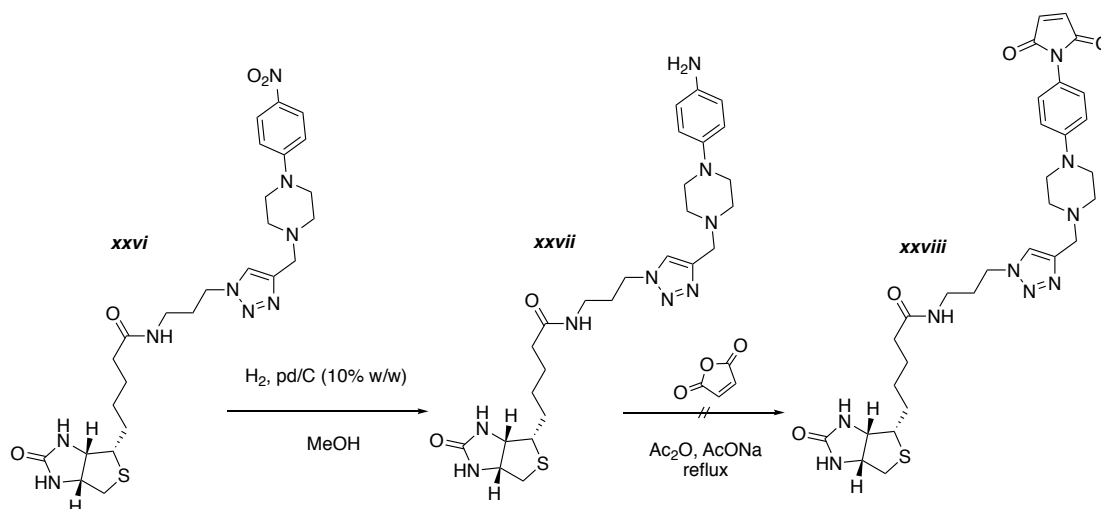


Figure 39 The biotinylated derivative of AHU3 was not obtained.

Given the amount of time spent trying to synthesise the biotinylated version of AHU3 it was decided that it was unsuitable to continue working on it.

3.12 Toxicological profiling of the AHU compounds

As part of any drug discovery programme, it is crucial to evaluate the toxicological profile of any potential lead compound, particularly if *in vivo* testing is being considered.

The AHU1-3 compounds were tested for toxicity in HEK 293 at the European Screening Port (Hamburg, Germany). Unfortunately, all three compounds showed to be highly toxic at a concentration of 100 μM . Dose-response studies on the compounds revealed pIC_{50} values of approximately 5 μM (table 15). Ideally, a lead compound in order to progress on a drug discovery campaign should have no toxicity at 10 μM . Thus, given the IC_{50} values obtained for the AHU compounds, it was concluded that they were not suitable for progression into *in vivo* testing.

Table 15 Toxicological evaluation of the AHU compounds.

Compound	Hill slope	pIC_{50}
AHU1	5.19 ± 0.47	5.10 ± 0.01
AHU2	4.30 ± 0.25	5.30 ± 0.01
AHU3	5.30 ± 0.30	5.09 ± 0.01

The toxicological profile of a lead compound can be modified by structural modifications, but care should be taken to prevent the loss of the desired activity. In the case of AHU3, a more thorough SAR study is required to find analogues that show a better toxicological profile.

3.13 Expression and purification of RecA

In order to produce RecA in large quantities, the *recA* gene from *E. coli* was cloned into the pTXB1 vector, which contains a self-cleavable intein tag from the *Mycobacterium xenopi gyrA* gene, and a chitin-binding domain (CBD)

(Singleton et al. 2002). RecA was inserted between the NdeI and SapI sites of pTXB1, which resulted in the fusion of the intein tag to the C-terminus of RecA, without addition of any extra amino acids. The advantage of using the pTXB1 vector is the ability to purify a native recombinant protein in a single chromatographic step without the use of proteases for its release. Instead, the intein undergoes self-cleavage at its N-terminus upon addition of thiols such as cysteine, DTT or β -mercaptoethanol, releasing the protein from the chitin-bound intein tag (Figure 40).

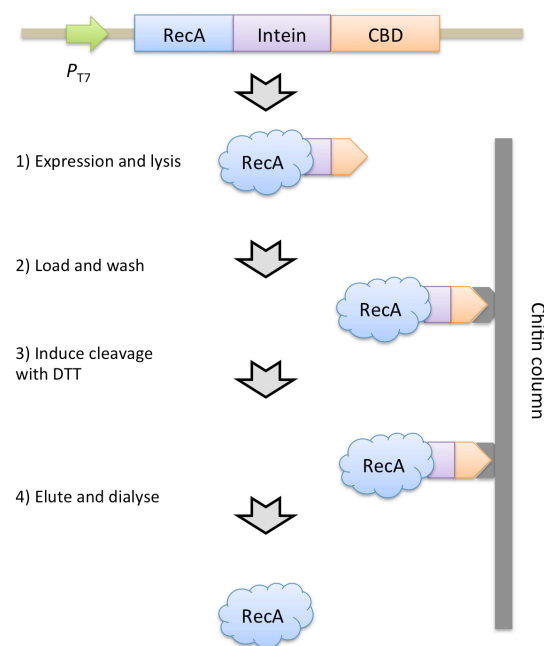


Figure 40 Intein-mediated purification of RecA.

The mini-intein Mxe *gyrA* and a chitin-binding domain (CBD) are fused to the C-terminal of RecA. The CBD allows its binding to the chitin resin. The fusion protein undergoes a N-S acyl rearrangement forming a thioester that is cleaved by DTT. RecA is eluted from the column while the intein-CBD fusion remains bound to the resin. Modified from Singleton et al. 2002

To overexpress RecA, the plasmid pTXB1-RecA was transformed into *E. coli* BL21(DE3) and the expression was induced by addition of 0.5 mM IPTG. The purification was performed using a chitin resin. SDS-PAGE analysis of the purification fractions showed successful production of RecA (Figure 41). RecA was obtained in good yields (8 mg/mL) without the need of further purification.

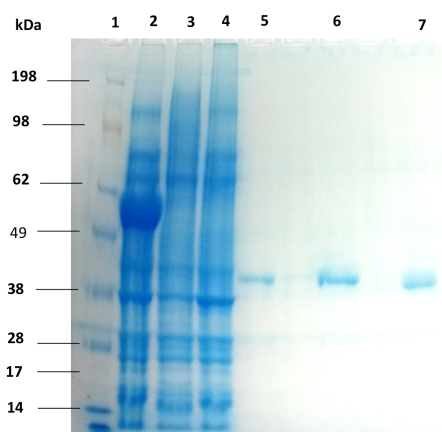


Figure 41 SDS-PAGE of purification fractions for RecA.

The protein bands were visualized by staining with 0.1% Coomassie brilliant blue R-250. 1, protein marker, 2 Crude extract from cells induced with IPTG at 16 °C for 16 h; note expression of RecA (38 kDa) fused to the Intein-CBD fragment (27 kDa). 3, Flow through from chitin column after loading of the cell lysate. 4, Wash with column buffer, 5, DTT flush to distribute it evenly in the column. 6, Elution of RecA after induced cleavage at 4 °C for 16 h. 7, RecA control from a commercial supplier.

In order to gain more insights into the mechanism of action of AHU3 on RecA, we decided to try to co-crystallize RecA and the compound. Since the crystal structure of RecA has been already described (PDB ID: 2REB, Story et al, 1992), we decided to try known crystallization conditions using the hanging drop method.

The hanging drop method for crystallization of macromolecules is a popular approach in structural biology (McPherson and Gavira 2014). The technique consists of suspending the protein of interest in the buffer. A drop of this mixture is then placed in a chamber that contains a reservoir filled only with the buffer. Typically the concentration of the buffer in the droplet is lower than the reservoir. Given this concentration difference, water vapour leaves the drop and ends up in the reservoir in order to achieve equilibrium. This concentration of the droplet promotes the formation of protein crystals in the droplet.

Shinohara and co-workers reported the DNA-free crystal structure of RecA using the hanging drop method using 24% PEG400, 10% glycerol, 10 mM MgCl₂ and 0.1 M MES pH 6.5 (Shinohara et al. 2015). Different concentrations of the

precipitating agent PEF400 were explored. Crystal trays were incubated at room temperature and monitored daily. No crystals were obtained in a two-month period. Given time constraints, we were unable to continue exploring more conditions.

3.14 Evaluation of a reported inhibitor of RecA

Recently, Alam and collaborators reported the activity of copper phthalocyanine-3,4',4'',4'''-tetrasulfonic acid (3,4-Cu-PcTs) and iron(III) phthalocyanine-4,4',4'',4'''-tetrasulfonic acid (Fe-PcTs) as RecA inhibitors (Alam et al. 2016). Their findings were based on the fact that metatungstate ($W_{12}O_{40}^{6-}$) salts were able to inhibit the ATPase, DNA-binding and DNA strand-exchange activities of MvRadA, a RecA homolog in *Methanococcus voltae* (Y. Li, He, and Luo 2009). Since metatungstate did not have the same effect on RecA, molecules with similar anionic nature were studied. Phthalocyanine tetrasulfonate-based molecules were found to inhibit RecA, potentially as a result of their interaction with the cationic DNA-binding site of RecA (Mecozzi, West, and Dougherty 1996). These compounds were able to block the ciprofloxacin-induced activation of the SOS response, potentiated the effect of bactericidal antibiotics and reduced the acquisition of ciprofloxacin resistance in a murine animal model (Alam et al. 2016)

We decided to study the ability of these compounds to suppress Stx2 expression. Fe-PcTs was shown to be the best performing compound at 100 μ M. Its potential to block *stx2* expression was assessed using the *pstx2::GFP* reporter fusion plasmid. Unfortunately, the coloured nature of the compound (intense blue) proved to be an issue in the reporter assay as it acted as a fluorescence-quenching agent.

Thus, we next assessed the effect that Fe-PcTs had on phage lytic development in the *E. coli* strain that carries only the lysogenic Stx2 prophage ϕ P27. Prophage induction was initiated by addition of mitomycin C (2 μ g/mL) in the presence and absence of Fe-PcTs (100 μ M) and AHU3 (50 μ M) as a control. The non-lysogenic *E. coli* K-12 MG16665 was used as the acceptor strain. In the absence

of MMC, basal levels of Stx2 phage (10^4 PFU/mL) were observed, whereas the addition of MMC produced a two orders of magnitude increase (10^6 PFU/mL) (Figure 42-A). The presence of FePcTs did not impair the phage lytic development as the phage titre was similar to the MMC induced control (10^6 PFU/mL). In contrast, the presence of AHU3 caused a significant decrease on the production of plaque forming units, close to the basal levels (10^4 PFU/mL). This was also studied in the *S. aureus* strain carrying the prophage ϕ SLT. The same results were obtained as shown in Figure 42-B. The presence of FePcTs did not reduce the phage titre.

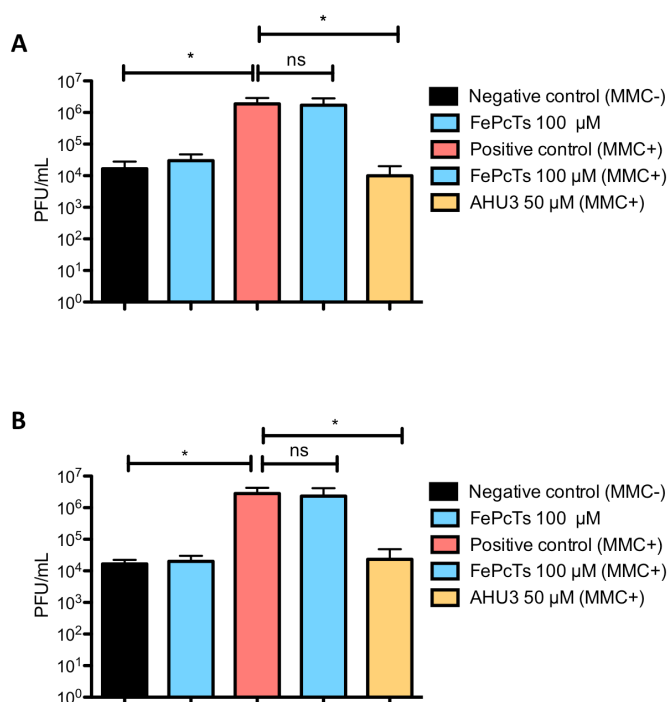


Figure 42 Effect of FePcTs on phage production.

A) FePcTs did not reduce the phage titer in *S. aureus* when cultures when grown in the presence of 100 μ M FePcTs B) FePcTs did not reduce the phage titer in *E. coli*. Data shown is the average of triplicates with standard deviation indicated as error bars

Table 16 Efficiency of the development of lambdoid bacteriophages in *E. coli* and *S. aureus* after mitomycin C induction and treatment with FePcTs

Strain	Phage titer (PFU/mL) obtained (mean)				
	MMC-	FePcTs, MMC-	MMC+	FePcTs, MMC+	AHU3, MMC+
<i>E. coli</i> (ϕ P27)	1.06×10^4	2×10^4	2.14×10^6	2.32×10^6	3×10^4
<i>S. aureus</i> (ϕ SLT)	1.66×10^4	3×10^4	1.88×10^6	1.72×10^6	1×10^4

We further investigated if FePcTs was able to regulate Stx2 expression by western blot analysis. As STEC is a category three microorganism under UK regulations, it is not possible to handle Stx+ strains in our laboratory. Thus, *Citrobacter rodentium* lysogenized with the Stx phage ϕ 1720a-02 was used for relative quantification of the toxin (Mallick et al. 2012).

C. rodentium (λ stx_{2dact}) was grown to early exponential phase (OD₆₀₀ = 0.25) followed by addition of either FePcTs (100 μ M) or AHU3 (50 μ M) and MMC. After 1 h incubation, cells were pelleted and the intracellular content of Stx2 was analysed by western blot (Figure 43). The presence of FePcTs did not suppress stx2 expression in comparison to AHU3.

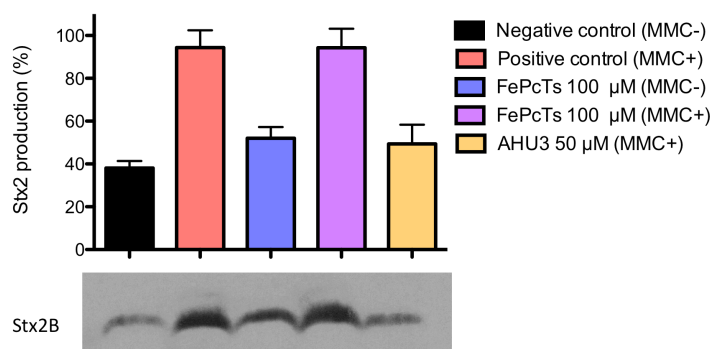


Figure 43 Effect of FePcTs on Stx2 expression in *C. rodentium* λ stx_{2dact}.

Cell lysate of *C. rodentium* non-induced and induced with MMC was blotted for Sxt2B. The presence of FePcTs in the MMC induced culture did not suppress *stx2* expression in contrast to AHU3 that clearly reduced the amount of *stx2* produced (50-60% expression). Pixel density was measured using the software ImageJ. The data shown are the average of three individual experiments with standard deviation from the mean displayed as error bars

The lack of activity of FePcTs made us wonder if the anionic nature (Figure 44) and size of the molecule was impeding the uptake by bacterial cells. To assess this, we decided to perform an uptake assay in order to quantify both the intracellular and extracellular distribution of the compound using mass spectrometry. The uptake of FePcTs was assessed in *E. coli* TUV 93-0 by incubating bacteria (OD₆₀₀=0.9) with the compound (25 μ M) in M9 minimum media for 1 h at room temperature. After this time, cells were pelleted through bromodecane oil to effectively isolate the bacterial cells from the surrounding supernatant. A solvent mixture made of CHCl₃:H₂O:MeOH (1:1:3) was added to the aqueous layer and this was considered as the supernatant fraction. Then,

bromodecane oil was removed from the cell pellet and cells were resuspended in the same solvent mixture previously described. This was considered as the cell fraction. The same procedure was performed with the AHU3 compound to be used as a control.

Samples were analysed at the Glasgow Polyomics facilities using hydrophilic interaction liquid chromatography (HILIC) and the metabolites analysed by electrospray ionisation mass spectrometry.

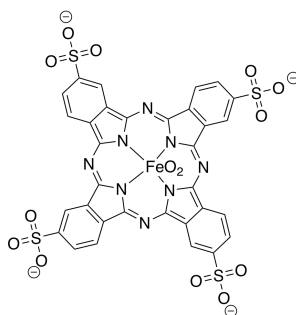


Figure 44 Chemical structure of FePcTs.

Table 17 Average peak intensities of compounds across different groups

Peak intensities	AHU3			FePcTs		
	Blank	Cells	Supernatant	Blank	Cells	Supernatant
Mean	656909581	14623091	49320131	-	-	-
SD	-	1983029.94	6672882.23	-	-	-

As shown in Table 17, only AHU3 was detected both inside and outside the cell, whereas FePcTs was not. Although the molecular size of FePcTs is within the scan range of the mass spectrometer, it could not be detected as the molecule might be multiply charged from the iron atom. This was unfortunate as it was not possible to demonstrate whether the lack of activity towards *stx2* expression is due to the poor uptake of the molecule.

It is worth mentioning that other RecA inhibitors previously described share the same anionic and aromatic nature. That is the case of suramin, reported by Singleton and collaborators (Wigle and Singleton 2007). Suramin inhibited the ATPase activity and the RecA-mediated DNA strand exchange reaction with an IC₅₀ of 2 μM. Its uptake in *E. coli* TUV 93-0 was also explored using the same methodology previously described. In this case suramin could not be detected as its molecular size is out of the scan range of the mass spectrometer.

3.15 Discussion

The work presented in this chapter shows the identification of the lead compound AHU3 with an inhibitory effect on *stx2* expression. The use of the *stx2::GFP* reporter assay in the HTS campaign ensured that any hits identified were active against intact bacteria. The selection criteria for the active compounds included a significant reduction in *stx2* expression, and a minimal effect on growth rate or off-target genes. Dose-response studies on the best performing compounds revealed that AHU3 showed inhibition of the *stx2* gene and phage production at a concentration that had minimal impact on bacterial growth.

Four lines of evidence led to the conclusion that AHU3 blocks Shiga toxin expression by acting as inhibitor of the SOS response and prophage induction, more specifically as an inhibitor of the RecA protein. First, when cultures of *E. coli* O157:H7 were incubated in the presence of AHU3, the compound blocked the MMC-induced lysis and phage lytic development compared to the non-treated control. Second, the compound was able to block phage production in both Gram-negative and positive organisms. Third, AHU3 had the ability to inhibit RecA-mediated ATP hydrolysis *in vitro* in a dose-dependent manner. Fourth, analytical ultracentrifugation revealed that AHU3 interferes with the oligomerisation dynamics of RecA, potentially explaining its inhibitory effect on *stx2* expression.

3.15.1 Electrophilic nature of AHU3 and its implications in the mode of action

One of the main features of AHU3 is its electrophilic nature. Maleimide moieties are susceptible to additions to their double bond either by Diels-Alder reactions or Michael additions. The maleimide moiety is rare in nature, but some natural products bearing this functionality have been reported. Pencolide is a maleimide with bacteriostatic and fungicidal activity produced by *Penicillium* strains

(Lucas, Castro, and Takahashi 2007). A compound isolated from *Streptomycin showdoensis*, showdomycin, was shown to target oxidoreductases and transferases involved in major cellular functions associated with virulence, growth and persistence in both Gram-negative and Gram-positive organisms (Böttcher and Sieber 2010).

Maleimides react readily with the highly nucleophilic thiol groups of cysteine residues in proteins at physiological pH (Bednar 1990). It is therefore highly likely that AHU3 reacts with RecA through this addition mechanism, covalently binding to one or more of the three cysteine residues present in *E. coli* RecA (Figure 45). This mechanism of inhibition has been reported for other small maleimide-based molecules, including a phenyl-substituted maleimide GNX-686, with anti-angiogenic properties for ocular pathologies and cancer (Nowak-Sliwinska et al. 2012), and a series of maleimide-based compounds with inhibitory activity on the monoamine oxidase B as a potential new therapy for Parkinson's disease (Manley-King et al. 2009).

Conservation analysis of cysteine across different bacterial species shows that it is not always present in RecA. For instance, as shown in figure 45, *Staphylococcus aureus* RecA does not have any cysteine residues. This observation suggests that the inhibitory activity of AHU3 on RecA's activity could be result of a different type of molecular interaction. Given the electrophilic nature of AHU3, covalent binding to other nucleophilic amino acids such as lysine, threonine and serine, could be possible. One approach to determine the binding of AHU3 to cysteine or other residues would be to genetically modify these residues and assess the impact that such modifications have on activity. Additionally, a protease digest and mass spectrometry of AHU3-bound RecA would also help to investigate which residues interact with RecA.

***E. coli* O157:H7**

MAIDENKQKALAAALGQIEKQFGKGSIMRLGEDRSMDVETISTGSLDIALGAGGLPMGRIVEIYGPESGKTTTLTQVIAAAQREGKTAFIDAEH
 ALDPYIARKLGVDIDNLLSQPDTGEQALEIDALARSGAVDVVVDSVAALTPKAEIEGEGDSDHMGLAARMMSQAMRKLKAGNLKQSNLTLIFINQI
 RMKIGVMFNGNPETTTGGNALKFYASVRLDIRRIGAVKEGENVVGSETRVKVVKKNKIAAPFKQAEFQILYGEINFGELVDLGVKEKLIKAGAWY
 SYKGEKIQGKANATAWLKDNPETAKEIEKKVRELLSNPNSTPDFSVDDSEGVAETNEDF

***S. aureus* MRSA252**

MDNDRQKALDVTIKNMEKSFSGKAVMKLGDNIGRRVSTTSTGSVTLDNALGVGGYPKGRRIEYGPESGKTTVALHAIAEVQSNNGGVAAFIDAEH
 ALDPEYAQALGVVDIDNLLSQPDTGEQALEIDALARSGAVDVVVDSVAALTPKAEIEGEGMDTHVGLQARLMSQALRKLKSGAISKNTTIAIFINQI
 REKVGVMFNGNPETTPGGRALKFYSSVRLVRRAEQLKQGGQIEVGNRTKIKVVKKNKVAAPPFRVAEVDIMYGGISKEGELIDLGVENDIVDKSGAWY
 SYNGERMGGQKENVKMYLKENPQIKEIDRKLREKLGISDGDVEETEDAPKSLFDEE

S. enterica

MAIDENKQKALAAALGQIEKQFGKGSIMRLGEDRSMDVETISTGSLDIALGAGGLPMGRIVEIYGPESGKTTTLTQVIAAAQREGKTAFIDAEH
 ALDPVYARKLGVDIDNLLSQPDTGEQALEIDALARSGAVDVVVDSVAALTPKAEIEGEGDSDHMGLAARMMSQAMRKLKAGNLKQSNLTLIFINQI
 IRMKIGVMFNGNPETTTGGNALKFYASVRLDIRRIGAVKEGDNVVGSETRVKVVKKNKIAAPFKQAEFQILYGEINFGELVDLGVKEKLIKAGAWY
 SYNGEKIQGKANATTWLKENPATAKEIEKRVRELLSNQNPATPDFAVDDSEGVAETNEDF

B. subtilis

MSDRQAALDMALKQIEKQFGKGSIMKLGEKTDTRISTVPSGSLALDTALGIGGYPRGRIEYVYGPESGKTTVALHAIAEVQQGGQAAAFIDAEHAL
 DPVYAQKLGVNIEELLSQPDTGEQALEIAEALVRSAGVDIVVVDSVAALVPAKAEIEGDMGDSHVGLQARLMSQALRKLKSGAINKSKTIAIFINQIREK
 VGVVMFNGNPETTPGGRALKFYSSVRLVRRAEQLKQGNVDMGNKTKIKVVKKNKVAAPPFRVAEVDIMYGGISKEGELIDLGTLDIVQKSGSWYSYE
 EERLQGGRENKQFLKENKDIMLMIQEQRREHYGLDNNGVVQQAAETQEELEFEE

C. difficile

MSVDQEKALKALNEALGKIEKDFGKGSVMKLGAEATSMIDVISTGAIGLDIAIGIGLPRGRIVEYVYGPESGKTTVALSIVASAQKDGGAIAAFIDAEH
 ALDPVYAKALGVVDNLIISQPDTGEQALEIAEALIRSGAIDIVVDSVAALVPAKAEIEGDMGDSHVGLQARLMSQALRKLKSGAINKSKTIAIFINQIREK
 KVGIMFNGNPETTTGGNALKFYSSVRLVRRAEQLKQGNVDMGNKTKIKVVKKNKVAAPPFRVAEVDIMYGGISKEGELIDLGTLDIVQKSGSWYSYN
 DTKLQGGRENKQFLKEDNLDLTTIDEKVRAFYNLNEEHEESGTSVSKIEVEE

***P. aeruginosa* LESB58**

MDENKRALAAALGQIERQFGKGVMMRGDHERQAIPAISTGSLGLDIALGIGLPPKGRIVEIYGPESGKTTTLTSLVIAEAQKQATAFVDAEHA
 LDPDYAGKLGVNVDLLYSQPDTGEQALEITDMLVRSNAVDVIVDSVAALVPAKAEIEGEMGDAHVGLQARLMSQALRKLKSGAINKSKTIAIFINQIREK
 RMKIGVMFNGNPETTTGGNALKFYASVRLDIRRIGAVKEGDEVVVGSETRVKVVKKNKVAAPPFRVAEVDIMYGGISKEGELIDLGTLDIVQKSGSWYSYN
 SYQSGKIQGKANAAKYLEDNPEIGSVLEKTIRDQLLAKSGPVKADAEVADAEAD

S. pneumoniae

MAKKPKLEEISKKFGAEREKALNDALKLIEKDFGKGSIMRLGERAEQKVQVMSGSLDIALGSGGYPKGRRIEYGPESGKTTVALHAVAQAQK
 EGGIAAFIDAEHALDPYAAAALGVNIDELLSQPDSEGEQLEIAGKLIDSGAVDLVVDSVAALVPAEIDGDIKDSHVGLQARMMSQAMRKLKAGSI
 NKTKTIAIFINQLREKVGVMFNGNPETTPGGRALKFYASVRLDVRGNTQIKGTGDKQKTNVVKETKIKVVKKNKVAAPPFRVAEVDIMYGGISKEGEL
 LKIASDLDIHKAGAWYSYKDEKIQGSENAKKYLAHPEIFDEIDKQVRSKFLGIDGEEVSEQDTENKDKPEPKKEEAVNEEVPDLGDLELEIEIE

Figure Cysteine conservation in RecA across selected bacteria species

Three cysteine residues (green) are present in *E. coli* RecA, whereas no cysteine residues are present in *S. aureus*, *B. subtilis* and *P. pneumoniae*.

As explained in Section 3.10, AUC analysis showed that AHU3 interferes with the formation of larger oligomeric RecA species in solution, possibly explaining the mechanism behind its inhibitory effect on *stx2* expression. An interesting finding in the literature was a chloroamide-based compound with inhibitory activity on RAD51, the human homologue of RecA (Budke et al. 2012). The compound RI-1 was found in a high-throughput screening platform that was looking for compounds able to modify the binding of RAD51 to ssDNA. RI-1 was found to bind directly to a surface of RAD51 that serves as an interface between protein subunits of the RAD51 filaments (Figure 46). The striking structural similarity between RI-1 and AHU3 reinforces the hypothesis that AHU3 could also be

inhibiting the activity of RecA by reducing the formation of larger oligomeric species.

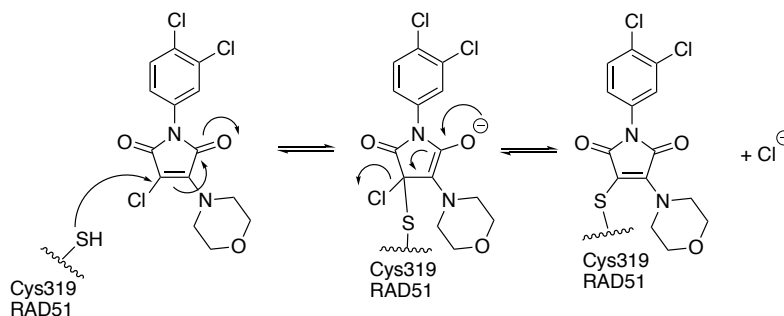


Figure 45 Proposed molecular mechanism of action of RI-1, an inhibitor of RAD51.

A cysteine residue in RAD51 is covalently modified by RI-1, thus interfering with the formation of functional RAD51 filaments (Adapted from Budke et al. 2012)

Although approximately 30% of drugs in the market are covalent inhibitors, there is reluctance in the pharmaceutical industry towards the development of drugs that bind irreversibly to their target protein(s), given the higher risk of off-target activity that can lead to toxicity (Mah, Thomas, and Shafer 2014). Off-target effects are a result of the covalent binding to other proteins that result in cell damage or immunological response. However, in the last few years there has been an increasing interest in this group of drugs. Covalent binding to the protein target provides higher potencies and prolonged effects in comparison to reversible drugs. This results in less-frequent dosing regimes, which widens the therapeutic margins of the drug (Bauer 2015). Furthermore, some studies have shown that covalent drugs could have a reduced risk for the development of resistance, particularly in areas like cancer or infectious diseases (Singh et al. 2011).

3.15.2 RecA as a drug target

The current antibiotic resistance problem and the urgent need for new antimicrobial strategies have prompted the search for novel drug targets. In recent years, RecA has been in the spotlight given the important role that it plays in bacterial physiology. Studies have shown that *recA*-deficient *E. coli* cells cannot cope with the hydroxyl radical damage caused by bactericidal antibiotics,

suggesting that targeting RecA can potentiate the current antibiotic arsenal (Kohanski et al. 2007). It has also been shown that inactivation of RecA abolishes the mutagenic effect induced by sublethal concentrations of antibiotics, reducing the generation of antibiotic-resistant mutants (Thi et al. 2011). Given the relationship between the SOS response and the spread of antibiotic resistance genes through horizontal gene transfer, it is clear that inactivation of RecA would diminish the efficiency of horizontal gene transfer, slowing the development of antimicrobial resistance (Beaber, Hochhut, and Waldor 2004). Based on our data, we propose that RecA could be a druggable target for the treatment of bacterial infectious diseases and, in particular, that RecA could be a good target to develop therapies for STEC infections.

While humans produce the RecA homologue Rad51, a recombinase also involved in DNA repair (Ristic et al. 2005), the low protein sequence similarity (25%, NCBI, BLAST) between RecA and Rad51 considerably decreases the risk of it being targeted by AHU3, although further studies would be needed to discard this possibility.

3.15.3 Challenges in the development of RecA inhibitors

Efforts to develop inhibitors of RecA have been attempted but little success has been achieved thus far. For instance, millimolar concentrations of the metal dications zinc(II), copper(II) and mercury(II) were shown to induce *in vitro* precipitation of RecA, effect which results from the metal-dependent initiation of RecA aggregation (A. M. Lee and Singleton 2004). The downside of this concept was the toxicity associated to these metals, limiting their use as therapeutics.

Similar to other ATPases, it has been shown that RecA can be inhibited *in vitro* by ADP and non-hydrolysable ATP derivatives (Moreau and Carlier 1989; Menetski and Kowalczykowski 1985). This rationale led to the development of N^6 -substituted ADP analogues capable of blocking the formation of RecA-DNA filaments (A. M. Lee et al. 2005). Unfortunately, the compounds discovered were of limited therapeutic utility given the membrane impermeability caused by the negatively charged 5'-diphosphate moiety at physiological pH. Interestingly,

many of the small molecules that have been found to inhibit RecA share this feature; they are rich in negatively charged moieties. For example, using an ATP hydrolysis plate assay, Wigle and Singleton discovered three polysulfated naphthyl compounds that inhibited RecA's ATPase activity *in vitro* (Wigle and Singleton 2007). These compounds were suramin, Congo Red and bis-ANS. Again, their lack of therapeutic utility was associated to the membrane impermeability caused by their negative charges.

The two cellular membranes and the lipopolysaccharide-coated outer membrane present in Gram-negative bacteria are very difficult for small molecules to cross (Hiroshi Nikaido 2003; H Nikaido 1994; Carpenter, Parkin, and Khalid 2016). To complicate things further, efflux pumps can also interfere with the accumulation of compounds inside bacterial cells (Silver 2011). Usually, small molecules that are able to cross the outer membrane do so through porins, cylinder-shaped channels that are lined with charged amino acids (Cowan et al. 1992). For a compound to enter the cell through these channels, the hydration shell of the amino acids has to be removed temporarily and replaced by the small molecule. For this reason, lipophilic molecules cannot cross the outer membrane easily. In fact, most of the antibiotics that are active against Gram-negative bacteria are highly polar and have a molecular weight of less than 600 Da (O'Shea and Moser 2008). In practice these principles are not always the case as there are antibiotics that meet these criteria but lack activity against Gram-negative bacteria.

The current understanding of the physicochemical properties that influence the uptake and accumulation of small molecules in Gram-negative organisms is mainly based on retrospective analyses of antibiotics (Brown et al. 2014). Recently, Richter and collaborators studied the ability of over 180 diverse compounds to accumulate in *E. coli*, in order to gain a better understanding of the parameters that govern the uptake of molecules in Gram-negative bacteria (Richter et al. 2017). Using accumulation assays in whole cells, followed by structure-activity (SAR) relationship studies and computational analyses, they found that compounds that are most likely to accumulate in *E. coli* contain an amine, are amphiphilic and rigid, and have low globularity. Experimental

findings like these will hopefully aid the development of compounds able to permeate Gram-negative organisms.

A different strategy to promote the uptake of large molecules in Gram-negative bacteria is the development of compounds that make the outer membrane more permeable. For instance, Muheim and co-workers performed a HTS looking for molecules able to make *E. coli* more susceptible to vancomycin. They discovered the compound MAC13243, a reported inhibitor of the essential chaperone LolA (Muheim et al. 2017). Inhibition of this chaperone affects the integrity of the outer membrane, making it more permeable. Indeed, the use of subinhibitory concentrations of MAC13243 made the outer membrane of *E. coli* permeable to the fluorescent dye 1-N-phenylnaphthylamine (NPN) and potentiated the effect of large scaffold antibiotics like novobiocin and erythromycin.

3.15.4 RecA-independent prophage induction

As previously explained, induction of all lambdoid prophages relies on the removal of the *cl* repressor from its corresponding DNA motif. The best understood mechanism of induction involves the RecA-mediated autoproteolysis of the *cl* repressor, via the SOS response. Self-cleavage of the *cl* repressor activates the phage lytic cycle, including production of Stx.

Nonetheless, RecA-independent mechanisms for the induction of lambdoid phages have also been reported. Rozanov and collaborators found that two *E. coli* genes, *rcaA* and *dsrA*, can cause partial induction of the phage λ in *recA*-deficient strains (Rozanov, D'ari, and Sineoky 1998). RcsA is a positive transcriptional regulator of the *cps* operons involved in capsular polysaccharide synthesis, also known as colanic acid. The synthesis of colanic acid is regulated by the RcsABC system (Stout and Gottesman 1990). Prophage induction by this system only occurs in the exponential phase, and it is thought to happen either from a reduction of *cl* synthesis or from a decreased repressor activity via an alternative RecA coprotease. DsrA is a small RNA molecule that derepresses *rcaA* transcription. Overexpression of this RNA was shown to efficiently cause prophage induction in both exponential and stationary phase. The mechanism

behind this regulation is still to be shown. Then, Imamovic and Muniesa discovered that chelating agents like EDTA and sodium citrate have the ability to induce Stx phages by causing damage to the outer membrane and by alkalinisation of the medium (Imamovic and Muniesa 2012).

Although RecA-independent prophage induction is possible, we consider that targeting RecA is still a viable approach to prevent Stx expression *in vivo*. Physiologically, when STEC colonizes the human gut, the main stressors encountered by bacteria are hydrogen peroxide produced by neutrophils (Wagner, Acheson, and Waldor 2001) and antibiotics administered by physicians. Though hydrogen peroxide is not as good inducing agents as MMC or UV radiation, it has been shown that is it able to induce the bacterial SOS response, which implies that small molecules able to inhibit RecA would be a viable therapeutic strategy for STEC infections.

CHAPTER 4

Identification of selective inhibitors of Shiga toxin expression by high throughput screening

4 Identification of selective inhibitors of Shiga toxin expression by high throughput screening

4.1 Introduction

As a result of the successful identification of a small molecule capable of inhibiting Stx2 expression in *E. coli* O157:H7, an additional high-throughput screening (HTS) of small molecules was performed. This was done at the Drug Discovery Unit, University of Dundee. The aim was to build on our experience from the previous series and hopefully find a new, more potent and less toxic series of Stx inhibitors.

Using the *stx2::GFP* reporter assay described in chapter 3, a total of 29,504 compounds were screened for activity against Stx expression. The cut-off for hit selection was anything above 40% inhibition of *stx2::GFP* expression. The primary screen identified 130 putative hit compounds. Analysis of the compounds using orthogonal assay to discard false positives showed that only 9 compounds exhibited activity in a dose-dependent manner and with no effect on bacterial growth. Further biological characterisation of the hit compounds revealed that only two molecules block expression of Stx2 in a specific and dose-dependent manner.

The work presented in this chapter goes from the development of the biological assay used in the primary screen, to the validation of hits and their biological evaluation.

4.2 Assay development and validation

4.2.1 DMSO tolerance

Since the libraries of compounds are stored as DMSO solutions, it is important to discard any undesirable effects that DMSO might have on the assay. To this end, three different concentrations of DMSO were tested in both *E. coli* O157 *stx2*::GFP and *E. coli* O157:H7 *rpsM*::GFP. As shown in Figure 47, DMSO concentrations up to 1% had no significant effect on bacterial growth in both reporter strains.

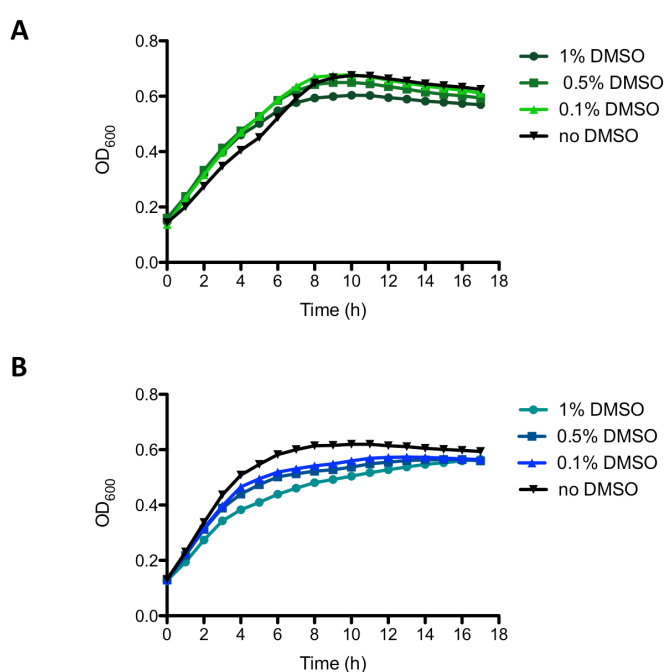


Figure 46 Effect of DMSO on bacterial growth.

Since all the compounds in the chemical library to be screened are dissolved in DMSO, it was important to discard any possible interference with bacterial growth. Concentrations of DMSO up to 1% v/v did not have any significant effect in both the A) *stx2*::GFP and B) *rpsM*::GFP reporter strains.

4.2.2 Statistical evaluation of the HTS assay

In order to identify bioactive compounds using a relevant biological model, certain quality metrics need to be taken into account in order to make sure that the data meet certain standards. In the Drug Discovery Unit, three parameters

are routinely assessed: *signal to background ratio*, *coefficient of variation* and *Z'-factor*.

Signal to background (S:B). It provides an indication of the separation between positive and negative controls. A good separation between controls is essential to identify changes in activity produced by active compounds. It is calculated using the following formula:

$$S:B = M_{\text{signal}} / M_{\text{background}}$$

Where M is the mean of the signal.

Coefficient of variation (CV): It is normally expressed as percentage and it provides a good indication of variability for the signal. It can be influenced by the assay stability, precision of liquid handling and detection instruments. It is calculated using the following formula

$$CV = 100 \times SD/M (\%)$$

Z' factor. In 1999, Zhang and collaborators introduced the Z-factor, a dimensionless statistical parameter that assesses the quality of the bioassay used in HTS campaigns. This parameter takes into account both the assay signal dynamic range and the data variation associated with the signal measurements (Zhang, Chung, and Oldenburg 1999). The Z factor can be calculated using equation 1. Note that for agonist/activation assays, *control* means the maximum activation signal data; for antagonist/inhibition assays the *control* is the minimum activation signal or negative control.

Equation 1

$$Z = 1 - \frac{(3 SD_{\text{sample}} + 3 SD_{\text{control}})}{|Mean_{\text{sample}} - Mean_{\text{control}}|}$$

Similar to the Z factor, the Z'-factor (Z-prime) can be calculated using only data from both positive (*p*) and negative (*n*) controls (equation 2). Equation 2 shows that a good Z' value is obtained when the means of both controls are strongly different to each other and have very low standard deviations.

Equation 2

$$Z' = 1 - \frac{(3 SD_p + 3 SD_n)}{|Mean_p - Mean_n|}$$

The Z' has a range of 0 to 1. The closer the value is to 1, the more robust and reliable the assay is. In HTS campaigns, assays with a Z' value above or equal to 0.5 are considered excellent assays. Table 18 shows the interpretation for different Z' values.

Table 18 Z' value and its interpretation (modified from Zhan, Chung, and Oldenburg, 1999).

Z' value	Interpretation
1	An ideal assay.
$1 > Z' \geq 0.5$	An excellent assay. Separation band is large
$0.5 > Z' > 0$	Separation band is small. More optimisation is needed
0	No separation band, the sample and control signal variations are very close
< 0	No separation band, the sample and control signal variations overlap

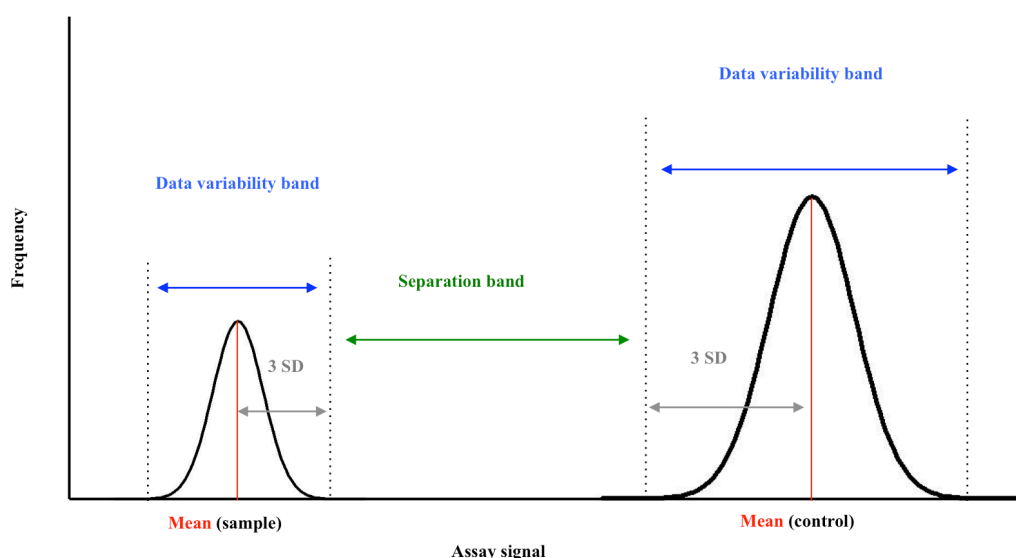


Figure 47 Separation band the suitability of an assay for HTS.

A good assay for a HTS campaign should have a clear separation between the tails of the distributions of the controls and a large signal window or separation band (>3-fold). Modified from Zhang, Chung, and Oldenburg 1999.

The robustness of the *stx2::GFP* assay was assessed by performing a pilot experiment with a small number of plates. This was to ensure that the assay would reliably detect compounds that have an effect on the biological model using the equipment and reagents available at the screening facilities. As shown in Figure 49, the assay produced low standard deviations and wide assay windows, therefore high Z' values were produced (>0.5).

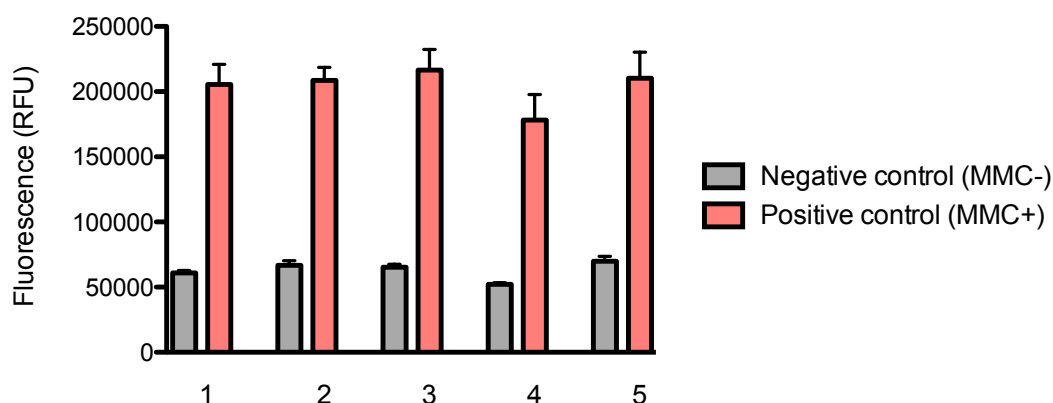


Figure 48 Assay performance of the *stx2::GFP* reporter strain.

Five different 384-well plates were used in a pilot experiment to assess the robustness and reproducibility of the assay. All five plates showed high Z' values (>0.4), good S:B ratio (>2) and acceptable %CV (<10%) suggesting that the assay was robust and reliable. The data shown are the average of five individual experiments with standard deviation from the mean displayed as error bars.

Table 19 Assay validation *stx2::GFP*

		Plate number				
		1	2	3	4	5
Negative control	Mean	60944	66678	65220	52274	69927
	Median	61221	67177	65283	52030	69342
	SD	1791	3568	2295	1203	3715
	%CV	2.94%	5.35%	3.52%	2.30%	5.31%
Positive control	Mean	205574	208749	216527	178253	210310
	Median	205139	205680	213373	181683	204997
	SD	15344	9863	15784	19540	19934
	%CV	7.46%	4.72%	7.29%	10.96%	9.48%
Robust Z' factor		0.64	0.71	0.64	0.77	0.49
S:B		3.3	3.13	3.31	3.40	3.0

The robustness of the *rpsM::GFP* assay was also assessed in a pilot experiment with five different plates. In this case the antibiotic ampicillin was used as positive control (a compound that interferes with bacterial growth). As shown in Figure 50, the assay also produced low standard deviations and wide assay windows, therefore high Z' values were produced (>0.5).

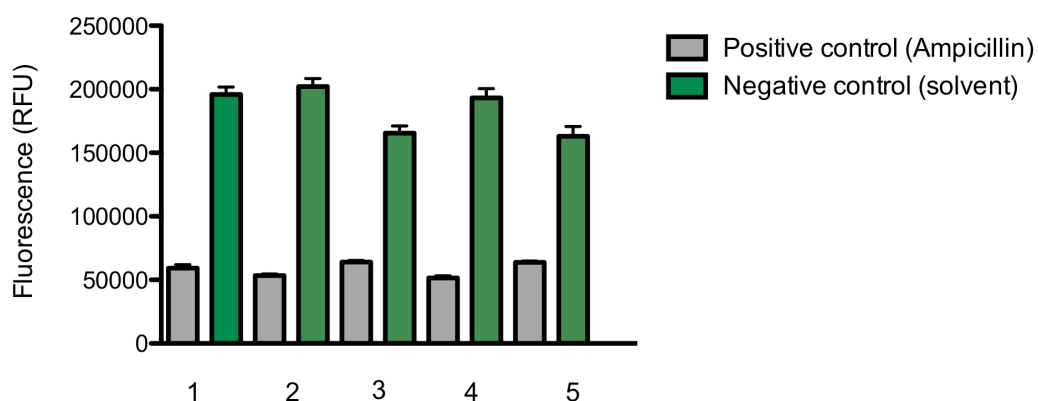


Figure 49 Assay performance of the *rpsM::GFP* reporter strain.

Five different 384-well plates were used in a pilot experiment to assess the robustness and reproducibility of the assay. All five plates showed high Z' values (>0.7), good S:B ratio (>2.5) and acceptable %CV (<10%) suggesting that the assay was robust and reliable. The data shown are the average of five individual experiments with standard deviation from the mean displayed as error bars.

Table 20 Assay validation *rpsM::GFP*

		Plate number				
		1	2	3	4	5
Negative control	Mean	59225	53494	64070	51589	63841
	Median	58656	53646	63726	51817	63695
	SD	2790	1296	1310	1714	1154
	%CV	4.71 %	2.42%	2.04%	3.32%	1.80%
Positive control	Mean	196035	202197	165513	193151	162963
	Median	194778	200256	163569	191705	162585
	SD	5721	6311	5585	7448	7844
	%CV	2.91%	3.12%	3.37%	3.85%	4.81%
Robust Z' factor		0.85	0.89	0.84	0.85	0.74
S:B		3.3	3.7	2.5	3.7	2.5

4.3 High throughput screening at the Drug Discovery Unit (DDU) University of Dundee

After optimisation and validation of the *stx2::GFP* assay, a single point screen of small molecules was carried out at the University of Dundee using the *stx2::GFP* expression assay. A total of 29,504 compounds from three different libraries were screened: the Gates and DDU targeting sets, the Epigenetics set and

Easysset. All of the compounds in the libraries are from synthetic origin, sourced from commercial suppliers and highly curated to cover diverse chemical space. The HTS was performed in a 384-well format, using the layout shown in Figure 51. The compounds were aliquoted in columns 1 to 22 to give a final concentration of 30 μM . Columns 23 and 24 were used as the positive (0% inhibition) and negative (100% inhibition) controls, respectively. The screening was carried out in 7 batches of 10-20 plates over the course of 3 weeks.

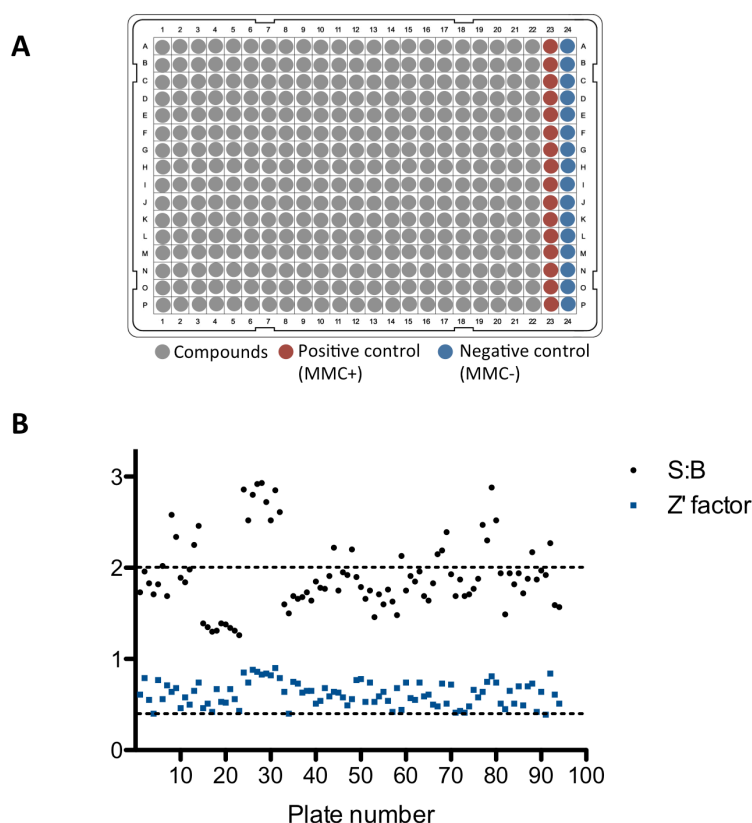


Figure 50 Single point HTS to identify inhibitors of Stx2 expression in *E. coli* O157:H7.

The screening of small molecules was performed at a final concentration of 30 μM using the *stx2::GFP* reporter assay. **A)** 384-well plate layout used for the screening of compounds; wells in columns 1 to 22 contained the compounds to test, wells in columns 23 and 24 were used as the positive (0% inhibition) and negative (100% inhibition) controls, respectively. **B)** Plot of S:B ratio and Z' factor for all the plates screened. Dotted lines indicate the quality control thresholds used in the DDU ($Z'=0.5$, $S:B=2$).

The quality and robustness of the screen was constantly monitored between plates and batches. The quality control criteria for acceptance of the assay were: $S:B$ ratio ≥ 2 , $CV\% < 10\%$ and $Z' \geq 0.4$. Although the screen performance was as expected, an important drop in S:B was observed as some plates had

values well below the acceptance limit (Figure 51B). However, the Z' factor of most of the plates remained above the 0.4 limit, suggesting that screen remained robust throughout the campaign.

Once the plates were screened, the hit identification process took place. The cut-off for hit selection was anything above 40% inhibition of *stx2*::GFP expression (Figure 52). The percentage effect for each compound tested was calculated using fluorescence (in relative fluorescence units or RFUs) of MMC treated cells to set the 0% effect and MMC untreated cells to set the 100% effect.

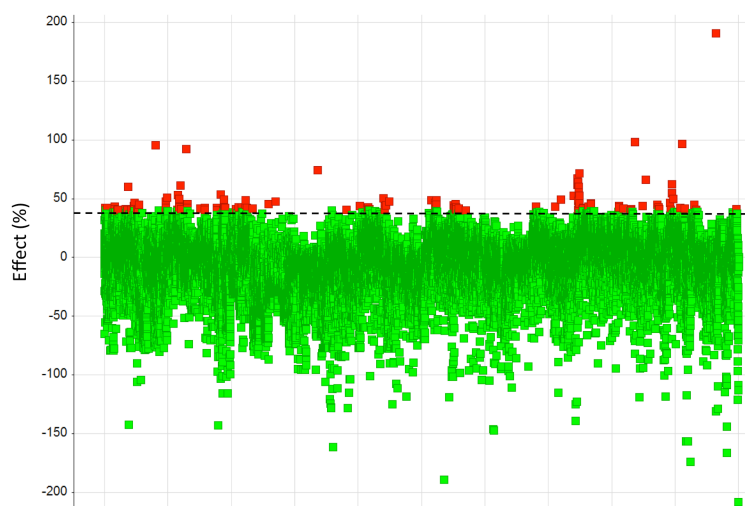


Figure 51 Hit selection from the HTS campaign.

Any compound that showed a decrease in *stx2*::GFP expression equal or superior to 40% (red dots) was considered a potential hit. Dotted line shows the 40% cut-off.

As shown in Figure 53, screening data is typically not normally distributed. Instead, it is asymmetrical with long tails or 'outliers' comprising the active compounds. As a result, using the average and standard deviation for hit selection is not a valid approach. To overcome this issue, a different parameter is taken, the median absolute deviation (MAD). MAD can be defined as:

$$\text{MAD} = 1.4826 \times \text{median} (| x_{ij} - \text{median}(x) |)$$

where x indicates all the values in the sample wells of a plate and x_{ij} the sample well at the row i and the column j . The number 1.4826 is used as a constant to make MAD comparable to SD when the data is normally distributed (Chung et al. 2008). Thus, in the Z' score formula, the mean and the SD are replaced with median and MAD.

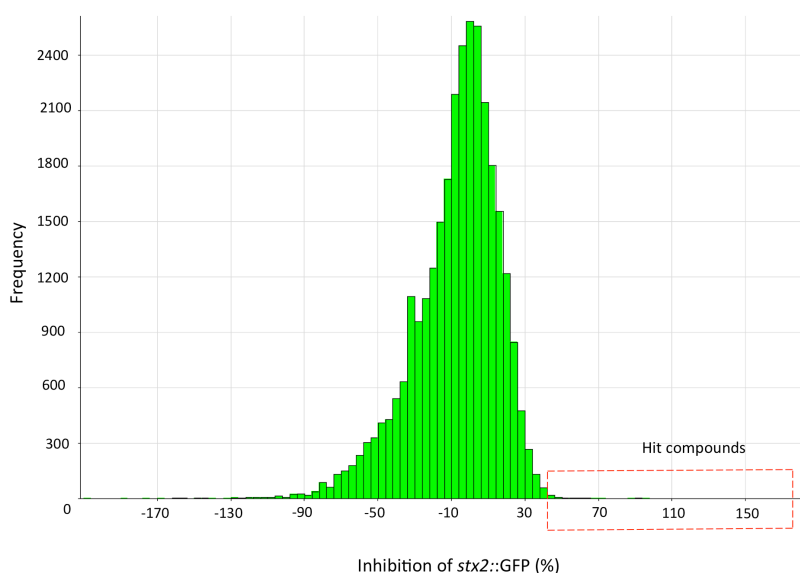


Figure 52 Response distribution of the HTS.

The screen output is represented as % inhibition of *stx2::GFP* and plotted as a frequency distributions of all compounds tested. Compounds that inhibited *stx2::GFP* by 40% (red square) or more were designated potential inhibitors.

Interestingly, the majority of the compounds screened appeared to enhance fluorescence rather than decrease it. This can also be seen in the distribution profile of the compounds shown in Figure 53 where it can be clearly seen that the number of enhancers of *stx2::GFP* surpassed the number of inhibitors. This can be attributed to possible autofluorescence properties of the compounds or potential triggers of the SOS response. Another possible factor for this behaviour could be a defective distribution of heat in the plates, a problem known as the edge effect (Lundholt, Scudder, and Pagliaro 2003).

4.4 Dose response evaluation of putative hit compounds and counter-screen

In order to confirm the activity of the compounds and to establish their potency, the 130 hit compounds identified in the primary screen were further re-tested in a dose-response assay. The assay consisted in a 10-point 2-fold serial dilution of the test compounds from 100 μM to 0.01 μM , using the same conditions used in the primary screen. Since compounds that affect bacterial growth would result in a decrease in GFP expression, a counter-screen using *E. coli rpsM::GFP* was performed in parallel to identify false positives. The *rpsM* promoter activity (30S ribosomal subunit) was chosen as a housekeeping gene control as it is not related to Stx expression (Roe et al. 2004). The plate layout used for the dose-response assay and counter-screen is shown in Figure 54. Columns 1 to 10 and 13 to 22 contained the compounds serially diluted. Columns 11 and 23 were used as the positive control (0% inhibition) and columns 12 and 24 as the negative control (100% inhibition). Both assays complied with the quality controls from the DDU.

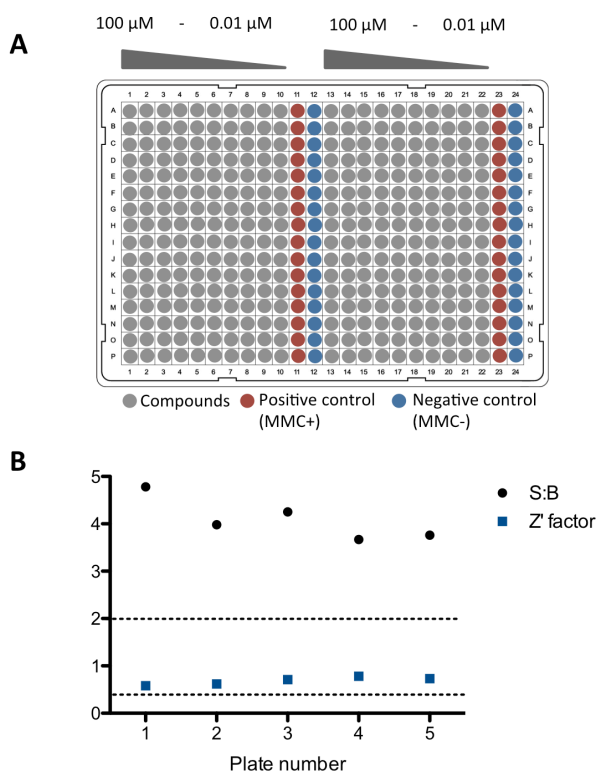


Figure 53 Secondary screening of the hit compounds using the *rpsM*::GFP.

In order to discard false positives, the hit compounds were evaluated using the *rpsM*::GFP reporter assay. **A)** 384-well plate layout used for the counter-screen; wells in columns 1 to 10 and 13 to 22 contained the compounds serially diluted. Columns 11 and 23 were used as the positive control (0% inhibition) and columns 12 and 24 as the negative control (100% inhibition) **B)** Plot of S:B ratio and Z' factor for all the plates screened. Dotted lines indicate the quality control thresholds used in the DDU (Z'=0.5, S:B=2).

From the 130 hit compounds identified, only 9 compounds exhibited activity in a dose-dependent manner without affecting bacterial growth (Table 22). The potency of these compounds was determined by calculation of their XC_{50} values, where 'X' denotes either antagonistic (IC_{50}) or agonistic (EC_{50}) activity. In HTS campaigns, the XC_{50} values are routinely reported as pXC_{50} values (negative logarithm of the molar concentration). Table 21 shows a conversion table between these two values. The higher the pXC_{50} , the more potent a compound is.

Table 21 Conversion table between pXC₅₀ and μM .

pXC ₅₀	μM
4	100
4.3	50
4.6	25
4.9	12.5
5.2	6.25
5.5	3.125
5.8	1.563
6.1	0.781
6.4	0.391
6.7	0.195
7.0	0.098

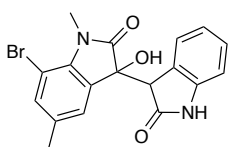
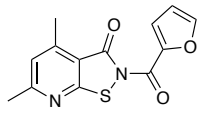
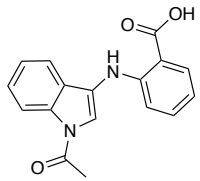
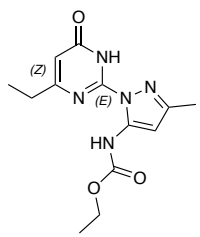
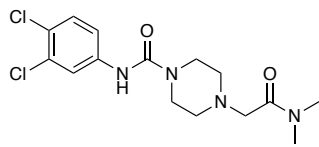
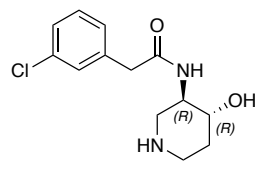
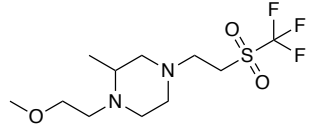
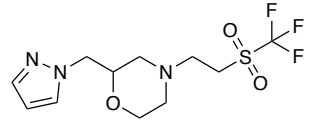
The pXC₅₀ values were obtained through the construction of dose-response curves, where different concentrations of the compounds are plotted against the corresponding assay response (GFP expression). A dose-response curve has four parameters: top asymptote (maximal response), bottom asymptote (baseline response), slope (Hill slope) and the XC₅₀ value (Goktug, Chai, and Chen 2013).

The dose response curves were fit using the following equation:

$$y = A + \frac{B - A}{1 + \left(\frac{10^C}{x}\right)^D}$$

where A is the minimum fold change, B is the maximum fold change, C is the Log XC₅₀ value and D is the slope factor; x is the drug concentration and Y is the fold change. Data were fitted using the Levenburg Marquardt algorithm. The dose response analysis identified 8 compounds as specific inhibitors of *stx2::GFP* expression in the primary assay, with pIC₅₀ values ranging from 4 to 5.64 (Figure 55).

Table 22 Chemical structures of the hit compounds, potency and activity.

Compound structure and name	Molecular formula	pXC ₅₀	Maximum effect (%)
 DDD00040598	C ₁₈ H ₁₅ BrN ₂ O ₃	5.64	77
 DDD00058801	C ₁₃ H ₁₀ N ₂ O ₃ S	5.55	89
 DDD00074091	C ₁₇ H ₁₄ N ₂ O ₃	4.83	91
 DDD01049435	C ₁₃ H ₁₇ N ₅ O ₃	4.67	56
 DDD01292781	C ₁₅ H ₂₀ Cl ₂ N ₄ O ₂	4.65	51
 DDD01257835	C ₁₃ H ₁₇ ClN ₂ O ₂	4.67	64
 DD01302463	C ₁₁ H ₂₁ F ₃ N ₂ O ₃ S	4.0	97
 DDD01304030	C ₁₁ H ₁₆ F ₃ N ₃ O ₃ S	4.1	86

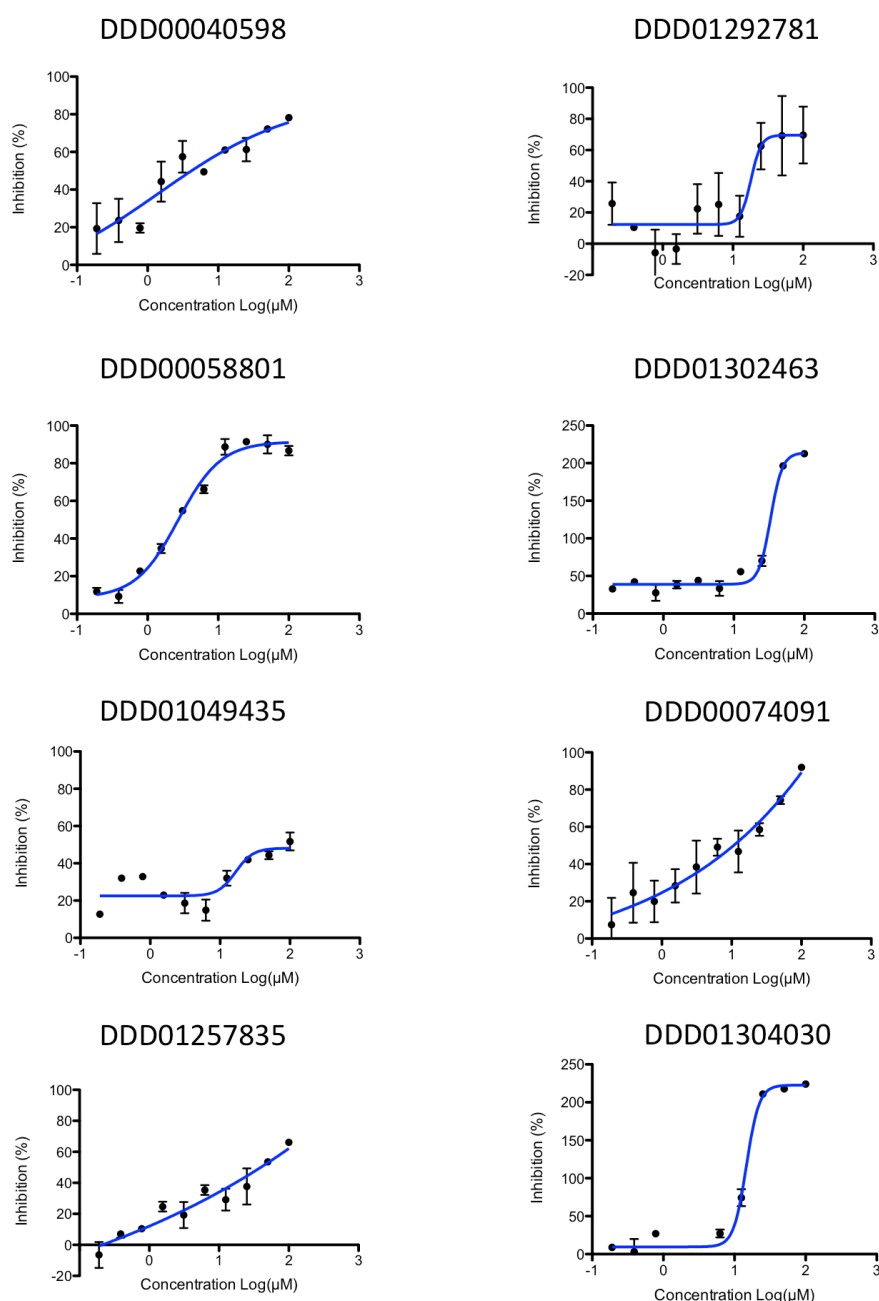


Figure 54 Dose-response curves from the hit compounds identified in the primary screen.

The potency of the hit compounds was assessed using the *stx2::GFP* assay, two-fold serial dilutions of the compounds. For all data analysis, the RFU of each well was normalised to as percentage effect (% Effect) of the positive control. Potency was determined using a 4-parameter logistic fit (minimum, maximum, hill slope and IC_{50}), being defined in reference to the negative logarithm of the molar value at the point of inflection of a sigmoidal dose-response curve (pIC_{50}). All the plates assessed were subject to quality control analysis, ensuring that the SB ratio ≥ 2 , CV % < 10% and $Z' \geq 0.4$.

4.5 Characterisation of hit compounds

To further evaluate the compounds, they were repurchased from commercial suppliers, and their purity was verified using LC-MS. It is important to repurchase or synthesise a new batch of the hit compounds as impurities could confer supposed activity in the primary assay. The compounds were re-tested in the *stx2*::GFP primary assay to confirm their activity. Upon re-evaluation, only the compounds DDD00040598, DDD00058801, DDD01049435, DDD01302463 and DD01304030 showed a dose-dependent reduction of fluorescence in the *stx2*::GFP reporter assay (Figure 56).

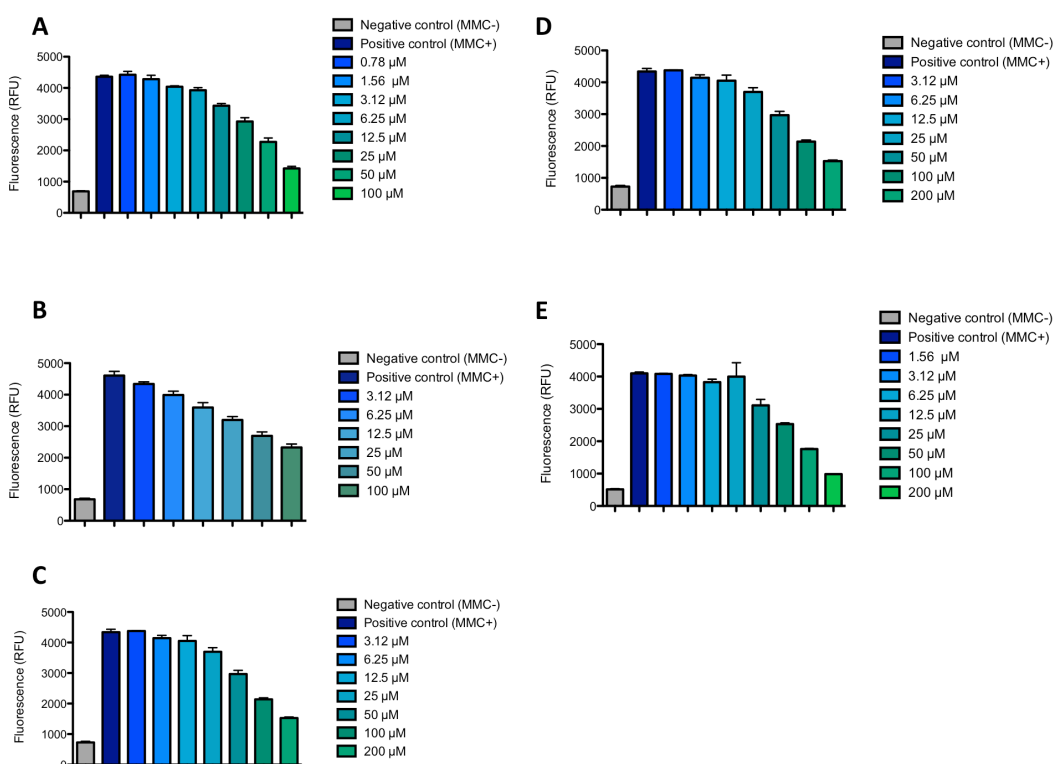


Figure 55 Re-evaluation of the hit compounds in the *stx2*::GFP reporter assay.

The freshly acquired compounds were tested in our laboratory to confirm the results obtained in the primary screen. Only 5 of the 8 hit compounds showed a dose-dependent reduction of fluorescence: (A) DDD00040598, (B) DDD00058801, (C) DDD01049435, (D) DDD01302463 and (E) DD01304030. The data shown are the average of three biological replicates with standard deviation from the mean displayed as error bars.

4.5.1 The compounds DDD01302463 and DDD01304030 block the phage lytic development

Next, we decided to test if the compounds had any effect on Stx prophage induction and phage lytic development. Transduction assays were performed using *E. coli* JP10819, which carries the lysogenic Stx2 prophage ϕ P27 with a tetracycline resistance cassette inserted into the *stx2* gene (Quiles-Puchalt et al. 2014). The non-lysogenic *E. coli* MG1665 was used as the acceptor strain. Only two hit compounds effectively reduced the production of phage particles: compounds DDD01302463 and DDD01304030. As shown in Figure 57, bacterial cultures that were not induced with MMC produced low levels of Stx phage (10^5 PFU/mL), whereas the presence of MMC increased the levels by four logs to 10^9 . The presence of 200 μ M of DDD01302463 significantly decreased the amount of Stx phage produced with a titre of 10^5 PFU/mL. This demonstrated that DDD01302463 inhibits the production of functional Stx phages. Similar results were observed for DDU01304030, although it appeared to be less potent in comparison to DDD01302463.

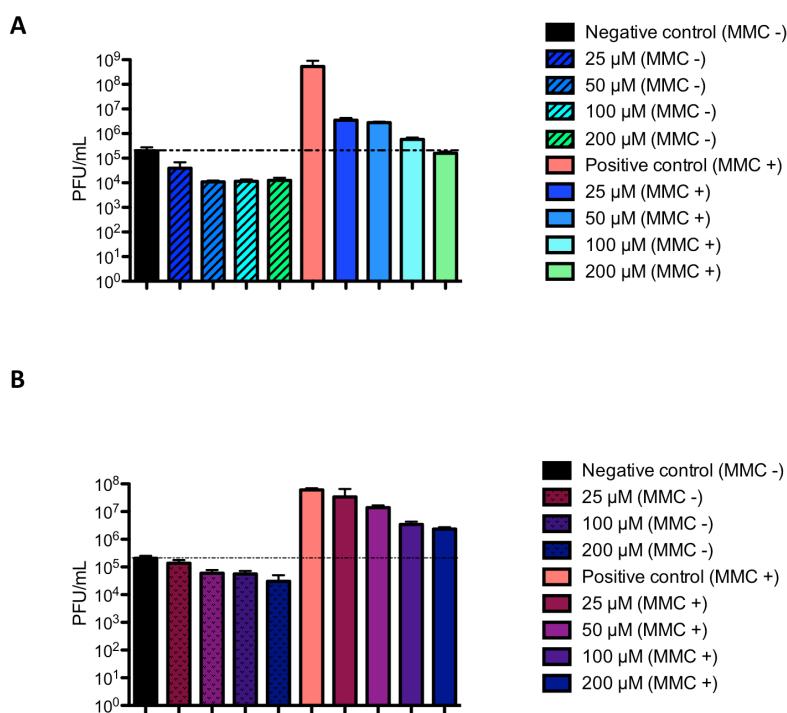


Figure 56 Effect of the compounds DDU01302463 and DDU01304030 on MMC-induced phage production.

Induction of JP10819 with 2 μg/ml MMC resulted in significantly increased Stx phage production. (A) DDU01302463 produced a significant decrease in phage production by both non-induced and MMC-induced JP10819. (B) Similarly, DDU01304030 decreased the production of phage particles in a dose-dependent manner. The data shown are the average of three independent experiments with standard deviation from the mean displayed as error bars.

As previously mentioned, prophage induction is intrinsically linked with bacterial lysis (Mauro and Koudelka 2011). Thus, inhibition of MMC-induced bacterial lysis is a confirmatory phenotype of the compound's ability to prevent Stx production.

To test this hypothesis, cultures of *E. coli* O157:H7 were incubated in the presence of DDU01302463 and DDU01304030, and induced with MMC. As shown in Figure 58, bacterial lysis was inhibited in a dose dependent manner. These results are in accordance with the data obtained in the transduction assay. The compounds seem to be effectively blocking phage lytic development.

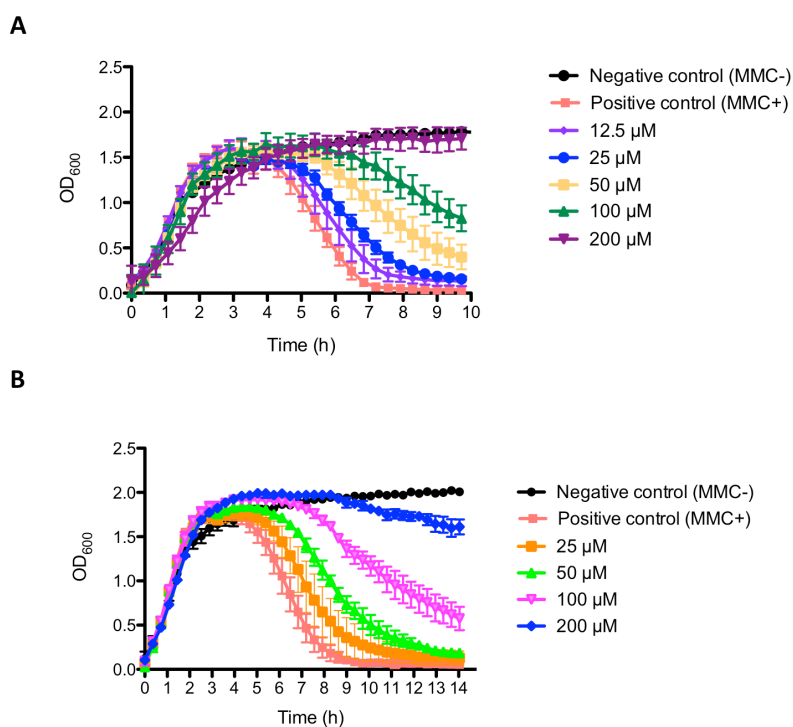


Figure 57 Effect of the compounds DDU01302463 and DDU01304030 on MMC-induced cell lysis.

Dose-dependent inhibition of bacteriophage mediated lysis in the presence of the compounds (A) DDU01302463 and (B) DDU01304030. The data shown are the average of three independent experiments with standard deviation from the mean displayed as error bars.

The pXC_{50} values for both compounds were recalculated using the freshly purchased compounds. For DDU01302463 the pXC_{50} was 4.0 and for DDU01304030 it was 4.1 (Figure 59), similar to the values previously obtained (table 22).

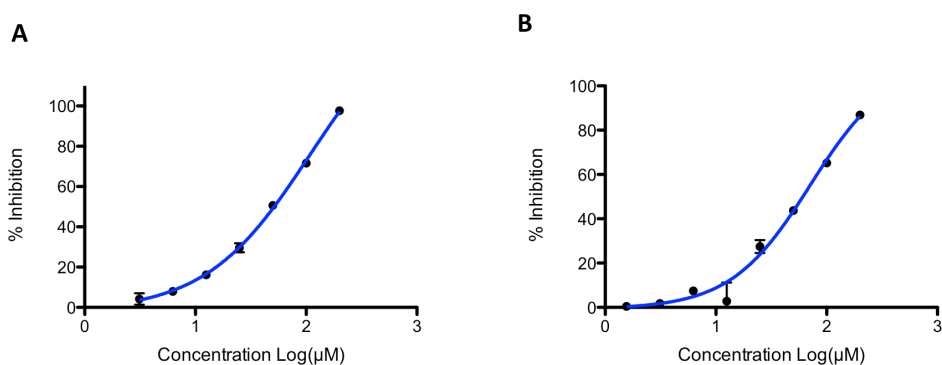


Figure 58 Potency of the hit compounds DDU01302463 and DDU01304030

The confirmed hit compounds were repurchased and tested in the *stx2::GFP* assay. *E. coli* O157:H7 was treated with 7-point, 2-fold serial dilution of the compounds. A) Calculated pXC_{50} for DDU01302463 B) Calculated pXC_{50} for DDU01304030

4.5.2 The compounds DDD01302463 and DDD01304030 do not affect bacterial growth and are specific against Stx expression.

It was essential to verify that the reduction in fluorescence in the *stx2::GFP* assay by the compounds DDD01302463 and DDD01304030 was not due to effects on bacterial growth. Bacterial cultures of *E. coli* O157:H7 were grown in the presence of different concentrations of the compounds. Ampicillin was used as a positive control i.e. inhibition of growth. As shown in Figure 60-A,C, DDD01302463 and DDD01304030 did not have a significant effect on bacterial growth. This was also confirmed using the *rpsM::GFP* reporter assay (Figure 60-B-D). The presence of the compound did not cause any significant decrease in fluorescence, confirming that the compounds are specific inhibitors of *stx* expression.

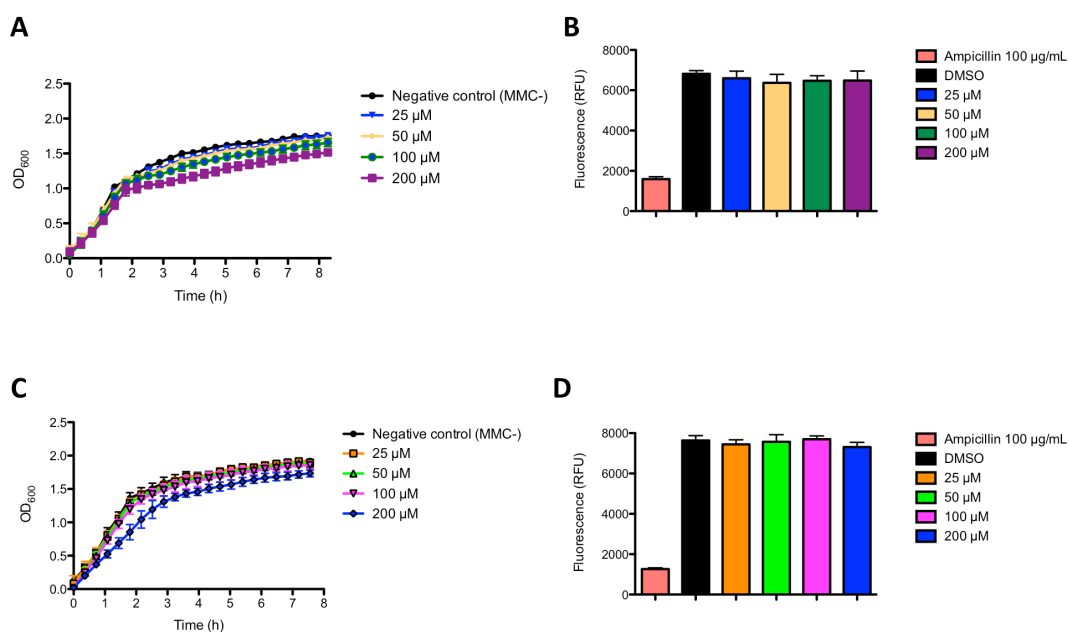


Figure 59 Evaluation of effect of compounds DDD01302463 and DDD01304030 in bacterial growth and *rpsM::GFP* expression.

A) Bacterial growth curve of *E. coli* O157:H7 in the presence of different concentrations of DDD01302463. **B)** Evaluation of DDD01302463 in the *rpsM::GFP* reporter assay demonstrated that the activity is specific only against Stx expression. Ampicillin was used as control to show a negative effect on growth and fluorescence measurements. **C)** Bacterial growth curve of *E. coli* O157:H7 in the presence of different concentrations of DDD01304030. **D)** Evaluation of DDD01302463 in the *rpsM::GFP* reporter. The data shown are the average of triplicate individual experiments with standard deviation from the mean displayed as error bars.

4.5.3 Evaluation of the compounds DDD01302463 and DDD01304030 in the Shiga toxin cytotoxicity assay

As previously discussed, when prophage induction occurs in STEC, the lysates of such cultures are toxic to Vero cells (Konowalchuk, Speirs, and Stavric 1977). Hence, testing the toxicity of the cell lysates in the presence and absence of the hit compounds is an indirect way of assessing their inhibitory activity on Stx expression.

To do this, we used the *C. rodentium* strain carrying the λ stx_{2dact} gene (Mallick et al. 2012). Cultures were treated with 200 μ M of DDD01302463 and DDD01304030. An additional culture treated with 50 μ M of the RecA inhibitor AHU3 was used as a control. Stx production was triggered by the addition of 1 μ g/mL of MMC to the samples containing the compounds and to the MMC-only control. Cultures were filter sterilised using 0.2 μ m syringe filters and serially diluted. The dilutions of the lysates were added to Vero cells plates and incubated for further 48 h at 37°C in a humidified 5% CO₂ incubator. Cytotoxicity was assessed using the methylthiazolyldiphenyl-tetrazolium bromide (MTT) assay (Denizot and Lang 1986).

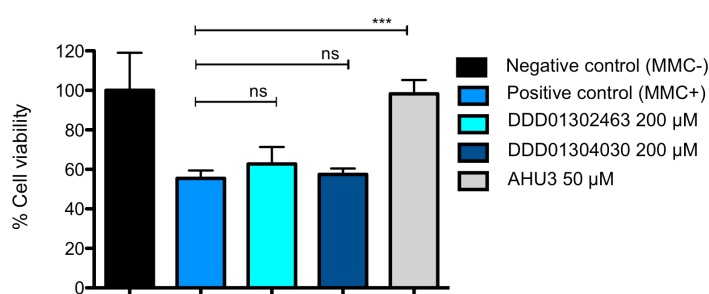


Figure 60 Effect of DDD01302463 and DDD01304030 on viability of Vero cells treated with lysates of *C. rodentium* λ stx_{2dact}.

Vero cells were treated with lysates of *C. rodentium* λ stx_{2dact} prepared from cultures: untreated (negative control), treated with 1 μ g/mL MMC to induce Stx expression (positive control), 200 μ M of DDD01302463 and DDD01304030 and 50 μ M of AHU3 as control. Results represent mean values from three independent experiments, with error bars indicating SD. Statistical significance is shown as P values obtained by *t* test (***) $p < 0.001$.

As shown in Figure 61, the compounds DDD01302463 and DDD01304030 did not show a significant decrease in the toxicity of *C. rodentium* λ stx_{2dact} lysates in comparison to the AHU3 compound. This result might be due higher potency that AHU3 has or the type of interaction involved in the biological effect. AHU3 could be more potent given the covalent nature of its binding its receptor, the RecA protein.

Western Blot analysis of *C. rodentium* λ stx_{2dact} supernatants showed that the compound DDD01302463 indeed inhibits Stx expression in a dose dependent manner, but that it is less effective than AHU3. Similarly to the effect seen in *E. coli* O157:H7, DDD01302463 also blocked phage-mediated lysis in *C. rodentium* λ stx_{2dact} (Figure 62).

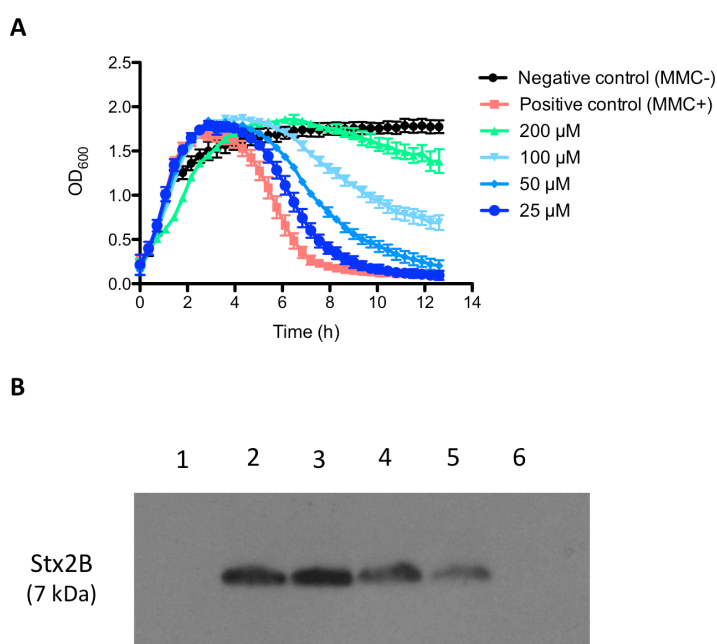


Figure 61 Effect of DDD01302463 on Stx production in *C. rodentium* λ stx_{2dact}.

A) DDD01302463 blocks phage-mediated lysis in *C. rodentium* λ stx_{2dact} in a dose-dependent manner. **B)** Supernatants of *C. rodentium* non-induced and induced with MMC was blotted for Sxt2B. Lane 1: non-induced culture, Lane 2: MMC -induced culture, Lane 3: 50 μ M DDD01302463, Lane 4: 100 μ M, Lane 5: 200 μ M, Lane 6: 50 μ M AHU3.

4.6 Discussion

Using a phenotypic GFP-based reporter assay, we successfully performed a HTS of small molecules to identify inhibitors of Shiga toxin expression in *E. coli* O157:H7.

The use of bacterial biosensors in HTS campaigns allows the screening of multiple targets simultaneously, in comparison to the target-based assays (Urban et al. 2007; Alksne et al. 2000). Cell-based assays also facilitate the identification of compounds able to cross the bacterial outer membrane, a common issue encountered in the development of drugs active against Gram-negative bacteria (Payne et al. 2007).

The performance of the screen was very good and in accordance with the Drug Discovery Unit guidelines. The *stx2::GFP* and the *rpsM::GFP* assays produced solid data, achieving S:B ratios ≥ 2 , CV % $< 10\%$ and $Z' \geq 0.4$, which are above pre-set industry standards (Iversen et al. 2006; Zhang, Chung, and Oldenburg 1999). The screen identified two hit compounds, DDD01302463 and DDD01304030 that specifically block expression of Stx2. The potency of these compounds was found to be in the micromolar range.

The secondary assay using the *rpsM::GFP* reporter fusion greatly facilitated the hit selection process. One of the main challenges in HTS campaigns is the differentiation between compounds that have genuine activity against compounds that interfere with elements of the biological assay (Thorne, Auld, and Inglese 2010). Since compounds that affect bacterial growth would result in a decrease in GFP expression, it was important to discard any compound with antimicrobial activity. There are other ways in which compounds can also interfere with the assay. For example, fluorescent compounds can affect light-based detection methods that rely on fluorescence or luminescence measurements. Alternatively, certain compounds can reduce the excited state of the fluorophore (quenching), which results in decreased light emission (Shapiro, Walkup, and Keating 2009). Although certain measures can be taken to avoid or solve assay interferences, the most logical option is to run an orthogonal assay to verify that the compounds are active against the target or phenotype of interest.

4.6.1 Potential of the compounds DDD01302463 and DDD01304030 as lead compounds

The evaluation of the compounds DDD01302463 and DDD01304030 in biological assays confirmed their inhibitory activity on Stx expression. The relatively high pXC₅₀ means that more work is required in order to optimize the activity. This will involve thorough structure-activity relationship studies (SARs) in order to obtain more potent and efficient derivatives.

Both DDD01302463 and DDD01304030 have the potential to be optimised and taken forward for development. For instance, they do not have functional groups that can cause problems later in drug development. Some functional groups are known to cause problems like toxicity or a higher susceptibility to biotransformation. A summary of the functional groups that can cause liabilities in drug development are listed in Table 23 (Huggins, Venkitaraman, and Spring 2011).

Table 23 Liable functional groups in drug discovery.

1,2 dicarbonyls	Metabolically unstable and potential mutagenic properties
1,2 dimethoxys	Susceptible to oxidation yielding reactive quinones
1,4 dimethoxys	
$\alpha\beta$ -unsaturated carbonyls	Reactive as Michael acceptors
Acetals	Metabolically unstable due to acetal hydrolysis
Acyhydrazides	
Aliphatic ketones	Metabolically unstable due to nucleophilic attack
Alkenes	Susceptible to epoxidation
Aminothiazoles	Toxicity
Anthracene/phenantrene derivatives	Possible DNA intercalation
Nitro groups	Susceptible to reduction and potential hepatotoxicity
Methylenedioxy	Metabolically unstable and prone to oxidation
Thioureas	Potential non-specific protein binding and metabolically unstable
Unflanked pyridyls	Can interfere with cytochrome P450 due to metal ion coordination

4.6.2 Stereochemistry and its implication in drug development

One of the features of the hit compounds identified is the presence of a chiral centre in the molecules (Figure 63). A molecule is 'chiral' when it cannot be superimposed on its mirror image, just like right and left hands. A chiral centre is usually a carbon atom that contains four different substituents. When one chiral carbon is present in the molecule it gives origin to enantiomers, the mirror images of one another (Gal 2013).

About half of the drugs commercially available are chiral molecules and near 90% of these are racemates, an equimolar mixture of two enantiomers (Nguyen, He, and Pham-Huy 2006).

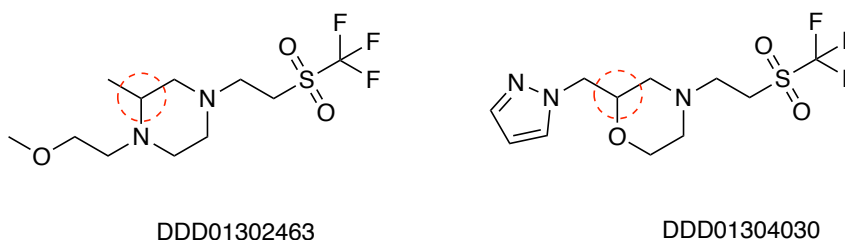


Figure 62 Chemical structures of the compounds DDD01302463 and DDD01304030.

The hit compounds DDD01302463 and DDD01304030 have a chiral carbon (red dotted circle) that gives origin to two enantiomers.

The importance of chirality in drug discovery resides in the chiral nature of the macromolecules that form biological systems, i.e. proteins, glycolipids and polynucleotides (Hutf and O'grady 1996). It is therefore not surprising that the interaction between a drug and a chiral macromolecule occurs in a stereoselective manner. In the case of drugs that are enantiomers, one enantiomer might have the desired pharmacological activity whereas the other may be inactive or produce undesired effects. A good example of this is the tragedy caused by thalidomide. Back in the 1960s, the sedative drug thalidomide was prescribed for morning sickness in pregnant women (J. H. Kim and Scialli 2011). The drug was being commercialised as a racemate, and back then little was know about the importance of stereochemistry in drug activity. Sadly, numerous babies were born with severe deformities as a consequence of the drug's toxicity. It was later discovered that the toxicity was due to the

teratogenic activity of one of the enantiomers, S(-)-thalidomide (S. W. Smith 2009). Although it has been proposed that the tragedy could have been prevented if only the R(+)-thalidomide enantiomer had been commercialised, more recent studies have shown that the humans interconvert both the (S) and (R) enantiomers *in vivo* (Reist et al. 1998). It is therefore important that both the racemate and the individual enantiomers of the compounds DDD01302463 and DDD01304030 are studied in an independent manner.

4.6.3 Target identification: future work

Since the compounds were identified using a phenotypic assay, the molecular target(s) remain to be elucidated. Although the identification of the target is not essential for approval of a drug candidate (Perola 2010), knowing the molecular mode of action allows the optimization of the pharmacokinetic and pharmacodynamic properties.

Part of the future work with the hit compounds will include the identification of the biological target(s). Despite the number of available techniques for target identification, affinity chromatography is still the most widely employed method (Sleno and Emili 2008; Sato et al. 2010). One of the main limitations of this technique is the need of SAR studies on the molecule prior to its use. It also requires the conjugation of the molecule to an affinity tag like biotin, which sometimes can be problematic or interfere with bioactivity (Lomenick, Olsen, and Huang 2011).

Drug Affinity Responsive Target Stability (DARTS) is a technique that is gaining popularity in the drug discovery setting. It relies on the principle that a small molecule drug stabilises the target protein that results in protease resistance (Figure 64).

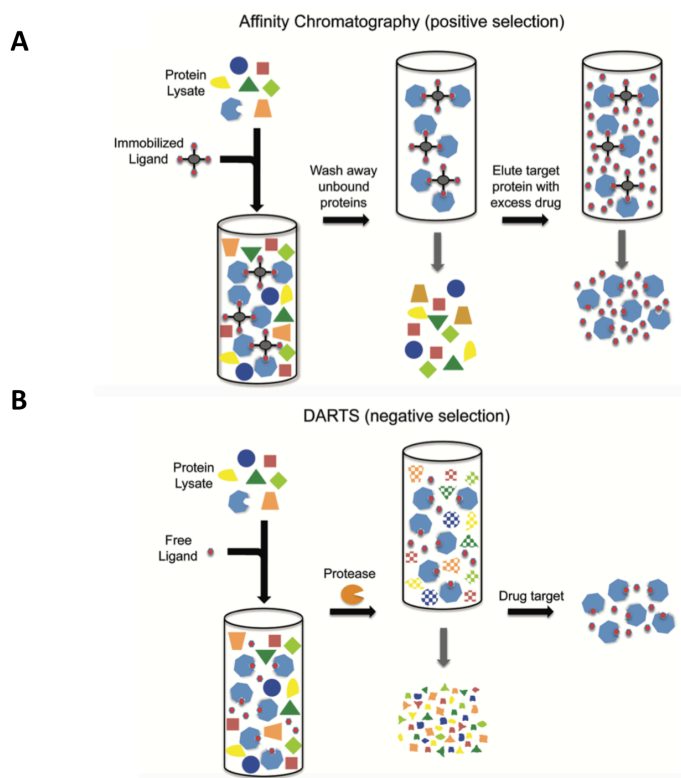


Figure 63 Target identification methods.

A) Affinity chromatography relies on the incubation of cell lysates with the immobilised small molecule of interest in order to ‘pull down’ the target protein. Unbound proteins are washed away and the target protein is eluted with an excess of free drug or denaturing conditions. **B)** In DARTS, cell lysates are incubated with the small molecule, followed by treatment with proteases. The drug-induced protease resistance promotes the negative enrichment of the target protein, while the non-target proteins are digested. Modified from Lomenick, Olsen and Huang, 2011.

In the particular case of this set of compounds, another possible approach would be to study the effect DDD01302463 and DDD01304030 have on the expression of bacteriophage genes crucial for lytic development (e.g. *N*, *Q*) or lysogenic state preservation (e.g. *ci*) (Vohradsky 2017). Bloch and collaborators applied this approach to investigate the mode of action of a set of compounds able to block the phage lytic development in *E. coli* (Bloch et al. 2018).

CHAPTER 5

Exploring the inhibition of quorum sensing as a potential strategy to prevent Shiga toxin expression in *Escherichia coli* O157:H7

5 Exploring the inhibition of quorum sensing as a potential strategy to prevent Shiga toxin expression in *Escherichia coli* O157:H7

5.1 Introduction

Quorum sensing (QS) can be defined as the production and secretion of signalling molecules that regulate gene expression in bacteria, in response to cell population density (M. B. Miller and Bassler 2001).

Studies have shown that QS plays a key role in virulence in enterohemorrhagic *E. coli*, including production of Shiga toxin and formation of attaching and effacing (AE) lesions on the intestinal epithelial cells (Sperandio et al. 2001). *E. coli* has several QS systems, including the LuxS/AI-2 system (Walters, Sircili, and Sperandio 2006; Sperandio et al. 1999), AI-3/epinephrine/norepinephrine system (Sperandio et al. 2003; Walters and Sperandio 2006), indole (D. Wang, Ding, and Rather 2001; J. Kim and Park 2015), and the LuxR homolog SdiA (Kanamaru et al. 2000). Different lines of evidence suggest that quorum sensing regulates production of Stx in EHEC. More specifically, expression of *stx* has been linked with two QS pathways, the adrenaline/noradrenaline/AI-3 and the LuxS/AI-2 signalling systems (Pacheco and Sperandio 2012).

EHEC has a membrane-embedded sensor histidine kinase, QseC, which recognises the host adrenergic signalling molecules adrenaline and noradrenaline, and the bacterial autoinducer-3 (AI-3) (Njoroge and Sperandio 2012). Sensing of these molecules causes autophosphorylation of QseC, which subsequently leads to phosphorylation of the transcription factor QseB. This leads to a series of events that promote activation of virulence factors, including Stx (Figure 65). Rasko and co-workers reported the discovery of a small molecule, LED209, able to inhibit QseC-dependent virulence gene activation in EHEC (Rasko et al. 2008). Concentrations in the picomolar range of LED209 prevented the formation of A/E lesions on cultural epithelial cells and decreased the expression of the *stxAB*

genes in EHEC. The compound also showed activity against QseC in other Gram-negative bacteria, including *S. typhimurium* and *Francisella* sp. One of the main features of LED209 is that it does not affect bacterial growth or induces the SOS response at the concentrations used, which makes it a promising lead that can be used as an anti-virulence therapy.

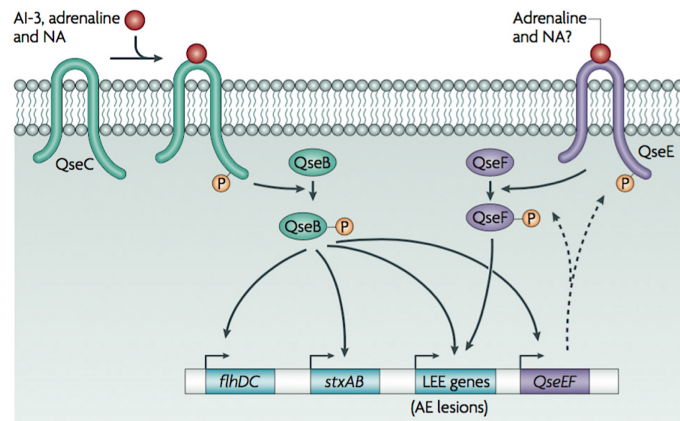


Figure 64 Adrenergic sensing in EHEC.

The bacterial membrane receptor QseC senses the host adrenaline and noradrenaline (NA), and the AI-3. Phosphorylation of QseC and QseB initiates a phosphorelay signalling cascade that activates expression of the two-component system QseEF, the locus of enterocyte effacement (LEE) genes, motility genes (*flhDC*) and Stx genes (*stxAB*). The QseEF system is also involved in expression of the LEE genes, and it is possible that adrenaline and/or NA play a role in its signalling. Adapted from Hughes and Sperandio 2008.

On the other hand, the autoinducer-2 (AI-2) is nonspecies-specific molecule involved in intra- and interspecies communication in Gram-negative and Gram-positive bacteria (Chen et al. 2002; Thiel et al. 2009). The LuxS/AI-2 system was first described in *V. harveyi* (Bassler, Wright, and Silverman 1994), and later work showed that it is also present in *E. coli* and *S. typhimurium* (Surette, Miller, and Bassler 1999). In fact, the gene responsible for AI-2 biosynthesis, *luxS*, has been identified in over 70 bacterial species (Lowery, Dickerson, and Janda 2008).

AI-2-dependent quorum sensing has been associated with regulation of genes in *E. coli*. For instance, exogenous addition of AI-2 to *E. coli* K12 cultures stimulated the formation of biofilm and motility (Gonzalez Barrios et al. 2006). This response was associated with the LsrK protein, suggesting that AI-2

signalling occurs through the Lsr system. Studies on *lsrR* and *lsrK* mutant strains provided evidence that support Lsr-dependent regulation of biofilm formation and motility in *E. coli* (Figure 66) (J. Li et al. 2007). In EHEC, AI-2 has also been associated with chemoattraction, motility and attachment to HeLa cells (Bansal et al. 2008). Overall, different studies show that in *E. coli*, the LuxS/AI-2 signaling system is important for the regulation of biofilm formation, colonisation, motility and other virulence traits.

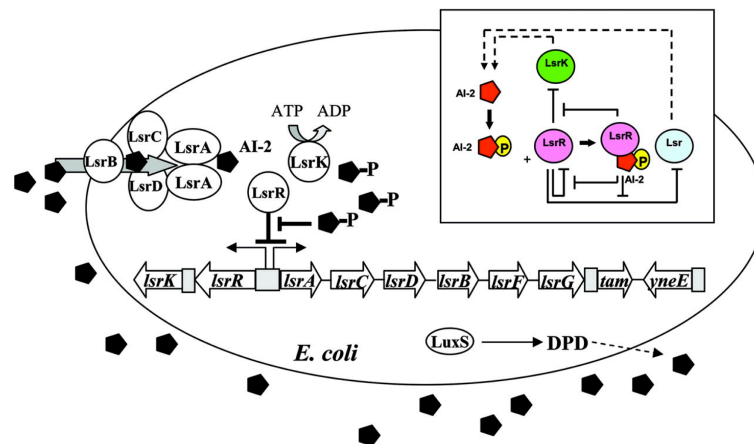


Figure 65 The LsrR/phospho-AI-2 circuit in *E. coli*.

LsrR represses the *lsr* operon (comprised of *lsrACDBFG*) and the *lsrRK* operon. The AI-2 is imported into the cells via LsrABCD; once inside the cell, AI-2 is phosphorylated by the kinase LsrK. Phospho-AI-2 binds to LsrR in order to relieve the repression of the *lsr* transporter genes. This stimulates additional AI-2. LsrR. DPD= 4,5-dihydroxy-2,3-pentanedione. Taken from Li et al, 2007.

Studies carried out by Sperandio and collaborators showed that genes involved in the SOS response are regulated by AI-2 (Sperandio et al. 2001). Using gene array technology in the EHEC strain 84-24 and an isogenic *luxS* mutant, they showed that genes involved in the SOS response were up-regulated in the wild-type strain in comparison to the *luxS* mutant. These genes were *recA* (20-fold), *uvrA* (20-fold) and *sulA* (25-fold). In addition, evaluation of the transcription of *stx* using a *stx::lacZ* fusion showed a threefold increase in the wild-type in comparison to the *luxS* mutant, results that were confirmed by Western blot analysis. A similar study carried out by Yang and co-workers also showed that deletion of *luxS* in STEC decreases production of Stx2e and expression of flagella *in vitro* (Yang et al. 2014).

Given the important role that AI-2 system has on the virulence of human pathogens, it has been proposed that inhibition of this pathway could be used for the development of antivirulence therapies (Guo et al. 2013). To date, inhibition of the LuxS/AI-2 pathway to prevent Stx expression in EHEC has not been explored. For this reason and given the evidence that AI-2 signalling is related to Stx expression, we decided to explore the inhibition of this QS pathway using a reported small molecule inhibitor of the AI-2 synthase, LuxS.

The work presented in this chapter shows that treatment of *E. coli* O157:H7 cultures with the synthetic compound furanone C-30 prevents phage lytic development and decreases production of Stx *in vitro*. Given the suitability of the compound for *in vivo* testing, the activity of furanone C-30 was assessed in a murine infection model using *C. rodentium* λ stx_{2dact} as a surrogate organism for STEC infections. Although it was not possible to draw conclusions from the *in vivo* work, to our knowledge this is the first report of the use of brominated furanones to prevent stx expression in EHEC.

5.2 Naturally occurring brominated furanones alter AI-2 signalling in *E. coli*

A series of different halogenated furanones were isolated from the marine algae *Delisea pulchra* by de Nys and collaborators (Rocky de Nys et al. 1993). These secondary metabolites were found to have antimicrobial and anti-fouling properties (Rocky de Nys et al. 1995). Later work suggested that the bioactivity of this class of compounds was result of their ability to interfere with quorum sensing systems (Givskov et al. 1996). The chemical structures of some of the isolated furanones from *D. pulchra* are shown in Figure 67.

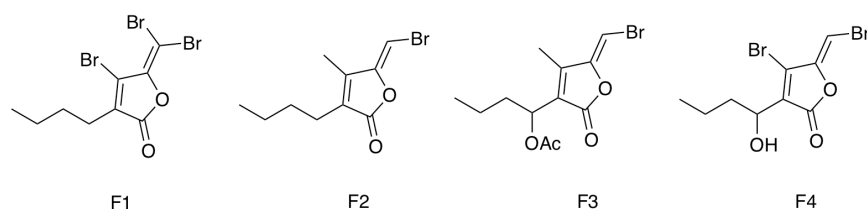


Figure 66 Chemical structures of the brominated furanones isolated from *D. pulchra*.

Studies showed that purified samples of the compounds F1 and F2 were able to block processes controlled by acyl homoserine lactones (AHL), including the swarming motility in *Serratia liquefaciens* and the bioluminescence of *Vibrio fischeri* and *Vibrio harveyi* (Givskov et al. 1996).

Later work revealed that brominated furanones could alter both AHL and LuxS/AI-2 signalling pathways. A DNA microarray done in *E. coli* K12 revealed that 90 genes were differentially expressed in the presence of brominated furanones (34 were induced and 56 were repressed) (Ren et al. 2004). 44 of the repressed genes were found to be induced by AI-2 and the majority of these genes were involved in chemotaxis, motility and flagellar synthesis. Interestingly, the transcription of *luxS* was not altered, suggesting that brominated furanones were affecting the AI-2 signalling pathway in a post-transcriptional way.

It was later discovered that brominated furanones covalently modify and inactivate LuxS, the AI-2 synthase (Zang et al. 2009). Using recombinant LuxS, *in vitro* inhibition assays of the enzyme were performed. A dose-dependent inhibition of LuxS enzymatic activity was observed. In addition, spectroscopic analysis of the reaction revealed that addition of the brominated furanone shifted the UV/vis absorbance of LuxS, likely as a result of covalent modification of one of the residues by the compound. To confirm the covalent binding, the LuxS-furanone complex was analysed by mass spectrometry. Protein fragments with changes in molecular size showed that brominated furanones were reacting covalently with LuxS. More specifically, the modified residue was found to be Cys126, a residue that has been shown to coordinate with a divalent cation, an essential step for enzymatic activity (Ruzheinikov et al. 2001). Treatment of LuxS with chloroacetone caused alkylation of all four cysteine residues present in LuxS, whereas the brominated furanone only modified Cys126, suggesting that this class of compounds act in a selective manner. Figure 68 shows the proposed molecular mechanism of the covalent modification of LuxS by brominated furanones.

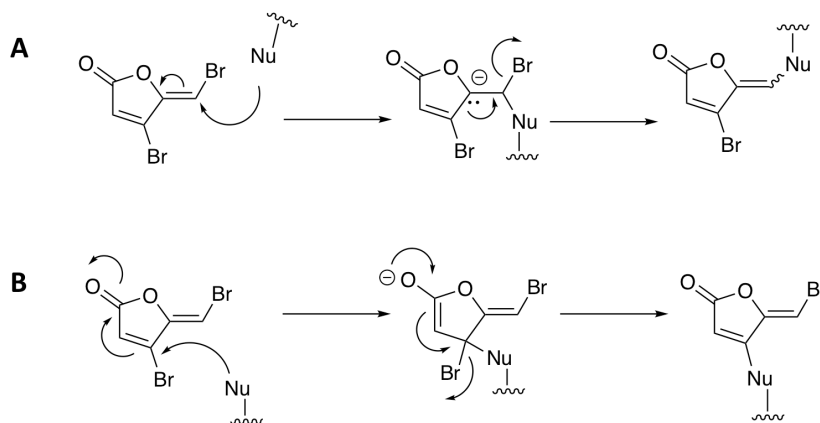


Figure 67 Proposed mechanisms for LuxS, by the brominated furanone C-30.

Based on the studies carried out by Zang and collaborators, two possible addition-elimination mechanisms are proposed. (A) A nucleophile in LuxS (Cys126) adds directly to the vinyl bromide, which leads to elimination of the bromide, and/or (B) the vinyl bromide can also be displaced by addition of Cys126. Modified from Zang et al. 2009.

Based on the evidence that brominated furanones can alter the AI-2 signalling in *E. coli*, we decided to explore if the synthetic furanone C-30 could prevent Stx expression in *E. coli* O157:H7.

5.3 The compound furanone C-30 reduces *stx2::GFP* expression

To assess if furanone C-30 had any activity against Stx expression, cultures of Stx-negative *E. coli* Sakai ZAP0273 strain transformed with the *stx2::GFP* reporter plasmid were treated with different concentrations of the compound. As shown in Figure 69, furanone C-30 decreased *stx2::GFP* expression in a dose dependent manner.

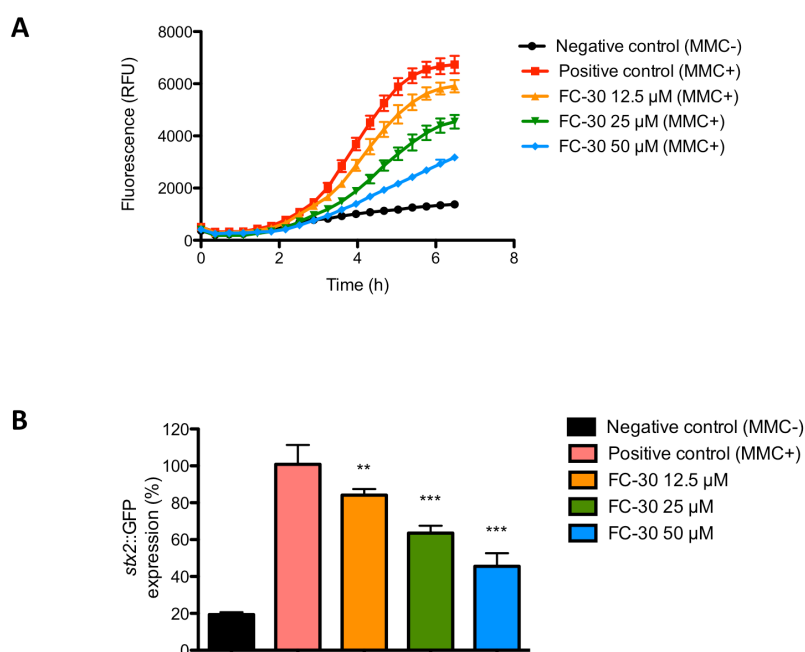


Figure 68 The compound furanone C-30 reduces *stx2::GFP* expression.

E. coli ZAP0273 transformed with *pstx2::GFP* was cultured in the presence of 12.5 - 50 μM furanone C-30 (FC-30), and induced with 1 $\mu\text{g}/\text{ml}$ MMC. Expression of *stx2::GFP* was measured by fluorescence. **(A)** Reduction of MMC-induced *stx2::GFP* expression by FC-30 over time. **(B)** FC-30 significantly decreases *stx2::GFP* expression in a dose dependent manner. Experiments were performed in triplicate, and data plotted as the mean with standard deviation from the mean displayed by error bars. Asterisks indicate a significant difference (** $p < 0.001$, *** $p < 0.0001$) from the culture treated with MMC only, determined by Student's unpaired *t*-test.

5.4 Furanone C-30 block phage mediated lysis and does not affect bacterial growth in *E. coli* O157:H7

As previously mentioned, bacterial lysis is intrinsically linked to Stx expression and release. Thus, prevention or delay of bacterial lysis is a phenotypic feature associated with the inhibitory effect of the furanone C-30 on *stx* expression. Bacterial cultures of *E. coli* ZAP0273 were incubated in the presence of various concentrations of the compound. Prophage induction was achieved by addition of 1 $\mu\text{g}/\text{ml}$ MMC. As shown in Figure 70, the presence of furanone C-30 prevented bacterial lysis in *E. coli* ZAP0273 in a concentration-dependent manner in comparison to the MMC-only culture.

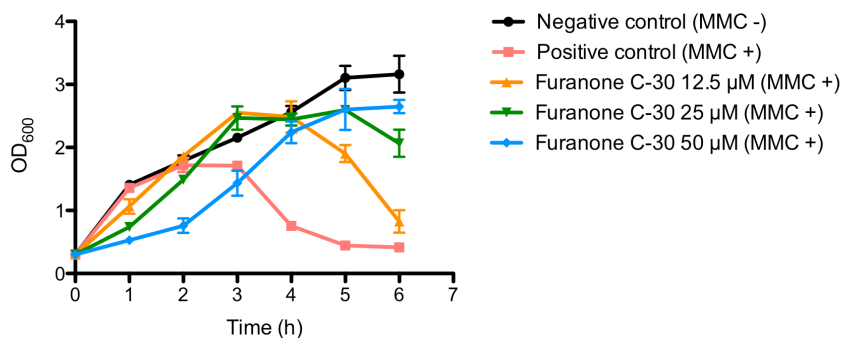


Figure 69 Furanone C-30 blocks phage mediated lysis in *E. coli* O157:H7.

Dose-dependent inhibition of bacteriophage mediated lysis in the presence of the various concentrations of furanone C-30. The data shown are the average of three independent experiments with standard deviation from the mean displayed as error bars.

The compound furanone C-30 did not affect bacterial growth at the concentrations used. Its specificity against *stx* expression was confirmed using the *rpsM*::GFP reporter strain (Figure 71). As previously mentioned, the *rpsM* promoter activity (30S ribosomal subunit) was chosen as a housekeeping gene control as it is not related to *Stx* expression (Roe et al. 2004).

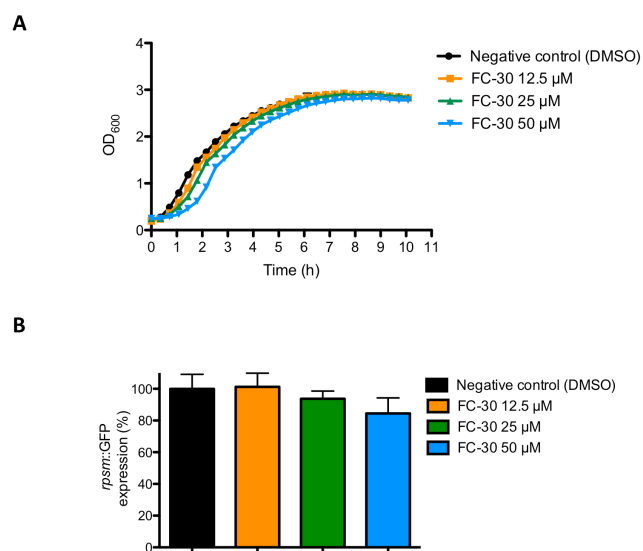


Figure 70 Evaluation of effect of furanone C-30 in bacterial growth and *rpsM*::GFP expression.

(A) Bacterial growth curve of *E. coli* O157:H7 in the presence of different concentrations of furanone C-30. (B) Evaluation of furanone C-30 in the *rpsM*::GFP reporter assay demonstrated that the activity is specific only against *Stx* expression. The presence of various concentration did not reduce expression of *rpsM*::GFP (data shown correspond to t=6 h after addition of the compound). The data shown are the average of triplicate individual experiments with standard deviation from the mean displayed as error bars.

5.5 Furanone C-30 prevents prophage induction and phage lytic development

Since the *stx2* genes are prophage encoded, production of Stx2 is intrinsically linked with the prophage lytic cycle. Hence, furanone C-30 is expected to reduce the number of Stx-encoding phages produced under SOS-inducing conditions. To test this hypothesis, transduction assays were performed using *E. coli* JP10819, which carries the lysogenic Stx2 prophage ϕ P27 with a tetracycline resistance cassette inserted into the *stx2* gene (Quiles-Puchalt et al. 2014). The non-lysogenic *E. coli* K-12 MG1665 was used as the acceptor strain. Cultures were treated with various concentrations of furanone C-30 and PFU were analysed 4 h after SOS-induction. As shown in Figure 72, in the absence of MMC, basal levels of Stx were around 10^4 PFU/mL, whereas the addition of MMC increased the number by four logs to 10^8 PFU/mL. The presence of furanone C-30 reduced the amount of Stx phages produced in a dose dependent manner. The highest concentration of furanone C-30 (50 μ M) reduced the titre to basal levels (10^4), demonstrating that the compound can effectively inhibit the production of Stx phage particles. Since 50 μ M of furanone C-30 also seemed to be affecting the basal levels of Stx phage in the non-induced cultures, the effect of the compound in the growth rate of JP10819 was studied. No significant reduction on growth rate was observed.

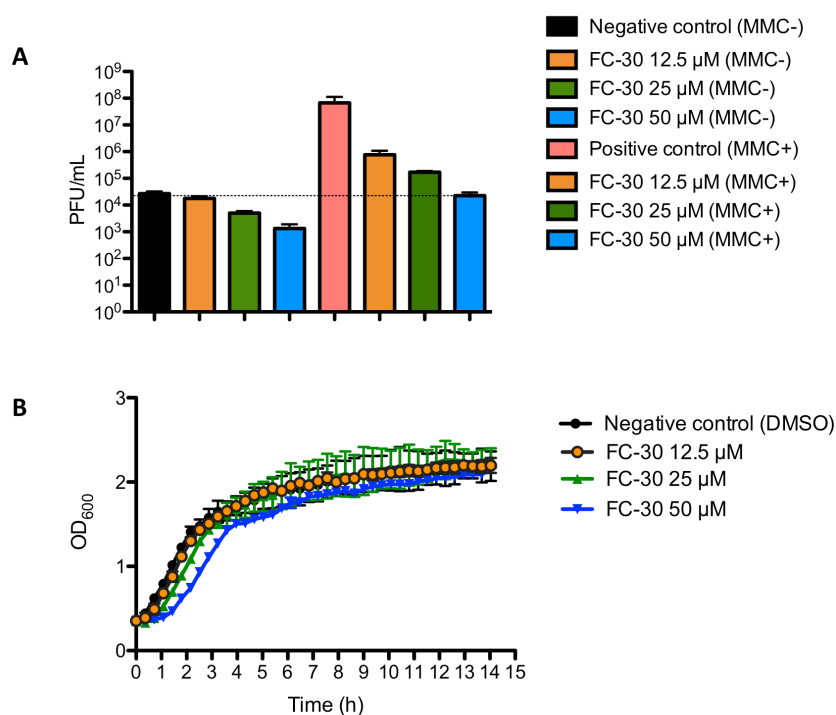


Figure 71 Effect of the furanone C-30 on MMC-induced phage production.

Induction of JP10819 with 2 μg/ml MMC resulted in significantly increased Stx phage production. (A) furanone C-30 produced a significant decrease in phage production by both non-induced and MMC-induced JP10819. (B) The compound does not affect the bacterial growth rate of JP10819. The data shown are the average of three independent experiments with standard deviation from the mean displayed as error bars.

5.6 Western blot analysis of the effect of furanone C-30 on Stx production in *C. rodentium* λ stx_{2dact}

Western Blot analysis of *C. rodentium* λ stx_{2dact} supernatants showed that furanone C-30 prevents Stx expression in a dose dependent manner (Figure 73). Similarly to *E. coli* O157:H7, the effect of furanone C-30 on the growth rate of *C. rodentium* was studied and no negative effect was observed. Phage mediated lysis was also prevented in the presence of the compound in a concentration-dependent manner.

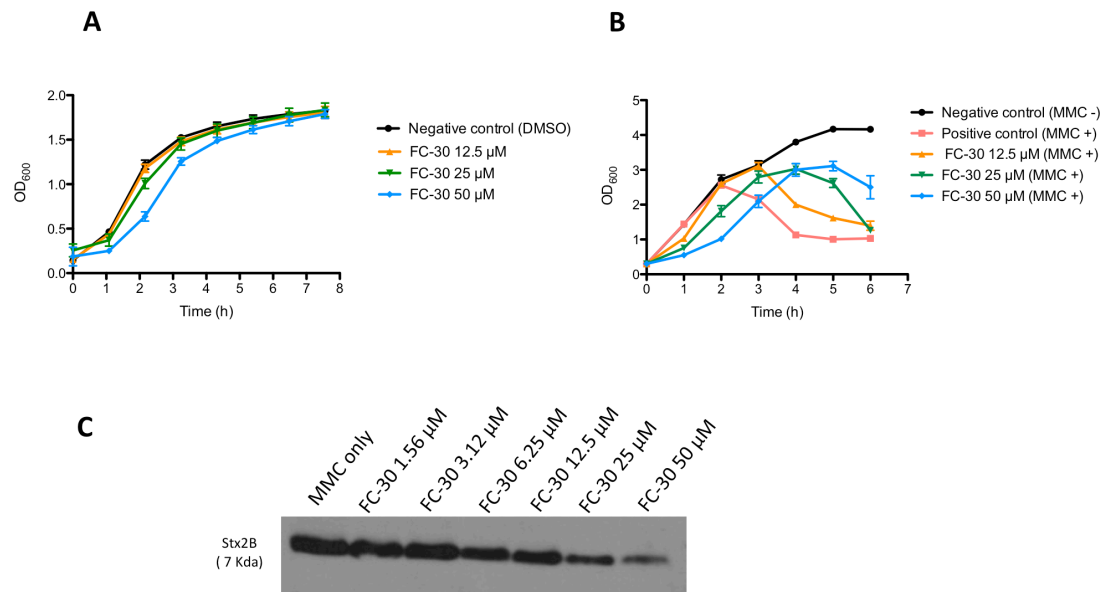


Figure 72 Furanone C-30 prevents phage-induced lysis in *C. rodentium* λ stx_{2dact} and decreases Stx_{2dact} production.

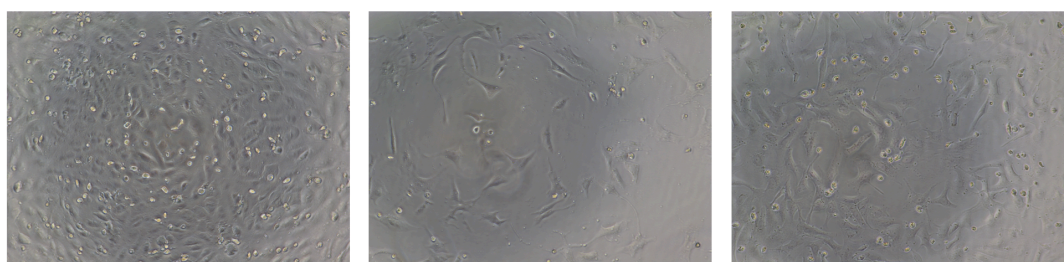
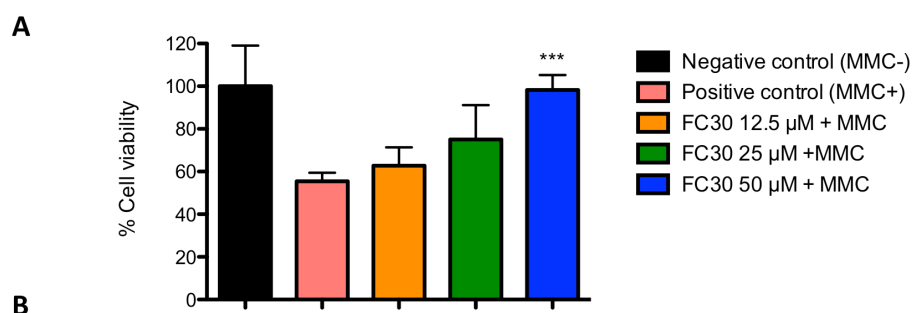
(A) Furanone C-30 does not interfere with *C. rodentium* growth rate. (B) Comparably to the results obtained with EHEC, the presence of furanone C-30 also showed an inhibitory effect on phage induced lysis in *C. rodentium* λ stx_{2dact}, particularly at the highest concentration (50 μM). (C) Western blot analysis of *C. rodentium* λ stx_{2dact} lysates showed a concentration dependent decrease in the production of Stx after prophage induction with MMC. The data shown are the average of three independent experiments with standard deviation from the mean displayed as error bars.

5.7 Evaluation of furanone C-30 in the Shiga toxin cytotoxicity assay

As previously discussed, analysis of the toxicity of STEC bacterial lysates to Vero cell cultures, is an indirect method to detect Stx production (Konowalchuk, Speirs, and Stavric 1977). Thus, we decided to test the ability of furanone C-30 to decrease Stx₂ production in *C. rodentium* λ stx_{2dact} (Mallick et al. 2012).

Cultures of *C. rodentium* λ stx_{2dact} were treated with 12.5 μM, 25 μM and 50 μM of furanone C-30. Stx₂ production was induced by the addition of 1 μg/mL of MMC to the samples containing the compound and to the MMC-only control. After 2-3 h incubation, cultures were filter sterilised using 0.2 μm syringe filters and

serially diluted. The dilutions were added to Vero cells plates and incubated for further 48 h at 37°C in a humidified 5% CO₂ incubator. Cytotoxicity was assessed using the methylthiazolyldiphenyl-tetrazolium bromide (MTT) assay (Denizot and Lang 1986). As shown in Figure 74, the presence of furanone C-30 in *C. rodentium* λ Stx_{2dact} cultures prevented the production of Stx and consequently reduced the cytotoxicity of the bacterial lysates. A significant difference was observed in the presence of 50 μ M furanone C-30.



DMSO only

MMC only

50 μ M FC-30 + MMC

Figure 73 Effect of furanone C-30 on viability of Vero cells treated with *C. rodentium* λ Stx_{2dact} lysates.

(A) Vero cells were treated with lysates of *C. rodentium* λ Stx_{2dact} prepared from cultures: untreated (negative control), treated with 1 μ g/mL MMC to induce Stx expression (positive control), 12.5, 25 and 50 μ M of furanone C-30. Results represent mean values from three independent experiments, with error bars indicating SD. Statistical significance is shown as P values obtained by *t* test (***p* < 0.001). (B) Representative micrographs from the experiment.

5.8 Is the activity of furanone C-30 on Stx expression a result of the inhibition of LuxS?

Our results showed that furanone C-30 is acting as an inhibitor of Stx expression in *E. coli* O157:H7. Preliminary studies on the molecular mode of action of brominated furanones in *E. coli* suggest that they act as inhibitors of the AI-2 signalling pathway by covalently binding to LuxS. Thus, we wanted to assess if the inhibitory activity of furanone C-30 on Stx production was due to the inhibition of LuxS. To do so, we planned to study the activity of furanone C-30 in *E. coli* with the *luxS* deletion and determine whether there was an effect on activity compared to the wild type strain. Using the lambda red recombineering system (Datsenko and Wanner 2000), the strains *E. coli* JP10819 Δ LuxS and *E. coli* ZAP0273 Δ LuxS were created. *E. coli* JP10819 Δ LuxS was used to study the effect on prophage induction and phage lytic development of the Stx2 prophage ϕ P27, whereas *E. coli* ZAP0273 Δ LuxS was transformed with the *stx2::GFP* reporter plasmid.

As observed in Figure 75, both *E. coli* JP10819 wild type and its Δ LuxS mutant showed the same phage titre in the presence of different concentrations of furanone C-30. No significant differences in the number of plaque forming units per millilitre (PFU/mL) were observed. The same result was observed when the compound was studied using the *stx2::GFP* reporter assay in the *E. coli* ZAP0273 Δ LuxS. Furanone C-30 was active in both the wild type and Δ LuxS mutant. These findings suggest that the inhibitory activity of furanone C-30 on Stx2 production is not a result of LuxS inhibition.

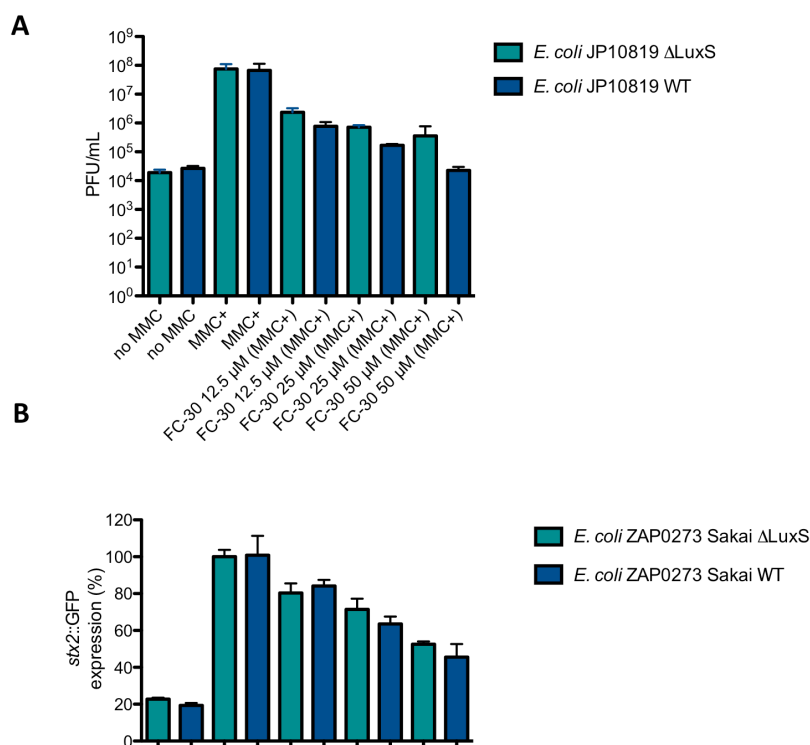


Figure 74 Effect of furanone C-30 on phage induction in *E. coli* JP10819 and its Δ LuxS mutant.

(A) Induction of JP10819 with 2 μ g/ml MMC resulted in significantly increased Stx phage production. Furanone C-30 produced a significant decrease in phage production in both *E. coli* JP10819 and its Δ LuxS mutant. (B) FC-30 decreases *stx2::GFP* expression in a dose dependent manner in both *E. coli* ZAP0273 Δ LuxS and wild type. The data shown are the average of three independent experiments with standard deviation from the mean displayed as error bars.

5.9 Does furanone C-30 inhibit RecA's activity?

In Chapter 3 we described the discovery of AHU3, a small molecule that interferes with the activity of RecA. The electrophilic nature of AHU3 suggests that the inhibitory activity on Stx production is a result of the covalent binding of the compound to RecA. Interestingly, furanone C-30 has a similar mode of action when it binds to LuxS (Zang et al. 2009). Given the shared reactivity of both compounds, we wanted to assess if furanone C-30 could also be interfering with RecA's function. To do so, the ability of furanone C-30 to inhibit RecA mediated ATP hydrolysis was investigated. As previously explained, RecA binds to ssDNA, forming nucleofilaments. These activated RecA filaments mediate autocleavage of the key SOS response repressor LexA and prophage repressors,

triggering gene expression and production of assembled phage particles. As shown in Figure 76, furanone C-30 did not affect RecA's ATP hydrolysis in comparison to AHU3. This suggests that the biological activity of furanone C-30 in STEC is not a result of the inhibition of RecA.

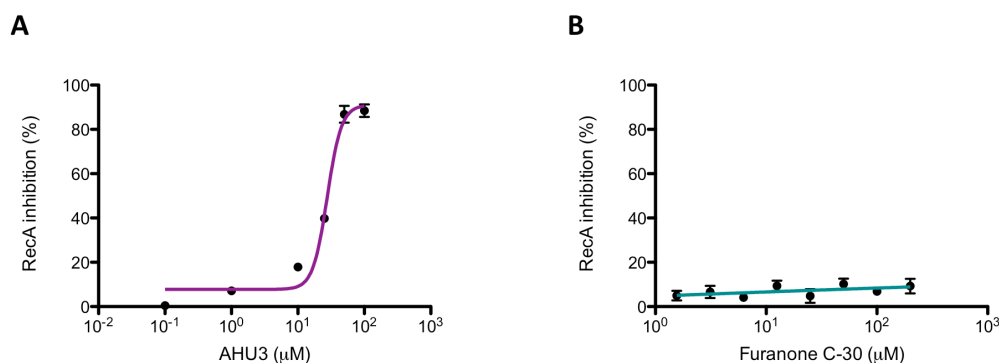


Figure 75 Furanone C-30 does not inhibit RecA's ATPase activity.

In order to assess if the inhibitory effect on *stx* expression was a result of the inhibition of the RecA protein, the ability of furanone C-30 to inhibit RecA-mediated ATP hydrolysis was investigated at concentrations between 1.56 and 200 μM. **(A)** The compound AHU3 inhibits the ATPase activity of RecA in a concentration-dependent manner, whereas furanone C-30 **(B)** does not. Data are plotted as a percentage of the inhibitory effect of ATP hydrolysis.

5.10 *In vivo* evaluation of furanone C-30 as a potential strategy to prevent Shiga toxin expression.

The ability of furanone C-30 to attenuate virulence *in vivo* has been explored in a mouse model of chronic lung infection with *Pseudomonas aeruginosa* PAO1 (H. Wu et al. 2004). As reported by Wu and collaborators, administration of furanone C-30 accelerated lung bacterial clearance of *P. aeruginosa* and reduced the severity of the lung pathology. In the case of *P. aeruginosa*, brominated furanones interfere with *N*-acyl homoserine lactone signalling. Given the positive results obtained *in vitro* and the precedent of an *in vivo* study using a murine model, we decided to assess if furanone C-30 was able to block Stx production *in vivo*.

5.10.1 Animal models for EHEC infections

In order to study EHEC pathogenesis and facilitate the development of therapeutic strategies, different animal models for EHEC infection have been developed (Mohawk and O'Brien 2011). One of the most popular models for *E. coli* O157:H7 infection is the streptomycin-treated mouse model. This model, developed by Wadolkowski and co-workers, requires a prior treatment with streptomycin in order to reduce the animals' normal intestinal microbiota and facilitate the colonisation by EHEC (Wadolkowski, Burriss, and O'Brien 1990). One of the main limitations of this model is the need of a high inoculum of *E. coli* O157:H7 in order to cause morbidity or mortality, and the lack of symptoms associated with STEC pathogenesis. Other models have been developed, including the protein-calorie malnutrition model or the use of germ-free mice (reviewed by Mohawk and O'Brien 2011), but the conflicting conclusions concerning their utility to study EHEC infections has prompted the development of novel alternatives.

Citrobacter rodentium is a mice pathogen that has an infection strategy and virulence profile similar to EPEC and EHEC (Mundy et al. 2005). In the same way as EPEC and EHEC, *C. rodentium* uses a type III secretion system (T3SS) to deliver effector proteins into infected enterocytes and promote the formation of attaching and effacing (A/E) lesions (Luperchio and Schauer 2001). Given their similarities, the use of *C. rodentium* as a surrogate organism of EHEC has been studied. However, one of the disadvantages of using *C. rodentium* is absence of the Stx genes, limiting its usefulness to study EHEC pathogenesis.

Recently, Mallick and collaborators created a Stx-producing *C. rodentium* strain (Mallick et al. 2012). *C. rodentium* DBS100 was lysogenized with the phage Φ 1720a-02, derived from the STEC strain EC1720a (Gobius, Higgs, and Desmarchelier 2003). The lysogenized strain *C. rodentium* λ stx_{2dact} strain produced the mucus-activatable Stx_{2dact} at levels comparable to STEC. Infection of C57BL/6 mice with approximately 1×10^9 CFU of this strain via oral gavage caused lethal infection, with most mice dying 4-9 days after inoculation. The course of the disease in mice was characterised by a significant weight loss

(10-20% of starting weight) and increased faecal water content and severe kidney and intestinal damage. Even though this murine model does not display all the features associated with EHEC infection, the formation of A/E lesions together with Stx-mediated damage make this model a plausible alternative for the study of EHEC pathogenesis.

5.10.2 Experimental design

The *C. rodentium* λ stx_{2dact} strain was a kind gift from Prof. John Leong (Tufts University). In order to monitor the infection in real time, the *lux* operon was integrated into the chromosome via homologous recombination. This was done using the p16*Slux* vector, a plasmid that carries the *P. luminescens lux* operon and 16S rRNA insertion site (Riedel et al. 2007).

A total of 26 female BALB/c mice, 6-8 weeks old, were used for the study. The mice were divided in four groups: Group 1 (8 mice) was infected and treated with furanone C-30; Group 2 (8 mice) was infected and given just pellet without the drug; Group 3 (5 mice) was not infected and treated with drug only and Group 4 (5 mice) was not infected and given just the pellet without the drug. The purpose of Group 3 was to assess any possible effect that the compound could have on the mice physiology, and Group 4 was to assess any possible effect that the vehicle could have.

5.10.3 Preparation of peanut butter/hazelnut spread pellets for the delivery of the drug.

Oral administration of drugs on animal models for human diseases is usually chosen given its practicality and non-invasive nature. Oral gavage is the most widely used technique for oral dosing in rodents but it has certain limitations. The animal resistance to the procedure usually causes complications, including esophageal and tracheal trauma and/or aspiration (Hoggatt et al. 2010). The stress induced by oral gavage can also influence different physiological processes

including immune function, metabolism, and inflammatory processes, amongst others (Corbett et al. 2012).

Recently, strategies for voluntary oral drug administration in mice have been developed. For example, a study carried out by Gonzales and co-workers showed that the inclusion of active principles into peanut butter pellets allows a non-stressful and precise drug administration in a short period of time and without the risks associated with oral gavage (Gonzales et al. 2014). Their findings showed that mice voluntarily took the pellets given their pleasant organoleptic properties. This approach is particularly useful in cases where chronic oral administration is required.

Given the nature of our study (continuous administration of the compound in order to assess its potential to block Stx expression), we decided to apply the approach described by Gonzales et al. Thus, pellets containing furanone C-30 were prepared mixing equal amounts of peanut butter and hazelnut cocoa spread. Approximately $100 \text{ mg} \pm 2.5 \text{ mg}$ of the mixture were dispensed in 1.5 mL eppendorf tubes. The compound furanone C-30 was added from a 10 mM ethanol stock in order to get doses of $4 \mu\text{g}$ per gram of weight. Placebo pellets contained an equal amount of vehicle only. The pellets were thoroughly mixed by hand with a spatula, spun down in a bench centrifuge, and stored at -20°C until use.

5.10.4 Infection of BALB/c mice with *C. rodentium* $\lambda\text{stx}_{2\text{dact}}$

Prior to infection, mice were subjected to administration of the pellets with and without the active compound, depending on the group they belonged to. This was done to familiarise the animals to the daily dosing in order to ensure the voluntary consumption of the drug. Administration was performed twice a day at 8:00 and 18:00 h, for five days. After this habituation step, mice were infected with the *lux* marked *C. rodentium* $\lambda\text{stx}_{2\text{dact}}$ strain. An overnight culture of the strain was subcultured in pre-warmed DMEM media and grown to an OD_{600} of 0.8. Bacteria were harvested by centrifugation and resuspended in sterile PBS to get a 100x concentrate of the original culture. The infection dose was 3.1×10^{10}

CFU/mL. Mock-infected mice were given an equal volume of PBS only. Faecal shedding was used to measure colonisation levels (Figure 77).

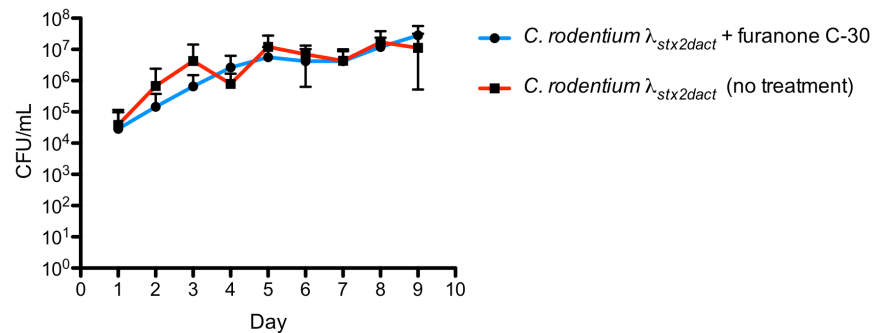


Figure 76 Colonisation of *C. rodentium* $\lambda_{stx2dact}$ in BALB/c mice.

Mice were infected with lux-marked *C. rodentium* $\lambda_{stx2dact}$. Colonisation was monitored by faecal shedding. Each group consisted of 8 animals at the start of the experiment, and data points represent the mean of each group with standard deviation from the mean displayed as error bars.

Colonisation was also monitored using an *in vivo* imaging system (IVIS) Spectrum. On day 2 post-infection, mice were anaesthetised by inhalation of 2% isoflurane and analysed using the IVIS spectrum. As shown in Figure 78, luminescence was detected after 1 minute exposure in mice infected with the lux-marked *C. rodentium* $\lambda_{stx2dact}$. Six mice from group 1 showed colonisation, whereas only four mice from group 2 appeared to be colonised. Faecal shedding showed that six mice of each group were colonised by day 3.

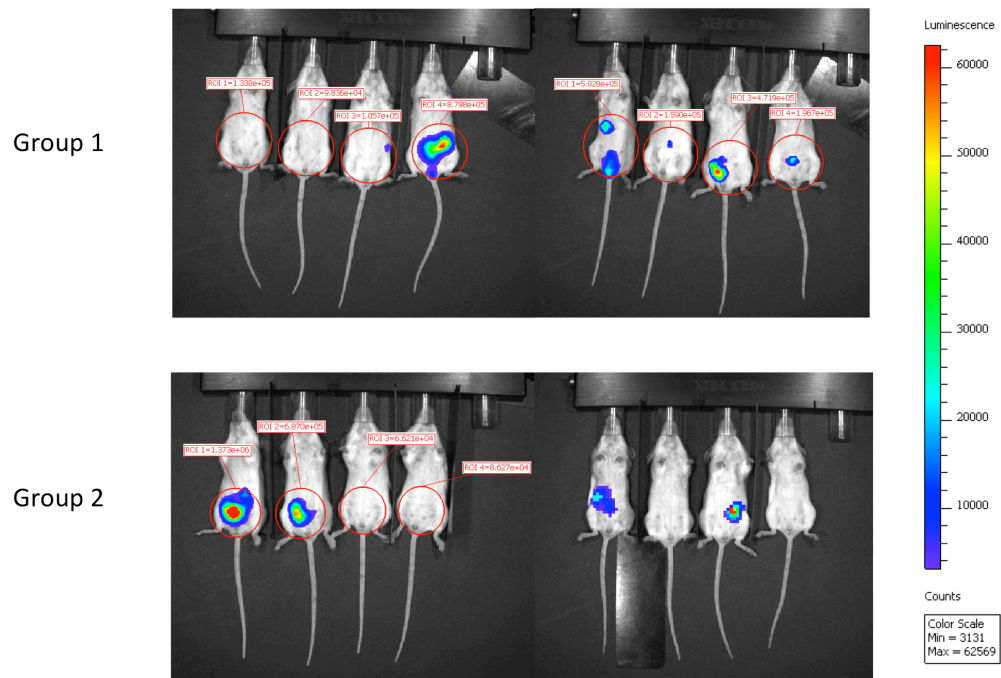


Figure 77 Colonisation of BALB/c mice with *C. rodentium* λ stx_{2dact}.

Images of mice taken from the IVIS at day 2 post infection. **Group 1**, infected with *C. rodentium* λ stx_{2dact}, no treatment; **Group 2**, infected with *C. rodentium* λ stx_{2dact} and treated with furanone C-30. The scale bar represents luminescence flux in photons per second per cm². Flux was normalised for all mice to allow comparison. On day two, only six mice from group 1 and four from group 2 were colonised.

After infection, pellets containing furanone C-30 were voluntarily administered by oral route twice a day at 8:00 and 18:00 h using sterile micropipette tips. As described by Mallick et al. 2012, weight loss was used as a main indicator of Stx-induced disease. Thus, mice were weighed twice every day (morning and afternoon) looking at any fluctuation throughout the experiment. As observed in Figure 79, no significant weight loss was seen in the infected groups 1 and 2 by day 10, contrary to the observations reported by Mallick et al. On the other hand, the non-infected mice treated with furanone C-30 only (group 3) did not show any changes in weight as expected.

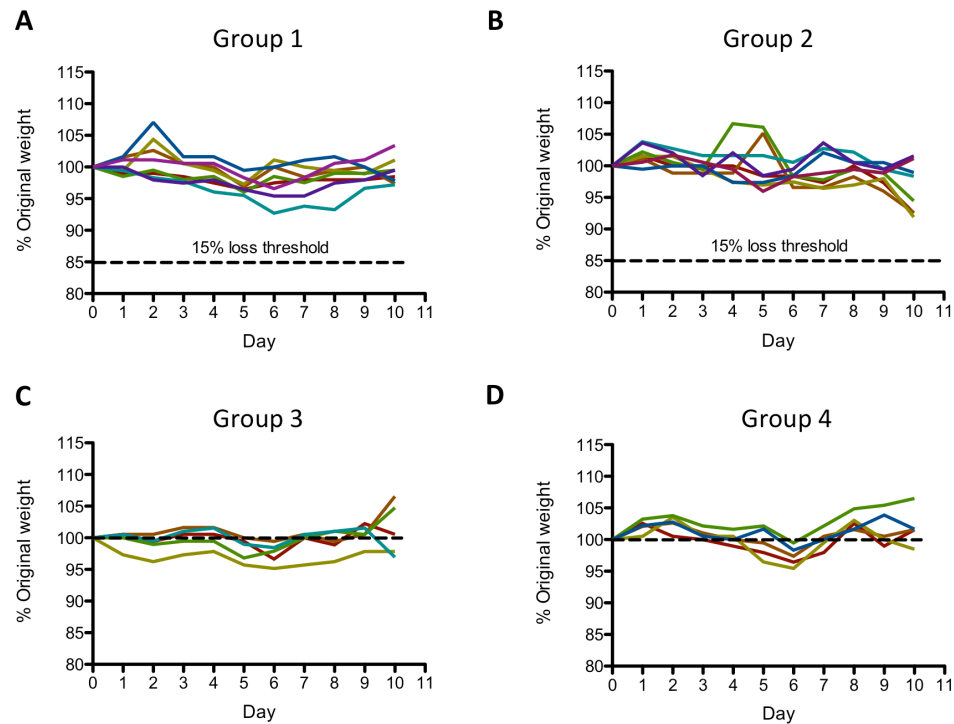


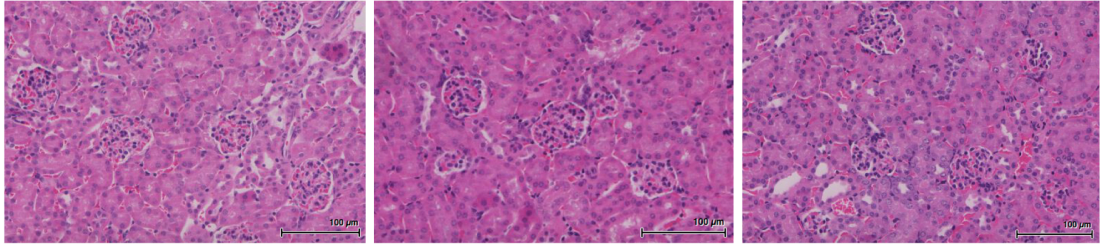
Figure 78 Weight monitoring of mice.

Mice were weighed twice a day just before the administration of the compound. **(A) Group 1** infected with *C. rodentium* λ Stx_{2dact}, no treatment; **(B) Group 2**, infected with *C. rodentium* λ Stx_{2dact} and treated with furanone C-30; **(C) Group 3**, non-infected but treated with furanone C-30 and **(D) Group 4** non-infected but given the vehicle only. Animals were monitored for weight loss of >15% from the starting weight. Each line represents an individual mouse.

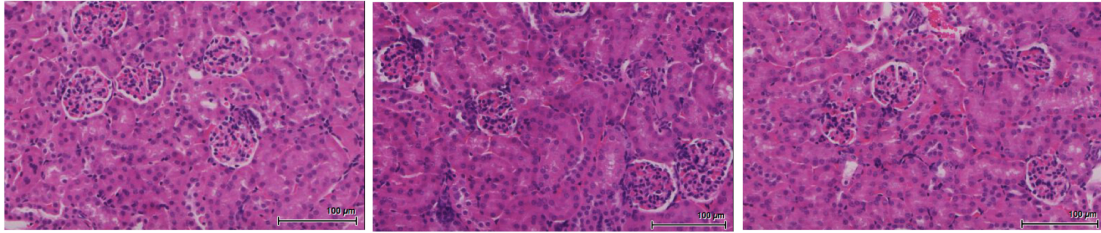
High faecal shedding and luminescence in the infected mice suggested that the lack of symptoms was not a result of poor bacterial colonization. Given the lack of symptoms in the infected mice, animals were euthanized on day 10 and kidneys were removed and prepared for histology using H&E staining.

Stx-mediated kidney damage in murine models is characterized by the presence of blood clots, spacing in the Bowman's capsule in the glomeruli, tubular dilation and the presence of degenerated, necrotic or sloughed epithelial cells (Torres et al. 2016). Histological assessment of the kidneys from infected mice did not show signs of Stx-mediated damage as observed in Figure 80. These results suggest that the lack of symptoms was probably due to the lack of production and release of Stx_{2dact}. Since no signs of disease were observed in the histological studies, the results of the experiment were taken as inconclusive

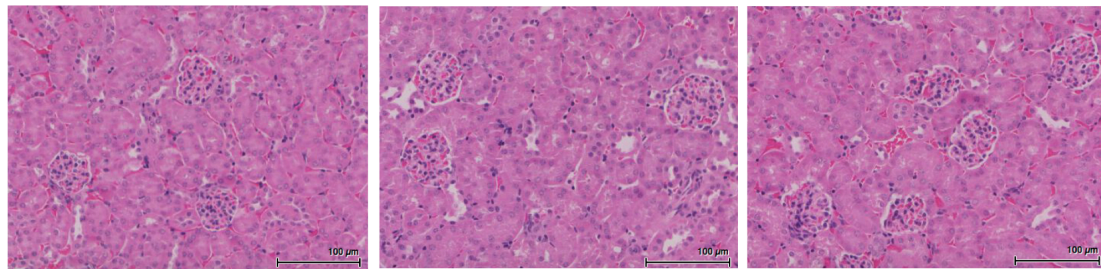
Group 1 – *C. rodentium* λ stx_{2dact} + furanone C-30



Group 2 – *C. rodentium* λ stx_{2dact} no treatment



Group 3 – Non-infected + furanone C-30



Group 4 – Non-infected + vehicle only

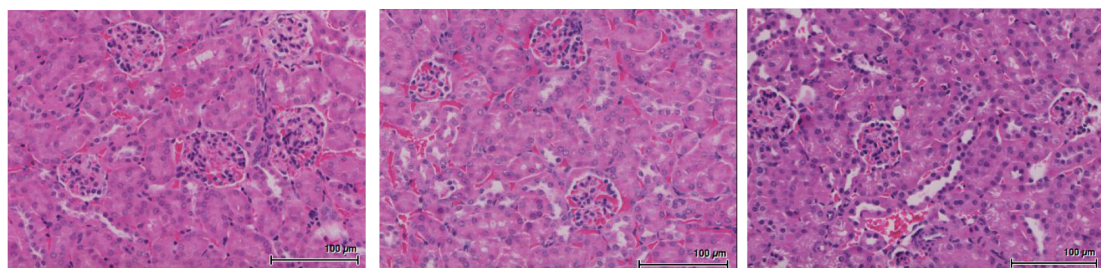


Figure 79 Micrographs of H&E-stained kidney sections from mock infected or *C. rodentium* λ stx_{2dact} infected mice at day 10 after infection.

Group 1 infected with *C. rodentium* λ stx_{2dact}, no treatment; **Group 2**, infected with *C. rodentium* λ stx_{2dact} and treated with furanone C-30; **Group 3**, non-infected but treated with furanone C-30; **Group 4** non-infected but given the vehicle only. No signals of Stx-mediated damage were observed in mice from groups 1 and 2.

5.11 Discussion

The AI-2 signaling pathway plays a key role in the production of virulence factors in bacteria of clinical relevance. Hence, the development of small molecules that modulate AI-2 activity is a plausible alternative to create anti-virulence therapies. Different attempts have been made to develop inhibitors of different components that are involved in the production or response to AI-2 (reviewed by Guo et al. 2013). Examples include synthesis of LuxS substrate analogues that prevent the synthesis of AI-2 (Greenberg et al. 2001), synthesis of analogues of AI-2 to interfere with AI-2 signaling (Lowery et al. 2005) or inhibitors of the AI-2 receptor (Peng et al. 2009).

The use of brominated furanones to modulate virulence in human pathogens has been previously explored in other systems. For example, a study showed that 4 µg/mL of furanone C-30 can inhibit biofilm formation by *Streptococcus mutans* without affecting bacterial growth (He et al. 2012). The anti-biofilm activity of brominated furanones has also been reported in *Pseudomonas aeruginosa* (Shetye et al. 2013), *Escherichia coli* (Han et al. 2008), *Salmonella enterica* serovar Agona (Vestby et al. 2014) and *Staphylococcus epidermidis* (Lonn-Stensrud et al. 2008).

To our knowledge, this is the first report of the activity of brominated furanones against Shiga toxin expression in EHEC. Our data shows that furanone C-30 effectively prevents the production of Stx2 *in vitro* under MMC-inducing conditions. Since it has been shown that brominated furanones target the AI-2 synthase LuxS, we investigated if the inhibitory on Stx expression was due to the inhibition of LuxS. Our results suggest that the activity could not be result of the inhibition of LuxS. There are several possible explanations for our observations. Furanone C-30 could be targeting another yet unknown *E. coli* quorum sensing system, the target could not be part of a quorum sensing system, or the observed activity against Stx expression is a result of the combination of effect on several targets.

Alternative pathways for the biosynthesis of AI-2 in *E. coli luxS* mutants have been identified. Tavender and co-workers reported the LuxS-independent formation of AI-2 via spontaneous conversion of ribulose-5-phosphate (Tavender et al. 2008). Their findings showed that this pathway does not contribute to the overall production of AI-2 in wild type *E. coli* strains but might be responsible for the synthesis of AI-2 in *luxS* mutants. Thus, it could be possible that our *luxS* mutant was still producing AI-2 through an alternative pathway, explaining the lack of differences between the wild type and $\Delta luxS$.

The use of small molecules to disrupt quorum sensing is an attractive approach to develop new anti-virulence therapies. It is however important to mention that other pathways, different to quorum sensing, can regulate the bacterial virulence, so anti-QS compounds should be considered in an adjuvant or synergistic approach with other therapies.

5.11.1 *In vivo* evaluation of furanone C-30 in the *Citrobacter rodentium* λstx_{2dact} infection model.

The use of *Citrobacter rodentium* to study the virulence of the closely related pathogens EPEC and EHEC has become the golden standard in recent years (Crepin et al. 2016). The lysogenisation with a Stx-producing phage by Mallick et al (2012) makes *C. rodentium* an even more accurate surrogate organism for STEC pathogenesis.

The *in vivo* evaluation of compounds with promising biological activity is an important step in the drug development process. Thus, we decided to assess the ability of furanone C-30 to suppress *stx* expression in a murine infection model. Unfortunately, infection of BALB/c mice with *C. rodentium* λstx_{2dact} did not produce the illness signs reported by Mallick (2012). According to his report, mice infected with the Stx-producing *C. rodentium* strain produced a lethal infection, with most mice dying 4-9 days after inoculation. In our study, no weight loss was observed and no signs of Stx-mediated kidney damage were seen in the histological analysis. Since faecal shedding showed that the mice were heavily colonised, the lack of symptoms could be attributed to the lack of Stx production in the infected mice.

There are many factors that could have interfered with the production of Stx. One of the most studied causes is the effect of the host microbiota on the induction of Stx-encoding prophages. For instance, it has been reported that elements produced by the human microbiota can interfere with prophage induction and *stx* expression in EHEC O157:H7. A study carried out by de Sablet and collaborators showed that molecules produced by the commensal microbiota are able to repress *stx2* mRNA expression and block RecA-mediated prophage induction (de Sablet et al. 2009). Their findings showed that *Bacteroides thetaiotaomicron*, a frequently encountered organism in the normal human microbiota, produces compounds that prevent Stx production in the intestine. Although the compounds have not been identified, the inhibitory effect on *stx2* expression was found to be independent of the quorum sensing pathways described in *E. coli* O157:H7, including SdiA, QseA, QseC or AI-3.

Other bacterial species have been reported to have an impact on *stx* expression. Studies carried out by Carey and collaborators showed that *Lactobacillus*, *Pediococcus* and *Bifidobacterium* strains down-regulate expression of *stx2* in *E. coli* O157:H7, both *in vivo* and *in vitro* (Carey et al. 2008). In the case of *Bifidobacterium*, the inhibitory effect against *stx* expression has been associated with the production of high concentrations of acetic acid (56 mM), lowering the pH of the intestine. *In vitro* studies confirmed that the low pH caused by acetic acid suppresses Stx production in *E. coli* O157:H7 (Asahara et al. 2004).

The presence of non-STEC strains in the gut microbiota has also been shown to influence toxin production. Goswami and collaborators performed a study *in vivo* in which germfree mice were co-colonised with the non-pathogenic strain *E. coli* C600 and *E. coli* O157:H7. Mice that were colonised with both strains showed greater kidney damage, a higher concentration of Stx2a in faeces and visible signs of illness in comparison with mice that were infected with *E. coli* O157:H7 only (Goswami et al. 2015). In fact, it has been shown that up to 10% of commensal *E. coli* in humans are susceptible to infection by Stx-encoding phages, which in turns leads to an increase of Stx production (Gamage et al. 2004).

It is also important to point out that the type of Shiga toxin produced by the *C. rodentium* strain used in this study, Stx2dact, requires to be 'activated' with mouse or human intestinal mucus, or purified mouse elastase (Melton-Celsa, Kokai-Kun, and O'Brien 2002). Interestingly, the composition of the mice gut microbiota has been shown to have an impact on the mucus barrier in mice (Jakobsson et al. 2015). Thus, if the microbiota of infected mice had an impact on the mucus barrier, it is possible that Stx2dact could have not been activated to exert its toxic activity.

The influence of the microbiota and commensal *E. coli* strains on toxin production by *E. coli* O157:H7 could explain how the infections with STEC can vary from being asymptomatic to the development of HUS (Figler and Dudley 2016). In the case of our study, it would be interesting to perform a 16S ribosomal RNA sequencing of the gut microbiota in order to investigate this further. Furthermore, the use of peanut butter and hazelnut cocoa spread as a dosage form could have had an impact on the microbiota composition or physiological state of the gut so this could be further explored.

CHAPTER 6

Final Discussion

6 Final discussion

Shiga toxin (Stx) is the causal agent for haemolytic uremic syndrome (HUS) in patients infected with Shiga toxin producing *E. coli* (STEC). Unfortunately, there are no available therapies to prevent the development of Stx-mediated HUS and the development of new therapies has been hampered by the sporadic nature of STEC outbreaks and the lack of financial investment.

The treatment of bacterial toxin-mediated diseases has always been a challenge given the lack of therapeutic strategies capable of neutralising the effects produced by the toxins and also the counterproductive effect of conventional antimicrobials. Most of the efforts to find new therapies against Stx-mediated HUS have focused on the neutralisation of the toxin using monoclonal antibodies against Stx1 and Stx2 or synthetic Stx binders that mimic the Gb3 receptor (E. A. Rahal et al. 2015). The outbreak nature of STEC infections complicates the statistics and finances to perform successful clinical trials. For example, according to the FDA guidelines, a clinical trial of two groups (STEC and STEC + HUS) with a 5% HUS rate would require over 600 individuals to demonstrate the efficacy of the drug (Hall et al. 2017). Most outbreaks are less than 100 patients (Luna-Gierke et al. 2014; Rangel et al. 2005), making the development of neutralising therapies unattractive for pharmaceutical companies. For this reason, other alternatives have started to be explored. These include, targeting the unfolded protein response (UPR) (Amaral et al. 2017), the ribotoxic stress response (Pinto et al. 2017), intracellular trafficking of Stx (Tepshi et al. 2018) or production of the toxin (Sheng, Rasco, and Zhu 2016).

6.1 Targeting the bacterial SOS response to prevent Shiga toxin expression

In chapter 3 we described the discovery of a small-molecule inhibitor of RecA, a key component of the SOS response in bacteria. Since the genes encoding Stx are located on temperate lysogenic phages integrated into the bacterial

chromosome, the production of the toxin is intrinsically associated with phage induction through the SOS response. For this reason, the inhibition of the SOS response in STEC is a promising approach for the prevention of Stx expression in infected patients. Unfortunately, given the toxicity profile of the lead compound AHU3 it was not possible to continue its development. Nevertheless, our findings are a proof-of-concept of the potential that RecA has as a target to regulate *stx2* expression.

The applications of targeting the SOS response go beyond the prevention of Stx expression. It has been proposed that inhibition of the SOS response could potentiate the current antimicrobial arsenal and stop the development of resistance to certain classes of antibiotics, such as fluoroquinolones (Recacha et al. 2017). Different elements of the SOS response pathway other than RecA have also been explored as potential drug targets. For instance, a recent study described the discovery of small molecules that specifically target the LexA autoproteolysis step in the SOS response (Mo et al. 2018). Mo and collaborators also showed that targeting both LexA or RecA are viable strategies for targeting the SOS response, and propose that the combination of an SOS inhibitor with a DNA-damaging antibiotic offers the potential for lowering the antibiotics MICs and decrease the acquired drug resistance (Mo et al. 2016)

Another proposed target is the endoribonuclease RNase E, an essential protein for the processing and degradation of all types of RNA. A study showed that deficiency of RNase E in *E. coli* severely limits the induction and maintenance of the SOS response (Manasherob et al. 2012). In fact, efforts to find small-molecules inhibitors of RNase E have already been reported (Kime et al. 2015).

6.2 The use of small molecules to modulate bacterial virulence

Recently, there has been a growing interest in the study of small molecules that are capable of blocking the production of bacterial toxins or disrupt the toxins normal functioning. This anti-virulence approach would provide an effective solution to the severe toxin-mediated diseases and could also help to overcome

the current antibiotic-resistance problem, as this type of drugs would put less selective pressure for the development of resistance mechanisms.

The discovery of new therapies against bacterial infections has faced numerous setbacks including the lack of financial support and interest by the pharmaceutical sector. On the academic side, the lack of progress is likely a result of the limited practical experience that academic laboratories have on the drug development process. A potential solution to this problem is the formation of partnerships between academia and industry. This type of collaborations would encourage the exploration of novel and less validated targets or phenotypes in industry, and provide support and guidance to academics in the drug discovery landscape.

Robust and quick high-throughput assays have greatly facilitated the identification of active compounds, as well as the technological advances that allow for the identification of the molecular targets in a more efficient manner. In collaboration with the Drug Discovery Unit, University of Dundee, we performed a high-throughput screening (HTS) of small-molecule libraries to identify inhibitors of Stx expression in *E. coli* O157:H7 using a fluorescence-based reporter assay. The use of *stx2*::GFP cell-based assay in the HTS maximised the chances of finding hit compounds that can penetrate the membrane. It also allowed the screening of multiple targets simultaneously, in comparison to the target-based approach (Urban et al. 2007; Alksne et al. 2000).

The work presented in chapter 4 describes the discovery of two hit compounds - DDD01302463 and DDD01304030 - that block *stx2* expression in a specific and dose-dependent manner. Future work with the compounds DDD01302463 and DDD01304030 will involve structure-activity relationship studies to improve the activity, the identification of the target and mode of action, and *in vivo* evaluation.

The assays and methods used in the HTS are an excellent platform to continue the study and development of small-molecule inhibitors of *stx* expression.

6.3 Concluding remarks

This study provides insights into the discovery and biological evaluation of small molecules with inhibitory activity against Shiga toxin expression. We report the discovery of novel inhibitor of the bacterial protein RecA. We propose that targeting RecA is a viable approach to develop new treatment strategies against STEC infections. Our work also provides an excellent framework for future research focused on the development of inhibitors of Shiga toxin expression.

List of References

- Aertsen, A., and Chris W. M. 2005. "Mrr Instigates the SOS Response after High Pressure Stress in *Escherichia coli*." *Molecular Microbiology* 58 (5): 1381-91.
- Alam, M. K., Areej A., DeCoteau J, Yu Luo, and Ronald G. 2016. "RecA Inhibitors Potentiate Antibiotic Activity and Block Evolution of Antibiotic Resistance." *Cell Chemical Biology* 23 (3). Elsevier Ltd: 381-91.
- Alksne, L. E., P Burgio, W. Hu, Feld B., Singh M. P., Tuckman M., Petersen P. J., et al. 2000. "Identification and Analysis of Bacterial Protein Secretion Inhibitors Utilizing a SecA-LacZ Reporter Fusion System." *Antimicrobial Agents and Chemotherapy* 44 (6): 1418-27.
- Allison, Heather E, Martin J Sergeant, Chloë E James, Jon R Saunders, Darren L Smith, Richard J Sharp, Trevor S Marks, and Alan J McCarthy. 2003. "Immunity Profiles of Wild-Type and Recombinant Shiga-like Toxin-Encoding Bacteriophages and Characterization of Novel Double Lysogens." *Infection and Immunity* 71 (6): 3409-18.
- Amaral, M., Girard M., Álvarez R., Paton A, Paton J, Repetto H., Sacerdoti F., and Ibarra C. 2017. "Ouabain Protects Human Renal Cells against the Cytotoxic Effects of Shiga Toxin Type 2 and Subtilase Cytotoxin." *Toxins* 9 (7): 226.
- Ammon, A., Petersen L. R., and Karch H.. 1999. "A Large Outbreak of Hemolytic Uremic Syndrome Caused by an Unusual Sorbitol-Fermenting Strain of *Escherichia Coli* O157:H-." *The Journal of Infectious Diseases* 179 (5). Oxford University Press: 1274-77.
- Arenson, T. A., Tsodikov O. V., and Cox M. M. 1999. "Quantitative Analysis of the Kinetics of End-Dependent Disassembly of RecA Filaments from ssDNA." *Journal of Molecular Biology* 288 (3): 391-401.

- Asahara, T., Shimizu K., Nomoto K., Hamabata T., Ozawa A., and Takeda Y. 2004. "Probiotic Bifidobacteria Protect Mice from Lethal Infection with Shiga Toxin-Producing *Escherichia coli* O157:H7." *Infection and Immunity* 72 (4): 2240-47.
- Baell J. B and Holloway G. A. "New Substructure Filters for Removal of Pan Assay Interference Compounds (PAINS) from Screening Libraries and for Their Exclusion in Bioassays". 2010. *J. Med. Chem.* 53(7):2719-2740
- Baell J. B and Holloway G. A. "Chemistry: Chemical con Artists Foil Drug Discovery". 2014. *Nature Comment.*
- Baharoglu, Z. and Didier M. 2014. "SOS, the Formidable Strategy of Bacteria against Aggressions." *FEMS Microbiology Reviews* 38 (6): 1126-45.
- Ban, T. A. 2006. "The Role of Serendipity in Drug Discovery." *Dialogues in Clinical Neuroscience* 8 (3). Les Laboratoires Servier: 335-44.
- Bansal, T., Jesudhasan P., Pillai S., Wood T., and Jayaraman A. 2008. "Temporal Regulation of Enterohemorrhagic *Escherichia coli* Virulence Mediated by Autoinducer-2." *Applied Microbiology and Biotechnology* 78 (5): 811-19.
- Barondess, J., and Beckwith J. 1990. "A Bacterial Virulence Determinant Encoded by Lysogenic Coliphage λ ." *Nature* 346 (6287): 871-74.
doi:10.1038/346871a0.
- Bassler, B., Wright M., and Silverman M. 1994. "Multiple Signalling Systems Controlling Expression of Luminescence in *Vibrio harveyi*: Sequence and Function of Genes Encoding a Second Sensory Pathway." *Molecular Microbiology* 13 (2): 273-86.
- Bauer, R. 2015. "Covalent Inhibitors in Drug Discovery: From Accidental Discoveries to Avoided Liabilities and Designed Therapies." *Drug Discovery Today* 20 (9). Elsevier Current Trends: 1061-73.
- Beaber, J., Hochhut B., and Waldor M.W. 2004. "SOS Response Promotes

Horizontal Dissemination of Antibiotic Resistance Genes.” *Nature* 427 (6969). Nature Publishing Group: 72-74.

Bednar, R. 1990. “Reactivity and pH Dependence of Thiol Conjugation to *N*-Ethylmaleimide: Detection of a Conformational Change in Chalcone Isomerase.” *Biochemistry* 29 (15). American Chemical Society: 3684-90.

Benedict, R C, and S C Kowalczykowski. 1988. “Increase of the DNA Strand Assimilation Activity of recA Protein by Removal of the C Terminus and Structure-Function Studies of the Resulting Protein Fragment.” *The Journal of Biological Chemistry* 263 (30): 15513-20.

Berg, R., and Straub B. 2013. “Advancements in the Mechanistic Understanding of the Copper-Catalyzed Azide-Alkyne Cycloaddition.” *Beilstein Journal of Organic Chemistry* 9: 2715-50.

Besser, T., Shaikh N., Holt N., Tarr P., Konkel M.E., Malik-Kale P., Walsh C., Whittam T., and Bono J. 2007. “Greater Diversity of Shiga Toxin-Encoding Bacteriophage Insertion Sites among *Escherichia coli* O157:H7 Isolates from Cattle than in Those from Humans.” *Applied and Environmental Microbiology* 73 (3). American Society for Microbiology: 671-79.

Bielaszewska, M., Idelevich E., Zhang W., Bauwens A., Schaumburg F., Mellmann A., Peters G., and Karch H. 2012. “Effects of Antibiotics on Shiga Toxin 2 Production and Bacteriophage Induction by Epidemic *Escherichia coli* O104:H4 Strain.” *Antimicrobial Agents and Chemotherapy* 56 (6): 3277-82.

Bitzan, M., Moebius E., Ludwig K., Müller-Wiefel D.E., Heesemann J., and Karch H. 1991. “High Incidence of Serum Antibodies to *Escherichia coli* O157 Lipopolysaccharide in Children with Hemolytic-Uremic Syndrome.” *The Journal of Pediatrics* 119 (3): 380-85.

Bloch, S., Nejman-Faleńczyk B., Pierzynowska K., Piotrowska Ewa., Węgrzyn A., Marminon C., Bouaziz Z. et al. 2018. “Inhibition of Shiga Toxin-Converting Bacteriophage Development by Novel Antioxidant Compounds.” *Journal of Enzyme Inhibition and Medicinal Chemistry* 33 (1). Taylor & Francis: 639-50.

- Bolsunovsky, A. Frolova T., Dementyev D., and Sinitsyna O. 2016. "Low Doses of Gamma-Radiation Induce SOS Response and Increase Mutation Frequency in *Escherichia coli* and *Salmonella typhimurium* Cells." *Ecotoxicology and Environmental Safety* 134: 233-38.
- Bommarius, B., Anyanful A., Izrayelit Y., Bhatt S., Cartwright E., Wang W., Swimm A., Benian G, Schroeder F., and Kalman D. 2013. "A Family of Indoles Regulate Virulence and Shiga Toxin Production in Pathogenic *E. coli*." *PLoS ONE* 8 (1).
- Bonifacino, Juan S., and Raul Rojas. 2006. "Retrograde Transport from Endosomes to the trans-Golgi Network." *Nature Reviews Molecular Cell Biology* 7 (8). Nature Publishing Group: 568-79.
- Bork, Julie M., Michael M. Cox, and Ross B. Inman. 2001. "RecA Protein Filaments Disassemble in the 5' to 3' Direction on Single-Stranded DNA." *Journal of Biological Chemistry* 276 (49): 45740-43.
- Böttcher, Thomas, and Stephan A. Sieber. 2010. "Showdomycin as a Versatile Chemical Tool for the Detection of Pathogenesis-Associated Enzymes in Bacteria." *Journal of the American Chemical Society* 132 (20): 6964-72.
- Boucher, Helen W., George H. Talbot, John S. Bradley, John E. Edwards, David Gilbert, Louis B. Rice, Michael Scheld, Brad Spellberg, and John Bartlett. 2009. "Bad Bugs, No Drugs: No ESKAPE! An Update from the Infectious Diseases Society of America." *Clinical Infectious Diseases* 48 (1). Wellcome Trust, Oxford, UK: 1-12.
- Boutte, Cara C., and Sean Crosson. 2013. "Bacterial Lifestyle Shapes Stringent Response Activation." *Trends in Microbiology* 21 (4). Elsevier Ltd: 174-80.
- Broach, J R, and J Thorner. 1996. "High-Throughput Screening for Drug Discovery." *Nature* 384 (6604): 14-14.
- Brown, Dean G., Tricia L. May-Dracka, Moriah M. Gagnon, and Ruben Tommasi. 2014. "Trends and Exceptions of Physical Properties on Antibacterial

Activity for Gram-Positive and Gram-Negative Pathogens.” *Journal of Medicinal Chemistry* 57 (23): 10144-61.

Budke, B., Logan H. L., Kalin J. H., Zelivianskaia A.S., McGuire W.C., Miller L.L., Stark J.M, Kozikowski A. P., Bishop D. K., and Connell P. 2012. “RI-1: A Chemical Inhibitor of RAD51 That Disrupts Homologous Recombination in Human Cells.” *Nucleic Acids Research* 40 (15): 7347-57.

Bujny, M. V., V. Popoff, Johannes L., and Cullen P. J. 2007. “The Retromer Component Sorting Nexin-1 Is Required for Efficient Retrograde Transport of Shiga Toxin from Early Endosome to the Trans Golgi Network.” *Journal of Cell Science* 120 (12): 2010-21.

Bunger, J., Melton-Celsa A., Maynard E., and O’Brien A. 2015. “Reduced Toxicity of Shiga Toxin (Stx) Type 2c in Mice Compared to Stx2d Is Associated with Instability of Stx2c Holotoxin.” *Toxins* 7 (6): 2306-20.

Butala, M., Žgur-Bertok D., and Busby S. J. W. 2009. “The Bacterial LexA Transcriptional Repressor.” *Cellular and Molecular Life Sciences* 66 (1): 82-93.

Calderwood, S. B., Auclair F., Donohue-Rolfe A., Keusch G. T., and Mekalanos J. J. 1987. “Nucleotide Sequence of the Shiga-like Toxin Genes of *Escherichia coli*.” *Proceedings of the National Academy of Sciences of the United States of America* 84 (13): 4364-68.

Calderwood, S. B., and Mekalanos J. J. 1987. “Iron Regulation of Shiga-like Toxin Expression in *Escherichia coli* is Mediated by the Fur Locus.” *Journal of Bacteriology* 169 (10): 4759-64.

Carey, Christine M., Kostrzynska M., Ojha S., and Thompson, S. 2008. “The Effect of Probiotics and Organic Acids on Shiga-Toxin 2 Gene Expression in Enterohemorrhagic *Escherichia coli* O157:H7.” *Journal of Microbiological Methods* 73 (2): 125-32.

Carpenter, T. S., Parkin, J., and Khalid, S. 2016. “The Free Energy of Small

Solute Permeation through the *Escherichia coli* Outer Membrane Has a Distinctly Asymmetric Profile.” *The Journal of Physical Chemistry Letters* 7 (17). American Chemical Society: 3446-51.

Casadevall, A, and L A Pirofski. 1999. “Host-Pathogen Interactions: Redefining the Basic Concepts of Virulence and Pathogenicity.” *Infection and Immunity* 67 (8). American Society for Microbiology (ASM): 3703-13.

Chan, Yau Sang, and Tzi Bun Ng. 2016. “Shiga Toxins: From Structure and Mechanism to Applications.” *Applied Microbiology and Biotechnology* 100 (4): 1597-1610.

Chart, H., Smith H. R., Scotland S. M., Rowe B., Milford D. V., and Taylor C. M. 1991. “Serological Identification of *Escherichia coli* O157:H7 Infection in Haemolytic Uraemic Syndrome.” *Lancet*, 337 (8734): 138-40.

Chase-Topping, M., Gally D., Low, C., Matthews, L. and Woolhouse, M. 2008. “Super-Shedding and the Link between Human Infection and Livestock Carriage of *Escherichia coli* O157.” *Nature Reviews Microbiology* 6 (12): 904-12.

Chen, X., Schauder, S., Potier N., Van Dorsselaer A., Pelczar I., Bassler B.L., and Hughson F.M. 2002. “Structural Identification of a Bacterial Quorum-Sensing Signal Containing Boron.” *Nature* 415 (6871): 545-49.

Cherla, R., Lee S, Mees P., and Tesh V. 2006. “Shiga Toxin 1-Induced Cytokine Production Is Mediated by MAP Kinase Pathways and Translation Initiation Factor eIF4E in the Macrophage-like THP-1 Cell Line.” *Journal of Leukocyte Biology* 79 (2). Society for Leukocyte Biology: 397-407.

Chinchilla, R., and Najera C. 2007. “The Sonogashira Reaction: A Booming Methodology in Synthetic Organic Chemistry.” *Chemical Reviews* 107 (3). American Chemical Society: 874-922.

Chung, N., Zhang X., Kreamer A., Locco L., Kuan P., Bartz S., Linsley P., Marc F., and Strulovici B. 2008. “Median Absolute Deviation to Improve Hit

Selection for Genome-Scale RNAi Screens.”

- Church, D. L., Emshey D., Semeniuk H., Lloyd T., and Pitout J. D. 2007. “Evaluation of BBL CHROMagar O157 versus Sorbitol-MacConkey Medium for Routine Detection of *Escherichia coli* O157 in a Centralized Regional Clinical Microbiology Laboratory.” *Journal of Clinical Microbiology* 45 (9). American Society for Microbiology (ASM): 3098-3100.
- Clatworthy, A., Pierson E., and Hung D. 2007. “Targeting Virulence: A New Paradigm for Antimicrobial Therapy.” *Nature Chemical Biology* 3 (9): 541-48.
- Corbett, A., McGowin A., Sieber S., Flannery T., and Sibbitt B. 2012. “A Method for Reliable Voluntary Oral Administration of a Fixed Dosage (mg/kg) of Chronic Daily Medication to Rats.” *Laboratory Animals* 46 (4). SAGE PublicationsSage UK: 318-24.
- Costa de Oliveira, R., Laval J., and Boiteux S. 1987. “Induction of SOS and Adaptive Responses by Alkylating Agents in *Escherichia coli* Mutants Deficient in 3-Methyladenine-DNA Glycosylase Activities.” *Mutation Research* 183 (1): 11-20.
- Cowan, S. W., Schirmer T., Rummel G., Steiert M., Ghosh R., Pauptit R. A., Jansonius J. N., and Rosenbusch J. P. 1992. “Crystal Structures Explain Functional Properties of Two *E. coli* Porins.” *Nature* 358 (6389): 727-33.
- Cox, M. 2007. “Regulation of Bacterial RecA Protein Function.” *Critical Reviews in Biochemistry and Molecular Biology* 42 (1): 41-63.
- Crane, J. K., Byrd I., and Boedeker E. 2011. “Virulence Inhibition by Zinc in Shiga-Toxigenic *Escherichia coli*.” *Infection and Immunity* 79 (4): 1696-1705.
- Crane, J., Broome J., Reddinger R., and Werth B. 2014. “Zinc Protects against Shiga-Toxigenic *Escherichia coli* by Acting on Host Tissues as Well as on Bacteria.” *BMC Microbiology* 14 (1): 145.

- Crepin, V., Collins J., Habibzay M., and Frankel G. 2016. “*Citrobacter rodentium* Mouse Model of Bacterial Infection.” *Nature Protocols* 11 (10): 1851-76.
- Datsenko, K. A., and Wanner B. L. 2000. “One-Step Inactivation of Chromosomal Genes in *Escherichia coli* K-12 Using PCR Products.” *Proceedings of the National Academy of Sciences* 97 (12): 6640-45.
- De Greve, H., Qizhi C., Deboeck F., and Hernalsteens J-P. 2002. “The Shiga-Toxin VT2-Encoding Bacteriophage ϕ 297 Integrates at a Distinct Position in the *Escherichia coli* Genome.” *Biochimica et Biophysica Acta (BBA) - Gene Structure and Expression* 1579 (2-3): 196-202. doi:10.1016/S0167-4781(02)00539-0.
- De Nys, R., Steinberg P., Willemsen P., Dworjanyn S., Gabelish C., and King R. 1995. “Broad Spectrum Effects of Secondary Metabolites from the Red Alga *Delisea Pulchra* in Antifouling Assays.” *Biofouling* 8 (4). Taylor & Francis Group : 259-71.
- de Nys, R, Wright A., König G., and Sticher O. 1993. “New Halogenated Furanones from the Marine Alga *Delisea Pulchra* (Cf. Fimbriata).” *Tetrahedron* 49 (48). Pergamon: 11213-20.
- De Sablet, T, Chassard C., Bernalier-Donadille A, Vareille M., Gobert A., and Martin C. 2009. “Human Microbiota-Secreted Factors Inhibit Shiga Toxin Synthesis by Enterohemorrhagic *Escherichia coli* O157:H7.” *Infection and Immunity* 77 (2): 783-90.
- Denizot, F., and Lang R. 1986. “Rapid Colorimetric Assay for Cell Growth and Survival. Modifications to the Tetrazolium Dye Procedure Giving Improved Sensitivity and Reliability.” *Journal of Immunological Methods* 89 (2): 271-77.
- Drees, J. C., Lusetti S., Chitteni-Pattu S., Inman R., and Cox M. 2004. “A RecA Filament Capping Mechanism for RecX Protein.” *Molecular Cell* 15 (5): 789-98.

- Dziva, F., van Diemen P., Stevens M., Smith A., and Wallis T. 2004. "Identification of *Escherichia coli* O157:H7 Genes Influencing Colonization of the Bovine Gastrointestinal Tract Using Signature-Tagged Mutagenesis." *Microbiology* 150 (11). Microbiology Society: 3631-45.
- Eisenhauer, P. B., Chaturvedi P., Fine R. E., Ritchie A. J., Pober J. S., Cleary T. G., and Newburg D. S. 2001. "Tumor Necrosis Factor Alpha Increases Human Cerebral Endothelial Cell Gb3 and Sensitivity to Shiga Toxin." *Infection and Immunity* 69 (3). American Society for Microbiology (ASM): 1889-94.
- Erill, I., Campoy S., and Barbé J. 2007. "Aeons of Distress: An Evolutionary Perspective on the Bacterial SOS Response." *FEMS Microbiology Reviews* 31 (6): 637-56.
- Fadlallah, S., Rahal E., Sabra A., Kissoyan K., and Matar G. 2015. "Effect of Rifampicin and Gentamicin on Shiga Toxin 2 Expression Level and the SOS Response in *Escherichia coli* O104:H4." *Foodborne Pathogens and Disease* 12 (1): 47-55.
- Falguières, T., Mallard F., Baron C., Hanau D., Lingwood C., Goud B, Salamero J, and Johannes L. 2001. "Targeting of Shiga Toxin B-Subunit to Retrograde Transport Route in Association with Detergent-Resistant Membranes." *Molecular Biology of the Cell* 12 (8). American Society for Cell Biology: 2453-68.
- Figler, H.M., and Dudley E. 2016. "The Interplay of *Escherichia coli* O157:H7 and Commensal *E. coli*: The Importance of Strain-Level Identification." *Expert Review of Gastroenterology & Hepatology* 10 (4): 415-17.
- Foster, G., and Tesh V. 2002. "Shiga Toxin 1-Induced Activation of c-Jun NH(2)-Terminal Kinase and p38 in the Human Monocytic Cell Line THP-1: Possible Involvement in the Production of TNF-Alpha." *Journal of Leukocyte Biology* 71 (1): 107-14.
- Foster, J. W. 2004. "*Escherichia coli* Acid Resistance: Tales of an Amateur Acidophile." *Nat Rev Microbiol* 2 (11): 898-907.

- Fuchs, G., Mobassaleh M., Donohue-Rolfe A, Montgomery R., Grand R., and Keusch G.T. 1986. "Pathogenesis of Shigella Diarrhea: Rabbit Intestinal Cell Microvillus Membrane Binding Site for Shigella Toxin." *Infection and Immunity* 53 (2): 372-77.
- Fuchs, S., Mühldorfer I, Donohue-Rolfe A., Kerényi M., Emödy L., Alexiev R., Nenkov P., and Hacker J. 1999. "Influence of RecA on in Vivo Virulence and Shiga Toxin 2 Production in *Escherichia coli* Pathogens." *Microbial Pathogenesis* 27 (1): 13-23.
- Fuller, C., Pellino C., Flagler M., Strasser J., and Weiss A. 2011. "Shiga Toxin Subtypes Display Dramatic Differences in Potency." *Infection and Immunity* 79 (3): 1329-37.
- Gal, J. 2013. "Molecular Chirality: Language, History, and Significance." In *Topics in Current Chemistry*, 340:1-20.
- Galstukhova N .B., Shchukina M. N., Zykova T. N., Pershin G.N. 1972. "Synthesis of Thiourea Derivatives" *Pharmaceutical Chemistry Journal* 6(3): 142-145
- Gamage, S., Patton A, Hanson J., and Weiss A. 2004. "Diversity and Host Range of Shiga Toxin-Encoding Phage." *Infection and Immunity* 72 (12). American Society for Microbiology (ASM): 7131-39.
- Garred, O, van Deurs B., and Sandvig K. 1995. "Furin-Induced Cleavage and Activation of Shiga Toxin." *The Journal of Biological Chemistry* 270 (18). American Society for Biochemistry and Molecular Biology: 10817-21.
- Ghilagaber, S., Hunter W., and Marquez R. 2007. "Efficient Coupling of Low Boiling Point Alkynes and 5-Iodonucleosides." *Tetrahedron Letters* 48 (3): 483-86.
- Givskov, M., de Nys R., Manefield M., Gram L., Maximilien R., Eberl L., Molin S., Steinberg P. D., and Kjelleberg S. 1996. "Eukaryotic Interference with Homoserine Lactone-Mediated Prokaryotic Signalling." *Journal of Bacteriology* 178 (22): 6618-22.

- Gobius, K. S., Higgs G., and Desmarchelier P. 2003. "Presence of Activatable Shiga Toxin Genotype (stx(2d)) in Shiga Toxigenic *Escherichia coli* from Livestock Sources." *Journal of Clinical Microbiology* 41 (8). American Society for Microbiology Journals: 3777-83.
- Goktug, A., Chai S., and Chen T. 2013. "Data Analysis Approaches in High Throughput Screening." *Drug Discovery*
- Gonzales, C., Zaleska M.M., Riddell D.R., Atchison K.P., Robshaw A., Zhou H., and Sukoff Rizzo S.J.. 2014. "Alternative Method of Oral Administration by Peanut Butter Pellet Formulation Results in Target Engagement of BACE1 and Attenuation of Gavage-Induced Stress Responses in Mice." *Pharmacology Biochemistry and Behavior* 126: 28-35.
- Gonzalez Barrios, A. F., Zuo R., Hashimoto Y., Yang L., Bentley W. E., and Wood T. K.. 2006. "Autoinducer 2 Controls Biofilm Formation in *Escherichia coli* through a Novel Motility Quorum-Sensing Regulator (MqsR, B3022)." *Journal of Bacteriology* 188 (1): 305-16.
- Goswami, K., Chen C., Xiaoli L., Eaton K., and Dudley E. 2015. "Coculture of *Escherichia coli* O157:H7 with a Nonpathogenic *E. coli* Strain Increases Toxin Production and Virulence in a Germfree Mouse Model." Edited by V. B. Young. *Infection and Immunity* 83 (11): 4185-93.
- Gouali, M., Ruckly C., Carle I., Lejay-Collin M., and Weill F.X. 2013. "Evaluation of CHROMagar STEC and STEC O104 Chromogenic Agar Media for Detection of Shiga Toxin-Producing *Escherichia coli* in Stool Specimens." *Journal of Clinical Microbiology* 51 (3): 894-900.
- Greenberg, R., Winans E. P., Bassler S. C., Xavier B. L. J., and Bassler K. B. 2001. "Synthesis of LuxS Inhibitors Targeting Bacterial Cell-Cell Communication." *Curr. Opin. Microbiol* 35 (2): 439.
- Guha, R. 2013. "On Exploring Structure-Activity Relationships." *Methods in Molecular Biology (Clifton, N.J.)* 993. NIH Public Access: 81-94.

- Guo, M., Gamby S., Zheng Y., and Sintim H. 2013. "Small Molecule Inhibitors of AI-2 Signaling in Bacteria: State-of-the-Art and Future Perspectives for Anti-Quorum Sensing Agents." *International Journal of Molecular Sciences* 14 (9): 17694-728.
- Haasen, D., Schopfer U., Antczak C., Guy C., Fuchs F., and Selzer P. 2017. "How Phenotypic Screening Influenced Drug Discovery: Lessons from Five Years of Practice." *ASSAY and Drug Development Technologies* 15 (6): 239-46.
- Hall, G., Kurosawa S., Stearns-Kurosawa D., Girbes T., Gillet D, and Barbier J. 2017. "Shiga Toxin Therapeutics: Beyond Neutralization."
- Han, Y., Hou S., Simon K., Ren D., and Yeung Luk Y. 2008. "Identifying the Important Structural Elements of Brominated Furanones for Inhibiting Biofilm Formation by *Escherichia coli*." *Bioorganic and Medicinal Chemistry Letters* 18 (3): 1006-10.
- Hansen, T.M., Engler M., and Forsyth C. 2003. "Total Synthesis of a Biotinylated Derivative of Phorboxazole A via Sonogashira Coupling." *Bioorganic & Medicinal Chemistry Letters* 13 (13): 2127-30.
- Hauswaldt, S., Nitschke M., Sayk F., Solbach W., and Knobloch J. 2013. "Lessons Learned From Outbreaks of Shiga Toxin Producing *Escherichia coli*." *Current Infectious Disease Reports* 15 (1): 4-9.
- Hazes, B., and Read R. 1997. "Accumulating Evidence Suggests That Several AB-Toxins Subvert the Endoplasmic Reticulum-Associated Protein Degradation Pathway To Enter Target Cells." *Biochemistry* 36 (37): 11051-54.
- He, Z., Wang Q., Hu Y., Liang J., Jiang Y., Ma R., Tang Z., and Huang Z. 2012. "Use of the Quorum Sensing Inhibitor Furanone C-30 to Interfere with Biofilm Formation by *Streptococcus Mutans* and Its luxS Mutant Strain." *International Journal of Antimicrobial Agents* 40 (1): 30-35.
- Head, S. C., Karmali M. A., and Lingwood C. A. 1991. "Preparation of VT1 and VT2 Hybrid Toxins from Their Purified Dissociated Subunits. Evidence for B

Subunit Modulation of a Subunit Function.” *The Journal of Biological Chemistry* 266 (6): 3617-21.

Hefti, F. 2008. “Requirements for a Lead Compound to Become a Clinical Candidate.” *BMC Neuroscience* 9 Suppl 3 (Suppl 3). BioMed Central: S7.

Hendrix, R. W., Hatfull G., and Smith M. 2003. “Bacteriophages with Tails: Chasing Their Origins and Evolution.” *Research in Microbiology* 154 (4): 253-57.

Henle, E. S., and Linn S. 1997. “Formation, Prevention, and Repair of DNA Damage by Iron/hydrogen Peroxide.” *The Journal of Biological Chemistry* 272 (31). American Society for Biochemistry and Molecular Biology: 19095-98.

Hepperle, M., Eckert J., and Gala D. 1999. “Sequential Mono-N-Arylation of Piperazine Nitrogens. Part 1: A Simplified Method and Its Application to the Preparation of a Key *N,N'*-Biaryl Piperazine Antifungal Intermediate.” *Tetrahedron Letters* 40 (31): 5655-59.

Herold, S., Karch H., and Schmidt H. 2004. “Shiga Toxin-Encoding Bacteriophages - Genomes in Motion.” *International Journal of Medical Microbiology* 294 (2-3): 115-21.

Hoggatt, A. F., Hoggatt J., Honerlaw M., and Pelus, L. M. 2010. “A Spoonful of Sugar Helps the Medicine Go down: A Novel Technique to Improve Oral Gavage in Mice.” *Journal of the American Association for Laboratory Animal Science : JAALAS* 49 (3). American Association for Laboratory Animal Science: 329-34.

Huggins, D. J., Venkitaraman A. R., and David R Spring. 2011. “Rational Methods for the Selection of Diverse Screening Compounds.” *ACS Chemical Biology* 6 (3). Europe PMC Funders: 208-17.

Hughes, D. T. and Sperandio V. 2008. “Inter-Kingdom Signalling: Communication between Bacteria and Their Hosts.” *Nature Reviews Microbiology* 6 (2): 111-

20.

- Hughes, J. P., Rees S. S., Kalindjian S. B., and Philpott K. L. 2011. "Principles of Early Drug Discovery." *British Journal of Pharmacology* 162 (6): 1239-49.
- Hurley, B. P., Thorpe C. M. and Acheson D. W. K.. 2001. "Shiga Toxin Translocation across Intestinal Epithelial Cells Is Enhanced by Neutrophil Transmigration." *Infection and Immunity* 69 (10): 6148-55.
- Hutf, A. J., and O'grady J. 1996. "Review Drug Chirality: A Consideration of the Significance of the Stereochemistry of Antimicrobial Agents." *Journal of Antimicrobial Chemotherapy*. Vol. 37.
- Ikeda, M., Gunji Y., Yamasaki S., and Takeda Y. 2000. "Shiga Toxin Activates p38 MAP Kinase through Cellular Ca(2+) Increase in Vero Cells." *FEBS Letters* 485 (1): 94-98.
- Imamovic, L., and Muniesa M. 2012. "Characterizing RecA-Independent Induction of Shiga toxin2-Encoding Phages by EDTA Treatment." *PLoS ONE* 7 (2).
- Iversen, Philip W., Brian J. Eastwood, G. Sitta Sittampalam, and Karen L. Cox. 2006. "A Comparison of Assay Performance Measures in Screening Assays: Signal Window, Z' Factor, and Assay Variability Ratio." *Journal of Biomolecular Screening* 11 (3): 247-52.
- Jakobsson, H. E., Rodriguez-Pineiro A. M., Schutte A., Ermund A., Boysen P., Bemark M., Sommer F., Backhed F., Hansson G. C., and Johansson M. E.. 2015. "The Composition of the Gut Microbiota Shapes the Colon Mucus Barrier." *EMBO Reports* 16 (2): 164-77.
- Jena, N R. 2012. "DNA Damage by Reactive Species: Mechanisms, Mutation and Repair." *Journal of Biosciences* 37 (3): 503-17.
- Jerabek-Willemsen, Moran, Timon André, Randy Wanner, Heide Marie Roth, Stefan Duhr, Philipp Baaske, and Dennis Breitsprecher. 2014. "MicroScale Thermophoresis: Interaction Analysis and beyond." *Journal of Molecular*

Structure 1077. Elsevier: 101-13.

Ludger J., Popoff V., Pepe S., Settembre C., Annunziata I., Surace E.M., Dierks T., et al. 2008. "Tracing the Retrograde Route in Protein Trafficking." *Cell* 135 (7). Academic Press: 1175-87.

Ludger J., and Römer W. 2010. "Shiga Toxins-from Cell Biology to Biomedical Applications." *Nature Reviews. Microbiology* 8 (2). Nature Publishing Group: 105-16.

Joo, C., McKinney S., Nakamura M., Rasnik I., Myong S., and Ha T. 2006. "Real-Time Observation of RecA Filament Dynamics with Single Monomer Resolution." *Cell* 126 (3): 515-27.

Kanamaru, K., Kanamaru K., Tatsuno I., Tobe T., and Sasakawa C. 2000. "SdiA, an *Escherichia coli* Homologue of Quorum-Sensing Regulators, Controls the Expression of Virulence Factors in Enterohaemorrhagic *Escherichia coli* O157:H7." *Molecular Microbiology* 38 (4): 805-16.

Karpman, D., Loos S, Tati R., and Arvidsson I. 2017. "Haemolytic Uraemic Syndrome." *Journal of Internal Medicine* 281 (2): 123-48.
doi:10.1111/joim.12546.

Keserú, G. M., and Makara G. 2006. "Hit Discovery and Hit-to-Lead Approaches." *Drug Discovery Today* 11 (15-16). Elsevier Current Trends: 741-48.

Kim, J. H., and Scialli A. 2011. "Thalidomide: The Tragedy of Birth Defects and the Effective Treatment of Disease." *Toxicological Sciences* 122 (1): 1-6.

Kim, J., and Park W. 2015. "Indole: A Signaling Molecule or a Mere Metabolic Byproduct That Alters Bacterial Physiology at a High Concentration?" *Journal of Microbiology* 53 (7): 421-28.

Kime, L., Vincent H., Gendoo, D. M. A., Jourdan S., Fishwick C., Callaghan A., and McDowall K. 2015. "The First Small-Molecule Inhibitors of Members of the Ribonuclease E Family." *Scientific Reports* 5 (1). Nature Publishing

Group: 8028.

- Kimmitt, P. T., Harwood C. R., and Barer M. R. 2000. "Toxin Gene Expression by Shiga Toxin-Producing *Escherichia coli*: The Role of Antibiotics and the Bacterial SOS Response." *Emerging Infectious Diseases* 6 (5): 458-65.
- Kintz, E., Brainard J., Hooper L., and Hunter P. 2017. "Transmission Pathways for Sporadic Shiga-Toxin Producing *E. coli* Infections: A Systematic Review and Meta-Analysis." *International Journal of Hygiene and Environmental Health* 220 (1): 57-67.
- Kitov, P., Sadowska J. M., Mulvey G., Armstrong G. D., Ling H., Pannu N. S., Read R. J., and Bundle D. R. 2000. "Shiga-like Toxins Are Neutralized by Tailored Multivalent Carbohydrate Ligands." *Nature* 403 (6770). Macmillan Magazines Ltd.: 669-72.
- Knegtel, R., Fogh R., Boelens R., Kaptein R., Otteleben G., Rüterjans H., Dumoulin P., and Schnarr M. 1995. "A Model for the LexA Repressor DNA Complex." *Proteins: Structure, Function, and Genetics* 21 (3): 226-36.
- Kohanski, M., Dwyer D., Hayete B., Lawrence C., and Collins J. 2007. "A Common Mechanism of Cellular Death Induced by Bactericidal Antibiotics." *Cell* 130 (5). Cell Press: 797-810.
- Kongmuang, U., Honda T., and Miwatani T. 1987. "Enzyme-Linked Immunosorbent Assay to Detect Shiga Toxin of *Shigella dysenteriae* and Related Toxins." *Journal of Clinical Microbiology* 25 (1). American Society for Microbiology (ASM): 115.
- Konowalchuk, J., Speirs J, and Stavric S. 1977. "Vero Response to a Cytotoxin of *Escherichia coli*." *Infection and Immunity* 18 (3): 775-79.
- Krishna, S., Maslov S., Sneppen K, Bailone A., and Ishibe S. 2007. "UV-Induced Mutagenesis in *Escherichia coli* SOS Response: A Quantitative Model." *PLoS Computational Biology* 3 (3). American Society of Microbiology: e41.

- Krüger, A., and Lucchesi P. 2015. "Shiga Toxins and Stx Phages: Highly Diverse Entities." *Microbiology (Reading, England)* 161: 451-62.
- Kunsmann, L., Rüter C., Bauwens A., Greune L., Glüder M., Kemper B., Fruth A., et al. 2015. "Virulence from Vesicles: Novel Mechanisms of Host Cell Injury by *Escherichia coli* O104:H4 Outbreak Strain." *Scientific Reports* 5 (1): 13252.
- Landi, F., Johansson C, Campopiano D., and Hulme A. 2010. "Synthesis and Application of a New Cleavable Linker For 'click'-Based Affinity Chromatography." *Organic & Biomolecular Chemistry* 8 (1). The Royal Society of Chemistry: 56-59. doi:10.1039/b916693a.
- Lauvrak, S. U., Torgersen M., and Sandvig K. 2004. "Efficient Endosome-to-Golgi Transport of Shiga Toxin Is Dependent on Dynamin and Clathrin." *Journal of Cell Science* 117 (11): 2321-31.
- Lee, A., Ross C., Zeng B., and Singleton S. 2005. "A Molecular Target for Suppression of the Evolution of Antibiotic Resistance: Inhibition of the *Escherichia coli* RecA Protein by N^6 -(1-Naphthyl)-ADP." *Journal of Medicinal Chemistry* 48 (17): 5408-11.
- Lee, A., and Singleton S. 2004. "Inhibition of the *Escherichia coli* RecA Protein: zinc(II), copper(II) and mercury(II) Trap RecA as Inactive Aggregates." *Journal of Inorganic Biochemistry* 98 (11): 1981-86.
- Lee, J., Kim Y., Cho H., Ryu S., Cho M., and Lee J. 2014. "Coumarins Reduce Biofilm Formation and the Virulence of *Escherichia coli* O157:H7." *Phytomedicine* 21 (8-9). Elsevier GmbH.: 1037-42.
- Lee, J., Wood T., and Lee J. 2015. "Roles of Indole as an Interspecies and Interkingdom Signaling Molecule." *Trends in Microbiology* 23 (11). Elsevier Ltd: 707-18.
- Lee, S., Lee M., Cherla R., and Tesh V. 2008. "Shiga Toxin 1 Induces Apoptosis through the Endoplasmic Reticulum Stress Response in Human Monocytic

Cells.” *Cellular Microbiology* 10 (3). Blackwell Publishing Ltd: 770-80.

- Li, J., Attila C, Wang L., Wood T., James J Valdes, and William E Bentley. 2007. “Quorum Sensing in *Escherichia coli* Is Signaled by AI-2/LsrR: Effects on Small RNA and Biofilm Architecture.” *Journal of Bacteriology* 189 (16). American Society for Microbiology Journals: 6011-20.
- Li, T., Tu W., Liu Y., Zhou P., Cai K., Li Z., Liu X., et al. 2016. “A Potential Therapeutic Peptide-Based Neutralizer That Potently Inhibits Shiga Toxin 2 *in vitro* and *in vivo*.” *Scientific Reports* 6. Nature Publishing Group: 21837.
- Li, Y., He Y., and Luo Y. 2009. “Crystal Structure of an Archaeal Rad51 Homologue in Complex with a Metatungstate Inhibitor.” *Biochemistry* 48 (29): 6805-10.
- Lin, J., Smith M., Chapin K., Baik H., Bennett G., and Foster J. 1996. “Mechanisms of Acid Resistance in Enterohemorrhagic *Escherichia coli*.” *Appl Environ Microbiol* 62 (9): 3094-3100.
- Ling, H., Boodhoo A., Hazes B., Cummings M., Armstrong G., Brunton J., and Read R. 1998. “Structure of the Shiga-like Toxin I B-Pentamer Complexed with an Analogue of Its Receptor Gb3.” *Biochemistry* 37 (7): 1777-88.
- Lingwood, C. A. 1999. “Verotoxin/Globotriaosyl Ceramide Recognition: Angiopathy, Angiogenesis and Antineoplasia.” *Bioscience Reports* 19 (5). Kluwer Academic Publishers-Plenum Publishers: 345-54.
- Little, J., and Mount D. 1982. “The SOS Regulatory System of *Escherichia coli*.” *Cell* 29 (1): 11-22.
- Lombardino, J., and Lowe J. 2004. “The Role Of The Medicinal Chemist In Drug Discovery. Then And Now” *Nat Rev Drug Disc.* 3(10):853-62
- Lomenick, B., Olsen R., and Huang J. 2011. “Identification of Direct Protein Targets of Small Molecules.” *ACS Chemical Biology* 6 (1): 34-46.
- Lonn-Stensrud, J., M. A. Landin, T. Benneche, F. C. Petersen, and A. A. Scheie.

2008. "Furanones, Potential Agents for Preventing *Staphylococcus epidermidis* Biofilm Infections" *Journal of Antimicrobial Chemotherapy* 63 (2): 309-16.
- Lowery, Colin A., Tobin J. Dickerson, and Kim D. Janda. 2008. "Interspecies and Interkingdom Communication Mediated by Bacterial Quorum Sensing." *Chemical Society Reviews* 37 (7): 1337.
- Lowery, Colin A., Kathleen M. McKenzie, Longwu Qi, Michael M. Meijler, and Kim D. Janda. 2005. "Quorum Sensing in *Vibrio Harveyi*: Probing the Specificity of the LuxP Binding Site." *Bioorganic & Medicinal Chemistry Letters* 15 (9): 2395-98.
- Lucas, Esther M.F., Mateus C. Monteiro de Castro, and Jacqueline A. Takahashi. 2007. "Antimicrobial Properties of Sclerotiorin, isochromophilone VI and Pencolide, Metabolites from a Brazilian Cerrado Isolate of *Penicillium sclerotiorum* van Beyma." *Brazilian Journal of Microbiology* 38 (4). SBM: 785-89.
- Luna-Gierke, R. E., P. M. Griffin, L. H. Gould, K. Herman, C. A. Bopp, N. Strockbine, And R. K. Mody. 2014. "Outbreaks of Non-O157 Shiga Toxin-Producing *Escherichia coli* Infection: USA." *Epidemiology and Infection* 142 (11): 2270-80.
- Lundholt, Betina Kerstin, Kurt M. Scudder, and Len Pagliaro. 2003. "A Simple Technique for Reducing Edge Effect in Cell-Based Assays." *Journal of Biomolecular Screening* 8 (5). SAGE Publications: 566-70.
- Luo, Jing, Jin Liang Kong, Bi Ying Dong, Hong Huang, Ke Wang, Li Hong Wu, Chang Chun Hou, Yue Liang, Bing Li, and Yi Qiang Chen. 2016. "Baicalein Attenuates the Quorum Sensing-Controlled Virulence Factors of *Pseudomonas aeruginosa* and Relieves the Inflammatory Response in *P. Aeruginosa*-Infected Macrophages by Downregulating the MAPK and NFκB Signal-Transduction Pathways." *Drug Design, Development and Therapy* 10: 183-203.

- Luo, Y, R A Pfuetzner, S Mosimann, M Paetzel, E A Frey, M Cherney, B Kim, J W Little, and N C Strynadka. 2001. "Crystal Structure of LexA: A Conformational Switch for Regulation of Self-Cleavage." *Cell* 106 (5): 585-94.
- Luperchio, S A, and D B Schauer. 2001. "Molecular Pathogenesis of *Citrobacter rodentium* and Transmissible Murine Colonic Hyperplasia." *Microbes and Infection* 3 (4): 333-40.
- Lusetti, Shelley L., Oleg N. Voloshin, Ross B. Inman, R. Daniel Camerini-Otero, and Michael M. Cox. 2004. "The DinI Protein Stabilizes RecA Protein Filaments." *Journal of Biological Chemistry* 279 (29): 30037-46.
- Mah, Robert, Jason R. Thomas, and Cynthia M. Shafer. 2014. "Drug Discovery Considerations in the Development of Covalent Inhibitors." *Bioorganic & Medicinal Chemistry Letters* 24 (1): 33-39.
- Majowicz, Shannon E., Elaine Scallan, Andria Jones-Bitton, Jan M. Sargeant, Jackie Stapleton, Frederick J. Angulo, Derrick H. Yeung, and Martyn D. Kirk. 2014. "Global Incidence of Human Shiga Toxin-Producing *Escherichia coli* Infections and Deaths: A Systematic Review and Knowledge Synthesis." *Foodborne Pathogens and Disease* 11 (6): 447-55.
- Mallick, Emily M, Megan E McBee, Vijay K Vanguri, Angela R Melton-Celsa, Katherine Schlieper, Brad J Karalius, Alison D O'Brien, Joan R Buttermont, John M Leong, and David B Schauer. 2012. "A Novel Murine Infection Model for Shiga Toxin-Producing *Escherichia coli*." *The Journal of Clinical Investigation* 122 (11): 4012-24. doi:10.1172/JCI62746.
- Malyukova, I., K. F. Murray, C. Zhu, E. Boedeker, A. Kane, K. Patterson, J. R. Peterson, M. Donowitz, and O. Kovbasnjuk. 2008. "Macropinocytosis in Shiga Toxin 1 Uptake by Human Intestinal Epithelial Cells and Transcellular Transcytosis." *AJP: Gastrointestinal and Liver Physiology* 296 (1): G78-92.
- Manasherob, Robert, Christine Miller, Kwang-sun Kim, and Stanley N Cohen. 2012. "Ribonuclease E Modulation of the Bacterial SOS Response." *PloS One*

7 (6). Public Library of Science: e38426.

- Manley-King, Clarina I., Gisella Terre'Blanche, Neal Castagnoli, Jacobus J. Bergh, and Jacobus P. Petzer. 2009. "Inhibition of Monoamine Oxidase B by N-Methyl-2-Phenylmaleimides." *Bioorganic & Medicinal Chemistry* 17 (8): 3104-10.
- Martinez-Castillo, A., and Muniesa M. 2014. "Implications of Free Shiga Toxin-Converting Bacteriophages Occurring Outside Bacteria for the Evolution and the Detection of Shiga Toxin-Producing *Escherichia coli*." *Frontiers in Cellular and Infection Microbiology* 4 (April): 1-8.
- Matar, G. M., and Rahal E. 2003. "Inhibition of the Transcription of the *Escherichia Coli* O157:H7 Genes Coding for Shiga-like Toxins and Intimin, and Its Potential Use in the Treatment of Human Infection with the Bacterium." *Annals of Tropical Medicine & Parasitology* 97 (3): 281-87.
- Matsushiro, A., Sato K., Miyamoto H., Yamamura T., and Honda T. 1999. "Induction of Prophages of Enterohemorrhagic *Escherichia coli* O157:H7 with Norfloxacin." *Journal of Bacteriology* 181 (7). American Society for Microbiology (ASM): 2257-60.
- Mauro, S., and Koudelka G. 2011. "Shiga Toxin: Expression, Distribution, and Its Role in the Environment." *Toxins* 3 (6): 608-25.
- McGannon, C., Fuller C., and Weiss A. 2010. "Different Classes of Antibiotics Differentially Influence Shiga Toxin Production." *Antimicrobial Agents and Chemotherapy* 54 (9): 3790-98.
- McPherson, A., and Gavira J. 2014. "Introduction to Protein Crystallization." *Acta Crystallographica. Section F, Structural Biology Communications* 70 *International Union of Crystallography*: 2-20.
- Mecozzi, S., West A., and Dougherty D. 1996. "Cation-Pi Interactions in Aromatics of Biological and Medicinal Interest: Electrostatic Potential Surfaces as a Useful Qualitative Guide." *Proceedings of the National*

Academy of Sciences of the United States of America 93 (20). National Academy of Sciences: 10566-71.

Meghna P., Jiang M., Woodgate R., Cox M., and Goodman M. 2010. "A New Model for SOS-Induced Mutagenesis: How RecA Protein Activates DNA Polymerase V." *Crit Rev Biochem Mol Biol* 45 (3): 171-84.

Melander, R., Minvielle M., and Melander C. 2014. "Controlling Bacterial Behavior with Indole-Containing Natural Products and Derivatives." *Tetrahedron* 70 (37). Elsevier Ltd: 6363-72.

Mellor, G., Sim E., Barlow R., D'Astek B., Galli L., Chinen I., Rivas M., and Gobius K. 2012. "Phylogenetically Related Argentinean and Australian *Escherichia coli* O157 Isolates Are Distinguished by Virulence Clades and Alternative Shiga Toxin 1 and 2 Prophages." *Applied and Environmental Microbiology* 78 (13). American Society for Microbiology: 4724-31.

Melton-Celsa, A.. 2014. "Shiga Toxin (Stx) Classification, Structure, and Function." *Microbiology Spectrum* 2 (3): 1-21.

Melton-Celsa, A. Kokai-Kun J., and O'Brien A. 2002. "Activation of Shiga Toxin Type 2d (Stx2d) by Elastase Involves Cleavage of the C-Terminal Two Amino Acids of the A2 Peptide in the Context of the Appropriate B Pentamer." *Molecular Microbiology* 43 (1): 207-15.

Menetski, J. P., and Kowalczykowski S. C. 1985. "Interaction of RecA Protein with Single-Stranded DNA. Quantitative Aspects of Binding Affinity Modulation by Nucleotide Cofactors." *Journal of Molecular Biology* 181 (2): 281-95.

Miller, C., Thomsen L., Gaggero C., Mosseri R., Ingmer H., and Cohen S. 2004. "SOS Response Induction by β -Lactams and Bacterial Defense Against Antibiotic Lethality." *Science* 305 (5690): 1629-31.

Miller, M., and Bassler B. 2001. "Quorum Sensing in Bacteria." *Annual Review of Microbiology* 55 (1): 165-99.

- Mo, C., Culyba M., Selwood T., Kubiak J., Hostetler Z., Jurewicz A., Keller P., et al. 2018. "Inhibitors of LexA Autoproteolysis and the Bacterial SOS Response Discovered by an Academic-Industry Partnership." *ACS Infectious Diseases* 4 (3). American Chemical Society: 349-59.
- Mo, C., Manning S., Roggiani M., Culyba M., Samuels A. M., Sniegowski P., Goulian M., and Kohli R. 2016. "Systematically Altering Bacterial SOS Activity under Stress Reveals Therapeutic Strategies for Potentiating Antibiotics." *mSphere* 1 (4): e00163-16.
- Mohawk, K., and O'Brien A. 2011. "Mouse Models of *Escherichia coli* O157:H7 Infection and Shiga Toxin Injection" 2011.
- Moreau, P. L., and Carlier M. 1989. "RecA Protein-Promoted Cleavage of LexA Repressor in the Presence of ADP and Structural Analogues of Inorganic Phosphate, the Fluoride Complexes of Aluminum and Beryllium." *The Journal of Biological Chemistry* 264 (4): 2302-6.
- Muheim, C., Götzke H., Eriksson A., Lindberg S., Lauritsen I., Nørholm M., and O'Daley D. 2017. "Increasing the Permeability of *Escherichia coli* Using MAC13243." *Scientific Reports* 7 (1). Nature Publishing Group: 17629.
- Mukhopadhyay, S., and Linstedt A. 2012. "Manganese Blocks Intracellular Trafficking of Shiga Toxin and Protects Against Shiga Toxicosis." *Science* 335 (6066): 332-35.
- Mukhopadhyay, S., and Linstedt A. 2013. "Retrograde Trafficking of AB₅ Toxins: Mechanisms to Therapeutics." *Journal of Molecular Medicine* 91 (10). NIH Public Access: 1131-41.
- Mundy, R., MacDonald T., Dougan G., Frankel G., and Wiles S. 2005. "Citrobacter Rodentium of Mice and Man." *Cellular Microbiology* 7 (12): 1697-1706.
- Nataro, J. P., and Kaper J. B. 1998. "Diarrheagenic *Escherichia coli*." *Clinical Microbiology Reviews* 11 (1): 142-201.

- Nguyen, L., He H. and Pham-Huy C. 2006. "Chiral Drugs: An Overview." *International Journal of Biomedical Science : IJBS* 2 (2). Master Publishing Group: 85-100.
- Nikaido, H. 1994. "Prevention of Drug Access to Bacterial Targets: Permeability Barriers and Active Efflux." *Science (New York, N.Y.)* 264 (5157): 382-88.
- Nikaido, H. 2003. "Molecular Basis of Bacterial Outer Membrane Permeability Revisited." *Microbiology and Molecular Biology Reviews : MMBR* 67 (4): 593-656.
- Njoroge, J., and Sperandio V. 2012. "Enterohemorrhagic *Escherichia coli* Virulence Regulation by Two Bacterial Adrenergic Kinases, QseC and QseE." *Infection and Immunity* 80 (2). American Society for Microbiology Journals: 688-703.
- Noris, M., and Remuzzi G. 2005. "Hemolytic Uremic Syndrome." *Journal of the American Society of Nephrology : JASN* 16 (4): 1035-50.
- Nowak-Sliwiska, P., Storto M, Cataudella T., Ballini J., Gatz R., Giorgio M., van den Bergh H., Plyte S., and Wagnières G. 2012. "Angiogenesis Inhibition by the Maleimide-Based Small Molecule GNX-686." *Microvascular Research* 83 (2): 105-10.
- Nowicki, D., Maciąg-Dorszyńska M., Kobiela W., Herman-Antosiewicz A., Węgrzyn A., Szalewska-Pałasz A., and Węgrzyn G. 2014. "Phenethyl Isothiocyanate Inhibits Shiga Toxin Production in Enterohemorrhagic *Escherichia coli* by Stringent Response Induction." *Antimicrobial Agents and Chemotherapy* 58 (4): 2304-15.
- Nowicki, D., Rodzik O., Herman-Antosiewicz A., and Szalewska-Pałasz A. 2016. "Isothiocyanates as Effective Agents against Enterohemorrhagic *Escherichia coli*: Insight to the Mode of Action." *Scientific Reports* 6 (November 2015). Nature Publishing Group: 22263.
- O'Shea, R., and Moser H. 2008. "Physicochemical Properties of Antibacterial

- Compounds: Implications for Drug Discovery.” *Journal of Medicinal Chemistry* 51 (10): 2871-78.
- Odumosu, O., Nicholas D., Yano H., and Langridge W. 2010. “AB Toxins: A Paradigm Switch from Deadly to Desirable,” 1612-45.
- Pacheco, A., and Sperandio V. 2012. “Shiga Toxin in Enterohemorrhagic *E. coli*: Regulation and Novel Anti-Virulence Strategies.” *Frontiers in Cellular and Infection Microbiology* 2 (June): 81.
- Pai, C. H., Gordon R., Sims H., and Bryan L. 1984. “Sporadic Cases of Hemorrhagic Colitis Associated with *Escherichia coli* O157:H7. Clinical, Epidemiologic, and Bacteriologic Features.” *Annals of Internal Medicine* 101 (6): 738-42.
- Panos, G. Z., Betsi G., and Falagas M. E. 2006. “Systematic Review: Are Antibiotics Detrimental or Beneficial for the Treatment of Patients with *Escherichia coli* O157:H7 Infection?” *Alimentary Pharmacology & Therapeutics* 24 (5): 731-42.
- Parsons, B., Zelyas N., Berenger B., and Chui L. 2016. “Detection, Characterization, and Typing of Shiga Toxin-Producing *Escherichia coli*.” *Frontiers in Microbiology* 7.
- Patel, K., and Telvekar V. 2014. “Design, Synthesis and Antitubercular Evaluation of Novel Series of *N*-[4-(piperazin-1-yl)phenyl]cinnamamide Derivatives.” *European Journal of Medicinal Chemistry* 75: 43-56.
- Payne, D., Gwynn M., Holmes D., and Pompliano D. 2007. “Drugs for Bad Bugs: Confronting the Challenges of Antibacterial Discovery.” *Nature Reviews Drug Discovery* 6 (1): 29-40.
- Penadés, J. R., Chen J., Quiles-Puchalt N., Carpena N., and P. Novick R. 2015. “Bacteriophage-Mediated Spread of Bacterial Virulence Genes.” *Current Opinion in Microbiology* 23: 171-78.

- Pendleton, J., Gorman S., and Gilmore B. 2013. "Clinical Relevance of the ESKAPE Pathogens." *Expert Review of Anti-Infective Therapy* 11 (3): 297-308.
- Peng, H., Cheng Y., Ni N., Minyong L., Gaurav C., Han T., Chung-Dar L., Phang C., and Wang B. 2009. "Synthesis and Evaluation of New Antagonists of Bacterial Quorum Sensing in *Vibrio harveyi*." *ChemMedChem* 4 (9): 1457-68.
- Perna, Nicole T., Guy Plunkett, Valerie Burland, Bob Mau, Jeremy D. Glasner, Debra J. Rose, George F. Mayhew, et al. 2001. "Genome Sequence of Enterohaemorrhagic *Escherichia coli* O157:H7." *Nature* 409 (6819): 529-33.
- Perola, E. 2010. "An Analysis of the Binding Efficiencies of Drugs and Their Leads in Successful Drug Discovery Programs." *Journal of Medicinal Chemistry* 53 (7). American Chemical Society: 2986-97.
- Persad, A. K, and Lejeune J. 2014. "Animal Reservoirs of Shiga Toxin-Producing *Escherichia coli*." *Microbiology Spectrum* 2 (4): 1-14.
- Peterson, E., Janzen W., Kireev D., and Singleton S. 2012. "High-Throughput Screening for RecA Inhibitors Using a Transcreeper Adenosine 5'-O-Diphosphate Assay." *Assay and Drug Development Technologies* 10 (3): 260-68.
- Pinto, A., Cangelosi A., Geoghegan P., and Goldstein J. 2017. "Dexamethasone Prevents Motor Deficits and Neurovascular Damage Produced by Shiga Toxin 2 and Lipopolysaccharide in the Mouse Striatum." *Neuroscience* 344 (March): 25-38.
- Popoff, V., Mardones G. A., Tenza D., Rojas R., Lamaze C., Bonifacino J. S., Raposo G., and Johannes L. 2007. "The Retromer Complex and Clathrin Define an Early Endosomal Retrograde Exit Site." *Journal of Cell Science* 120 (12): 2022-31.
- Prentiss, M., Prévost C., and Danilowicz C. 2015. "Structure/function Relationships in RecA Protein-Mediated Homology Recognition and Strand

Exchange.” *Critical Reviews in Biochemistry and Molecular Biology* 50 (6): 453-76.

Priyadarsini K. I. "Chemical and Structural Features Influencing the Biological Activity of Curcumin". 2013. *Curr Pharm Des* 19(11):2093-100.

Quiles-Puchalt, N., Carpena N., Alonso J., Novick R., Marina A., and Penadés J. 2014. "Staphylococcal Pathogenicity Island DNA Packaging System Involving Cos-Site Packaging and Phage-Encoded HNH Endonucleases." *Proceedings of the National Academy of Sciences of the United States of America* 111 (16): 6016-21.

Rahal, E., Fadlallah S., Nassar F., Kazzi N., and Matar G. 2015. "Approaches to Treatment of Emerging Shiga Toxin-Producing *Escherichia coli* Infections Highlighting the O104:H4 Serotype." *Frontiers in Cellular and Infection Microbiology* 5: 24.

Rahal, E., Kazzi N., Sabra A., Abdelnoor A., and Matar G. 2011. "Decrease in Shiga Toxin Expression Using a Minimal Inhibitory Concentration of Rifampicin Followed by Bactericidal Gentamicin Treatment Enhances Survival of *Escherichia coli* O157:H7-Infected BALB/c Mice." *Annals of Clinical Microbiology and Antimicrobials* 10: 34.

Rainard, J., Pandarakalam G., and McElroy S. 2018. "Using Microscale Thermophoresis to Characterize Hits from High-Throughput Screening: A European Lead Factory Perspective." *Advancing Life Sciences R&D* 23 (3). SAGE Publications: 225-41.

Rangel, J., Sparling P., Crowe C., Griffin P., and Swerdlow D. 2005. "Epidemiology of *Escherichia coli* O157:H7 Outbreaks, United States, 1982-2002." *Emerging Infectious Diseases* 11 (4): 603-9.

Rasko, D., Moreira C., Li D., Reading N., Ritchie J., Waldor M., Williams N., et al. 2008. "Targeting QseC Signaling and Virulence for Antibiotic Development." *Science*, 321 (5892): 1078-80.

- Recacha, E., Machuca J, Díaz de Alba P., Ramos-Güelfo M., Docobo-Pérez F., Rodríguez-Beltrán J, Blázquez J., Pascual A/, and Rodríguez-Martínez J. 2017. "Quinolone Resistance Reversion by Targeting the SOS Response." *mBio* 8 (5). American Society for Microbiology
- Reist, M., Carrupt P., Francotte E., and Testa B. 1998. "Chiral Inversion and Hydrolysis of Thalidomide: Mechanisms and Catalysis by Bases and Serum Albumin, and Chiral Stability of Teratogenic Metabolites." *Chemical Research in Toxicology* 11 (12): 1521-28.
- Ren, D., Bedzyk L., Ye R., Thomas S., and Wood T. 2004. "Differential Gene Expression Shows Natural Brominated Furanones Interfere with the Autoinducer-2 Bacterial Signaling System of *Escherichia coli*." *Biotechnology and Bioengineering* 88 (5): 630-42.
- Richter, M., Drown B., Riley A., Garcia A., Shirai T., Svec R., and Hergenrother P. 2017. "Predictive Compound Accumulation Rules Yield a Broad-Spectrum Antibiotic." *Nature* 545 (7654): 299-304.
- Riedel, C. U., Casey P. G., Mulcahy H., O'Gara F., Gahan C. G. M., and Hill C. 2007. "Construction of p16Slux, a Novel Vector for Improved Bioluminescent Labeling of Gram-Negative Bacteria." *Applied and Environmental Microbiology* 73 (21): 7092-95.
- Riley, L W, R S Remis, S D Helgerson, H B McGee, J G Wells, B R Davis, R J Hebert, et al. 1983. "Hemorrhagic Colitis Associated with a Rare *Escherichia coli* Serotype." *The New England Journal of Medicine* 308 (12): 681-85.
- Risseuw, Martijn D P, Dries J H De Clercq, Sam Lievens, Ulrik Hillaert, Davy Sinnaeve, Freya Van den Broeck, José C Martins, Jan Tavernier, and Serge Van Calenbergh. 2013. "A 'clickable' MTX Reagent as a Practical Tool for Profiling Small-Molecule-Intracellular Target Interactions via MASPIT." *ChemMedChem* 8 (3): 521-26.
- Ristic, D., Mauro Modesti, Thijn van der Heijden, John van Noort, Cees Dekker, Roland Kanaar, and Claire Wyman. 2005. "Human Rad51 Filaments on

Double- and Single-Stranded DNA: Correlating Regular and Irregular Forms with Recombination Function.” *Nucleic Acids Research* 33 (10). Oxford University Press: 3292-3302.

Robinson, C M, J F Sinclair, M J Smith, and A D O’Brien. 2006. “Shiga Toxin of Enterohemorrhagic *Escherichia coli* Type O157:H7 Promotes Intestinal Colonization.” *Proc Natl Acad Sci* 103 (25): 9667-72.

Roe, Andrew J., Stuart W. Naylor, Kevin J. Spears, Helen M. Yull, Tracy A. Dransfield, Matthew Oxford, Iain J. McKendrick, et al. 2004. “Coordinate Single-Cell Expression of LEE4- and LEE5-Encoded Proteins of *Escherichia coli* O157:H7.” *Molecular Microbiology* 54 (2): 337-52.

Römer, Winfried, Ludwig Berland, Valérie Chambon, Katharina Gaus, Barbara Windschiegel, Danièle Tenza, Mohamed R. E. Aly, et al. 2007. “Shiga Toxin Induces Tubular Membrane Invaginations for Its Uptake into Cells.” *Nature* 450 (7170): 670-75.

Rozañov, Dmitry V, Richard D ’ari, and Sergey P Sineoky. 1998. “RecA-Independent Pathways of Lambdoid Prophage Induction in *Escherichia coli*.” *Journal Of Bacteriology* 180 (23): 6306-15.

Ruggenenti, Piero, Marina Noris, and Giuseppe Remuzzi. 2001. “Thrombotic Microangiopathy, Hemolytic Uremic Syndrome, and Thrombotic Thrombocytopenic Purpura.” *Kidney International* 60 (3): 831-46.

Ruzheinikov, S.N, S.K Das, S.E Sedelnikova, A Hartley, S.J Foster, M.J Horsburgh, A.G Cox, et al. 2001. “The 1.2 Å Structure of a Novel Quorum-Sensing Protein, *Bacillus subtilis* LuxS 1 Edited by J. Thornton.” *Journal of Molecular Biology* 313 (1): 111-22.

Saint-Pol, Agnès, Belén Yélamos, Mohamed Amessou, Ian G Mills, Marc Dugast, Danièle Tenza, Peter Schu, et al. 2004. “Clathrin Adaptor epsinR Is Required for Retrograde Sorting on Early Endosomal Membranes.” *Developmental Cell* 6 (4): 525-38.

- Salmond, George P. C., and Peter C. Fineran. 2015. "A Century of the Phage: Past, Present and Future." *Nature Reviews Microbiology* 13 (12). Nature Publishing Group: 777-86.
- Sams-Dodd, F. 2005. "Target-Based Drug Discovery: Is Something Wrong?" *Drug Discovery Today* 10 (2): 139-47.
- Sandvig, K, S Olsnes, J E Brown, O W Petersen, and B van Deurs. 1989. "Endocytosis from Coated Pits of Shiga Toxin: A Glycolipid-Binding Protein from *Shigella dysenteriae* 1." *The Journal of Cell Biology* 108 (4): 1331-43.
- Sato, Shin-ichi, Asako Murata, Takashi Shirakawa, and Motonari Uesugi. 2010. "Biochemical Target Isolation for Novices: Affinity-Based Strategies." *Chemistry & Biology* 17 (6): 616-23.
- Scheutz, F., L. D. Teel, L. Beutin, D. Pierard, G. Buvens, H. Karch, A. Mellmann, et al. 2012. "Multicenter Evaluation of a Sequence-Based Protocol for Subtyping Shiga Toxins and Standardizing Stx Nomenclature." *Journal of Clinical Microbiology* 50 (9): 2951-63.
- Schnarr, M, M Granger-Schnarr, S Hurstel, and J Pouyet. 1988. "The Carboxy-Terminal Domain of the LexA Repressor Oligomerises Essentially as the Entire Protein." *FEBS Letters* 234 (1): 56-60.
- Schröder, M. 2008. "Endoplasmic Reticulum Stress Responses." *Cellular and Molecular Life Sciences* 65 (6): 862-94.
- Secher, T., A. Shima, K. Hinsinger, J. C. Cintrat, L. Johannes, J. Barbier, D. Gillet, and E. Oswald. 2015. "Retrograde Trafficking Inhibitor of Shiga Toxins Reduces Morbidity and Mortality of Mice Infected with Enterohemorrhagic *Escherichia coli*." *Antimicrobial Agents and Chemotherapy* 59 (8): 5010-13.
- Serra-Moreno, R, J Jofre, and M Muniesa. 2008. "The CI Repressors of Shiga Toxin-Converting Prophages Are Involved in Coinfection of *Escherichia coli* Strains, Which Causes a down Regulation in the Production of Shiga Toxin

2.” *Journal of Bacteriology* 190 (13). American Society for Microbiology (ASM): 4722-35.

Sexton, Jonathan Z, Tim J Wigle, Qingping He, Mark a Hughes, Ginger R Smith, Scott F Singleton, Alfred L Williams, and Li-An Yeh. 2010. “Novel Inhibitors of *E. coli* RecA ATPase Activity.” *Current Chemical Genomics* 4: 34-42.

Shaikh, Nurmohammad, and Phillip I Tarr. 2003. “*Escherichia coli* O157:H7 Shiga Toxin-Encoding Bacteriophages: Integrations, Excisions, Truncations, and Evolutionary Implications.” *Journal of Bacteriology* 185 (12): 3596-3605.

Shapiro, Adam B., Grant K. Walkup, and Thomas A. Keating. 2009. “Correction for Interference by Test Samples in High-Throughput Assays.” *Journal of Biomolecular Screening* 14 (8). SAGE PublicationsSage CA: Los Angeles, CA: 1008-16.

Sheng, Lina, Barbara Rasco, and Mei-jun Zhu. 2016. “Cinnamon Oil Inhibits Shiga Toxin Type 2 Phage Induction and Shiga Toxin Type 2 Production in *Escherichia coli* O157:H7” 82 (22): 6531-40.

Shetye, Gauri S., Nischal Singh, Xiang Gao, Debjyoti Bandyopadhyay, Aixin Yan, and Yan-Yeung Luk. 2013. “Structures and Biofilm Inhibition Activities of Brominated Furanones for *Escherichia coli* and *Pseudomonas seruginosa*.” *MedChemComm* 4 (7). The Royal Society of Chemistry: 1079.
doi:10.1039/c3md00059a.

Shimizu, Takeshi, Yuko Ohta, and Masatoshi Noda. 2009. “Shiga Toxin 2 Is Specifically Released from Bacterial Cells by Two Different Mechanisms ” 77 (7): 2813-23.

Shinohara, Takeshi, Shukuko Ikawa, Wakana Iwasaki, Toshiki Hiraki, Takaaki Hikima, Tsutomu Mikawa, Naoto Arai, Nobuo Kamiya, and Takehiko Shibata. 2015. “Loop L1 Governs the DNA-Binding Specificity and Order for RecA-Catalyzed Reactions in Homologous Recombination and DNA Repair.” *Nucleic Acids Research* 43 (2). Oxford University Press: 973-86.

- Shringi, Smriti, Carrie Schmidt, Kaya Katherine, Kelly A. Brayton, Dale D. Hancock, and Thomas E. Besser. 2012. "Carriage of stx2a Differentiates Clinical and Bovine-Biased Strains of *Escherichia coli* O157." Edited by A. Mark Ibekwe. *PLoS ONE* 7 (12). Public Library of Science: e51572.
- Shu, Yue-Zhong, Benjamin M Johnson, and Tian J Yang. 2008. "Role of Biotransformation Studies in Minimizing Metabolism-Related Liabilities in Drug Discovery." *The AAPS Journal* 10 (1). Springer: 178-92.
- Silver, L. L. 2011. "Challenges of Antibacterial Discovery." *Clinical Microbiology Reviews* 24 (1): 71-109.
- Sinclair, James F, and Alison D O'Brien. 2002. "Cell Surface-Localized Nucleolin Is a Eukaryotic Receptor for the Adhesin Intimin-Gamma of Enterohemorrhagic *Escherichia coli* O157:H7." *The Journal of Biological Chemistry* 277 (4). American Society for Biochemistry and Molecular Biology: 2876-85.
- Singh, Juswinder, Russell C. Petter, Thomas A. Baillie, and Adrian Whitty. 2011. "The Resurgence of Covalent Drugs." *Nature Reviews Drug Discovery* 10 (4). Nature Publishing Group: 307-17.
- Singleton, Scott F, Rebecca A Simonette, Neil C Sharma, and Alberto I Roca. 2002. "Intein-Mediated Affinity-Fusion Purification of the *Escherichia coli* RecA Protein." *Protein Expression and Purification* 26 (3): 476-88.
- Sleno, Lekha, and Andrew Emili. 2008. "Proteomic Methods for Drug Target Discovery." *Current Opinion in Chemical Biology* 12 (1): 46-54.
- Slilaty, S N, and J W Little. 1987. "Lysine-156 and Serine-119 Are Required for LexA Repressor Cleavage: A Possible Mechanism." *Proceedings of the National Academy of Sciences of the United States of America* 84 (12): 3987-91.
- Smith, J.L., and P.M. Fratamico. 2017. "*Escherichia coli* as a Pathogen." In *Foodborne Diseases*, Third Edit, 26:189-208. Elsevier.

- Smith, Silas W. 2009. "Chiral Toxicology: It's the Same Thing...Only Different." *Toxicological Sciences* 110 (1). Oxford University Press: 4-30.
- Smith, Wendy E, Anne V Kane, Sausan T Campbell, David W K Acheson, Brent H Cochran, and Cheleste M Thorpe. 2003. "Shiga Toxin 1 Triggers a Ribotoxic Stress Response Leading to p38 and JNK Activation and Induction of Apoptosis in Intestinal Epithelial Cells." *Infection and Immunity* 71 (3). American Society for Microbiology: 1497-1504.
- Sommer, Suzanne, Francois Boudsocq, Raymond Devoret, and Adriana Bailone. 1998. "Specific RecA Amino Acid Changes Affect RecA-UmuD'C Interaction." *Molecular Microbiology* 28 (2). Blackwell Science Ltd, UK: 281-91.
- Sousa, Francisco J.R., Luis M.T.R. Lima, Ana B.F. Pacheco, Cristiano L.P. Oliveira, Iris Torriani, Darcy F. Almeida, Debora Foguel, Jerson L. Silva, and Ronaldo Mohana-Borges. 2006. "Tetramerization of the LexA Repressor in Solution: Implications for Gene Regulation of the *E. coli* SOS System at Acidic pH." *Journal of Molecular Biology* 359 (4): 1059-74.
- Sperandio, V., A. G. Torres, B. Jarvis, J. P. Nataro, and J. B. Kaper. 2003. "Bacteria-Host Communication: The Language of Hormones." *Proceedings of the National Academy of Sciences* 100 (15): 8951-56.
- Sperandio, V, J L Mellies, W Nguyen, S Shin, and J B Kaper. 1999. "Quorum Sensing Controls Expression of the Type III Secretion Gene Transcription and Protein Secretion in Enterohemorrhagic and Enteropathogenic *Escherichia coli*." *Proceedings of the National Academy of Sciences of the United States of America* 96 (26): 15196-201.
- Sperandio, V, a G Torres, J a Giron, and J B Kaper. 2001. "Quorum Sensing Is a Global Regulatory Mechanism in Enterohemorrhagic *Escherichia coli* O157:H7." *J Bacteriol* 183 (17): 5187-97.
- Spooner, Robert a, Daniel C Smith, Andrew J Easton, Lynne M Roberts, and J Michael Lord. 2006. "Retrograde Transport Pathways Utilised by Viruses and Protein Toxins." *Virology Journal* 3: 26.

- Ståhl, Anne-lie, Ida Arvidsson, Karl E. Johansson, Milan Chromek, Johan Rebetz, Sebastian Loos, Ann-Charlotte Kristoffersson, Zivile D. Békássy, Matthias Mörgelin, and Diana Karpman. 2015. "A Novel Mechanism of Bacterial Toxin Transfer within Host Blood Cell-Derived Microvesicles." Edited by Steven R. Blanke. *PLOS Pathogens* 11 (2). Public Library of Science: e1004619.
- Stayrook, Steven, Peera Jaru-ampornpan, Jenny Ni, Ann Hochschild, and Mitchell Lewis. 2008. "Crystal Structure of the L Repressor and a Model for Pairwise Cooperative Operator Binding" 452 (April): 2-6.
- Stechmann, B., Bai S., Gobbo E., Lopez R., Merer G., Pinchard S, Panigai L, et al. 2010. "Inhibition of Retrograde Transport Protects Mice from Lethal Ricin Challenge." *Cell* 141 (2): 231-42.
- Stohl, Elizabeth A., Joel P. Brockman, Kristin L. Burkle, Katsumi Morimatsu, Stephen C. Kowalczykowski, and H. Steven Seifert. 2003. "*Escherichia coli* RecX Inhibits RecA Recombinase and Coprotease Activities *in Vitro* and *in Vivo*." *Journal of Biological Chemistry* 278 (4): 2278-85.
- Stout, V., and Gottesman S. 1990. "RcsB and RcsC: A Two-Component Regulator of Capsule Synthesis in *Escherichia coli*." *Journal of Bacteriology* 172 (2). American Society for Microbiology: 659-69.
- Story R. M, Weber I.T., and Steitz T.A. 1992. "The structure of *E. coli* RecA protein monomer and polymer". *Nature*, 23;355(6358):318-25.
- Strovel, J., Sittampalam S, Coussens N., Hughes M, Inglese J., Kurtz A., Andalibi, A., et al. 2004. Early Drug Discovery and Development Guidelines: For Academic Researchers, Collaborators, and Start-up Companies. *Assay Guidance Manual*. Eli Lilly & Company and the National Center for Advancing Translational Sciences.
- Surendrannair, M., Kollanoor-Johny A, Ananda-Baskaran S., Norris C., Lee J., and Venkitanarayanan K. 2016. "Selenium Reduces Enterohemorrhagic *Escherichia coli* O157 : H7 Verotoxin Production and Globotriaosylceramide Receptor Expression on Host Cells" 11: 745-56.

- Surette, M. G., Miller M. B., and Bassler B. 1999. "Quorum Sensing in *Escherichia coli*, *Salmonella typhimurium*, and *Vibrio harveyi*: A New Family of Genes Responsible for Autoinducer Production." *Proceedings of the National Academy of Sciences of the United States of America* 96 (4): 1639-44.
- Taldone, T., Rodina A, DaGama Gomes E., Riolo M, Patel H, Alonso-Sabadell R, Zatorska D, Patel M, Kishinevsky S, and Chiosis G. 2013. "Synthesis and Evaluation of Cell-Permeable Biotinylated PU-H71 Derivatives as Tumor Hsp90 Probes." *Beilstein Journal of Organic Chemistry* 9: 544-56.
- Tam, P. J., and Lingwood C. A. 2007. "Membrane Cytosolic Translocation of Verotoxin A1 Subunit in Target Cells." *Microbiology* 153 (8): 2700-2710.
- Tarr, P., Gordon C., and Chandler W.. 2005. "Shiga-Toxin-Producing *Escherichia coli* and Haemolytic Uraemic Syndrome." *Lancet* 365 (9464): 1073-86.
- Tateishi, S., Horii T., Ogawa T., and Ogawa H. 1992. "C-Terminal Truncated *Escherichia coli* RecA Protein RecA5327 Has Enhanced Binding Affinities to Single- and Double-Stranded DNAs." *Journal of Molecular Biology* 223 (1): 115-29.
- Tavender, T., Halliday N., Hardie K., and Winzer K. 2008. "LuxS-Independent Formation of AI-2 from Ribulose-5-Phosphate." *BMC Microbiology* 8 (1): 98.
- Tepshi, L., Gupta N., Noel R., Goudet A., Hinsinger K., Michau A., Pons V., et al. 2018. "Retro-2, a Small Molecule Able to Protect Cells against a Broad Spectrum of Menacing Agents: Toxins, Viruses, Parasites and Intracellular Bacteria." *Toxicon* 149 (July). Pergamon: 96-97.
- Terstappen, G., Schlüpen C., Raggiaschi R., and Gaviraghi G. 2007. "Target Deconvolution Strategies in Drug Discovery." *Nature Reviews Drug Discovery* 6 (11). Nature Publishing Group: 891-903.
- Tesh, V. L., Burris J. A., Owens J. W., Gordon V. M., Wadolowski E. A., O'Brien A. D., and Samuel J. E. 1993. "Comparison of the Relative Toxicities of Shiga-like Toxins Type I and Type II for Mice." *Infection and Immunity* 61

(8). American Society for Microbiology (ASM): 3392-3402.

- Tesh, V. L. 2012. "Activation of Cell Stress Response Pathways by Shiga Toxins." *Cellular Microbiology* 14 (1): 1-9.
- Thi, T. D., Lopez E., Rodriguez-Rojas A., Rodriguez-Beltran J., Couce A., Guelfo J. R., Castaneda-Garcia A., and Blazquez J. 2011. "Effect of *recA* Inactivation on Mutagenesis of *Escherichia coli* Exposed to Sublethal Concentrations of Antimicrobials." *Journal of Antimicrobial Chemotherapy* 66 (3): 531-38.
- Thiel, V., Vilchez R., Sztajer H., Wagner-Döbler I., and Schulz S. 2009. "Identification, Quantification, and Determination of the Absolute Configuration of the Bacterial Quorum-Sensing Signal Autoinducer-2 by Gas Chromatography-Mass Spectrometry." *ChemBioChem* 10 (3): 479-85.
- Thorne, N, Auld D., and Inglese J. 2010. "Apparent Activity in High-Throughput Screening: Origins of Compound-Dependent Assay Interference." *Current Opinion in Chemical Biology* 14 (3). NIH Public Access: 315-24.
- Tilden, J., Young T., McNamara A., Custer C., Boesel B., Lambert-Fair M., Majkowski J., et al. 1996. "A New Route of Transmission for *Escherichia coli*: Infection from Dry Fermented Salami." *American Journal of Public Health* 86 (8): 1142-45.
- Torres, A., Tesh V., Palermo M., Bentancor L, Weiss A., Pradhan S., Pellino C., Macmaster K., and Coyle D. 2016. "Shiga Toxin Mediated Neurologic Changes in Murine Model of Disease." *Frontiers in Cellular and Infection Microbiology*
- Trachtman, H., Cnaan A., Christen E., Gibbs K., Zhao S., Acheson D., Weiss R., Kaskel F., Spitzer A., and Hirschman G. 2003. "Effect of an Oral Shiga Toxin-Binding Agent on Diarrhea-Associated Hemolytic Uremic Syndrome in Children: A Randomized Controlled Trial." *JAMA* 290 (10): 1337-44.
- Trofa, A. F., Ueno-Olsen H., Oiwa R., and Yoshikawa M. 1999. "Dr. Kiyoshi Shiga: Discoverer of the Dysentery Bacillus." *Clinical Infectious Diseases* 29 (5):

1303-6.

- Túri, S., Németh I., Vargha I., and Matkovics B. 1994. "Oxidative Damage of Red Blood Cells in Haemolytic Uraemic Syndrome." *Pediatric Nephrology (Berlin, Germany)* 8 (1): 26-29.
- Tyler, J. S., Mills M. J., and Friedman D. I. 2004. "The Operator and Early Promoter Region of the Shiga Toxin Type 2-Encoding Bacteriophage 933W and Control of Toxin Expression." *Journal of Bacteriology* 186 (22): 7670-79.
- Tyrrell, G., Ramotar K., Toye B., Boyd B., Lingwood C., and Brunton J. 1992. "Alteration of the Carbohydrate Binding Specificity of Verotoxins from Gal α -1-4Gal to GalNAc B1-3Gal α 1-4Gal and Vice Versa by Site-Directed Mutagenesis of the Binding Subunit." *Proceedings of the National Academy of Sciences of the United States of America* 89 (2): 524-28.
- Urban, A., Eckermann S., Fast B., Metzger S., Gehling M., Ziegelbauer K., RübSamen-Waigmann H., and Freiberg C. 2007. "Novel Whole-Cell Antibiotic Biosensors for Compound Discovery." *Applied And Environmental Microbiology* 73 (20): 6436-43.
- van Diemen, P. M., F. Dziva, M. P. Stevens, and T. S. Wallis. 2005. "Identification of Enterohemorrhagic *Escherichia coli* O26:H11 Genes Required for Intestinal Colonization in Calves." *Infection and Immunity* 73 (3): 1735-43.
- VanderWel, S., Harvey P., McNamara D., Repine J, Keller P., Quin J, Booth J., et al. 2005. "Pyrido[2,3D]pyrimidin-7-ones as Specific Inhibitors of Cyclin-Dependent Kinase 4." *Journal of Medicinal Chemistry* 48 (7). American Chemical Society: 2371-87.
- Vestby, L.K., Johannesen K.C.S., Witsø I.L., Habimana O., Scheie A.A., Urdahl A.M., Benneche T., Langsrud S., and Nesse L.L. 2014. "Synthetic Brominated Furanone F202 Prevents Biofilm Formation by Potentially Human Pathogenic *Escherichia coli* O103:H2 and *Salmonella* Ser. Agona on Abiotic Surfaces." *Journal of Applied Microbiology* 116 (2): 258-68.

- Vohradsky, J. 2017. "Lambda Phage Genetic Switch as a System with Critical Behaviour." *Journal of Theoretical Biology* 431 (October): 32-38.
- Wadolowski, E. A., Burris J. A., and O'Brien A. D. 1990. "Mouse Model for Colonization and Disease Caused by Enterohemorrhagic *Escherichia coli* O157:H7." *Infection and Immunity* 58 (8). American Society for Microbiology (ASM): 2438-45.
- Wagner, P. L., Acheson D. W., and Waldor M. K. 2001. "Human Neutrophils and Their Products Induce Shiga Toxin Production by Enterohemorrhagic *Escherichia coli*." *Infection and Immunity* 69 (3). American Society for Microbiology (ASM): 1934-37.
- Walters, M., Sircili M. P., and Sperandio V. 2006. "AI-3 Synthesis Is Not Dependent on *luxS* in *Escherichia coli*." *Journal of Bacteriology* 188 (16): 5668-81.
- Walters, M., and Sperandio V. 2006. "Autoinducer 3 and Epinephrine Signaling in the Kinetics of Locus of Enterocyte Effacement Gene Expression in Enterohemorrhagic *Escherichia coli*." *Infection and Immunity* 74 (10): 5445-55.
- Wang, D., X. Ding, and P. N. Rather. 2001. "Indole Can Act as an Extracellular Signal in *Escherichia coli*." *Journal of Bacteriology* 183 (14): 4210-16.
- Wang, D., Zetterström C., Gabrielsen M, Beckham K., Tree J, Macdonald S, Byron O., et al. 2011. "Identification of Bacterial Target Proteins for the Salicylidene Acylhydrazide Class of Virulence-Blocking Compounds." *The Journal of Biological Chemistry* 286 (34): 29922-31.
- Watanabe, M., Matsuoka K., Kita E., Igai K., Higashi N., Miyagawa A., Watanabe T., et al. 2004. "Oral Therapeutic Agents with Highly Clustered Globotriose for Treatment of Shiga Toxigenic *Escherichia coli* Infections." *The Journal of Infectious Diseases* 189 (3): 360-68. doi:10.1086/381124.
- Wigle, Tim J., and Singleton S. 2007. "Directed Molecular Screening for RecA

ATPase Inhibitors.” *Bioorganic and Medicinal Chemistry Letters* 17 (12): 3249-53.

Wigle, T., Sexton J., Gromova A., Hadimani M., Hughes M, Smith G., Yeh L., and Singleton S. 2009. “Inhibitors of RecA Activity Discovered by High-Throughput Screening: Cell-Permeable Small Molecules Attenuate the SOS Response in *Escherichia coli*.” *Journal of Biomolecular Screening : The Official Journal of the Society for Biomolecular Screening* 14 (9): 1092-1101.

Wu, H., Song Z., Hentzer M., Andersen J. B., Molin S., Givskov M., and Høiby N. 2004. “Synthetic Furanones Inhibit Quorum-Sensing and Enhance Bacterial Clearance in *Pseudomonas aeruginosa* Lung Infection in Mice.” *Journal of Antimicrobial Chemotherapy* 53 (6): 1054-61.

Wu, M. T., MacCoss M., Ikeler T. J., Hirshfield J., Arison B. H., and Tolman R. L. 1990. “Annelated Piperazinyl-7,8-Dihydro-6 H-thiopyrano[3,2-D]Pyrimidines.” *Journal of Heterocyclic Chemistry* 27 (6): 1559-63.

Wylie, J. L., Van Caesele P., Gilmour M. W., Sitter D., Guttek C., and Giercke S.. 2013. “Evaluation of a New Chromogenic Agar Medium for Detection of Shiga Toxin-Producing *Escherichia coli* (STEC) and Relative Prevalences of O157 and Non-O157 STEC in Manitoba, Canada.” *Journal of Clinical Microbiology* 51 (2): 466-71.

Yang, Y, Mingxu Z., Huayan H., Jun Z., Fenghua Y., Xinjun Z., Xiaofang Z., Hardwidge P., and Zhu G. 2014. “Quorum-Sensing Gene *luxS* Regulates Flagella Expression and Shiga-like Toxin Production in F18ab *Escherichia coli*.” *Canadian Journal of Microbiology* 60 (6): 355-61.

Yazdanbakhsh, K. 2005. “Controlling the Complement System for Prevention of Red Cell Destruction.” *Current Opinion in Hematology* 12 (2): 117-22.

Youn, J., Yoon J., and Hovde C. 2010. “A Brief Overview of *Escherichia coli* O157 : H7 and Its Plasmid O157”

- Yu, F., Wang Q., Zhang Z., Peng Y., Qiu Y., Shi Y., Zheng Y., et al. 2013. "Development of Oleanane-Type Triterpenes as a New Class of HCV Entry Inhibitors." *Journal of Medicinal Chemistry* 56 (11). American Chemical Society: 4300-4319.
- Yu, M., and D. B. Haslam. 2005. "Shiga Toxin Is Transported from the Endoplasmic Reticulum Following Interaction with the Luminal Chaperone HEDJ/ERdj3." *Infection and Immunity* 73 (4): 2524-32.
- Zang, T., Lee B., Cannon L., Ritter K., Dai S., Ren D., Wood T., and Zhou S. 2009. "A Naturally Occurring Brominated Furanone Covalently Modifies and Inactivates LuxS." *Bioorganic and Medicinal Chemistry Letters* 19 (21). Elsevier Ltd: 6200-6204.
- Zelyas, N., Poon A., Patterson-Fortin L., Johnson R., Lee W., and Chui L. 2016. "Assessment of Commercial Chromogenic Solid Media for the Detection of Non-O157 Shiga Toxin-Producing *Escherichia coli* (STEC)." *Diagnostic Microbiology and Infectious Disease* 85 (3): 302-8.
- Zhang, C., and Oldenburg A. 1999. "A Simple Statistical Parameter for Use in Evaluation and Validation of High Throughput Screening Assays." *Journal of Biomolecular Screening*.

Annex